

Applied asymmetric hydroformylation with rhodium-bisdiazaphospholane catalysts: Expanded substrate scope and industrial scale synthesis of chiral aldehydes

By

Martha Leigh Abrams

A dissertation submitted in partial fulfillment

of the requirements for the degree of

Doctor of Philosophy

(Chemistry)

at the

UNIVERSITY OF WISCONSIN-MADISON

2014

Date of final oral examination: 8/1/14

The dissertation is approved by the following members of the Final Oral Committee:

Clark R. Landis, Professor, Chemistry

Robert J. McMahon, Professor, Chemistry

Tehshik P. Yoon, Professor, Chemistry

Steven D. Burke, Professor, Chemistry

Eric Strieter, Assistant Professor, Chemistry

Applied asymmetric hydroformylation with rhodium-bisdiazaphospholane catalysts: Expanded substrate scope and industrial scale synthesis of chiral aldehydes

Martha Leigh Abrams

Under the supervision of Professor Clark R. Landis

At the University of Wisconsin-Madison

The conversion of olefins into aldehydes by hydroformylation with rhodium catalysts is one of the largest homogeneously catalyzed industrial reactions, producing millions of tons of linear aldehydes per year. However, the production of chiral, branched aldehydes via *asymmetric* hydroformylation (AHF) remains underutilized in synthesis. To improve the application of rhodium BisDiazaphos catalyzed AHF, high selectivity for previously uninvestigated disubstituted olefins including enol esters and enamides is demonstrated, which yield more complex α -functionalized aldehyde building blocks. Additionally, process-scale asymmetric hydroformylation to yield chiral, enantioenriched aldehyde feedstocks has not yet been demonstrated. In collaboration with Eli Lilly, asymmetric hydroformylation in a research scale flow reactor is realized through the development of a flow synthesis of naproxen. To support scale-up of asymmetric hydroformylation technologies the synthesis of bisdiazaphospholane ligands is re-examined to optimize the cost of the material and synthesis on a larger scale is demonstrated. Access to enantiopure ligand via classical resolution in place of preparative SFC chromatography has also been developed, and will improve accessibility to selective AHF catalysts. Finally, the direct observation of catalytic intermediates and rate information in asymmetric hydroformylation by circulating high-pressure NMR will be described.

Acknowledgements

I am incredibly thankful for my time spent in the Landis group, and for the people I interacted with along the way. From talking about recent literature to afternoon ice cream runs, it's been a pleasure working in the group. Gene Wong was a good friend and a passionate mentor. He will be missed. Clark has been an excellent mentor and guide for my graduate career. I've learned I should be ready to prove my side if he ever offers me a bet about a research problem.

Much of the work in this thesis is the result of not just my efforts, but of those around me. I am sincerely grateful for the excellent staff in this department, and in particular Dr. Charlie Fry, Dr. Martha Vestling, Bob Shanks, and Matt Martin in the machine shop. The crystal structure of the diastereomeric salt from our ligand resolution ended up being far more of an adventure than anyone expected; I am indebted to the tireless work of Dr. Ilia Guzei for not just his time but his recruitment of other experts including Matt Benning from Bruker, and Katrina Forest and Ken Satyshur from biochemistry.

I appreciate the time that Steve Burke, Bob McMahon, Eric Strieter and Tehshik Yoon are taking to sit on my committee. I would also like to thank Shannon Stahl and Jen Schomaker for their roles in my development at Wisconsin.

Thanks is also due to Scott May, Marty Johnson, Joel Calvin, Jim Stout, Joe Martinelli, and all of my other collaborators at Eli Lilly. Every interaction I had with the Lilly team was a genuine pleasure and a learning experience.

Larry Welch and Mary Crawford deserve credit for making me fall in love with chemistry, and Diana Cermak is the reason I chose to come to graduate school.

Finally, thanks to all of my friends both at Wisconsin and afar who have provided a terrific support network and cheering squad for me throughout the last five years.

Table of Contents

Abstract	i
Acknowledgements	ii
Chapter 1. Introduction for a lay audience	1
1.1. Chemistry and catalysis.	2
Scheme 1.1. Activation energy and catalysis.	3
1.2. Hydroformylation.	3
Scheme 1.2: Hydroformylation	3
Figure 1.1: Enantiomers	5
Figure 1.2: Carvone enantiomers	5
Figure 1.3: A bisdiazaphospholane ligand	7
1.3. Asymmetric hydroformylation in a flow reactor.	7
1.4. References.	8
Chapter 2. Asymmetric hydroformylation of <i>Z</i>-enamides and enol esters with rhodium-BisDiazaphos catalysts.	9
2.1 Introduction.	10
Figure 2.1: Bisdiazaphospholane ligand used for hydroformylation.	10
Scheme 2.1. AHF in the synthesis of (+)-Patulolide C	11
Table 2.1. Some representative examples of AHF of 1,1- and 1,2-disubstituted alkenes	11
Table 2.2. Asymmetric hydroformylation of <i>para</i> -substituted <i>Z</i> enol esters	13
Table 2.3. Selectivity of AHF is maintained at higher temperatures.	14
Table 2.4. Selectivity of AHF is maintained at higher temperatures.	14
Figure 2.2. AHF of enamide N-((<i>Z</i>)-1-hexen-1-yl)benzamide with time.	15

Table 2.5. Asymmetric hydroformylation of enamides.	16
Figure 2.3. Pressure effects on AHF of styrenyl enamides	17
Scheme 2.2. AHF of enamides applied to the synthesis of protected analog of L-DOPA	
aldehyde	18
2.2 Experimental.	20
2.3 References	54

Chapter 3. Improvements to the synthesis of enantiopure BisDiazaphospholane ligands

	57
3.1 Introduction.	58
Scheme 3.1. Synthesis of bisdiazaphospholane ligands.	58
Table 3.1. Routine syntheses of tetra-acid in the Landis group.	59
3.2a. Synthesis of 2,2'-(azinodimethyldiyne)bis-benzoic acid and identification of conformers and byproducts	60
Figure 3.1: ^1H NMR of azine and minor component	61
Figure 3.2: Possible structures of the minor component.	62
Figure 3.3: Variable-temperature ^1H NMR of azine.	62
Figure 3.4: 1D NOESY spectra of azine.	64
3.2b. Improving the yield and reproducibility of the synthesis of tetra-acid	65
Table 3.2: Revised synthesis of tetra-acid	66
Figure 3.5: color changes during tetra-acid synthesis	68
3.3. Classical resolution of racemic tetra-acid with chiral amine bases	68
Scheme 3.2: Tetra-acid resolution by salt formation.	68
Figure 3.6: Chiral amine bases screened for resolution.	69

Figure 3.7: <i>ee</i> comparison with increase in water % of crystallization solution.	70
Figure 3.8: ^{31}P and ^1H NMR spectra of diastereomers at each step in a resolution.	71
Figure 3.9: Crystal structure with disordered waters visible.	72
Figure 3.10: Simplified structure of the tetra-acid pseudoephedrine 1:4 salt.	73
3.4a. Issues with ligand potency and revised synthesis of ligand	74
Table 3.3: Potency of ligand samples	75
Scheme 3.3: Synthetic routes to bisdiazaphospholane tetra-amide ligands.	76
Table 3.4: Modifications to acyl fluoride coupling	78
3.4b. “The acetone trick”: isolation of high-potency ligand	78
Figure 3.11: $^{31}\text{P}\{^1\text{H}\}$ and ^1H NMR of ligand sample after various workup techniques.	79
3.5. Experimental.	81
3.6. References.	99
 Chapter 4. High-pressure, circulating NMR apparatus as a tool to study asymmetric hydroformylation: Observation of reaction timecourses and catalyst speciation under realistic reaction conditions	100
4.1. Introduction.	101
Figure 4.1. Mechanism of hydroformylation.	101
Figure 4.2: High-pressure, circulating NMR apparatus with injection capability (HP-NMR).	103

4.2 Equipment setup and design issues	104
<i>4.2.a: Starvation</i>	104
Figure 4.3: Catalyst speciation under static (starved) conditions.	105
<i>4.2.b: Lineshape</i>	105
Figure 4.4: Monitoring pre-activation of tetraphenyl catalyst at different flow rates.	106
<i>4.2c: Post-acquisition deconvolution to improve lineshape and sample autoshimming</i>	106
Figure 4.5: Reference deconvolution to improve lineshape.	107
<i>4.2d: Circulation rate vs. lineshape and capillary design</i>	108
Figure 4.6: Lineshape with different flow rates and bubble size changes with different capillary designs and flow rates	109
<i>4.2.e Temperature calibration and variation with flow</i>	109
Figure 4.7: Temperature profile after circulation	110
4.3. HP-NR runs with styrene.	110
Figure 4.8. AHF of styrene with step changes in temperature (starved)	111
Figure 4.9: AHF of styrene at 80 °C and lower catalyst loadings: starved vs. non-starved behavior.	112
Table 4.1: Comparing HP-NMR runs of styrene	114
4.4 HP-NMR studies with Z-1-(benzoyloxy)-1 hexene	114
Figure 4.10: Ligands for asymmetric hydroformylation.	115
<i>4.4.a Development of pulse program for circulation during d1 delay</i>	115
Figure 4.11: Modified pulse program with circulation during the inter-scan delay.	116
<i>4.4.b Batch and HP-NMR studies with Z-1-(benzoyloxy)-1 hexene</i>	116

Table 4.2: Batch AHF of Z-1-(benzoyloxy)-1-hexene.	117
Figure 4.12: Proton NMR stacked plot and timecourse of the AHF of Z-1-(benzoyloxy)-1-hexene under three pressure regimes.	118
Figure 4.13: Average H ₂ concentration and observed rate constant varies with pressure during the AHF of Z-1-(benzoyloxy)-1-hexene.	119
Figure 4.14: Observation of catalyst species by ³¹ P NMR and speciation with pressure changes.	120
Figure 4.15: AHF of enol ester substrate with step changes between 80 and 500 psi.	121
4.5. Experimental.	121
4.6. References.	125
Chapter 5. Asymmetric hydroformylation in a flow reactor for industrial-scale applications	126
5.1. Introduction.	127
5.1.a Advantages to developing asymmetric hydroformylation as a continuous flow process.	127
5.1.b Highlighting AHF in flow by performing the continuous asymmetric synthesis of Naproxen	130
Scheme 5.1: Synthesis of naproxen highlighting the use of reagent gasses.	131
5.1.c Equipment setup	131
Figure 5.1: Segmented flow in 13 mL tubular reactor.	132
Figure 5.2: Flow system overview	133
Figure 5.3. A similar 38 mL pipes in series reactor.	134
5.2.a Batch studies to establish flow rates: Styrene	134

Figure 5.4: Selectivity of styrene AHF changes with pressure.	135
5.2.b React-NMR at Lilly and reaction timecourses.	135
Figure 5.5: Decay of Rh(acac)(bisdiazaphospholane) during pre-activation of the catalyst.	136
Figure 5.6: Selectivity under starvation kinetics in the React-NMR.	137
5.2.c Flow runs with styrene	138
Figure 5.7: Ligands used for AHF flow studies	138
Figure 5.8: AHF with Ph-BPE: effect of catalyst age on selectivity.	138
5.3.a Batch studies with naproxen olefin	139
Table 5.1: Initial runs at UW: batch runs in glass pressure bottles.	139
Figure 5.9: HP-NMR timecourse of Naproxen hydroformylation showing starvation kinetics	140
Tables 5.2-5.5: Screening catalyst loading at two temperatures to observe approximate rate.	141
Table 5.6: Endeavor screens at Eli Lilly compared to batch work at Wisconsin.	143
5.3.b Flow studies with naproxen olefin	143
Table 5.7: Flow studies with naproxen olefin: Adjusting catalyst source and loading	144
Table 5.8: Flow studies with naproxen olefin: Probing the effect of pre-activation, running longer to reach steady state.	145
Table 5.9: Endeavor batch studies: matching flow studies in table 5.8 and determining the role of temperature and pressure	146
Table 5.10: Endeavor batch studies with naproxen olefin at different temperatures.	147

Table 5.11: Endeavor batch studies with naproxen olefin to determine stability of pre-activated catalyst under a N ₂ atmosphere.	149
Figure 5.10: Graphical representations of table 5.11 .	150
Figure 5.11: Pressure and temperature effects on sample composition.	151
5.4 Heck reaction and oxidation for completion of synthesis.	151
Scheme 5.2: Heck reaction with ethylene.	152
Scheme 5.3: Oxidation of chiral aldehydes developed by the Stahl lab.	153
5.5 Experimental.	154
5.6 References.	157

Appendix A: Expanding the scope of asymmetric hydroformylation: various novel substrates

	159
A.1. Asymmetric Hydroformylation of Z-Alkenes Produced by Metathesis	160
A.2. Asymmetric Hydroformylation of 1,1-disubstituted olefins	167
Appendix B: Spectra and supporting data for Chapters 2-5.	188
Appendix C: Crystal structure of tetra-acid / pseudoephedrine salt	259

Chapter 1

Introduction for a lay audience

1.1. Chemistry and catalysis.

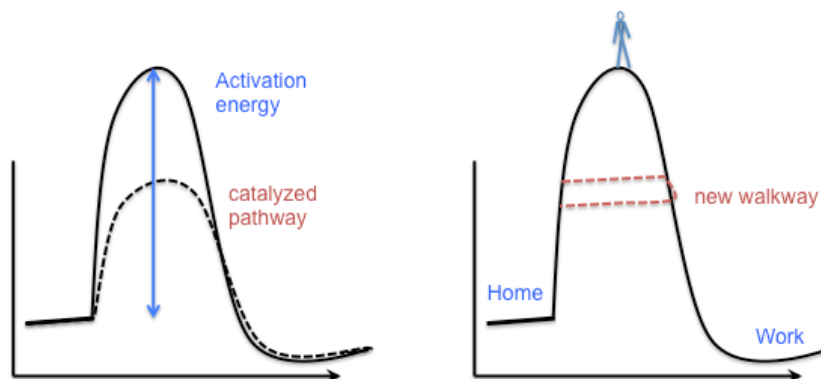
Chemistry, as a subject, is a vast field of knowledge. The diversity of research in chemistry spans from understanding how your cells sense hormones, to finding regular, nonrepeating patterns in nature, to computational modeling of how molecules stretch and bend and collide in the dance we chemists call a reaction. These examples are just a few to highlight the breadth of chemistry research in the world today, and they happen to be the subject of the three most recent Nobel prizes in chemistry.¹

If we look back one year further, to the Nobel prize from 2010, it was awarded to the people who figured out how to bond, or stick together, the carbon atoms of two molecules in a controlled way by first introducing them to a palladium atom.² This kind of reaction, called cross-coupling, is at the heart of the kind of chemistry that this thesis is related to. That palladium atom, in a lot of ways, makes all the difference. Organometallic chemistry is the merger of organic and inorganic chemistry, and much of modern catalysis comes from our understanding of how that palladium atom helps bond two carbons together.

When a catalyst (the palladium, in our example so far) lowers the activation energy of a chemical process (the two carbon atoms bonding together), the result is that the process goes more quickly. This phenomenon is known as catalysis. An easy way to think of this is as a big hill on your way to work. Let's say your walk to work each morning takes you half an hour, mostly because you have to go over the top of that big hill. One day, you set out only to find that a new walkway has been installed, which means you no longer have to climb all the way up the hill. Your walk to work now takes only 15 minutes, or what chemists would call a "twofold rate enhancement." Now, this seems like a pretty good improvement on your daily commute, until you realize that some catalysts can provide a million-fold rate enhancement, which for the purposes of our analogy would get you to work in just under two milliseconds.³

The energy it takes to get over the hill is the activation energy, and the role of a catalyst is to reduce the magnitude of this barrier. The reaction (your walk to work) is graphed as energy versus reaction progress (Scheme 1.1).

Scheme 1.1: Activation energy and catalysis.

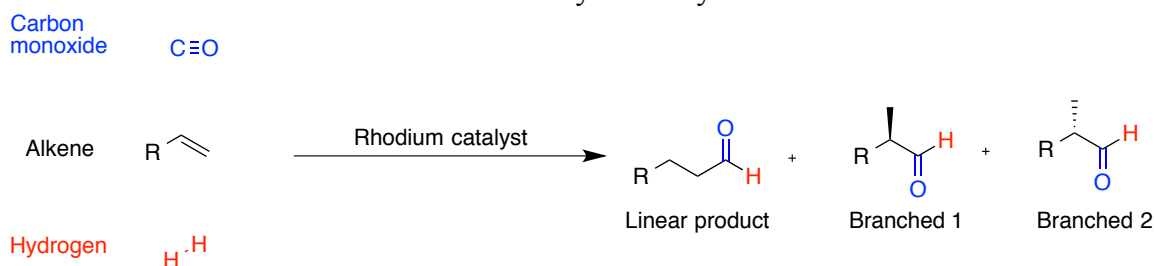


1.2: Hydroformylation.

The particular type of catalysis that this work concerns is a reaction called hydroformylation. Hydroformylation takes gasses produced during steam refining, hydrogen and carbon monoxide, and adds them to another commonly oil-derived compound, an alkene. In this particular case, the catalyst is rhodium, not palladium, but a new bond between carbon atoms is still formed, this time in between carbon monoxide and the alkene (Scheme 1.2). This new product is called an aldehyde.

Aldehydes can be made in other ways too—not just by hydroformylation. You are most likely familiar with a number of aldehydes, as they tend to be fragrant compounds. The smell of cinnamon and vanilla are both due to aldehydes. An aldehyde is a type of functional group, or a fragment in a molecule. The aldehyde functional group is a carbon that is double bonded to an oxygen and also bonded to a hydrogen.

Scheme 1.2: Hydroformylation



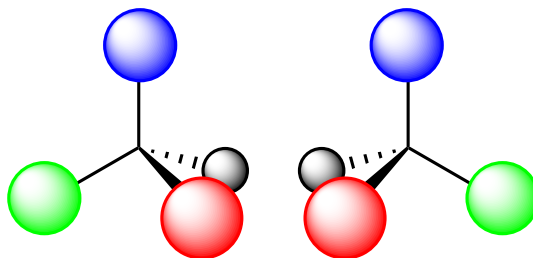
You may have noticed that there are three products shown in scheme 1.2: indeed, there are three potential ways that the carbon monoxide and hydrogen can add to the alkene. First of all, let's cover some definitions.

The molecules drawn above use a sort of shorthand where sticks are used to draw the bonds between atoms, and the carbon atoms are implied wherever there is an intersection of straight lines or a bend in the line. Carbon monoxide, in blue, is made up of a carbon and an oxygen and gets incorporated into the product to form the aldehyde functional group. The carbon of carbon monoxide is still connected to the oxygen illustrated in blue, it just isn't drawn explicitly in the shorthand structure.

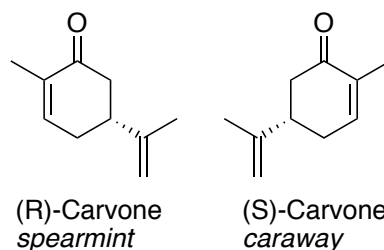
The "R" on the alkene stands for any kind of variable group. Depending on its identity, the reaction might be faster or slower, or lead to one product in greater quantities than another. The work in Chapter 2 is concerned with versions of alkenes where there are two "R" groups on either end of the alkene—something that has been less well studied to date. This makes it more difficult to form just one of the (now four!) possible products in large quantities while suppressing the formation of others.

There are three possible products drawn in Scheme 1.2, two that appear nearly identical and one that has the atoms connected in a different order. The one with the atoms in a different order is the linear product. It is called this because the aldehyde ends up on the end of the molecule, as far away from the R group as possible. There are lots of catalysts that select for making the linear product and very little of the branched product, these are "linear-selective" hydroformylation catalysts, and they are used commercially to prepare billions of pounds of linear aldehydes per year.⁴ These aldehydes end up in industrial solvents, plasticizers, and detergents.

The other two products drawn in Scheme 1.2 are identical in composition and in how the atoms are connected, and only vary in the direction that the top carbon sticks out. Remember, our two-dimensional shorthand for molecules is just that, and sometimes we need a way to also represent three-dimensional orientation (Figure 1.1).

Figure 1.1: Enantiomers

One way to do this is with wedges (the bold bond in the branched aldehyde on the left) representing bonds that stick out in front of the drawing plane, and hashes (seen in the branched aldehyde on the right) representing bonds that stick out behind the drawing plane. Just like your hands, if you take one and try to exactly superimpose it on the other, you will never find an orientation that succeeds. The two branched aldehydes (and your hands) are mirror images of one another. In molecules, this means that they have all identical properties except for the direction in which they rotate plane-polarized light. These are called enantiomers. Of course, if that was the only way in which they differed, we would maybe not be so concerned with the difference. However, nearly everything biological relies on the difference between enantiomers for recognition and binding. The “handedness” of a molecule is often crucially important to its biological function. For example, limonene and carvone (Figure 1.2) are enantiomers of each other, and our noses can tell the difference, with the (R) enantiomer smelling like mint and the (S) enantiomer like caraway.

Figure 1.2: Carvone enantiomers

Returning to hydroformylation, the formation of one of the branched isomers selectively is referred to as *asymmetric* hydroformylation. This reaction is done on a much smaller scale than the commodity scale linear hydroformylation, and tends to use more expensive catalysts as well. However,

catalysts for asymmetric hydroformylation are able to make a single enantiomer of aldehyde as the major product, with only the stereochemical information they contain to induce this selectivity.

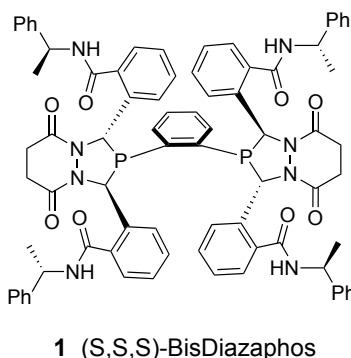
Understanding the way in which this information is transferred, and the reaction conditions that favor formation of one type of reaction over another is the subject of Chapter 4 of this thesis. Much has been done before to determine this kind of information, but we will be using a new tool to be able to see what is happening during the entire reaction, instead of just at the end. This means that we get to watch things like changes in how fast the linear aldehyde is formed versus how fast the branched aldehyde is formed simultaneously. We are also able to see exactly what the catalyst looks like while it's doing catalysis, something that will tell us more about how it behaves. We hope to be able to get a full snapshot of the interplay between lots of effects (like what temperature and pressure the reactions are run at) and the form the catalyst is in during each of those reaction types.

Now, the catalyst is certainly important to hydroformylation (nothing happens without it), but what makes it have this special behavior? If many of the catalysts for linear hydroformylation contain rhodium metal, how do they differ from the asymmetric hydroformylation catalysts that are also rhodium based? The difference between catalysts is largely determined by the *ligand* that the metal is bound to. Remember, many catalysts are organometallic compounds. The “metallic” part of the catalyst is the rhodium, and the “organo” part of the catalyst is the ligand, which is usually an organic molecule that coordinates to the metal in a particular way. The ligand has certain groups on it, often phosphorus atoms, that have electrons that can be “donated” to the metal center to help stabilize it and change the kind of chemistry it performs.

For the work in this thesis there is one particular ligand that is our favorite, the bisdiazaphospholane **1** (Figure 1.3). This is because it has properties that make it fast, even at lower temperatures (remember that “hill” of activation energy? heating a reaction is the other way to get over that), and because it is relatively straightforward to make. However, we recently discovered that it isn't quite as easy to make as we had thought, and we are losing a lot of our expensive ligand along the way.

Chapter 3 is the story of how we discovered this, and how many of the problems have been solved by looking closely at each step in the synthesis and coming up with small changes that add up to a big improvement in the purity and yield of catalyst we can make.

Figure 1.3: A bisdiazaphospholane ligand



1.3: Asymmetric hydroformylation in a flow reactor.

One of the main drivers in chemical industry is to reduce cost and reduce waste. Performing reactions in a flow reactor is one way to do this because control of temperature is more easily managed, and because it provides the opportunities to recycle back to the front end components that may have otherwise been thrown out. In pharmaceutical synthesis, flow reactors are also seen as a way to perform reactions that may not have made it very far in scale up because of safety concerns, expensive equipment, or difficulty with scale. Flow reactors are just a tube in their most simple form, so they generally cost less than many types of specialized equipment. For reactions like hydroformylation, or other reactions that use hazardous gasses like hydrogenations, important safety problems are solved by flow reactors. Running a reaction in flow means that less gas can be used and the total volume in the reactor is far less than that required to perform the same reaction on the same scale in batch.

When running in a flow reactor, there are a few key terms to understanding what is happening. First, in a batch reactor the material all goes in and out of the reaction at the same time, like cooking a casserole. The analogous value in a flow reactor is the residence time, tau, which is the average time that the material takes to flow from one end of the reactor to another. However, as it moves down the pipe, the material begins to mix so some of it takes a little longer to come out the other end and some

takes a little less time. The amount of material converted to product in six hours in a batch reactor will not be the same as the amount coming out of the reactor at a six hour tau unless mixing up and down the reactor is minimized (axial dispersion) or accounted for, and the reaction is at steady state (the material coming out of the back end of the reactor is always the same mixture of things). These are features of a well-controlled flow reaction, and what we are aiming to accomplish.

Chapter 5 is related to research done with Eli Lilly on employing asymmetric hydroformylation in a flow reactor. Recall that hydroformylation is atom economical, with all the atoms entering into the reaction (carbon monoxide, hydrogen, and alkene) incorporated into the product. Pair this with the energy, design and scale up advantages that flow reactors can confer and together, these two “green” components have the potential to greatly reduce the cost of synthesis. The reaction we want to use to demonstrate how valuable this might be is the synthesis of naproxen—the active ingredient in Aleve. Even if this project becomes wildly successful, the synthesis described here won’t replace commercial processes in place, which have been optimized to reduce cost as much as possible over the four decades naproxen has been approved as a drug. Instead, this project is designed to highlight the possibilities that asymmetric hydroformylation offers and provide a precedent for their implementation on the industrial scale, in the synthesis of new medicines.

1.4. References.

¹ All Nobel Prizes in chemistry. http://www.nobelprize.org/nobel_prizes/chemistry/laureates/ (Accessed 7/26/2014).

² Nobel Prize in chemistry for 2010. http://www.nobelprize.org/nobel_prizes/chemistry/laureates/2010/ (Accessed 7/26/2014).

³ Hastings, C. J., Bergman, R. G. and Raymond, K. N. *Chem. Eur. J.*, **2014** *20*, 3966–3973.

⁴ Gual, A.; Godard, C.; Castellón, S.; Claver, C. *Tetrahedron: Asymmetry* **2010**, *21*, 1135-1146.

Chapter 2

Asymmetric hydroformylation of *Z*-enamides and enol esters with rhodium-BisDiazaphos catalysts.

Portions of this chapter are the work of:

Floriana Foarta, who did the vast majority of work on enol ester substrates.

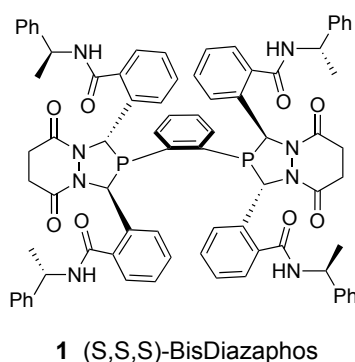
Yicong Ge, who performed the synthesis and characterization of the L-DOPA aldehyde. These contributions are also noted within the text.

This chapter was submitted for publication to the Journal of the American Chemical Society on July 28, 2014.

2.1. Introduction

Chiral aldehydes are versatile building blocks in organic synthesis. Although the conversion of simple, terminal alkenes into aldehydes by hydroformylation with rhodium catalysts constitutes a long-standing commodity process, applications to the synthesis of chiral aldehydes have been less common.¹ The emergence of new chiral catalysts that effect rapid, enantioselective, and regioselective hydroformylation of monosubstituted, and to a lesser extent, disubstituted alkenes provide new opportunities for efficient syntheses of chiral aldehydes. In this chapter, we demonstrate that disubstituted alkenes comprising *Z*-enol esters and *Z*-enamides undergo efficient hydroformylation with excellent selectivity and functional group tolerance using rhodium catalysts in the presence of the (S,S,S)-BisDiazaphos ligand, **1**.

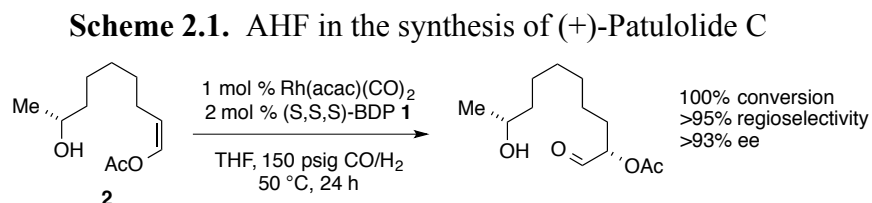
Figure 2.1: Bisdiazaphospholane ligand used for hydroformylation.



Effective, modern asymmetric hydroformylation (AHF) technology began with the development of the Rh(BINAPHOS) catalyst system.² Applications of this catalyst system demonstrated that useful regio- and enantioselectivities could be effected for a variety of alkenes, especially monosubstituted alkenes. Following these initial demonstrations, several notable ligand systems for AHF have been reported. These ligands include diphosphites such as Chiraphite,³ mixed phosphine-phosphoramidites such as Yanphos,⁴ mixed phosphine-phosphite ligands with small bite angles,⁵ Duphos-related diphosphines such as Ph-BPE,⁶ and so-called scaffolding monophosphine ligands.⁷ Rhodium complexes of the bisdiazaphospholane (BDP) class of ligands exhibit unusual activity and selectivity in

AHF reaction for a broad range of alkene substrates. High (> 90% ee) enantioselectivities have been achieved with aryl alkene, 1,3-diene, vinyl acetate and *N*-vinyl acetamide, dihydrofuran, and other substrates using BDP-derived catalysts.⁸

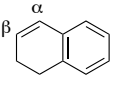
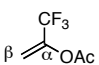
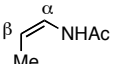
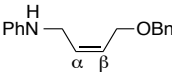
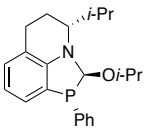
Effective AHF with disubstituted alkene substrates would expand the application of AHF in complex molecule synthesis. AHF provides a fundamentally different disconnection than other C-C bond forming reactions in the design of complex molecules. An excellent example is provided by Burke's recent report of a highly efficient synthesis of Patulolide C that features AHF of the *Z*-enol ester **2**.^{8c} Additional examples include the enantioselective synthesis of Garner's aldehyde⁹ and Leighton's synthesis of Dictyostatin.¹⁰



Many simple, terminal alkenes have been converted into chiral aldehydes with high selectivity by asymmetric hydroformylation. However, AHF of more complex substrates is far less established, and requires overcoming a number of new obstacles to achieve selective reactions. Prior examples of enantioselective AHF of disubstituted alkenes with enantioselectivities that exceed 90% ee are given in Table 2.1.

Table 2.1. Some representative examples of AHF of 1,1- and 1,2-disubstituted alkenes

	Substrate	Ligand	Sub/Cat t Ratio	P _{H₂/CO} (psi)	T (°C)	t (h)	Conv. (%)	α:β	ee (%)
1		Binaphos ^{2b}	250	1470	60	50	10	97: 3	92
2		BDP 1 ^{8b}	500	150	40	24	37	92: 8	94
3		BDP 1 ^{8b}	500	70	40	24	67	-	93

4		Binaphos ^{2b}	300	1470	60	20	79	96: 4	96
5		QuinoxP* ¹¹	100	145	85	8	46	> 100	91
6		BDP 1 ^{8c}	200	140	70	20	99	97: 3	90
7			57 ^a	50	45	14	77	> 100	91

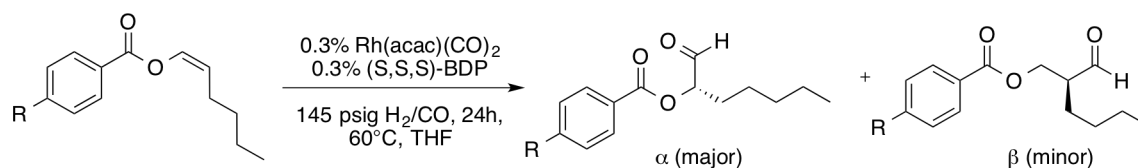
^a Run with 15 mol% ligand (6.7:1 substrate:ligand) and 0.05 mol% pTsOH as an additive.

The AHF of 1,2-disubstituted alkenes requires controlling the regioselectivity of CO insertion between two positions that are less sterically differentiated than in monosubstituted or 1,1-disubstituted alkenes. To date, control of regioselectivity has been addressed mostly for substrates with a heteroatom in the allylic position, which are amenable to scaffolding catalysis.⁷ The overall increased steric bulk of disubstituted substrates frequently requires long reaction times and/or high catalyst loading. With Rh-bisdiazaphospholane catalysts, alkenes substituted with inductively electron-withdrawing groups, such as acetoxy- or acetamido-substituents, generally yield high regioselectivity and good overall activity of AHF.^{8c} With the exception of particularly electron-deficient alkenes, AHF of 1,1-disubstituted alkenes is sluggish.¹¹ A small set of data indicates that the geometry of the double bond also impacts AHF selectivity, with *Z* alkenes giving higher regio- and enantioselectivities as well as higher activity.^{2b, 8c} These guiding principles are crucial for expanding the application of AHF to *Z*-enol esters and enamides.

Enol ester substrates are attractive candidates for investigation of AHF because the two carbons of the alkene are well-differentiated electronically. Benzoyloxy-substituted alkenes are synthetically accessible as the *Z* isomer selectively via Ru-catalyzed addition of alkynes to carboxylic acids.^{12,13} Hydroformylation of these alkenes produced only the alpha-substituted, 2-benzoyloxy aldehyde with

excellent enantioselectivity (90-97% *ee*) and low catalyst loadings (0.3%) (Table 2). In addition, results on the gram scale (Table 2, entry 1) are comparable to small scale (Table 2). Hydroformylation is tolerant of a wide variety of functional groups, including potential catalyst poisoning groups such as thioether, benzylic chloride, and free phenol (Table 2, entries 3, 6 and 7). The substituent in the *para* position has little effect on the hydroformylation activity and all substrates tested give high regio- and enantioselectivity under the screening conditions.

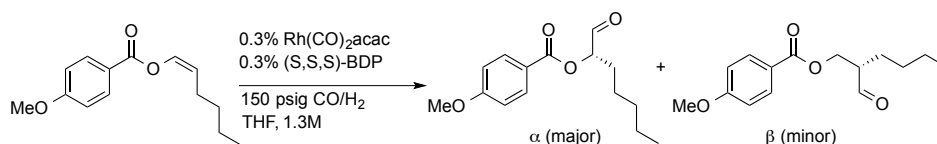
Table 2.2: Asymmetric hydroformylation of *para*-substituted *Z* enol esters.



Entry	R=	Conc. alkene	Conv. ^a	$\alpha:\beta^a$	Isolated yield	% <i>ee</i> ^c
1 ^b	H	1.5 M	>99%	>50:1	92%	97
2	OMe	1.3M	>99%	>50:1	84%	96
3	SMe	1.8M	>99%	>50:1	85%	90
4	Cl	1.3M	>99%	>50:1	88%	96
5	Br	1.3M	>99%	>50:1	82%	92
6 ^d	CH ₂ Cl	1.5M	94%	>50:1	78%	92
7	OH	1.3M	93%	>50:1	82%	nd

Run with 100 mg alkene. ^a Determined by ¹H NMR of crude reaction mixture. ^b Run with 1 g alkene. ^c *ee* determined by SFC or HPLC after NaBH₄ reduction. ^d 0.5% catalyst loading. Entries 2-7 by F. Foarta.

While the results in Table 2.2 are all run for 24 hours, many substrates go to complete conversion at 60 °C in under 16 hours. Additionally, at higher temperatures, the reaction time is reduced with no effect on the enantio- or regioselectivity. For (*Z*)-hex-1-en-1-yl 4'-methoxybenzoate, AHF is complete within 1.5 hours at 100 °C, and the resultant aldehyde is produced in 96 % *ee* (Table 2.3, entry 3). The enantioselectivity only drops modestly when the temperature is further increased to 120 °C.

Table 2.3: Selectivity of AHF is maintained at higher temperatures.

Entry	Temp (°C)	Time (h)	Conv. ^a	$\alpha:\beta^a$	% ee ^b
1	60	24	>99%	>50:1	96
2	80	5	>99%	>50:1	96
3	100	1.5	>99%	>50:1	95
4	120	0.5	>99%	>50:1	89

Run with 100 mg alkene. ^aDetermined by ¹H NMR of crude reaction mixture. ^bee determined by HPLC after NaBH₄ reduction. Data in this table from F. Foarta.

AHF of enol esters is effective with both acetyl and benzoyl protecting groups (Table 2.4, entry 1). This is significant because acetyl groups are also common in multi-step syntheses. Chiral, amino acid derived enol esters undergo AHF with high diastereoselectivity that appears to be catalyst-controlled, with little mismatch effect (Table 2.4, entries 2 and 3). Trifluoroacetyl enol esters also were investigated, but these underwent undesirable elimination of trifluoroacetic acid under catalytic conditions and gave low conversion (37-60%) to the desired product.

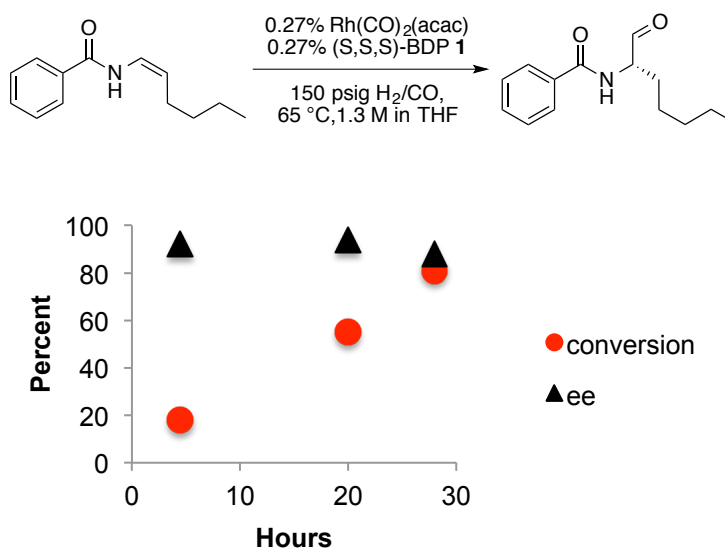
Table 2.4. AHF of other enol esters

Substrate	Product	Conc. alkene	Temp (°C)	Time (h)	Conv. ^a	$\alpha:\beta^a$	Isolated Yield	% ee or de
		1.3M	60	24	>99%	>50:1	88%	93 ^b
		1.1M	60	24	>99%	>50:1	83%	92 ^a
		1.1M	60	24	>99%	>50:1	75%	92 ^c

Run with 150 psig H₂/CO. ^aDetermined by ¹H NMR of crude reaction mixture. ^bee determined by HPLC after NaBH₄ reduction. ^cRun with (R,R,R) BisDiazaphos. Data from F. Foarta.

Z-enamides can be synthesized by a Ru-catalyzed coupling of primary amides to alkynes that is analogous to the synthesis used for enol esters.¹⁸ These substrates also undergo AHF with high selectivity for the α -amino aldehyde product. The AHF of enamides is slower than that of the corresponding enol esters (Figure 2.2), and complete conversion within a day requires higher catalyst loading (1%).

Figure 2.2. AHF of enamide N-((*Z*)-1-hexen-1-yl)benzamide with time.



Both *E*- and *Z*-enamides were tested under standard AHF conditions (Table 2.5, entries 1 and 2); consistent with past results the *Z*-enamide gives both higher enantioselectivity and faster rates. Under standard conditions, the AHF of most enamides proceeds with high selectivity and excellent functional group tolerance, including groups that often react with metal catalysts, like alkyl chlorides and nitriles (Table 2.5, entries 4 and 5). Important limitations of AHF with BisDiazaphos catalysts are revealed by two substrates. The α - β unsaturated substrate ethyl-(2-benzamido)ethenoate undergoes hydroformylation but also shows extensive hydrogenation of the double bond and degradation of starting material (entry 10). Second, the tertiary amide *N*-4-

phenyl-1-butenylpyrrolidinone is far slower than other enamides giving only 27% conversion to the aldehyde in 24 hours, with extensive isomerization to the *E* alkene (entry 11).

Table 2.5. Asymmetric hydroformylation of enamides.

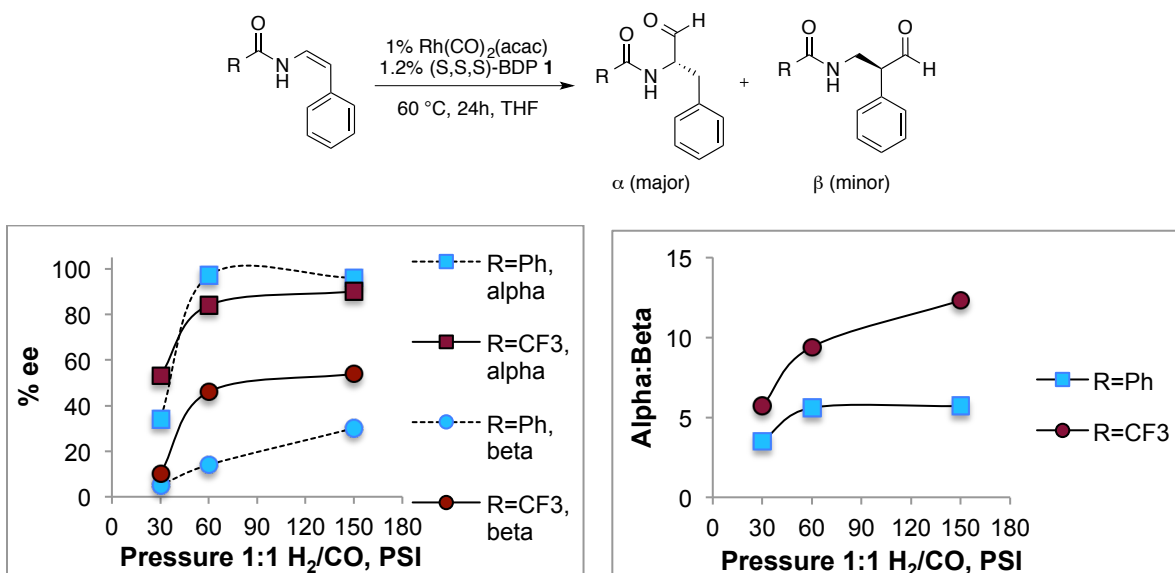
$ \begin{array}{c} \text{R}-\text{C}(=\text{O})-\text{NH}-\text{CH}=\text{CH}-\text{R}' \\ \xrightarrow[150 \text{ psig H}_2/\text{CO, THF}]{1\% \text{ Rh}(\text{CO})_2(\text{acac}), 1.2\% (\text{S,S,S})\text{-BDP } 1} \\ \text{R}-\text{C}(=\text{O})-\text{NH}-\text{CH}(\text{R}')-\text{CH}_2-\text{CHO} \quad + \quad \text{R}-\text{C}(=\text{O})-\text{NH}-\text{CH}_2-\text{CH}(\text{R}')-\text{CHO} \\ \alpha \text{ (major)} \quad \quad \quad \beta \text{ (minor)} \end{array} $						
Entry	Substrate	Temp (°C)	Conc. alkene	% Conv. ^a	α:β ^a	%ee ^b
1		65	1.1M	100	>99	85
2		65	1.1M	68	>99	56
3		60	1.0M	87	>99	90
4		60	0.8M	79	14.3	92
5		60	0.8M	100	>99	94
6		55	0.8M	80	>99	84
7		65	1.1M	86	6.3	α: 98 β: 32
8		60	1.1M	100	12.3	α: 90 β: 54
9		60	0.9M	100	21.0	n.d.
10		60	0.9M	70	n.d.	n.d.
11		60	1.8M	27	6.7	n.d.

Reactions run with 100 mg alkene. ^a Determined by ¹H NMR of crude reaction mixture. ^b ee determined by SFC or HPLC after NaBH₄ reduction.

The *N*-styryl enamides examined undergo hydroformylation with lower regioselectivity than that seen for enamides with pendant alkyl chains. Presumably this reflects competition between

the aryl (which directs formyl insertion in the β position) vs carboxamido (which directs formyl insertion in the α position) directing effects. Because styrene exhibits strongly CO-pressure dependent selectivity, we examined the hydroformylation of *N*-((*Z*)-2-phenylvinyl) benzamide as a function of pressure (Figure 2.3).

Figure 2.3. Pressure effects on AHF of styrenyl enamides.



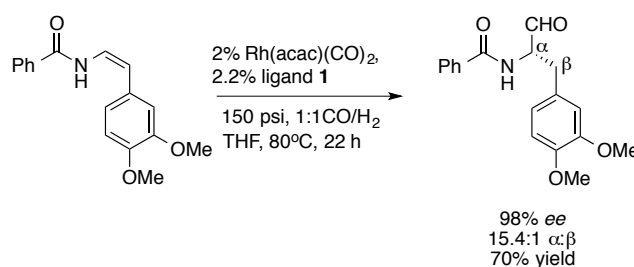
As seen for simple styrenes, the regio- and enantioselectivity of (*Z*)-styreneamides decrease with decreased syngas pressure. Increasing the electron-withdrawing nature of the carboxamide (trifluoroacetamido vs. benzamido) improves the regioselectivity at a given syngas pressure and the trend of increasing regio- and enantioselectivity with increased syngas pressure persevere. Such results demonstrate the importance of manipulating reaction conditions to control selectivity in the hydroformylation of styrenyl substrates.

AHF provides more atom efficient and direct access to highly enantioenriched α -amino aldehydes than methods involving multiple-step reactions and multiple changes in oxidation state to reach the desired aldehyde functionality.¹⁹ Although alpha substituted aldehydes potentially

are susceptible to racemization via enolization, the intrinsically neutral conditions unique to aldehyde synthesis by hydroformylation obviate racemization even at temperatures in excess of 100 °C.²⁰ As a demonstration of the practical utility of AHF, the synthesis of a protected L-DOPA aldehyde was performed. While the acid form is accessible through various synthetic methods (the most notable of which is Knowles' asymmetric hydrogenation), the aldehyde form is a valuable intermediate for formation of peptides and analogs.²¹

The desired *Z*-enamide was accessed by Ru-catalyzed coupling of benzamide to an alkyne derived from vanillin.²² Asymmetric hydroformylation of this substrate proceeds cleanly to produce the aldehyde with 98% *ee* and 15.4:1 branch selectivity. The improved selectivity relative to the styrenyl enamides in Figure 3 is likely due to the electron-donating methoxy substituents on the aryl ring disfavoring acyl formation at the β position.^{8b}

Scheme 2.2. AHF of enamides applied to the synthesis of protected analog of L-DOPA aldehyde.



ee Determined by HPLC after NaBH₄ reduction to the alcohol. Synthesis by Y. Ge.

AHF provides a direct, catalytic, and atom-efficient route to useful chiral building blocks, including unnatural amino aldehydes. A variety of *Z* enol esters and enamides undergo asymmetric hydroformylation in the presence of **1** and Rh(acac)(CO)₂ to produce α -chiral aldehydes with high regio- and enantioselectivity. These studies highlight critical attributes of the BisDiazaphos hydroformylation catalysts: high intrinsic reactivity (with complete

conversion and > 90% *ee* in just 90 minutes at 0.3 mol% catalyst loading), reliably (>90% *ee*) high enantioselectivities for a variety of *Z*-enol esters and enamides, and tolerance of functional groups such as phenols, thioethers, aryl bromides, and benzylic chlorides. For 1,2-disubstituted alkenes with competing regiodirecting substituents, such as styrenyl enamides, increased pressure can effect increased regio- and enantioselectivities for the α -carboxamido aldehyde. Overall, these results significantly expand efficient access to chiral α -functionalized aldehydes.

Experimental.

I. General:

All manipulations were carried out under nitrogen using standard Schlenk, high vacuum, and glovebox techniques. Ethyl acetate, hexane, dichloromethane and anhydrous DMF were obtained from Sigma-Aldrich. Dichloro(*p*-cymene)Ru(II) dimer and Ru(COD)(2-methallyl)₂ were purchased from Alfa Aesar. Dicyclohexylphosphinobutane, *tris*-(*p*-Cl-C₆H₄) phosphine, DMAP, and all alkynes, carboxylic acids, and primary amides were purchased from Sigma-Aldrich. Unless mentioned below, all chemicals were purchased and used without further purification. Enol esters and enamides were prepared by literature methods and purified by silica column chromatography prior to use (see section II). Bisdiazaphospholane ligands were prepared as reported in literature (Adint, T.T; Wong, G.W.; Landis, C.R. *J. Org. Chem.* **2013**, 78 4231-4238). [Rh(acac)(CO)₂] was used as received from Dow Chemical and stored in a N₂-filled glovebox. 1:1 CO:H₂ was purchased from Airgas. THF and toluene were either distilled from sodium/benzophenone ketyl under N₂ or dried by safety columns prior to use. Alkynes were degassed prior to use by either three freeze-pump-thaw cycles or sparging with N₂. Flash chromatography was performed on Silicycle Siliaflash P60 silica gel (40-63μm, 230-400 mesh). Chiral HPLC analysis was performed on a Gilson analytical HPLC with Chiralpak IA, IB, IC, and ID columns. Chiral super critical fluid chromatography (SFC) analysis was performed on a Berger SFC with Chiracel OJ-H or AD-H columns. Optical rotations were measured at room temperature using a 1 mL cell with a 0.5 dm path length on a Randolph digital polarimeter. Absolute configuration was determined by optical rotation for (-)(2*S*)-(benzoyloxy)heptanal, and assigned by analogy for other reported aldehydes. All pressures given are gauge pressures unless otherwise noted.

NMR spectra were recorded at ambient temperature on Varian Mercury-300, Inova-500 or Unity-500 and Bruker AC-300, Avance III 400, or Avance III 500 spectrometers. ^1H and ^{13}C NMR chemical shifts were referenced to tetramethylsilane if present or residual solvent. ^{31}P and ^{19}F NMR chemical shifts were referenced to TMS in the proton spectrum using the unified scale. ^1H NMR splitting patterns were designated as singlet (s), doublet (d), triplet (t), quartet (q), doublet of doublets (dd), apparent (ap), broad (br). First-order splitting patterns were assigned on the basis of the multiplet. For the alcohols reported here, ABX splitting patterns are all of the type where $\nu_{\text{AB}} \gg J_{\text{AB}}$, and ambiguous assignment of subquartets makes an exact solution difficult. Instead, an approximate AMX type solution deviates little from the values found by treating the AB part as first order. This has been demonstrated in the chemical shift values reported for (*S*)-*N*-(4-cyclohexyl-1-hydroxybutan-2-yl)benzamide, which vary by less than 0.01ppm from the calculated value. Calculated δ 3.778 ($J_{\text{AX}} = 3.43$ Hz, $J_{\text{AB}} = 11.0$ Hz, 1H, *A* of ABX), 3.678 ($J_{\text{BX}} = 5.48$ Hz, $J_{\text{AB}} = 11.0$ Hz, 1H, *B* of ABX), vs. first-order analysis δ 3.78 (app. dd, $J = 11.1, 3.5$ Hz, 1H, *A* of ABX), 3.67 (app. dd, $J = 11.0, 5.4$ Hz, 1H, *B* of ABX). Multiplets that are of this ABX type are reported as apparent but labeled as ABX, and the values measured are found by treating the multiplet as first order. Splitting patterns that could not be interpreted are designated as multiplet (m) or broad (br). Mass spectra were collected on a Waters (Micromass) LCT® for electrospray ionization experiments with a sample cone voltage of 20.

II. Synthesis and characterization of (*Z*)- enol ester and enamide substrates

All enol ester substrates were prepared according to procedures slightly modified from the reported procedures, as reported below.

General procedure for the synthesis of enol esters (Method 1)

Based on Gooßen, L. J.; Paetzold, J.; Koley, D. *Chem. Commun.* **2003**, 706-707.

An oven-dried Schlenk flask equipped with a magnetic stir bar and carboxylic acid (1 eq, 5 mmol) was brought into a N₂ glove box. A vial was charged with [Ru(p-cumene)Cl₂]₂ (1 mol%, 0.05 mmol), P(p-Cl-C₆H₄)₃ (3 mol%, 0.15 mmol), DMAP (4 mol%, 0.20 mmol), dry toluene (15 mL) and transferred to the Schlenk flask via a Pasteur pipette, followed by 1-hexyne (1.3 eq, 6.5 mmol) via a syringe. In a fume hood, the flask was immersed in a silicone oil bath and stirred for 16 h at 60°C under N₂. When the reaction is complete, the solution was allowed to cool down at room temperature for 30 min, then passed through a plug of silica gel and washed with dichloromethane. The solvent was removed in vacuo and the product was purified via silica gel flash chromatography with hexane/ethyl acetate as eluents. The enol ester was filtered through a plug of silica prior to hydroformylation.

General procedure for the synthesis of enol esters (Method 2)

Based on Doucet, H.; Martin-Vaca, B.; Bruneau, C.; Dixneuf, P. H. *J. Org. Chem.* **1995**, 60, 7247-7255.

An oven-dried Schlenk flask equipped with a magnetic stir bar and carboxylic acid (1 eq, 10 mmol) was brought into a N₂ glove box. A vial was charged with Ru(2-methallyl)₂-bis(diphenylphosphino)butane (1 mol%, 0.1 mmol) and solvent (5 mL) and transferred to the Schlenk flask via a Pasteur pipette. Degassed 4-Phenyl-1-butyne (1 eq, 10 mmol) was added via a syringe in a fume hood. The flask was immersed in a silicone oil bath and stirred for 24h under N₂. When the reaction is complete, the solution was allowed to cool down at room temperature

for 30 min, then passed through a plug of silica gel and washed with dichloromethane. The solvent was removed in vacuo and the product was purified via silica gel flash chromatography with hexane/ethyl acetate as eluents. The enol ester was filtered through a plug of silica prior to hydroformylation.

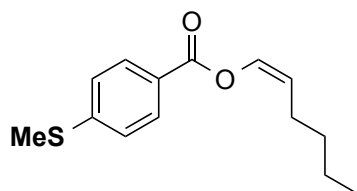
General procedure for the synthesis of enamides

All enamide substrates were prepared according to a procedure slightly modified from the reported procedure, as reported below. Their spectroscopic properties match those previously reported, or are reported below.

-Butyl, $-(\text{CH}_2)_2\text{Ph}$, $-(\text{CH}_2)_3\text{Cl}$, $-\text{CH}_2\text{Cy}$, and Ph substituted benzamides were reported in: Gooßen, L. J.; Salih, K. S. M.; Blanchot, M. *Angew. Chem. Int. Ed.* **2008**, 47, 8492. (Z)-N-(5-cyanopent-1-en-1-yl)benzamide was reported in: Honjo, T.; Phipps, R.J.; Rauniyar, V.; Toste, F.D.; *Angew. Chem. Int. Ed.* **2012**, 51, 9684-9688.

In an oven-dried Schlenk flask inside a nitrogen-filled glovebox, *bis*(2-methallyl)(COD)ruthenium(II) (5%, 0.25 mmol), 1,4-*bis*(dicyclohexylphosphino)butane (6%, 0.30 mmol), ytterbium triflate (4%, 0.20 mmol), and amide (5.0 mmol) were combined, and anhydrous DMF (15 mL) was added. On a Schlenk line, degassed alkyne (10.0 mmol) was added via syringe, followed by N_2 -sparged H_2O (0.540 mL, 30 mmol). The resulting solution was stirred for 6-18h in a 60 °C oil bath, then poured into a saturated aqueous sodium bicarbonate solution (150 mL). This mixture was extracted with ethyl acetate (3x60 mL), the combined organics were washed with water (5x50 mL) and brine (1x50 mL), dried over magnesium sulfate, filtered, and the volatiles were removed by rotary evaporation. The dark

brown oil was purified by column chromatography on silica gel with 9:1 Hexane/EtOAc. Two or more columns were frequently necessary for clean product isolation.



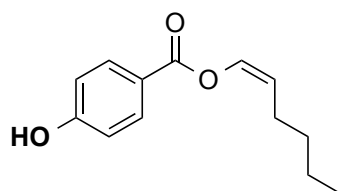
(Z)-hex-1-en-1-yl 4-(methylthio)benzoate

Prepared according to method 1. Product purified by silica gel flash chromatography (10:1 hexane/ethyl acetate) to afford a yellow oil in 72% isolated yield.

¹H NMR (400 MHz, Chloroform-*d*) δ 7.99 (d, J = 8.5 Hz, 2H), 7.33 – 7.20 (m, 3H), 5.05 – 4.93 (m, 1H), 2.53 (s, 3H), 2.35 – 2.23 (m, 2H), 1.48 – 1.33 (m, 4H), 0.93 (t, J = 7.0 Hz, 3H).

¹³C NMR (101 MHz, CDCl₃) δ 163.39, 146.26, 134.17, 130.15, 125.46, 124.98, 114.72, 31.38, 24.36, 22.26, 14.80, 13.93.

HRMS (ESI-TOF) m/z : [M]⁺ calcd for C₁₄H₁₈O₂S 250.1023; found 250.1019.



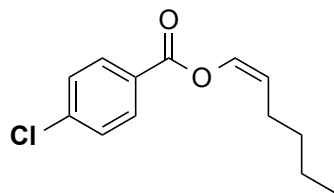
(Z)-hex-1-en-1-yl 4-hydroxybenzoate

Prepared according to method 1. Reaction refluxed in THF. Product purified by silica gel flash chromatography (5:1 hexane/ethyl acetate) to afford a dark yellow oil in 40% isolated yield.

¹H NMR (500 MHz, Chloroform-*d*) δ 8.08 – 7.96 (m, 2H), 7.24 – 7.21 (m, 1H), 6.97 – 6.83 (m, 2H), 4.98 (tdd, J = 7.5, 6.4, 1.3 Hz, 1H), 2.31 – 2.24 (m, 2H), 1.46 – 1.34 (m, 4H), 0.93 (t, J = 7.1 Hz, 3H).

¹³C NMR (126 MHz, CDCl₃) δ 164.10, 160.95, 134.09, 132.33, 121.30, 115.56, 114.98, 31.34, 24.34, 22.24, 13.90.

HRMS (ESI-TOF) m/z : [M]⁺ calcd for C₁₃H₁₆O₃ 220.1094; found 220.1095.



(Z)-hex-1-en-1-yl 4-chlorobenzoate

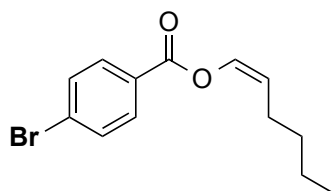
Prepared according to method 1. Product purified by silica gel flash chromatography (10:1 hexane/ethyl acetate) to afford a yellow oil in 26% isolated yield.

Characterization data agrees with previously reported results (Das, U.K.; Bhattacharjee, M. *J. Organomet. Chem.* **2012**, *700*, 78-82).

¹H NMR (400 MHz, Chloroform-*d*) δ 8.19 – 7.92 (m, 2H), 7.57 – 7.38 (m, 2H), 7.31 – 7.17 (m, 1H), 5.13 – 4.94 (m, 1H), 2.36 – 2.21 (m, 2H), 1.51 – 1.27 (m, 4H), 0.93 (d, *J* = 7.0 Hz, 3H).

¹³C NMR (126 MHz, CDCl₃) δ 162.79, 139.93, 134.03, 131.22, 128.92, 127.90, 115.22, 31.30, 24.35, 22.23, 13.90.

HRMS (ESI-TOF) *m/z*: [M]⁺ calcd for C₁₃H₁₅ClO₂ 238.0756; found 238.0759.



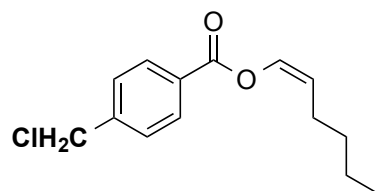
(Z)-hex-1-en-1-yl 4-bromobenzoate

Prepared according to method 1. Product purified by silica gel flash chromatography (10:1 hexane/ethyl acetate) to afford a yellow oil in 22% isolated yield.

¹H NMR (400 MHz, Chloroform-*d*) δ 8.01 – 7.90 (m, 2H), 7.69 – 7.57 (m, 2H), 7.23 (dt, *J* = 6.4, 1.6 Hz, 1H), 5.03 (td, *J* = 7.5, 6.3 Hz, 1H), 2.33 – 2.21 (m, 2H), 1.49 – 1.30 (m, 4H), 0.93 (t, *J* = 7.0 Hz, 3H).

¹³C NMR (126 MHz, CDCl₃) δ 162.92, 134.02, 131.91, 131.33, 128.62, 128.36, 115.24, 31.29, 24.35, 22.23, 13.89.

HRMS (ESI-TOF) *m/z*: [M]⁺ calcd for C₁₃H₁₅BrO₂ 282.0250; found 282.0252.



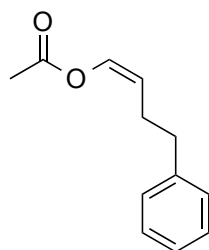
(Z)-hex-1-en-1-yl 4-(chloromethyl)benzoate

Prepared according to method 1. Product purified by silica gel flash chromatography (10:1 hexane/ethyl acetate) to afford a light yellow oil in 15% isolated yield.

¹H NMR (500 MHz, Chloroform-*d*) δ 8.13 – 8.07 (m, 2H), 7.54 – 7.47 (m, 2H), 7.25 (dt, *J* = 6.3, 1.6 Hz, 1H), 5.02 (td, *J* = 7.5, 6.3 Hz, 1H), 4.63 (s, 2H), 2.35 – 2.25 (m, 2H), 1.48 – 1.33 (m, 4H), 0.93 (t, *J* = 7.1 Hz, 3H).

¹³C NMR (126 MHz, CDCl₃) δ 162.05, 141.72, 133.07, 129.26, 128.39, 127.59, 114.07, 44.27, 30.28, 23.31, 21.20, 12.86.

HRMS (ESI-TOF) *m/z*: [M]⁺ calcd for C₁₄H₁₇ClO₂ 252.0912; found 252.0903.



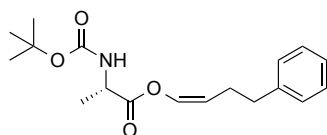
(Z)-4-phenylbut-1-en-1-yl acetate

Prepared according to method 2, using 2 mol% catalyst loading. Reaction run in hexane at 40°C for 24 h. Product purified by silica gel flash chromatography (10:1 hexane/ethyl acetate) to afford a clear oil in 75% isolated yield.

¹H NMR (500 MHz, Chloroform-*d*) δ 7.31 – 7.27 (m, 2H), 7.20 (d, *J* = 7.3 Hz, 2H), 7.01 (dt, *J* = 6.4, 1.4 Hz, 1H), 4.90 (td, *J* = 7.4, 6.2 Hz, 1H), 2.70 (t, *J* = 7.7 Hz, 2H), 2.54 – 2.40 (m, 2H), 2.11 (s, 3H).

¹³C NMR (126 MHz, CDCl₃) δ 168.04, 141.55, 134.39, 128.43, 128.31, 125.95, 112.97, 35.35, 26.21, 20.72.

HRMS (ESI-TOF) *m/z*: [M]⁺ calcd for C₁₂H₁₄O₂ 190.0989; found 190.0990.



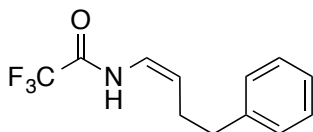
(S,Z)-4-phenylbut-1-en-1-yl 2-((tert-butoxycarbonyl)amino)propanoate

Prepared according to method 2. Reaction ran in toluene for 24 h at 75°C. Product purified by silica gel flash chromatography (10:1 hexane/ethyl acetate) to afford a light orange oil in 55% isolated yield.

¹H NMR (500 MHz, Chloroform-*d*) δ 7.31 – 7.24 (m, 2H), 7.23 – 7.14 (m, 3H), 7.00 (d, *J* = 6.3 Hz, 1H), 5.03 (d, *J* = 8.0 Hz, 1H), 4.96 (td, *J* = 7.4, 6.2 Hz, 1H), 4.37 (h, *J* = 6.3, 5.2 Hz, 1H), 2.69 (t, *J* = 7.6 Hz, 2H), 2.54 – 2.42 (m, 2H), 1.44 (s, 9H), 1.39 (d, *J* = 7.2 Hz, 3H).

¹³C NMR (126 MHz, CDCl₃) δ 170.47, 155.04, 141.37, 134.29, 128.44, 125.98, 113.96, 80.01, 53.43, 49.04, 35.23, 28.30, 26.22, 18.47.

HRMS (ESI-TOF) *m/z*: [M+NH₄]⁺ calcd for C₁₈H₂₅NO₄ 337.2122; found 337.2119.



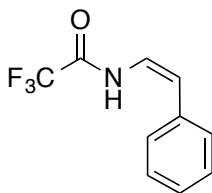
20% yield. Yellow oil.

¹H NMR (400 MHz, Chloroform-*d*) δ 7.37 – 7.12 (m, 6H), 6.57 (t, *J* = 9.7 Hz, 1H), 5.12 (ap. q, *J* = 8.2 Hz, 1H), 2.74 (t, *J* = 7.1 Hz, 2H), 2.36 (ap. q, *J* = 7.3 Hz, 2H).

¹⁹F NMR (377 MHz, CDCl₃) δ -75.64 (Z isomer), -75.87 (E isomer).

¹³C NMR (101 MHz, CDCl₃) δ 154.22 (q, *J* = 37.8 Hz), 140.79, 128.80, 128.43, 126.51, 119.67, 115.63, 115.49 (q, *J* = 287 Hz), 34.96, 28.23.

HRMS (EI) *m/z*: [M•⁺] Calcd for C₁₂H₁₂F₃NO 243.0866; found 243.0857.



69% yield (after two flash column chromatography purifications). Yellow oil.

¹H NMR (400 MHz, Chloroform-*d*) δ 8.31 (br s, 1H), 7.49 – 7.39 (m, 2H), 7.39 – 7.29 (m, 1H), 7.30 – 7.25 (m, 2H), 6.90 (dd, *J* = 10.9, 9.4 Hz, 1H), 6.10 (d, *J* = 9.4 Hz, 1H).

¹⁹F NMR (377 MHz, CDCl₃) δ -75.81.

¹³C NMR (101 MHz, CDCl₃) δ 154.57 (q, *J* = 38 Hz), 134.13, 129.57, 128.16, 127.93, 119.46, 115.78, 115.69 (q, *J* = 287 Hz), 77.16.

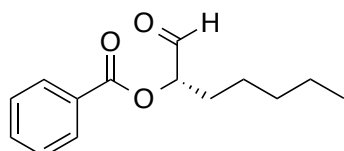
HRMS (EI) *m/z*: [M•+]⁺ Calcd for C₁₀H₈F₃NO 215.0553; found 215.0551.

III. General method for hydroformylation.

Inside a N₂-purged glovebox, an oven-dried 15mL Ace Glass pressure bottle equipped with a magnetic stir bar was charged with THF stock solutions of Rh(acac)(CO)₂ and bisdiazaphospholane ligand **1** using 1000μL and 200μL Eppendorf® pipets. The pressure bottle was attached to a pressure reactor and removed from the glovebox, placed in a fume hood, subjected to 5 pressurization (140 psi)/depressurization (15 psi) cycles with syngas to ensure replacement of the dinitrogen atmosphere with syngas, then filled to the appropriate syngas pressure. The solution was allowed to stir at high speed to ensure gas mixing for 30-60 min in an oil bath at the reaction temperature. The reaction vessel was then removed from the oil bath and allowed to cool for 5 minutes, then the pressure was reduced to <10 psig and the olefin was injected with a gas-tight syringe with a 12" needle. Solid olefins were injected as a solution in THF. Reactions were run at 0.8-1.3 M final concentration of olefin. The reaction was then repressurized to the reaction pressure after additional pressurization/depressurization cycles and replaced in the oil bath. Upon completion of the reaction, the pressure bottle was removed from the oil bath, allowed to cool to room temperature, and vented in a fume hood. NMR spectra are initially obtained of the crude reaction mixture by adding acetone-d₆, MeOD, or CDCl₃ directly to the reaction mixture. NMR yields were determined by addition of a solution of internal standard (1,3,5-trimethoxybenzene or mesitylene) in NMR solvent and acquiring spectra with a

sufficiently long delay. Enantiomeric excess of the branched hydroformylation product was determined by chiral SFC or HPLC.

IV. Data for enol ester AHF



(-)(2S)-(Benzoyloxy)heptanal:

Yield 1.09g (92.0%), 97% *ee*, colorless oil.

$[\alpha]_D^{20} = -14.7$, $c = 1.24$ in CHCl_3 (Lit. $[\alpha]_D^{20} = -31.1$ ($c = 1.41$, CH_2Cl_2). (Chattopadhyay, A.; Mamdapur, V.R. *J. Org. Chem.* **1995**, *60*, 585-587.)

^1H NMR (400 MHz, Chloroform-*d*) δ 9.57 (d, $J = 1.0$ Hz, 1H), 8.12 – 7.88 (m, 2H), 7.53 (tt, $J = 7.5, 1.2$ Hz, 1H), 7.44 – 7.37 (m, 2H), 5.15 (ddd, $J = 8.1, 4.9, 1.0$ Hz, 1H), 1.96 – 1.73 (m, 2H), 1.49 – 1.39 (m, 2H), 1.32 – 1.21 (m, 4H), 0.90 – 0.74 (m, 3H).

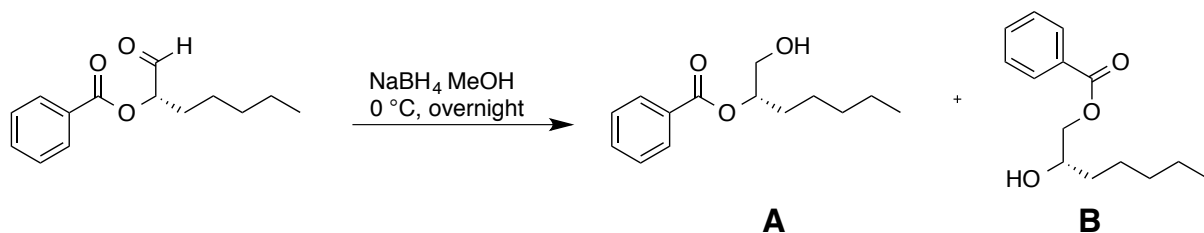
^{13}C NMR (101 MHz, CDCl_3) δ 198.59, 166.19, 133.55, 129.87, 129.24, 128.55, 78.83, 31.45, 28.90, 24.70, 22.40, 13.96.

Enantiomeric excess was determined to be 97% by chiral SFC analysis, after NaBH_4 reduction in MeOH at 0°C .

The reduction conditions afford a mixture of two alcohol isomers, **A** and **B**, after partial migration of the benzoyl protecting group from the secondary alcohol to the primary alcohol (identified by HMBC and COSY experiments).

The four peaks observed by SFC are due to the two enantiomers of each isomer. $t_r = 4.40$ min (isomer **A**, (*S*)), $t_r = 5.53$ min (isomer **B**, (*R*)), $t_r = 6.0$ min (isomer **B**, (*S*)), $t_r = 6.23$ min (isomer **A**, (*R*)).

Separation by SFC: Chiralcel AD-H, MeOH modifier ramp 5-50% over 10 min, 3 mL/min flow, $\lambda = 233$ nm.

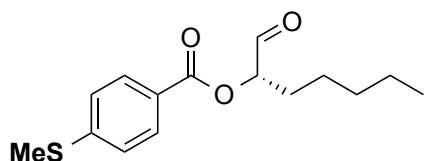


Alcohol isomers:**A: (S)-1-hydroxyheptan-2-yl benzoate**

¹H NMR (400 MHz, Chloroform-*d*) δ 8.09 – 8.04 (m, 2H), 7.61 – 7.54 (m, 1H), 7.47 – 7.41 (m, 2H), 5.20 – 5.12 (m, 1H), 3.83 (dd, J = 12.1, 3.4 Hz, 1H), 3.76 (dd, J = 12.1, 6.2 Hz, 1H), 1.81 – 1.66 (m, 2H), 1.66 – 1.27 (m, 6H), 0.93 – 0.83 (m, 3H).

B: (S)-2-hydroxyheptyl benzoate (*rearranged*)

¹H NMR (400 MHz, Chloroform-*d*) δ 8.08 – 8.01 (m, 2H), 7.56 (tt, J = 7.5, 1.2 Hz, 1H), 7.47 – 7.39 (m, 2H), 4.38 (dd, J = 11.4, 3.2 Hz, 1H), 4.22 (dd, J = 11.4, 7.1 Hz, 1H), 4.02 – 3.94 (m, 1H), 1.61 – 1.52 (m, 2H), 1.52 – 1.27 (m, 6H), 0.89 (t, J = 6.9 Hz, 3H).

**(S)-1-oxoheptan-2-yl 4-(methylthio)benzoate**

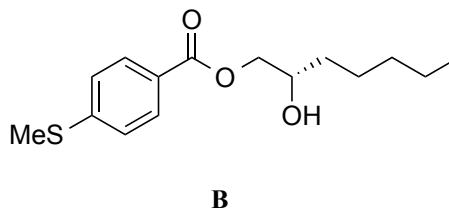
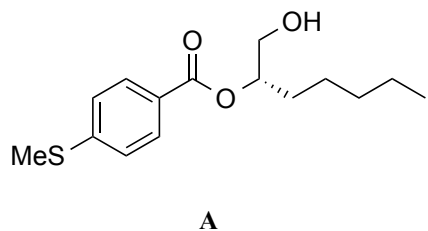
Crude hydroformylation mixture filtered through a plug of silica and washed with dichloromethane. 84% isolated yield, yellow oil.

¹H NMR (400 MHz, Chloroform-*d*) δ 9.63 (d, J = 0.9 Hz, 1H), 7.99 (d, J = 8.5 Hz, 2H), 7.28 (d, J = 8.5 Hz, 2H), 5.19 (ddd, J = 8.2, 5.0, 1.0 Hz, 1H), 2.53 (s, 3H), 2.05 – 1.79 (m, 2H), 1.63 – 1.45 (m, 2H), 1.44 – 1.23 (m, 4H), 0.92 – 0.87 (m, 3H).

¹³C NMR (101 MHz, CDCl₃) δ 198.70, 165.94, 146.44, 130.13, 125.20, 124.98, 78.72, 31.45, 28.90, 24.70, 22.40, 14.82, 13.96.

Enantiomeric excess was determined to be 90% by chiral HPLC analysis, after NaBH₄ reduction in MeOH at room temperature for 16 h, followed by addition of sat. aq. NH₄Cl solution, extraction with dichloromethane and drying over MgSO₄. The reduction conditions afford a mixture of two alcohol isomers, **A** and **B**, after partial migration of the benzoyl protecting group from the secondary alcohol to the primary alcohol, as well as a transesterification by-

product in the presence of MeOH. The mixture of alcohols was purified by silica gel flash chromatography (2:1 hexanes/ethyl acetate) prior to HPLC analysis.



Alcohol isomers:

A: (S)-1-hydroxyheptan-2-yl 4-(methylthio)benzoate

¹H NMR (500 MHz, Chloroform-*d*) δ 7.92 – 7.82 (m, 2H), 7.22 – 7.14 (m, 2H), 5.10 – 5.03 (m, 1H), 3.74 (dd, J = 12.1, 3.3 Hz, 1H), 3.67 (dd, J = 12.1, 6.2 Hz, 1H), 2.44 (s, 3H), 2.21 (s, 1H), 1.73 – 1.55 (m, 2H), 1.54 – 1.12 (m, 6H), 0.90 – 0.74 (m, 3H).

¹³C NMR (126 MHz, CDCl₃) δ 165.83, 144.68, 128.82, 125.19, 123.86, 75.33, 63.96, 30.59, 29.62, 23.99, 21.43, 13.76, 12.93.

B: (S)-2-hydroxyheptyl 4-(methylthio)benzoate (rearranged)

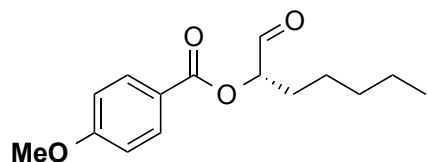
¹H NMR (500 MHz, Chloroform-*d*) δ 7.92 – 7.82 (m, 2H), 7.22 – 7.14 (m, 2H), 4.29 (A of ABX, ap dd, J = 11.4, 3.2 Hz, 1H), 4.18 – 4.10 (m, 1H), 3.93 – 3.86 (m, 1H), 2.44 (s, 3H), 2.21 (br, 1H), 1.54 – 1.12 (m, 8H), 0.90 – 0.74 (m, 3H).

¹³C NMR (126 MHz, CDCl₃) δ 165.47, 144.79, 128.90, 124.90, 123.86, 69.11, 68.12, 32.41, 30.72, 24.06, 21.53, 13.75, 12.98.

HRMS (ESI-TOF) m/z : [M]⁺ calcd for C₁₅H₂₂O₃S 282.1285; found 282.1290.

Separation by HPLC: CHIRALPAK 1A (AD-H), 3% iPrOH/hexanes, 0.9 ml/min, ambient temperature, 220 nm, t_R

(**A**): 31.5 min (major, (*S*)), 36.7 min (minor, (*R*)), t_R (**B**): 44.7 min (major, (*S*)), 51.6 min (minor, (*R*))



(S)-1-oxoheptan-2-yl 4-methoxybenzoate

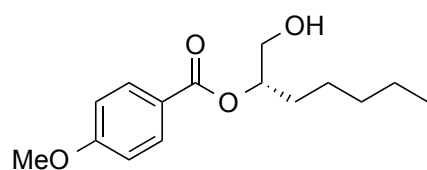
Crude hydroformylation mixture filtered through a plug of silica and washed with dichloromethane. 85% isolated yield, yellow oil.

¹H NMR (500 MHz, Chloroform-*d*) δ 9.63 (d, J = 1.0 Hz, 1H), 8.06 (d, J = 8.9 Hz, 2H), 7.05 – 6.84 (d, J = 8.9 Hz, 2H), 5.17 (ddd, J = 8.2, 4.9, 1.0 Hz, 1H), 3.88 (s, 3H), 2.02 – 1.79 (m, 2H), 1.55 – 1.45 (m, 2H), 1.40 – 1.15 (m, 4H), 1.05 – 0.74 (m, 3H).

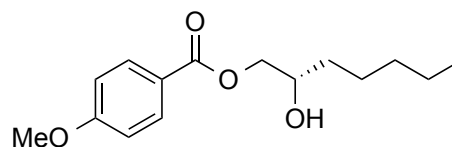
¹³C NMR (126 MHz, CDCl₃) δ 198.97, 165.91, 163.83, 131.94, 121.54, 113.80, 78.54, 55.50, 31.44, 28.93, 24.68, 22.38, 13.94.

HRMS (ESI-TOF) m/z : [M+H]⁺ calcd for C₁₅H₂₀O₄ 265.1435; found 265.1438.

Enantiomeric excess was determined to be 96% by chiral HPLC analysis, after NaBH₄ reduction in MeOH at room temperature for 6 h, followed by addition of sat. aq. NH₄Cl solution, extraction with dichloromethane and drying over MgSO₄. The reduction conditions afford a mixture of two alcohol isomers, **A** and **B**, after partial migration of the benzoyl protecting group from the secondary alcohol to the primary alcohol.



A



B

Alcohol isomers:

A: (S)-1-hydroxyheptan-2-yl 4-methoxybenzoate

¹H NMR (500 MHz, Chloroform-*d*) δ 7.96 – 7.89 (m, 2H), 6.87 – 6.81 (m, 2H), 5.10 – 4.99 (m, 1H), 3.77 (s, 1H), 3.75 – 3.64 (m, 2H), 2.39 (br, 1H), 1.72 – 1.55 (m, 2H), 1.52 – 1.16 (m, 6H), 0.87 – 0.75 (m, 3H).

¹³C NMR (126 MHz, CDCl₃) δ 166.77, 163.47, 131.71, 122.57, 113.62, 76.15, 65.03, 55.43, 31.65, 30.72, 25.05, 22.48, 13.98.

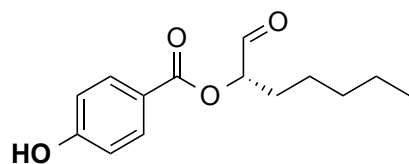
***B* (S)-2-hydroxyheptyl 4-methoxybenzoate (rearranged)**

¹H NMR (500 MHz, Chloroform-*d*) δ 7.96 – 7.89 (m, 2H), 6.87 – 6.81 (m, 2H), 4.27 (A of ABX, ap dd, J = 11.5, 3.2 Hz, 1H), 4.11 (B of ABX, ap dd, J = 11.4, 7.1 Hz, 1H), 3.94 – 3.84 (X of ABX, m, 1H), 3.77 (s, 1H), 2.39 (br, 1H), 1.52 – 1.16 (m, 8H), 0.87 – 0.75 (m, 3H).

¹³C NMR (126 MHz, CDCl₃) δ 166.54, 163.50, 131.71, 122.29, 113.65, 70.17, 69.01, 55.43, 33.46, 31.78, 25.12, 22.58, 14.02.

HRMS (ESI-TOF) m/z : [M+H]⁺ calcd for C₁₅H₂₂O₄ 267.1591; found 267.1599.

Separation by HPLC: CHIRALPAK 1A (AD-H), 5% iPrOH/hexanes, 0.8 ml/min, ambient temperature, 254 nm, t_R (**A**): 20.3 min (major, (*S*)), 23.6 min (minor, (*R*)), t_R (**B**): 26.0min (major, (*S*)), 28.7 min (minor, (*R*)).

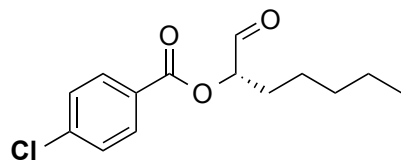
**(Z)-hex-1-en-1-yl 4-hydroxybenzoate**

Crude hydroformylation mixture filtered through a plug of silica and washed with dichloromethane. 82% isolated yield, dark yellow oil stored under dinitrogen.

¹H NMR (500 MHz, Chloroform-*d*) δ 9.64 (s, 1H), 8.00 (d, J = 7.9 Hz, 2H), 7.00 – 6.81 (m, 2H), 6.31 (broad s, 1H), 5.19 (dd, J = 8.3, 4.8 Hz, 1H), 2.04 – 1.79 (m, 2H), 1.57 – 1.45 (m, 2H), 1.40 – 1.29 (m, 4H), 0.96 – 0.87 (m, 3H).

¹³C NMR (126 MHz, CDCl₃) δ 198.12, 165.16, 159.65, 131.24, 120.29, 114.43, 77.64, 30.40, 27.83, 23.66, 21.34, 12.90.

HRMS (ESI-TOF) m/z : [M+H]⁺ calcd for C₁₄H₁₈O₄ 251.1278; found 251.1280.



(S)-1-oxoheptan-2-yl 4-chlorobenzoate

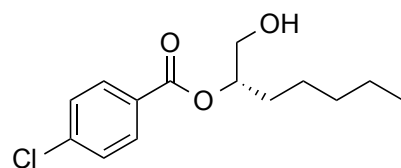
Crude hydroformylation mixture filtered through a plug of silica and washed with dichloromethane. 88% isolated yield, yellow oil.

¹H NMR (500 MHz, Chloroform-*d*) δ 9.63 (d, J = 0.8 Hz, 1H), 8.15 – 7.97 (m, 2H), 7.53 – 7.39 (m, 2H), 5.23 (dd, J = 8.3, 4.7 Hz, 1H), 2.04 – 1.81 (m, 2H), 1.63 – 1.43 (m, 2H), 1.34 (dtp, J = 7.4, 5.0, 2.6 Hz, 4H), 1.00 – 0.85 (m, 3H).

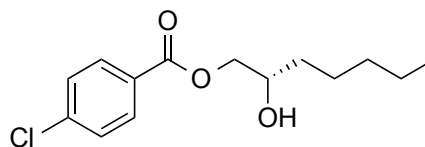
¹³C NMR (101 MHz, CDCl₃) δ 198.07, 165.29, 140.06, 131.24, 128.92, 127.69, 79.00, 31.43, 28.78, 24.70, 22.38, 13.95.

HRMS (ESI-TOF) m/z : [M]⁺ calcd for C₁₄H₁₇ClO₃ 268.0861; found 268.0851.

Enantiomeric excess was determined to be 96% by chiral HPLC analysis, after NaBH₄ reduction in MeOH at room temperature for 6 h, followed by addition of sat. aq. NH₄Cl solution, extraction with dichloromethane and drying over MgSO₄. The reduction conditions afford a mixture of two alcohol isomers, **A** and **B**, after partial migration of the benzoyl protecting group from the secondary alcohol to the primary alcohol. Another by-product was detected in the region 3.4-3.73 ppm in ¹HNMR, tentatively assigned as a diol formed upon reduction of the ester group. The mixture was purified by silica gel flash chromatography (3:1 hexanes/ethyl acetate) prior to HPLC analysis.



A



B

Alcohol isomers:

A: (S)-1-hydroxyheptan-2-yl 4-chlorobenzoate

¹H NMR (500 MHz, Chloroform-*d*) δ 7.99 (d, J = 8.2 Hz, 2H), 7.45 – 7.39 (m, 2H), 5.22 – 5.11 (m, 1H), 3.87 – 3.73 (m, 2H), 1.81 – 1.64 (m, 2H), 1.60 – 1.17 (m, 6H), 0.94 – 0.83 (m, 3H).

^{13}C NMR (126 MHz, CDCl_3) δ 165.07, 138.53, 130.03, 127.71, 127.61, 75.66, 63.80, 30.58, 29.57, 23.99, 21.43, 12.93.

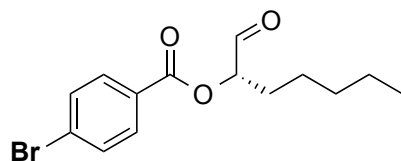
B: (S)-2-hydroxyheptyl 4-chlorobenzoate (*rearranged*)

^1H NMR (500 MHz, Chloroform-*d*) δ 7.99 (d, $J = 8.2$ Hz, 2H), 7.45 – 7.39 (m, 2H), 4.43 – 4.33 (m, 1H), 4.23 (ap dd, $J = 11.5, 7.1$ Hz, 1H), 4.03 – 3.93 (m, 1H), 1.60 – 1.17 (m, 8H), 0.94 – 0.83 (m, 3H).

^{13}C NMR (126 MHz, CDCl_3) δ 164.90, 138.62, 130.02, 127.76, 127.32, 69.05, 68.36, 32.43, 30.72, 24.06, 21.54, 12.99.

HRMS (ESI-TOF) m/z : $[\text{M}]^+$ calcd for $\text{C}_{14}\text{H}_{19}\text{ClO}_3$ 270.1018; found 270.1026.

Separation by HPLC: CHIRALPAK 1A (AD-H), 2% iPrOH/hexanes, 0.6 ml/min, ambient temperature, 254 nm, t_R (A): 48.4 min (major, (*S*)), 55.3 min (minor, (*R*)).



(S)-1-oxoheptan-2-yl 4-bromobenzoate

Crude hydroformylation mixture filtered through a plug of silica and washed with dichloromethane. 82% isolated yield, yellow oil.

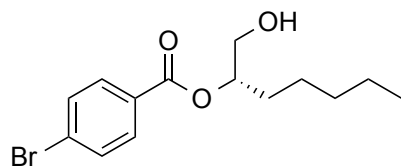
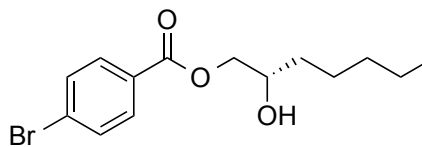
^1H NMR (500 MHz, Chloroform-*d*) δ 9.63 (s, 1H), 7.96 (d, $J = 8.5$ Hz, 2H), 7.62 (d, $J = 8.5$ Hz, 2H), 5.23 (ddd, $J = 8.0, 5.0, 0.8$ Hz, 1H), 2.02 – 1.75 (m, 2H), 1.56 – 1.44 (m, 2H), 1.40 – 1.28 (m, 4H), 0.98 – 0.81 (m, 3H).

^{13}C NMR (126 MHz, CDCl_3) δ 196.98, 164.38, 130.87, 130.29, 127.70, 127.09, 77.97, 30.37, 27.72, 23.65, 21.33, 12.89.

HRMS (ESI-TOF) m/z : $[\text{M}]^+$ calcd for $\text{C}_{14}\text{H}_{17}\text{BrO}_3$ 312.0356; found 312.0364.

Enantiomeric excess was determined to be 92% by chiral SFC analysis, after NaBH_4 reduction in MeOH at room temperature for 6 h, followed by addition of sat. aq. NH_4Cl solution, extraction with dichloromethane and drying

over MgSO_4 . The reduction conditions afford a mixture of two alcohol isomers, **A** and **B**, after partial migration of the benzoyl protecting group from the secondary alcohol to the primary alcohol. Another by-product was detected, tentatively assigned as transesterification product in the presence of MeOH.

**A****B**

Alcohol isomers:

A: (S)-1-hydroxyheptan-2-yl 4-bromobenzoate

^1H NMR (500 MHz, Chloroform-*d*) δ 7.97 – 7.85 (m, 2H), 7.62 – 7.55 (m, 2H), 5.23 – 5.11 (X of ABX, m, 1H), 3.83 (A of ABX, ap dd, $J = 12.1, 3.2$ Hz, 1H), 3.76 (B of ABX, ap dd, $J = 12.1, 6.2$ Hz, 1H), 1.85 – 1.63 (m, 2H), 1.62 – 1.16 (m, 6H), 0.97 – 0.80 (m, 3H).

^{13}C NMR (126 MHz, CDCl_3) δ 165.17, 130.71, 130.16, 128.64, 128.07, 75.69, 63.84, 30.58, 29.55, 23.99, 21.43, 12.94.

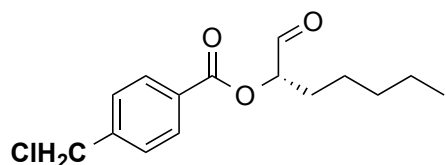
B: (S)-2-hydroxyheptyl 4-bromobenzoate (*rearranged*)

^1H NMR (500 MHz, Chloroform-*d*) δ 7.97 – 7.85 (m, 2H), 7.62 – 7.55 (m, 2H), 4.38 (A of ABX, ap dd, $J = 11.4, 3.2$ Hz, 1H), 4.28 – 4.18 (B of ABX, m, 1H), 4.02 – 3.94 (m, 1H), 1.62 – 1.16 (m, 8H), 0.97 – 0.80 (m, 3H).

^{13}C NMR (126 MHz, CDCl_3) δ 165.00, 130.76, 130.15, 128.63, 127.79, 69.06, 68.40, 32.43, 30.71, 24.05, 21.54, 12.99.

HRMS (ESI-TOF) m/z : $[\text{M}+\text{H}]^+$ calcd for $\text{C}_{14}\text{H}_{19}\text{BrO}_3$ 315.0591; found 315.0589.

Separation by SFC: Chiralcel OJ-H, 4% modifier, 4 ml/min, methanol, 50°C, 150 bar, t_R (**A**): 5.0 min (major, (*S*)), 6.5 min (minor, (*R*)), t_R (**B**): 7.3 min (minor, (*R*)), 9.8 min (major, (*S*)).



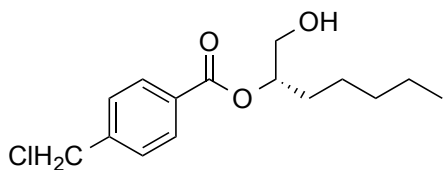
(S)-1-oxoheptan-2-yl 4-(chloromethyl)benzoate

Crude hydroformylation mixture filtered through a plug of silica and washed with dichloromethane. 78% isolated yield, yellow oil.

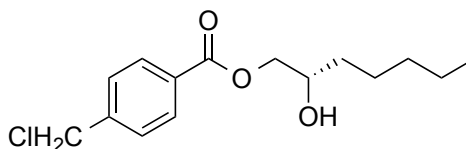
¹H NMR (400 MHz, Chloroform-*d*) δ 9.63 (d, J = 0.9 Hz, 1H), 8.13 – 8.06 (m, 2H), 7.53 – 7.47 (m, 2H), 5.23 (dd, J = 8.2, 4.9 Hz, 1H), 4.63 (s, 2H), 2.02 – 1.83 (m, 2H), 1.57 – 1.45 (m, 2H), 1.40 – 1.30 (m, 4H), 0.95 – 0.86 (m, 3H).

¹³C NMR (101 MHz, CDCl₃) δ 198.31, 161.54, 142.94, 130.31, 129.18, 128.66, 78.92, 45.30, 31.43, 28.83, 24.70, 22.39, 13.96.

Enantiomeric excess was determined to be 92% by chiral HPLC analysis, after NaBH₄ reduction in MeOH at room temperature for 6 h, followed by addition of sat. aq. NH₄Cl solution, extraction with dichloromethane and drying over MgSO₄. The reduction conditions afford a mixture of two alcohol isomers, **A** and **B**, after partial migration of the benzoyl protecting group from the secondary alcohol to the primary alcohol. The mixture was purified by silica gel flash chromatography (3:1 hexanes/ethyl acetate) prior to HPLC analysis.



A



B

Alcohol isomers:

A: (S)-1-hydroxyheptan-2-yl 4-(chloromethyl)benzoate

¹H NMR (500 MHz, Chloroform-*d*) δ 8.05 (d, J = 8.1 Hz, 2H), 7.47 (d, J = 8.1 Hz, 2H), 5.23 – 5.12 (m, 1H), 4.62 (s, 2H), 3.84 (ap dd, J = 12.1, 3.3 Hz, 1H), 3.77 (ap dd, J = 12.1, 6.3 Hz, 1H), 2.09 (s, 1H), 1.83 – 1.64 (m, 2H), 1.62 – 1.22 (m, 6H), 0.95 – 0.83 (m, 3H).

^{13}C NMR (126 MHz, CDCl_3) δ 166.40, 142.45, 130.16, 130.12, 128.52, 76.60, 64.98, 45.34, 31.62, 30.62, 25.02, 22.47, 13.97.

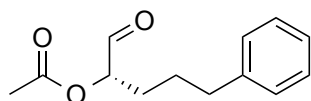
B: (S)-2-hydroxyheptyl 4-(chloromethyl)benzoate (rearranged)

^1H NMR (500 MHz, Chloroform-*d*) δ 8.09 – 8.02 (m, 2H), 7.47 (d, J = 8.1 Hz, 2H), 4.62 (s, 2H), 4.39 (A of ABX, ap dd, J = 11.4, 3.1 Hz, 1H), 4.23 (B of ABX, ap dd, J = 11.4, 7.1 Hz, 1H), 4.04 – 3.94 (m, 1H), 2.09 (br s, 1H), 1.62 – 1.22 (m, 8H), 0.95 – 0.83 (m, 3H).

^{13}C NMR (126 MHz, CDCl_3) δ 166.22, 142.51, 130.10, 129.86, 128.54, 70.14, 69.34, 45.32, 33.45, 31.76, 25.09, 22.57, 14.02.

HRMS (ESI-TOF) m/z : $[\text{M}+\text{H}]^+$ calcd for $\text{C}_{15}\text{H}_{21}\text{ClO}_3$ 285.1252; found 285.1249.

Separation by HPLC: CHIRALPAK 1A (AD-H), 5% iPrOH/hexanes, 0.8 ml/min, ambient temperature, 254 nm, t_R (**A**): 20.3 min (major, (*S*)), 23.6 min (minor, (*R*)), t_R (**B**): 26.0 min (major, (*S*)), 28.7 min (minor (*R*)).



(S)-1-oxo-5-phenylpentan-2-yl acetate

Crude hydroformylation mixture filtered through a plug of silica and washed with dichloromethane. 88% isolated yield, yellow oil.

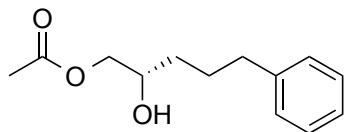
^1H NMR (400 MHz, Chloroform-*d*) δ 9.50 (d, J = 0.8 Hz, 1H), 7.32 – 7.25 (m, 2H), 7.24 – 7.14 (m, 3H), 5.01 (dd, J = 7.5, 4.3 Hz, 1H), 2.69 – 2.62 (m, 2H), 2.17 (s, 3H), 1.92 – 1.70 (m, 4H).

^{13}C NMR (126 MHz, CDCl_3) δ 198.18, 170.59, 141.31, 128.46, 128.37, 126.07, 78.13, 35.38, 28.17, 26.67, 20.62.

HRMS (ESI-TOF) m/z : $[\text{M}+\text{H}]^+$ calcd for $\text{C}_{13}\text{H}_{16}\text{O}_3$ 221.1173; found 221.1174.

Enantiomeric excess was determined to be 93% by chiral HPLC analysis, after NaBH_4 reduction in MeOH at room temperature for 5 h, followed by addition of sat. aq. NH_4Cl solution, extraction with dichloromethane and drying over MgSO_4 . The reduction conditions afford a mixture of two alcohol isomers, **A** and **B**, after partial migration of

the benzoyl protecting group from the secondary alcohol to the primary alcohol. The mixture was purified and the two isomers separated by silica gel flash chromatography (3:1 hexanes/ethyl acetate) prior to HPLC analysis.



Alcohol isomer:

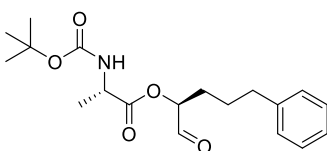
(S)-2-hydroxy-5-phenylpentyl acetate (*rearranged*):

¹H NMR (500 MHz, Chloroform-*d*) δ 7.30 – 7.24 (m, 2H), 7.20 – 7.15 (m, 3H), 4.11 (A of ABX, ap dd, J = 11.4, 3.0 Hz, 1H), 3.93 (B of ABX, ap dd, J = 11.4, 7.4 Hz, 1H), 3.88 – 3.81 (m, 1H), 2.64 (t, J = 7.6 Hz, 2H), 2.22 (d, J = 4.3 Hz, 1H), 2.07 (s, 3H), 1.88 – 1.75 (m, 1H), 1.74 – 1.62 (m, 1H), 1.54 – 1.47 (m, 2H).

¹³C NMR (126 MHz, CDCl₃) δ 171.26, 142.01, 128.42, 128.36, 125.86, 69.75, 68.71, 35.72, 32.83, 27.17, 20.91.

HRMS (ESI-TOF) m/z : [M+H]⁺ calcd for C₁₃H₁₈O₃ 223.1329; found 223.1329.

Separation by HPLC: CHIRALPAK 1D, 6% iPrOH/hexanes/0.1% TFA, 0.6 ml/min, ambient temperature, 220 nm, t_R : 31.3min (major, (*S*)), 38.8 min (minor, (*R*)).



(S)-(S)-1-oxo-5-phenylpentan-2-yl 2-((tert-butoxycarbonyl)amino)propanoate

Reaction mixture filtered through a pad of celite and washed with DCM. 83% isolated yield, orange oil.

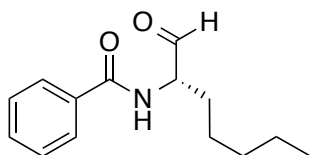
¹H NMR (400 MHz, Chloroform-*d*) δ 9.48 (s, 1H), 7.34 – 7.25 (m, 2H), 7.24 – 7.13 (m, 3H), 5.09 (dd, J = 7.6, 4.5 Hz, 1H), 5.02 (d, J = 7.8 Hz, 1H), 4.47 – 4.35 (m, 1H), 2.66 (dd, J = 8.0, 6.0 Hz, 2H), 1.48 (d, J = 7.2 Hz, 3H), 1.44 (s, 9H).

¹³C NMR (126 MHz, CDCl₃) δ 197.26, 173.14, 155.14, 141.19, 128.45, 128.38, 126.05, 80.00, 78.54, 49.12, 35.31, 28.29, 27.96, 26.50, 18.55.

HRMS (ESI-TOF) m/z : $[M+H]^+$ calcd for $C_{19}H_{27}NO_5$ 350.1962; found 350.1953.

Enantiomeric excess was determined to be 92% by integration of aldehyde signals in crude 1H NMR.

V. Data for enamide AHF



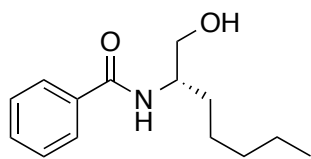
2-benzamido-heptanal.

Started with 100 mg enamide, 100% conversion.

1H NMR (400 MHz, Chloroform- d) δ 9.67 (s, 1H), 7.91 – 7.76 (m, 2H), 7.58 – 7.49 (m, 1H), 7.49 – 7.37 (m, 2H), 6.86 (d, J = 6.9 Hz, 1H, *NH*), 4.76 (q, J = 6.6 Hz, 1H), 2.13 – 1.97 (m, 1H), 1.82 – 1.70 (m, 1H), 1.51 – 1.20 (m, 6H), 0.96 – 0.80 (m, 3H).

^{13}C NMR (101 MHz, $CDCl_3$) δ 199.46, 167.41, 133.80, 131.88, 128.66 (2C), 127.10 (2C), 59.24, 31.60, 29.09, 24.86, 22.42, 13.96.

HRMS (ESI-TOF) m/z : $[M+H]^+$ calcd for $C_{14}H_{20}NO_2$ 234.1489; found 234.1492.



Alcohol: (S)-N-(1-hydroxyheptan-2-yl)benzamide

1H NMR (400 MHz, Chloroform- d) δ 7.82 – 7.69 (m, 2H), 7.51 – 7.43 (m, 1H), 7.42 – 7.32 (m, 2H), 6.61 (d, J = 8.3 Hz, 1H, *NH*), 4.12 (m, 1H, *X of ABX*), 3.78 – 3.70 (m, 1H, *A of ABX*), 3.70 – 3.60 (m, 1H, *B of ABX*), 3.50 (br s, 1H, *OH*), 1.70 – 1.51 (m, 2H), 1.46 – 1.33 (m, 2H), 1.34 – 1.22 (m, 4H), 0.95 – 0.80 (m, 3H).

^{13}C NMR (101 MHz, $CDCl_3$) δ 168.35, 134.50, 131.61, 128.61, 127.09, 65.37, 52.33, 31.80, 31.36, 25.98, 25.95, 22.63, 14.12.

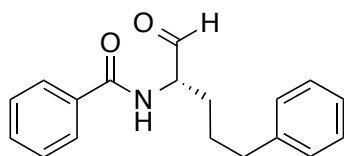
HRMS (ESI-TOF) m/z : $[M+H]^+$ calcd for $C_{14}H_{22}NO_2$ 236.1646; found 236.1638.

Separation by SFC: 85% *ee*.

Chiralcel OJ-H, 50 °C, 150 bar, MeOH modifier 2% for 1 min, then ramp to 8% over 6 min, hold 20 min, 2 mL/min flow, λ = 210 nm. t_r = 14.8 min (*S*), 16.9 min (*R*).

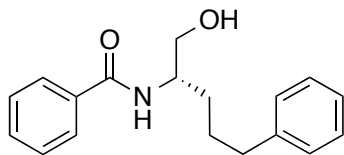
Separation by HPLC: 84% *ee*.

Chiralpak IA, 8% 2-propanol / 92% hexane, 1 mL/min flow, ambient temperature, λ =254 or 220 nm. t_r = 8.5 min (*S*), 11.4 min (*R*).



2-benzamido-5-phenylpentanal.

Started with 104 mg of enamide. 87% conversion, 81.1% yield (aldehyde).



Alcohol: (*S*)-*N*-(1-hydroxy-5-phenylpentan-2-yl)benzamide

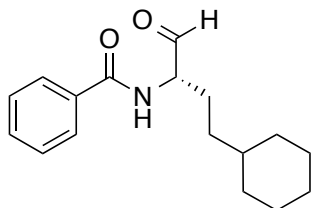
¹H NMR (500 MHz, Chloroform-*d*) δ 7.73 (d, J = 7.7 Hz, 2H), 7.46 (t, J = 7.4 Hz, 1H), 7.37 (t, J = 7.6 Hz, 2H), 7.26 (t, J = 7.4 Hz, 2H), 7.21 – 7.11 (m, 3H), 6.46 (d, J = 8.4 Hz, 1H), 4.23 – 4.08 (m, 1H, *X* of *ABX*), 3.79 – 3.68 (m, 1H, *A* of *ABX*), 3.68 – 3.57 (m, 1H, *B* of *ABX*), 3.10 (t, J = 5.0 Hz, 1H, OH), 2.74– 2.54 (m, 2H), 1.78– 1.68 (m, 2H), 1.68 – 1.55 (m, 2H).

¹³C NMR (126 MHz, CDCl₃) δ 168.28, 142.02, 134.42, 131.69, 128.66, 128.52, 128.48, 127.08, 125.98, 65.41, 52.08, 35.74, 30.94, 28.08.

HRMS (ESI-TOF) m/z : [M+H]⁺ calcd for C₁₈H₂₂NO₂ 284.1646; found 284.1652.

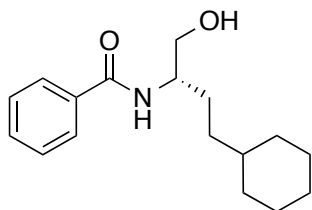
Separation by HPLC: 90% *ee*.

Chiralpak IA, 8% 2-propanol / 92% hexane, 1 mL/min flow, ambient temperature, $\lambda=254$ or 220 nm. $t_r = 10.2$ min (major, *S*), 13.4 min (*R*).



2-benzamido-4-cyclohexylbutanal.

80% conversion, 78% isolated yield (alcohol). Started with 150 mg enamide, isolated 131.9 mg alcohol.



Alcohol: (*S*)-*N*-(4-cyclohexyl-1-hydroxybutan-2-yl)benzamide

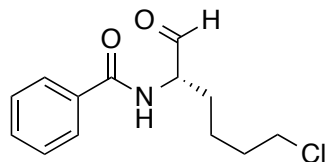
¹H NMR (400 MHz, Chloroform-*d*) δ 7.81 – 7.72 (m, 2H), 7.50 (ddt, $J = 8.7, 6.3, 1.2$ Hz, 1H), 7.42 (tt, $J = 6.7, 1.6$ Hz, 2H), 6.37 (d, $J = 7.9$ Hz, 1H, *NH*), 4.16 – 4.05 (m, 1H, *X of ABX*), 3.78 (app. dd, $J = 11.1, 3.5$ Hz, 1H, *A of ABX*), 3.67 (app. dd, $J = 11.0, 5.4$ Hz, 1H, *B of ABX*), 2.96 (br. s, 1H, *OH*), 1.79 – 1.51 (m, 7H), 1.34 – 1.05 (m, 6H), 0.96 – 0.79 (m, 2H).

¹³C NMR (101 MHz, CDCl₃) δ 168.26, 134.43, 131.60, 128.60 (2C), 126.99 (2C), 65.72, 52.67, 37.62, 33.84, 33.34, 33.29, 28.69, 26.62, 26.33 (2C).

HRMS (ESI-TOF) m/z : [M+H]⁺ calcd for C₁₇H₂₆NO₂ 276.1959; found 276.1956.

Separation by HPLC: 84% *ee*.

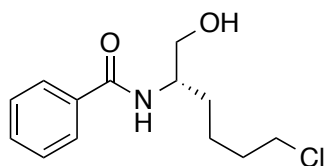
Chiralpak IA, 8% 2-propanol / 92% hexane, 1 mL/min flow, ambient temperature, $\lambda=254$ or 220 nm. $t_r = 8.5$ min (major, *S*), 12.6 min (*R*).



Aldehyde: 2-Benzamido-6-chlorohexanal.

79% conversion, 68% isolated yield. Started with 67 mg of enamide. Isolated alcohol as a yellow oil, 52 mg.

¹H NMR (400 MHz, Chloroform-*d*) δ 9.69 (s, 1H), 7.88 – 7.77 (m, 2H), 7.57 – 7.50 (m, 1H), 7.50 – 7.41 (m, 2H), 6.85 (d, J = 6.8 Hz, 1H), 4.78 (td, J = 6.9, 5.5 Hz, 1H), 3.54 (td, J = 6.4, 2.1 Hz, 2H), 2.18 – 2.04 (m, 1H), 1.95 – 1.72 (m, 3H), 1.69 – 1.48 (m, 2H).



Alcohol: (S)-N-(6-chloro-1-hydroxyhexan-2-yl)benzamide

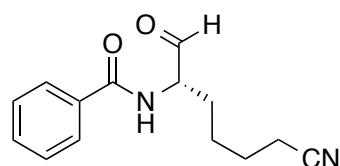
¹H NMR (500 MHz, Chloroform-*d*) δ 7.78 – 7.74 (m, 2H), 7.48 (tt, J = 7.5, 1.4 Hz, 1H), 7.40 (t, J = 7.5 Hz, 2H), 6.53 (d, J = 8.3 Hz, 1H), 4.21 – 4.09 (m, 1H, *X of ABX*), 3.82 – 3.73 (m, 1H, *A of ABX*), 3.69 (dt, J = 10.7, 4.6 Hz, 1H, *B of ABX*), 3.54 (t, J = 6.5 Hz, 2H), 3.08 (t, J = 4.9 Hz, 1H, *OH*), 1.89 – 1.73 (m, 2H), 1.73 – 1.61 (m, 2H), 1.61 – 1.47 (m, 2H).

¹³C NMR (126 MHz, CDCl₃) δ 168.28, 134.41, 131.76, 128.71 (2C), 127.09 (2C), 65.23, 51.93, 44.90, 32.32, 30.63, 23.54.

HRMS (ESI-TOF) *m/z*: [M+H]⁺ calcd for C₁₃H₁₉ClNO₂ 256.1099; found 256.1096.

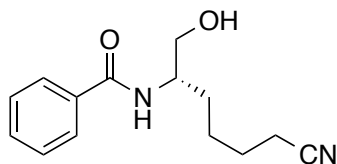
Separation by HPLC: 92% *ee*.

Chiralpak IA, 8% 2-propanol / 92% hexane, 1.2 mL/min flow, ambient temperature, λ =254 or 220 nm. t_r = 9.2 min (major, *S*), 15.0 min (*R*).



Aldehyde: 2-Benzamido-6-cyanoheptanal.

100% conversion.

**Alcohol: (S)-N-(6-cyano-1-hydroxyheptan-2-yl)benzamide**

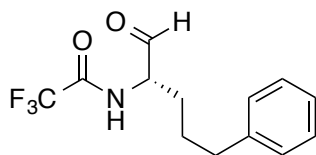
¹H NMR (400 MHz, Chloroform-*d*) δ 7.81 – 7.73 (m, 2H), 7.53 – 7.47 (m, 1H), 7.45 – 7.39 (m, 2H), 6.54 (d, *J* = 8.3 Hz, 1H), 4.22 – 4.07 (m, 1H, X of ABX), 3.82 – 3.66 (m, 2H, AB of ABX), 2.89 (br. s, 1H), 2.35 (t, *J* = 6.7 Hz, 2H), 1.79 – 1.62 (m, 4H), 1.62 – 1.49 (m, 2H).

¹³C NMR (126 MHz, CDCl₃) δ 168.13, 134.35, 131.86, 128.78 (2C), 127.10 (2C), 119.72, 77.16, 65.13, 51.53, 30.65, 25.36, 25.21, 17.21.

HRMS (ESI-TOF) *m/z*: [M+H]⁺ calcd for C₁₄H₁₉N₂O₂ 247.1442; found 247.1438.

Separation by HPLC: 94% ee.

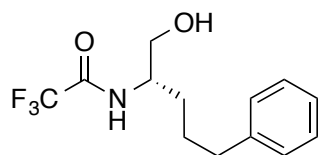
Chiralpak IA, 10% 2-propanol / 90% hexane, 1.2 mL/min flow, ambient temperature, λ =254 or 220 nm. *t_r* = 13.4 min (major, *S*), 24.1 min (*R*).

**Aldehyde: (S)-2,2,2-trifluoro-N-(1-oxo-5-phenylpentan-2-yl)acetamide**

100% conversion, 91% crude yield. Started from 100 mg enamide, isolated 103.4 mg alcohol.

¹H NMR (400 MHz, Chloroform-*d*) δ 9.49 (s, 1H), 8.30 (d, *J* = 8.7 Hz, 1H, NH), 7.31 – 7.21 (m, 2H), 7.21 – 7.06 (m, 3H), 4.52 (td, *J* = 8.4, 4.9 Hz, 1H), 2.77 – 2.54 (m, 2H), 1.77 – 1.56 (m, 4H).

¹⁹F NMR (377 MHz, CDCl₃) δ -75.73.



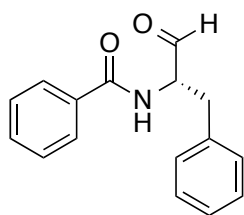
Alcohol: (S)-2,2,2-trifluoro-N-(1-hydroxy-5-phenylpentan-2-yl)acetamide

¹H NMR (400 MHz, Chloroform-*d*) δ 7.32 – 7.24 (m, 2H), 7.23 – 7.13 (m, 3H), 6.51 (d, J = 8.4 Hz, 1H), 4.12 – 3.98 (m, 1H, X of ABX), 3.73 (app. dd, J = 11.0, 3.6 Hz, 1H, A of ABX), 3.67 (app. dd, J = 11.1, 4.1 Hz, 1H, B of ABX), 2.71 – 2.57 (m, 2H), 1.80 (br s, 1H), 1.75 – 1.54 (m, 4H).

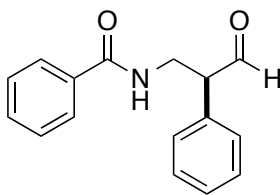
¹³C NMR (126 MHz, Chloroform-*d*) δ 157.38 (q, J = 37.0 Hz), 141.66, 128.60 (2C), 128.52 (2C), 126.16, 116.01 (q, J = 288.0 Hz), 63.83, 51.74, 35.57, 30.40, 27.75.

¹⁹F NMR (377 MHz, CDCl₃) δ -75.83.

HRMS (ESI-TOF) m/z : [M+H]⁺ calcd for C₁₃H₁₇F₃NO₂ 276.1206; found 276.1198.



α (major)



β (minor)

Aldehyde, alpha: N-(1-Formyl-2-phenylethyl) benzamide

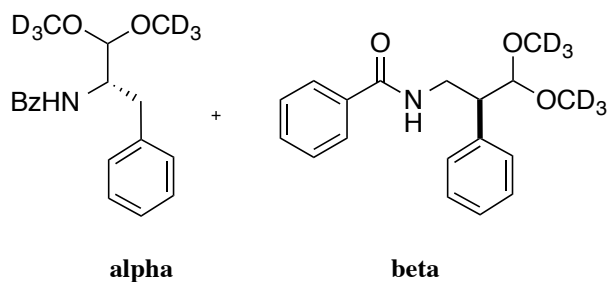
86.3% conversion, 81.2% isolated yield (aldehyde), 6.3:1 α : β .

Characterization data are consistent with literature report. (Pan, H.; Xie, Y.; Liua, M.; Shi, Y. *RSC Adv.* **2014**, *4*, 2389-2392.)

¹H NMR (400 MHz, Acetone-*d*₆) δ 9.73 (s, 1H), 8.08 (s, 1H), 7.85 (dd, J = 7.5, 1.7 Hz, 2H), 7.58 – 7.50 (m, 1H), 7.50 – 7.41 (m, 2H), 7.35 – 7.23 (m, 4H), 7.24 – 7.15 (m, 1H), 4.64 (ddd, J = 9.5, 7.3, 4.8 Hz, 1H), 3.36 (dd, J = 14.1, 4.8 Hz, 1H), 3.09 (dd, J = 14.1, 9.6 Hz, 1H).

HRMS (ESI-TOF) m/z : [M+H]⁺ calcd for C₁₆H₁₆NO₂ 254.1176; found 254.1170.

When the NMR is taken in methanol- d_4 (to obtain accurate b:l ratios), the dimethoxyacetal forms spontaneously:

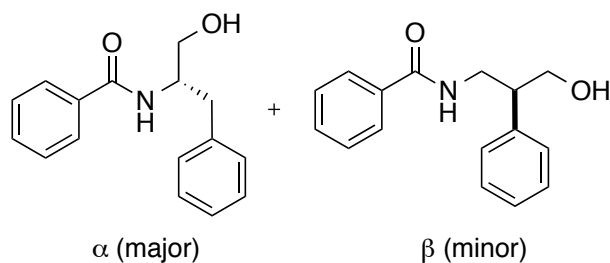


Dimethoxyacetal, alpha: (*S*)-*N*-(1,1-dimethoxy-3-phenylpropan-2-yl)benzamide

^1H NMR (500 MHz, Methanol- d_4) δ 7.74 – 7.67 (m, 2H), 7.52 – 7.35 (m, 3H), 7.34 – 7.20 (m, 4H), 7.18 – 7.12 (m, 1H), 4.66 (t, J = 3.4 Hz, 1H), 4.47 – 4.32 (m, 1H), 3.13 (app. ddd, J = 13.1, 7.7, 4.7 Hz, 1H), 2.92 (app. ddd, J = 14.8, 9.9, 6.1 Hz, 1H).

Dimethoxyacetal, beta: *N*-(3,3-dimethoxy-2-phenylpropyl)benzamide

^1H NMR (500 MHz, Methanol- d_4) δ 7.76 – 7.10 (m, 10H), 4.81 (d, J = 4.5 Hz, 1H, acetal H), 3.94 – 3.82 (m, 1H, A of ABX), 3.79 – 3.70 (m, 1H, B of ABX), 3.29 – 3.21 (m, 1H, X of ABX).



Alcohol, Alpha insertion: (*S*)-*N*-(1-hydroxy-3-phenylpropan-2-yl)benzamide

^1H NMR (500 MHz, Methanol- d_4) δ 7.76 – 7.71 (m, 2H), 7.52 (tt, J = 7.4, 1.1 Hz, 1H), 7.47 – 7.40 (m, 2H), 7.33 – 7.25 (m, 4H), 7.19 (tt, J = 6.9, 1.6 Hz, 1H), 4.36 (dq, J = 8.5, 5.7 Hz, 1H), 3.67 (d, J = 5.5 Hz, 2H), 3.04 (dd, J = 13.7, 6.1 Hz, 1H), 2.88 (dd, J = 13.7, 8.5 Hz, 1H).

^{13}C NMR (126 MHz, MeOD) δ 170.35, 139.97, 136.00, 132.49, 130.34 (2C), 129.42 (2C), 129.36 (2C), 128.27 (2C), 127.33, 64.29, 54.96, 49.00, 37.99.

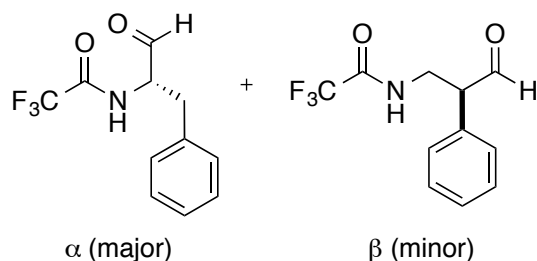
Alcohol, Beta insertion: *N*-(3-hydroxy-2-phenylpropyl)benzamide

¹H NMR (400 MHz, Methanol-*d*₄) δ 7.68 (dd, *J* = 7.2, 1.6 Hz, 2H), 7.53 – 7.45 (m, 2H), 7.44 – 7.36 (m, 2H), 7.33 – 7.21 (m, 4H), 3.82 (d, *J* = 6.4 Hz, 2H), 3.77 (dd, *J* = 13.5, 7.2 Hz, 1H), 3.63 (dd, *J* = 13.7, 7.9 Hz, 1H), 3.23 – 3.11 (m, 1H).

HRMS (ESI-TOF) *m/z*: [M+H]⁺ calcd for C₁₆H₁₈NO₂ 256.1333; found 256.1342.

Separation by HPLC: 98.3% *ee* α, 31.9% *ee* β.

Chiralpak IA, 8% 2-propanol / 92% hexane, 1 mL/min flow, ambient temperature, λ=220 nm. *t*_r (alpha isomer) = 11.5 min (major, *S*), 13.9 min (minor, *R*). *t*_r (beta isomer) = 19.3 min (minor), 21.8 min (major).

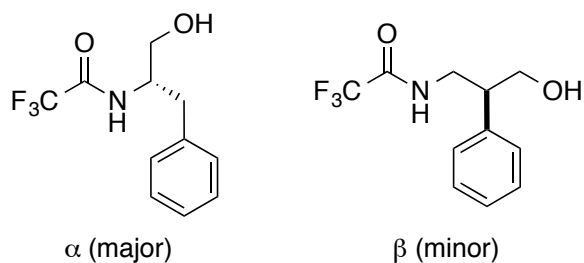
**Aldehyde, alpha: 2,2,2-Trifluoro-*N*-[(1*S*)-1-formyl-2-phenylethyl]acetamide**

100% conversion, 65.5% isolated yield (alcohol).

Characterization data are consistent with literature report. (Myers, A. G.; Kung, D. W.; Zhong, B.; Movassaghi, M.; Kwon, S. *J. Am. Chem. Soc.*, **1999**, *121*, 8401–8402.)

¹H NMR (400 MHz, CDCl₃) δ 9.64 (s, 1H), 7.50 – 7.09 (m, 5H), 7.02 (br. s, 1H), 4.82 (app. q, *J* = 6.6 Hz, 1H), 3.30 (dd, *J* = 14.2, 5.5 Hz, 1H), 3.22 (dd, *J* = 14.2, 7.2 Hz, 1H).

¹⁹F NMR (377 MHz, CDCl₃) δ -75.86 (alpha), -76.05 (beta).



Alcohol, alpha: (S)-2,2,2-trifluoro-N-(1-hydroxy-3-phenylpropan-2-yl)acetamide

Characterization data agrees with literature reports. (Myers, A. G.; Kung, D. W.; Zhong, B.; Movassaghi, M.; Kwon, S. *J. Am. Chem. Soc.*, **1999**, *121*, 8401–8402. Jiang, H.; Yan, L.; Xu, M.; Lu, W.; Cai, Y.; Wan, W.; Yao, J.; Wu, S.; Zhu, S.; Hao, J. *J. Org. Chem.* **2013**, *78*, 4261–4269.)

^1H NMR (400 MHz, Methanol- d_4) δ 7.38 – 7.13 (m, 5H), 4.17 (dq, J = 8.7, 5.9 Hz, 1H), 3.60 (qd, J = 11.2, 5.7 Hz, 2H), 2.96 (dd, J = 13.8, 5.9 Hz, 1H), 2.75 (dd, J = 13.8, 8.9 Hz, 1H).

^{19}F NMR (377 MHz, MeOD) δ -77.17.

Alcohol, beta: 2,2,2-trifluoro-N-(3-hydroxy-2-phenylpropyl)acetamide

^1H NMR (400 MHz, Methanol- d_4) δ 7.34 – 7.15 (m, 5H), 3.76 (dd, J = 6.5, 2.4 Hz, 2H), 3.67 (dd, J = 13.4, 6.7 Hz, 1H), 3.60 – 3.52 (m, 1H), 3.10 (dq, J = 8.5, 6.7 Hz, 1H).

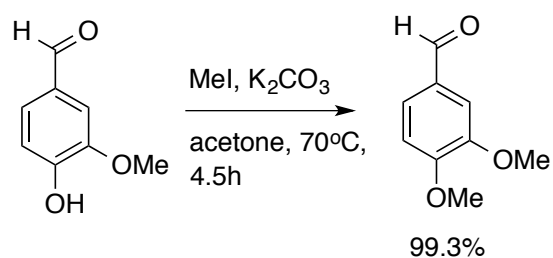
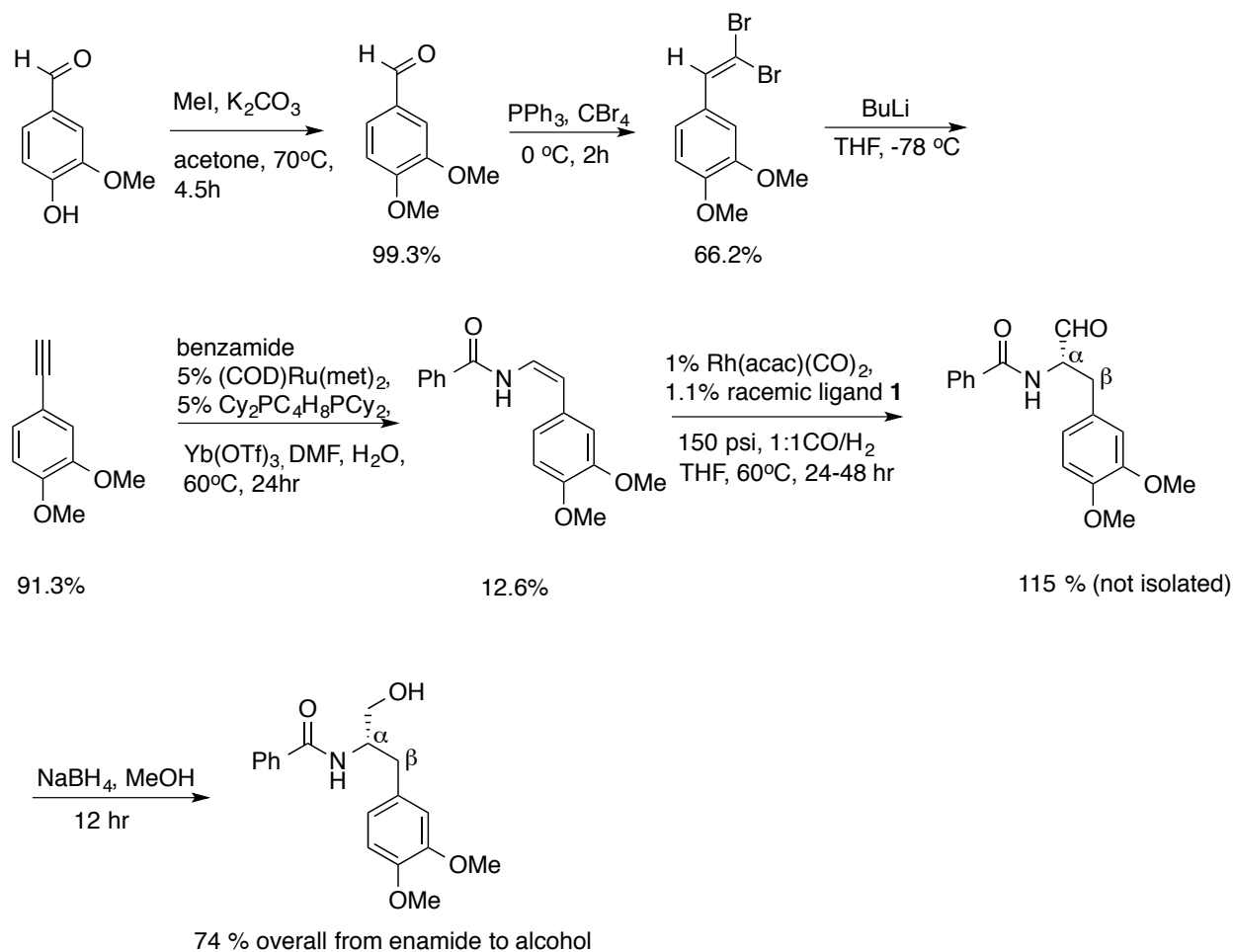
^{19}F NMR (377 MHz, Methanol- d_4) δ -77.37.

HRMS (ESI-TOF) m/z : $[\text{M}+\text{H}]^+$ calcd for $\text{C}_{11}\text{H}_{13}\text{F}_3\text{NO}_2$ 248.0893; found 248.0897.

Separation by HPLC: 90% *ee* α , 54% *ee* β .

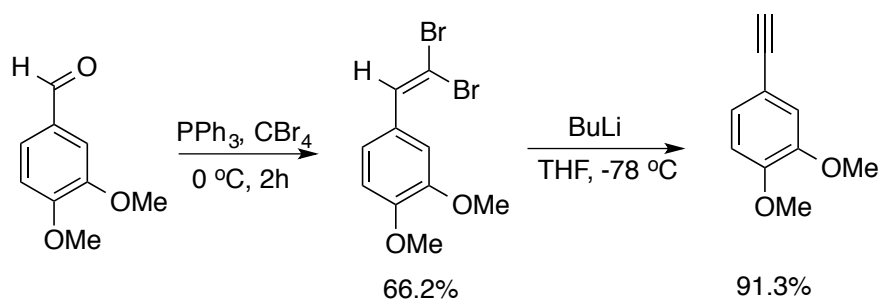
Chiralpak IA, 5% 2-propanol / 95% hexane, 1 mL/min flow, ambient temperature, λ =220 nm. t_r (alpha isomer) = 8.2 min (major, *S*), 9.5 min (minor, *R*). t_r (beta isomer) = 12.9 min (major), 14.1 min (minor).

VI. Synthesis of L-DOPA precursor



Methylation: 12.172 g (80 mmol) of vanillin was added into 130 mL of acetone, and the mixture was warmed to 60 °C to dissolve the vanillin. Then 11.222 g (80 mmol) of K₂CO₃ and 8 mL (120 mmol) of MeI were added, and the mixture was stirred at 60-70 °C overnight (17 hours) under reflux. The reaction mixture was filtered and the solids washed with acetone, then the filtrate was

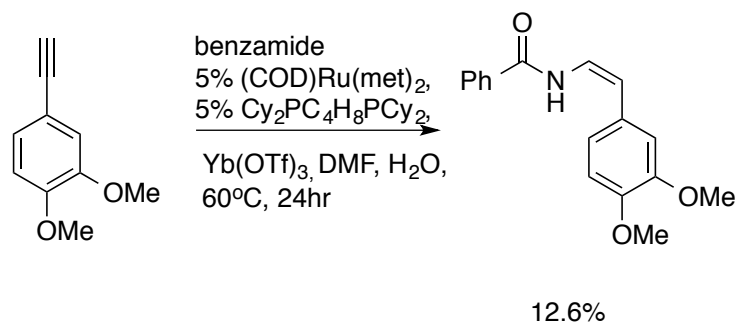
concentrated under vacuum to yield the desired product, which was further purified by flash column chromatography, to give 13.2 g (99.3% yield) of pure product. Characterization data are consistent with previously reported results. (Jiang, H.; Yan, L.; Xu, M.; Lu, W.; Cai, Y.; Wan, W.; Yao, J.; Wu, S.; Zhu, S.; Hao, J. *J. Org. Chem.* **2013**, 78, 4261–4269.)



Corey-Fuchs:

1) To a solution of the methylated aldehyde (6.646g, 40 mmol) in dry DCM, triphenylphosphine (20.983g, 80mmol) was added. The mixture was cooled to $0\text{ }^\circ\text{C}$, and a solution of carbon tetrabromide (14.592g, 44 mmol) in dry DCM was added dropwise. The reaction mixture was allowed to gradually warm up to room temperature and stirred for another two hours after reaching room temperature. The reaction mixture was quenched with water, and the organic layer was separated and washed with brine. The crude mixture was dried over magnesium sulfate, filtered, concentrated under vacuum, and purified by flash column chromatography to give the dibromoethene derivative (8.521g, 66.2%). Characterization data are consistent with previously reported results. (Rosiak, A.; Frey, W.; Christoffers, J. *Eur. J. Org. Chem.* **2006**, 4044–4054.)

2) *n*BuLi (26.46 mL of 2.5 M solution in hexane, 66.15 mmol) was added dropwise to a solution of the dibromoethene derivative (8.521g, 26.46 mmol) in dry THF at -78 °C. The resulting solution was stirred at -78 °C for 1h, and then gradually warmed to room temperature. The reaction was quenched using saturated aqueous NH₄Cl, and the mixture was extracted with EtOAc. The organic layer was washed with water (x1) and brine (x1). After drying over magnesium sulfate and concentration under vacuum, the crude product was purified by column chromatography to yield alkyne (3.915g, 91.3%). Characterization data are consistent with previously reported results. (Rosiak, A.; Frey, W.; Christoffers, J. *Eur. J. Org. Chem.* **2006**, 4044–4054.)



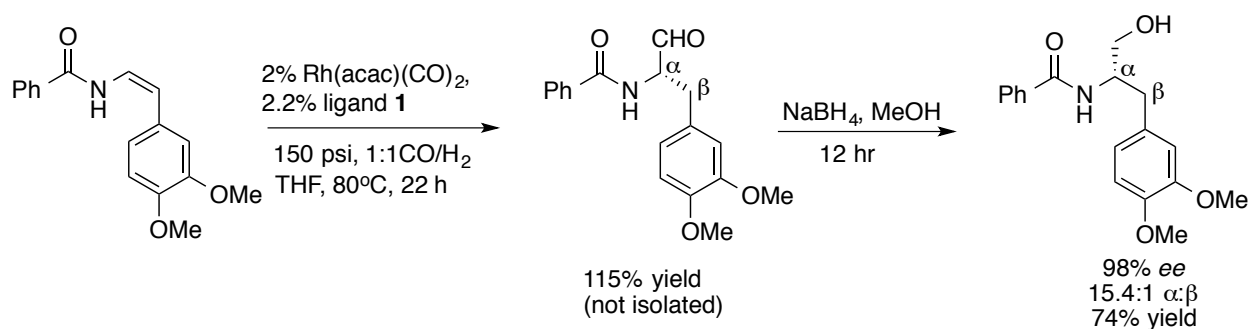
Enamide formation: The enamide was synthesized by the general procedure reported above, starting from 3.915g (24.17 mmol) of the alkyne. After the typical extractive workup and removal of the solvent under vacuum, the crude mixture was left overnight. Upon standing, the desired product precipitated out, and the dark liquid impurities were dissolved in EtOAc (the product does not dissolve in EtOAc). The product was separated using filtration, and the solids were washed with EtOAc. The product was recrystallized from a mixture of DCM and hexane four times to yield 0.8624g of light green crystals (12.6% yield). Characterization data are

consistent with previously reported results. (Wendlandt, A.E.; Stahl, S.S.; *Org. Biomol. Chem.*, **2012**, *10*, 3866.)

¹H NMR (500 MHz, Chloroform-*d*) δ 8.37 (d, *J* = 11.0 Hz, 1H), 7.80 – 7.73 (m, 2H), 7.58 – 7.50 (m, 1H), 7.50 – 7.41 (m, 2H), 7.16 (dd, *J* = 11.1, 9.4 Hz, 1H), 6.94 (d, *J* = 2.1 Hz, 2H), 6.83 (d, *J* = 1.5 Hz, 1H), 5.85 (d, *J* = 9.4 Hz, 1H), 3.92 (s, 3H), 3.89 (s, 3H).

¹³C NMR (126 MHz, Chloroform-*d*) δ 164.19, 149.51, 148.13, 133.41, 132.15, 128.87, 128.51, 127.02, 121.75, 119.99, 111.73, 111.29, 110.94, 55.98, 55.93.

HRMS (ESI-TOF) *m/z*: [M+H]⁺ calcd for C₁₇H₁₇NO₃ 284.1282; found 284.1279.



AHF and reduction: 0.5 mL of 20 mM Rh(acac)(CO)₂ solution in THF was combined with 1.1 mL of 20 mM ligand solution in THF with about 50% potency. The mixture was stirred in a pressure bottle under 150 psi of syngas (1:1 H₂/CO) at 70-80 °C for 1hr, then the entire mixture was removed via syringe and injected into another pressure bottle containing 0.1418g (0.5 mmol) of the olefin. The mixture was pressurized to 155 psi of syngas, submerged in an 80 °C oil bath, and stirred at a high rate to ensure sufficient gas-liquid mixing for 22 hours. The crude mixture was passed through a short pad of silica, rinsed with THF. Then the mixture was concentrated in vacuum to give the aldehyde (>100% crude yield).

The crude aldehyde was dissolved in MeOH, and excess NaBH₄ was added to the solution at 0 °C, and the resulting mixture was stirred overnight. The crude material was purified using small-scale flash column chromatography (60% EtOAc in hexane) to give 0.116g of the alcohol product (74% yield from enamide).

Aldehyde:

¹H NMR (500 MHz, 3:1 Toluene-*d*₈:CDCl₃) δ 9.39 (s, 1H), 7.64 (d, *J* = 7.5 Hz, 2H), 7.27 (t, *J* = 7.3 Hz, 1H), 7.19 (t, *J* = 7.5 Hz, 2H), 6.62 (d, *J* = 5.1 Hz, 1H), 6.59 – 6.51 (m, 3H), 4.61 (q, *J* = 6.1 Hz, 1H), 3.59 (s, 4H), 3.55 (s, 3H), 3.13 – 2.99 (m, 2H).

¹³C NMR (126 MHz, 3:1 Toluene-*d*₈:CDCl₃) δ 198.95, 167.39, 149.71, 148.80, 134.21, 132.23, 129.05 (2C), 128.64, 127.50 (2C), 121.84, 113.13, 111.88, 60.79, 56.027, 55.961, 34.86.

HRMS (ESI-TOF) *m/z*: [M+H]⁺ calcd for C₁₈H₁₉NO₄ 314.1387; found 314.1392.

Alcohol:

¹H NMR (500 MHz, Chloroform-*d*) δ 7.71 – 7.66 (m, 2H), 7.52 – 7.46 (m, 1H), 7.45 – 7.37 (m, 2H), 6.83 – 6.76 (m, 3H), 6.46 (d, *J* = 7.4 Hz, 1H), 4.42 – 4.25 (m, 1H), 3.86 (s, 3H), 3.83 (s, 3H), 3.82 – 3.68 (m, 2H), 2.95 (d, *J* = 7.2 Hz, 2H), 2.91 (br. s, 1H).

¹³C NMR (126 MHz, Chloroform-*d*) δ 168.15, 149.25, 148.01, 134.38, 131.85, 131.82, 130.18, 128.75, 127.03, 121.37, 112.40, 111.46, 64.35, 56.04, 55.99, 53.48, 36.70.

HRMS (ESI-TOF) *m/z*: [M+H]⁺ calcd for C₁₈H₂₁NO₄ 316.1544; found 316.1550.

Separation by HPLC:

Chiralpak IA, 10% 2-propanol / 90% hexane, 1.2 mL/min flow, ambient temperature, λ=220 nm. *t*_r (alpha isomer) = 12.7 min (major, *S*), 15.7 min (minor, *R*). *t*_r (beta isomer) = 23.5 min (minor), 24.9 min (major).

2.3. References.

- 1 For hydroformylation reviews, see: (a) Agbossou, F.; Carpentier, J. F.; Mortreaux, A. *Chem. Rev.* **1995**, *95*, 2485-2506. (b) Claver, C.; van Leeuwen, P. W. N. M. *Rhodium Catalyzed Hydroformylation*; Kluwer Academic Publishers: Dordrecht, The Netherlands, 2000. (c) Wiese, K. D.; Obst, D. *Top. Organomet. Chem.* **2006**, *18*, 35–64. (d) Franke, R.; Selent, D.; Börner, A. *Chem. Rev.* **2012**, *112*, 5675–5732. (e) Whiteker, G.T.; Cobley, C.J. *Top. Organomet. Chem.* **2012**, *42*, 35–46. For reviews of asymmetric hydroformylation, see: (f) Klosin, J.; Landis, C. R. *Acc. Chem. Res.* **2007**, *40*, 1251–1259. (g) Breit, B. *Top. Curr. Chem.* **2007**, *279*, 139–172. (h) Gual, A.; Godard, C.; Castillon, S.; Claver, C. *Tetrahedron: Asymmetry* **2010**, *21*, 1135 – 1146.
- 2 (a) Sakai, N.; Mano, S.; Nozaki, K.; Takaya, H. *J. Am. Chem. Soc.* **1993**, *115*, 7033–7034. (b) Sakai, N.; Nozaki, K.; Takaya, H. *J. Chem. Soc., Chem. Commun.* **1994**, 395-396. (c) Nanno, T.; Sakai, N.; Nozaki, K.; Takaya, H. *Tetrahedron: Asymmetry* **1995**, *6*, 2583-2591. (d) Nozaki, K.; Sakai, N.; Nanno, T.; Higashijima, T.; Mano, S.; Horiuchi, T.; Takaya, H. *J. Am. Chem. Soc.* **1997**, *119*, 4413– 4423. (e) Horiuchi, T.; Ohta, T.; Shirakawa, E.; Nozaki, K.; Takaya, H. *J. Org. Chem.* **1997**, *62*, 4285–4292. (f) Nozaki, K.; Li, W.; Horiuchi, T.; Takaya, H. *Tetrahedron Lett.* **1997**, *38*, 4611–4614.
- 3 Babin, J. E.; Whiteker, G. T. World Patent, WO 9303839, 1993.
- 4 Yan, Y.; Zhang, X. *J. Am. Chem. Soc.* **2006**, *128*, 7198-7202.
- 5 Fernández-Pérez, H.; Benet-Buchholz, J.; Vidal-Ferran, A., *Org. Lett.* **2013**, *15*, 3634-3637.
- 6 Zhang, X. W.; Cao, B. N.; Yan, Y. J.; Yu, S. C.; Ji, B. M.; Zhang, X. M. *Chem.—Eur. J.* **2010**, *16*, 871-877.
- 7 (a) Lightburn, T. E.; Dombrowski, M. T.; Tan, K. L. *J. Am. Chem. Soc.* **2008**, *130*, 9210–9211. (b) Grünanger, C. U.; Breit, B. *Angew. Chem., Int. Ed.* **2008**, *47*, 7346–7349. (c)

-
- Grünanger, C. U.; Breit, B. *Angew. Chem., Int. Ed.* **2010**, *49*, 967–970. (d) Worthy, A. D.; Joe, C. L.; Lightburn, T. E.; Tan, K. L. *J. Am. Chem. Soc.* **2010**, *132*, 14757–14759. (e) Sun, X.; Frimpong, K.; Tan, K. L. *J. Am. Chem. Soc.* **2010**, *132*, 11841–11843. (f) Joe, C. L.; Tan, K. L. *J. Org. Chem.* **2011**, *76*, 7590–7596. (g) Usui, I.; Nomura, K.; Breit, B. *Org. Lett.* **2011**, *13*, 612–615. (h) Ueki, Y.; Ito, H.; Usui, I.; Breit, B. *Chem. Eur. J.* **2011**, *17*, 8555–8558. (i) Joe, C. L.; Blaisdell, T. P.; Geoghan, A. F.; Tan, K. L. *J. Am. Chem. Soc.* **2014**, *136*, 8556–8559.
- 8 (a) Clark, T. P.; Landis, C. R.; Freed, S. L.; Klosin, J.; Abboud, K. A. *J. Am. Chem. Soc.* **2005**, *127*, 5040–5042. (b) Watkins, A. L.; Hashiguchi, B. G.; Landis, C. R. *Org. Lett.* **2008**, *10*, 4553–4556. (c) McDonald, R. I.; Wong, G. W.; Neupane, R. P.; Stahl, S. S.; Landis, C. R. *J. Am. Chem. Soc.* **2010**, *132*, 14027–14029. (d) Watkins, A. L.; Landis, C. R. *Org. Lett.* **2011**, *13*, 164–167. (e) Risi, R. M.; Burke, S. D. *Org. Lett.* **2012**, *14*, 1180 – 1182. (f) Risi, R. M.; Burke, S. D. *Org. Lett.* **2012**, *14*, 2572 – 2575. (g) Adint, T. T.; Wong, G. W.; Landis, C. R. *J. Org. Chem.* **2013**, *78*, 4231–4238. (h) Adint, T. T.; Landis, C. R. *J. Am. Chem. Soc.* **2014**, *136*, 7943–7953.
- 9 Clemens, A. J. L.; Burke, S. D. *J. Org. Chem.* **2012**, *77*, 2983–2985.
- 10 Ho, S.; Bucher, C.; Leighton, J. L. *Angew. Chem., Int. Ed.* **2013**, *52*, 6757–6761.
- 11 Wang, X.; Buchwald, S. L. *J. Org. Chem.* **2013**, *78*, 3429–3433. Wang, X.; Buchwald, S. L. *J. Am. Chem. Soc.* **2011**, *133*, 19080–19083.
- 12 Doucet, H.; Martin-Vaca, B.; Bruneau, C.; Dixneuf, P. H. *J. Org. Chem.* **1995**, *60*, 7247–7255.
- 13 Gooßen, L. J.; Paetzold, J.; Koley, D. *Chem. Commun.* **2003**, 706–707.
- 18 Gooßen, L. J.; Salih, K. S. M.; Blanchot, M. *Angew. Chem. Int. Ed.* **2008**, *47*, 8492.
- 19 (a) Chen, X.; Chen, J.; De Paolis, M.; Zhu, J. *J. Org. Chem.* **2005**, *70*, 4397–4408. (b) De Paolis, M.; Chen, X.; Zhu, J. *Synlett* **2004**, 729–731.

20 Myers, A. G.; Zhong, B.; Movassaghi, M.; Kung, D. W.; Lanman, B. A.; Kwon, S. *Tetrahedron Lett.* **2000**, *41*, 1359–1362.

21 Knowles, W. S. *Acc. Chem. Res.* **1983**, *16*, 106-112.

22 See supporting information for synthesis and references to procedures utilized.

Chapter 3

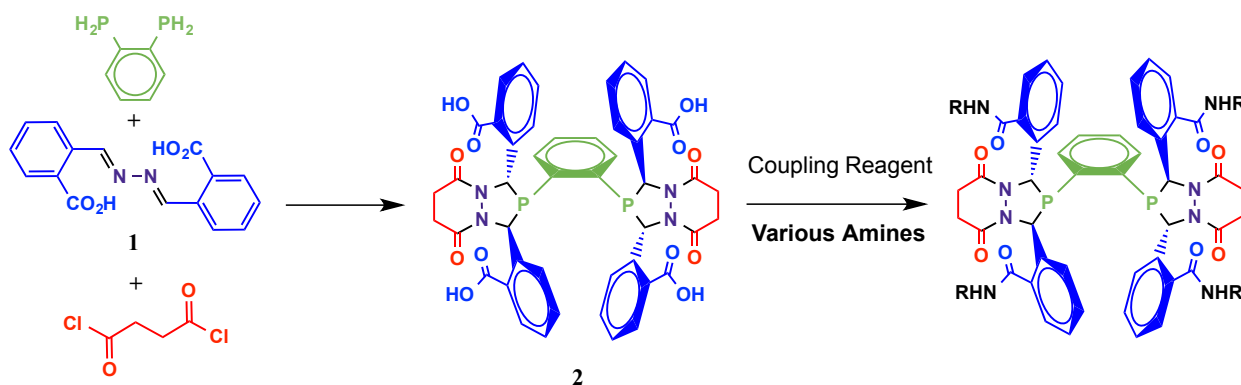
Improvements to the synthesis of enantiopure BisDiazaphospholane ligands

Portions of this work were done in collaboration with Eli Lilly and Co. and their contractee Freeslate. Some experimental procedures were performed with or by Joseph R. Martinelli, Joel Calvin, Michael E. Laurila (Eli Lilly and Co.), and Bradley R. Jones (University of Wisconsin-Madison). These contributions are noted within the text.

3.1. Introduction.

The family of bisdiazaphospholane ligands developed in the Landis group provide highly selective asymmetric hydroformylation (AHF) catalysts when bound to rhodium.¹ These bisdiazaphospholane catalysts are highly active at relatively low pressures (150 psi) of synthesis gas, allowing for the use of glass pressure bottles.² Their development has greatly expanded the number of α -chiral aldehydes accessible through AHF.³ These ligands are modular, allowing for modification of steric and electronic properties without substantial changes to the synthetic procedure (Scheme 3.1). A library of these tetra-amide ligands has been synthesized,⁴ as well as bead-immobilized variants.⁵ In addition, they show activity in hydroacylation in some preliminary studies.⁶ We aim to demonstrate the straightforward synthesis, resolution, and coupling of the bisdiazaphospholane ligands to facilitate their use in AHF by organic chemists. To do so, the reaction is performed on two scales: one that is easily run on the bench in a round-bottom flask, and one that produces larger amounts of ligand to sustain the development of AHF on a production scale.

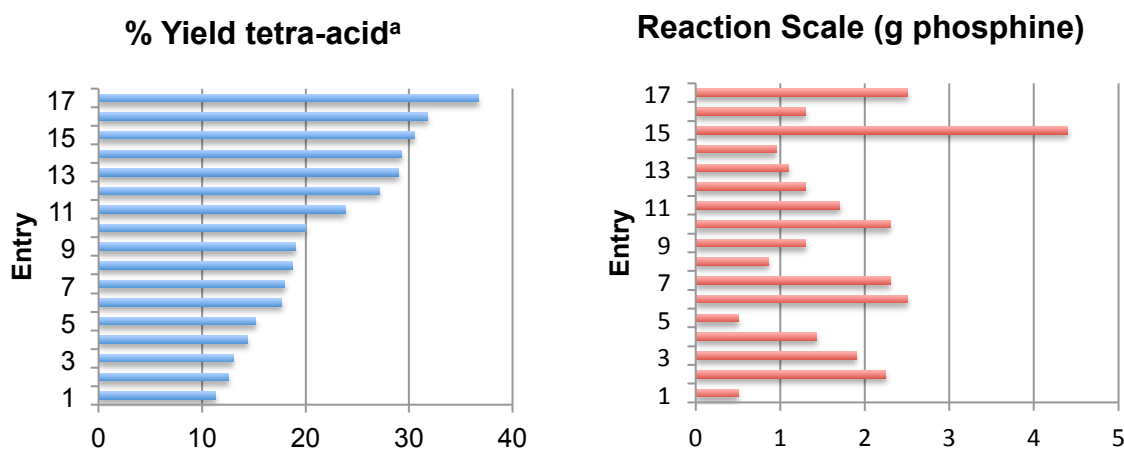
Scheme 3.1. Synthesis of bisdiazaphospholane ligands.



The synthesis of the precursor to these tetra-amide ligands, **2** (“tetra-acid,” rel-2,2',2'',2'''-(1,2-phenylenebis((1*R*,3*R*)-tetrahydro-5,8-dioxo-1H-

(1,2,4)diazaphospholo(1,2-a)pyridazine-2,1,3(3H)-triyl))tetrakis-benzoic acid), has had inconsistent yields in the past decade of synthesis in our research group. The goal of this project is to standardize the reaction to give consistent results regardless of the chemist running it and to re-optimize the synthesis for larger scale, to facilitate industrial-scale AHF. The original reported scale for synthesis of tetra-acid was 1.5 mmol, though the typical scale on which this synthesis has been run in the group is 17.6 mmol. The scale and yields of reactions performed over the last 5 years in our lab are reproduced in Table 3.1. In section 3.2, the purity of the starting azine and other materials are examined to determine the source of variability in yield, and then the reaction conditions are modified to improve the yield.

Table 3.1. Routine syntheses of tetra-acid in the Landis group.



^a Not adjusted for coordinated THF, actual yields are lower and may vary based on drying technique.

The *rac* C_2 symmetric isomer of tetra-acid crashes out of solution preferentially. This allows for efficient isolation of the desired isomer from the other possible diastereomers. However, the separation of the two enantiomers has historically been carried out through preparative SFC chromatography, limiting the accessibility of enantiopure tetra-acid to researchers with access to this technology. In addition, the resolved material is not currently

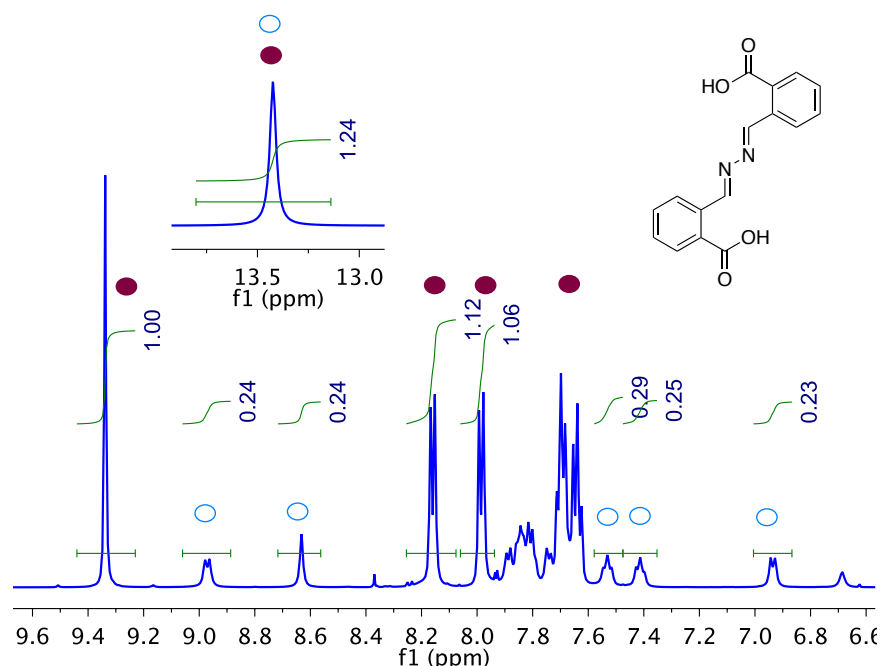
commercially available. To circumvent the need for chromatographic separation, classical resolution *via* diastereomeric salt formation is carried out using enantiopure pseudoephedrine (Section 3.3).

During studies of scale-up of AHF in a flow reactor, it was determined that the tetra-amide ligand used for catalysis was of low purity. This is true of material synthesized by the original route using PyBOP as a coupling agent, as well as the material synthesized through a tetra-acyl fluoride intermediate synthesized using Deoxo-Fluor®. In section 3.4 we re-examine the synthesis of ligand to determine if a different coupling method would improve the yield and purity of isolated material. In addition, a new, straightforward technique to purify low-potency ligand is developed.

3.2a. Synthesis of 2,2'-(azinodimethyldiynyl)bis-benzoic acid and identification of conformers and byproducts

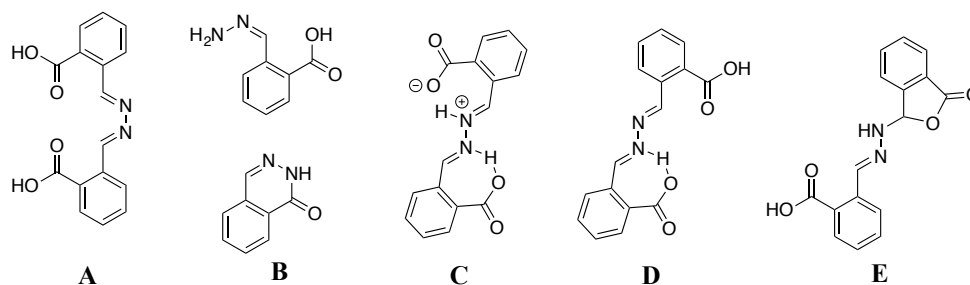
The original report of synthesis of the azine **1** proceeds in high yield (91%), crashing out of ethanol as a yellow solid.⁷ However, during routine synthesis of the azine, the NMR of the product shows about 20% of the material is a different species (Figure 3.1). Understanding the identity of this species will enable higher yielding synthesis of this important ligand precursor.

Figure 3.1: ^1H NMR of azine and minor component.

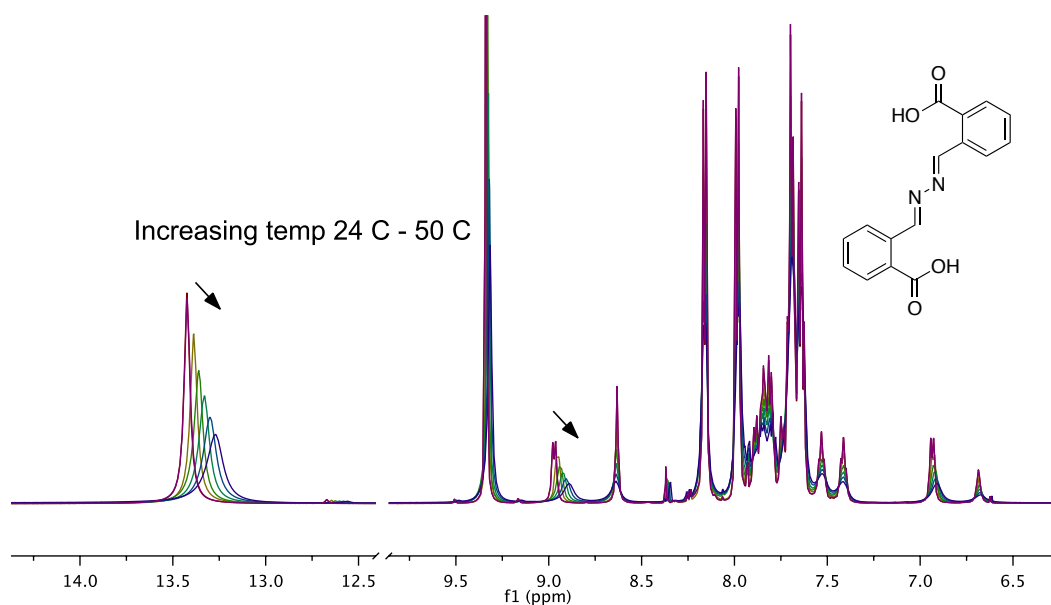


Three initial hypotheses of the identity of this minor component are proposed (Figure 3.2).

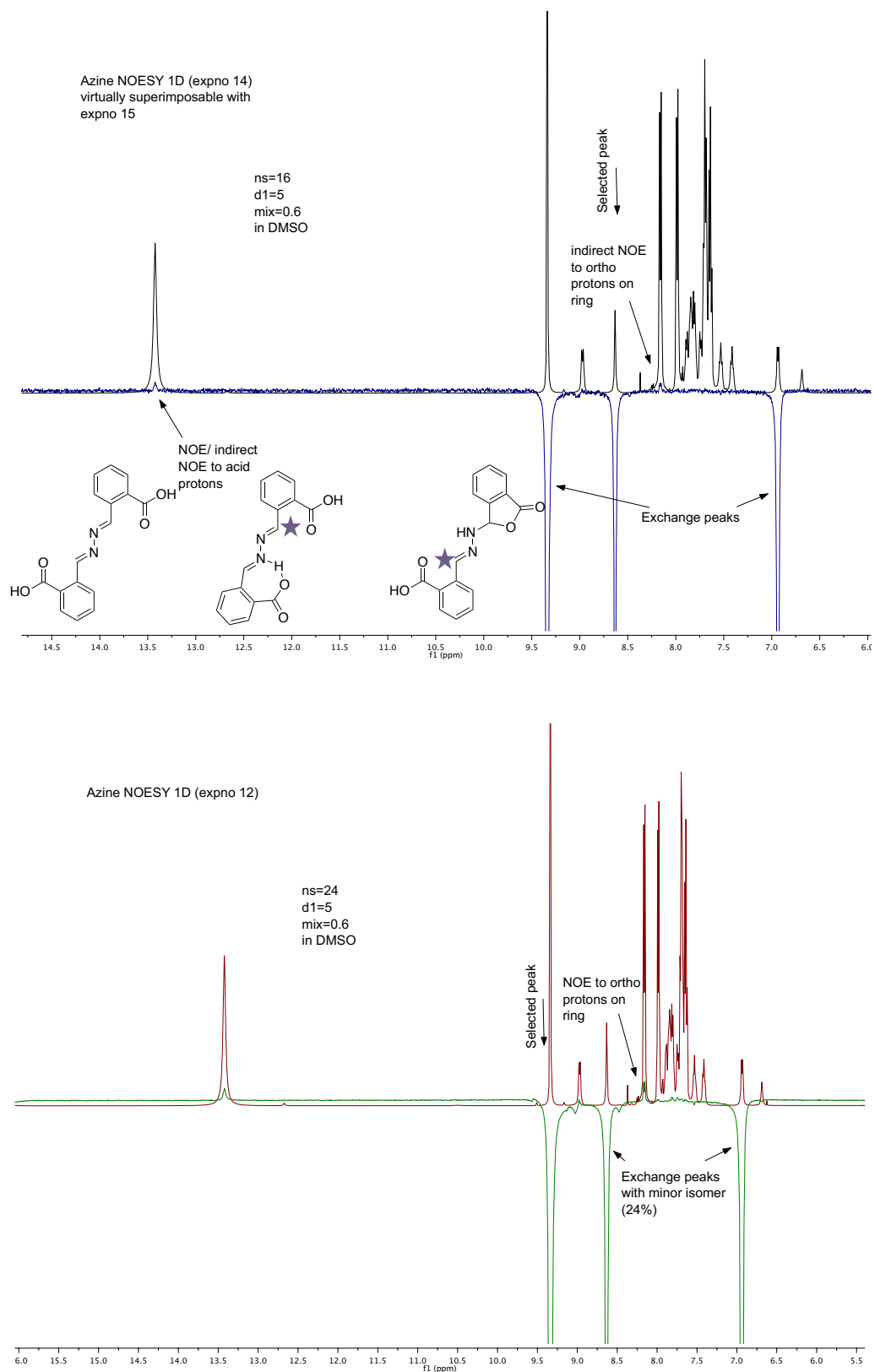
First, the minor species is a geometric conformer. Second, the minor species is a hydrogen-bonded form. Third, the minor species is a byproduct from the synthesis. Mass spectrometry provides limited help in identifying the composition of the mixture, as the compounds are extremely insoluble in all solvents but DMSO, and efforts to examine the composition of the solid by LC/MS led to degradation. However, we analyzed the composition of the filtrate after the reaction was complete, and it contains a material isolated as a white solid that LC/MS shows is the ethyl ester of 2-carboxybenzaldehyde, from the condensation of ethanol and starting material. However, this material is not present in the isolated azine and is only a minor component in the overall mass balance. For identification of the two components in the solid azine, NMR proved to be the most valuable technique.

Figure 3.2: Possible structures of the minor component.

To test the first hypothesis, variable-temperature NMR was performed to examine what is expected to be a strong temperature dependence of the equilibrium between the postulated conformers. While one peak of the minor component moves with temperature variations between 24 and 50 °C, an analogous peak on the azine also moves, suggesting that the observed shifts are due to two separate components with functional groups hydrogen-bonding with the solvent (Figure 3.3).

Figure 3.3: Variable-temperature ^1H NMR of azine.

To gather more information on the structure of the minor component and test the second and third hypotheses, a series of 1D NOESY NMR spectra were acquired (Figure 3.4). In NOESY spectra, through-space interactions up to about 5 Å are observed as positive resonances, with the intensity of the peaks in proportion to the spacial distance from the irradiated peak.⁸ In the spectra acquired on a sample of the azine, the peaks seen are instead strong negative signals, indicating rapid chemical exchange with the irradiated resonance. This implies that the minor component is in exchange with the major component on the NMR timescale, and should therefore be accessible for further reaction. In addition, indirect NOE is also observed in the spectra, which is the result of the irradiated nuclei undergoing exchange with the other component, followed by NOE enhancement of the spatially proximal protons. Based on the imine protons in the minor component being inequivalent (one appears at δ 8.6 the other at δ 6.9), one imine showing coupling to the hydrogen-bonding peak at 9.0 ppm (distinguished by the variable-temperature experiment), and the integral of the major acid (1.24 relative to the imine on the major component, Figure 3.1), the minor species appears to have one half of the molecule in some sort of hydrogen bonded or cyclic form, and the other imine “free” in the form typically drawn for the molecule. The hydrogen-bonded isomer labeled **D** in Figure 3.2, or its fully deprotonated, zwitterionic form, is the most consistent structure. A cyclic form like **E** has not been fully ruled out.

Figure 3.4: 1D NOESY spectra of azine.

While these data do not fully distinguish between the proposed hydrogen-bonded, zwitterionic and cyclic structures, they do suggest that the minor component in the azine is rapidly interconverting with the major component. This means that both components can access the reaction pathway that leads to formation of tetra-acid, and the purity of the azine is both high and not adversely affecting the yield of tetra-acid in the next synthetic step. With this knowledge, the synthesis of the tetra-acid is examined more closely.

3.2b. Improving the yield and reproducibility of the synthesis of tetra-acid

A reproducible, optimized synthesis of tetra-acid on the academic bench scale was necessary before scaling up the synthesis to a large scale. A number of the starting materials were of unknown quality in some of the runs included in Table 3.1. To standardize subsequent results, the THF used is distilled from Na⁰/benzophenone, the succinyl chloride is distilled within a week of use, and the purity of the azine is evaluated (see section 3.2a, above). After controlling these sources of error, the rate of addition of materials, the concentration, and the reaction temperature are modified.

On scaling up the reaction from the original report of 1.5 mmol to a 17.5-35 mmol scale, the addition of succinyl chloride is noted to produce a substantial exotherm. If the addition of succinyl chloride is too fast, the yield of the reaction is lower, and in some cases the reaction mixture changes in appearance. Instead of the typical milky suspension, the solids in the reaction clump up. Based on these observations, the rate at which succinyl chloride is added is more closely controlled and the reaction is cooled in an ice and water bath (0 °C). These modifications reproducibly provide yields close to 40%. Cooling the reaction further does not appear to be beneficial, as running the reaction at -40 °C (MeCN/CO₂ bath) did not substantially

improve the yield (Table 3.2, entry 5). In addition, the color change from a suspension of yellow azine to white tetra-acid does not begin until the reaction is warmed to above -20 °C.

Another factor that appears to have an effect on the yield of tetra-acid is the concentration at which the reaction is run. At higher concentrations, yield of the product tetra-acid is lower: at about 30 mL/ g of phosphine starting material the yield is only 24%, whereas at 100 mL/ g phosphine the yield is 42% (Table 3.2, entries 8 and 9). More dilute conditions were not attempted because of concern about the efficiency of isolation of C₂ tetra-acid when it is sparingly soluble. Again, control of the exotherm upon succinyl chloride addition appears to be crucial to a high-yielding reaction. Lowering the reaction temperature, running the reaction at a low concentration, and adding the acid chloride slowly all accomplish this and the revised procedure produces consistent yields in the hands of at least three different chemists (entries 4, 6 and 9).

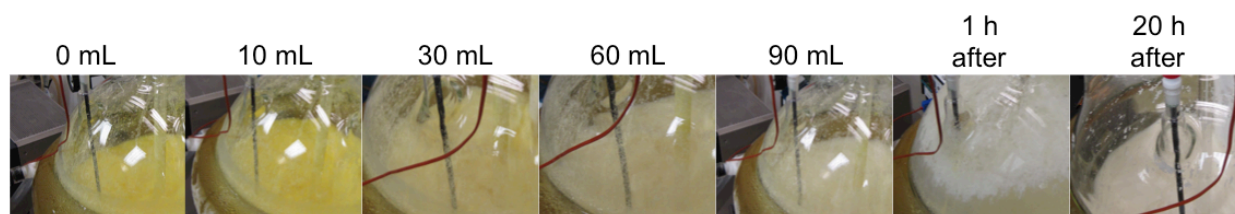
Table 3.2: Revised synthesis of tetra-acid

Entry/ Reaction ID	Scale ^a	Temperature (°C)	mL THF / g phosphine	Succinyl Chloride addition notes	Yield ^b
1 MLA2063	2.5 g	21 °C	30	Details of addition rate not recorded	36.7%
2 MLA2191	2.5 g	21 °C	60	Details of addition rate not recorded	17.7%
3 MLA2211	5 g	0° → rt	100	Details of addition rate not recorded	35%
4 MLA2241	5 g	0° → rt	100	Added over 25 min	39.1%
5 MLA2306	5 g	-40° → -15° → rt 1h → 1.5h → 48h	100	Added over 50 min Color change only above -20 °C	39.5%
6 F. Foarta	5 g	0° → rt	100	Added over 65 min	39.2%

7 J. Martinelli (Eli Lilly)	2.5 g	21 °C	32	Added slowly, no temp control	2.5%*
8 J. Martinelli (Eli Lilly)	2.5 g	13-15° internal, jacketed flask, overnight	32	Added over 2h, maintain 13°-15 °C	24%*
9 J. Martinelli (Eli Lilly)	5 g	5° jacketed flask, ~6h slow warm to rt	100	Added over 1.75h, maintain 5-9 °C	36%
10 Large Scale (Eli Lilly)	43 g	-8 °C internal, jacketed flask, ~5h slow warm to rt	102	Added over 4h, maintain -8.2 to -6.1 °C	36.2%

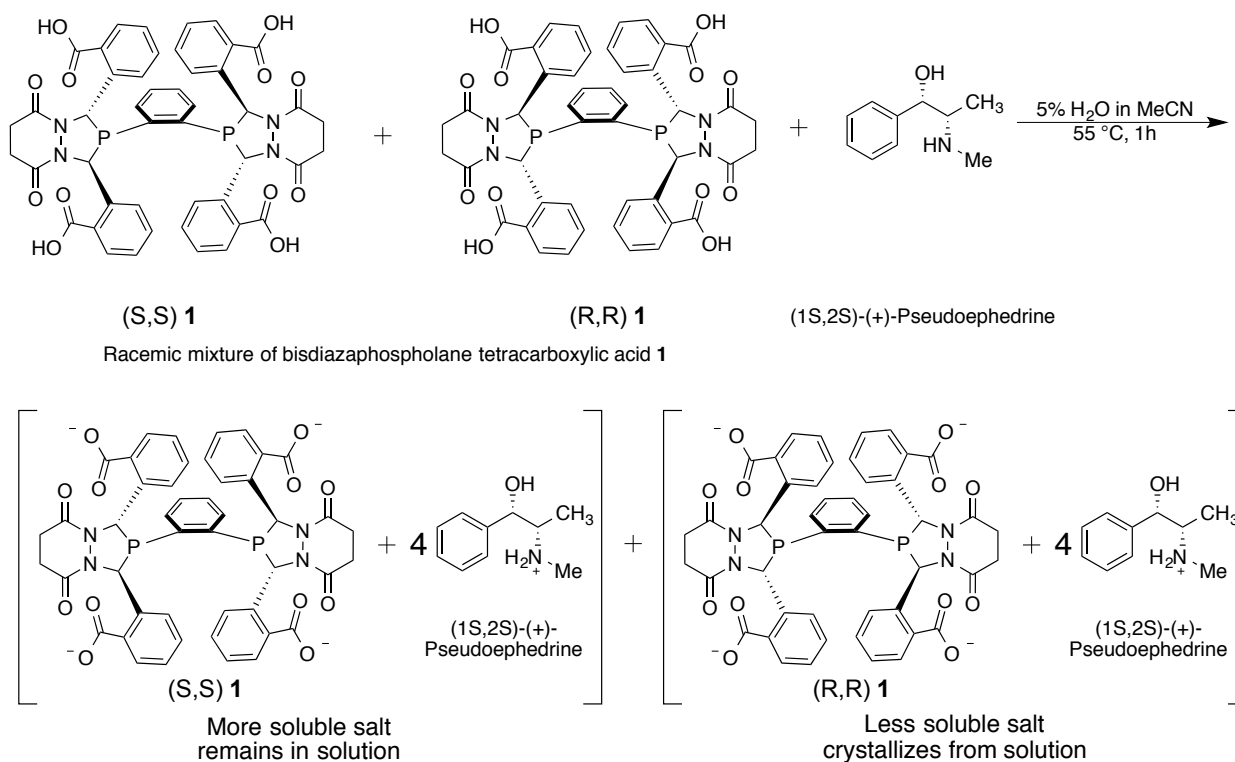
^aGrams of 1,2-*bis*(phosphino)benzene. ^bYield adjusted for mass of coordinated THF after vacuum drying. *Actual yield slightly lower because solvate mass not accounted for.

The revised and scaled up synthesis of tetra-acid on a routine scale allows a bench chemist to reproducibly synthesize grams of the ligand precursor. However, further work in our group involves industrial-scale hydroformylation in a continuous flow reactor, and that necessitates a larger ligand supply than what the 35 mmol scale provides. In collaboration with Eli Lilly, we ran a 297 mmol scale reaction that proceeded to yield 105 g (39.5 % yield, corrected to 36.2% with THF removed, Table 3.2 entry 10). The reaction is run in a 22 L jacketed flask with a chiller set to -10 °C, which provides tight internal temperature control within a range of -8.2 to -6.1 °C over the entire course of succinyl chloride addition, indicating effective control of the exotherm. We expect that the demonstrated scalability and increased yield of tetra-acid synthesis makes it more attractive to chemical suppliers, which we hope will facilitate the commercial availability of bisdiazaphospholane ligands. Additionally, the consumption of ligand in the 23.8 mL continuous flow reactor described in Chapter 5 is about 3.6 mmol per kilogram of alkene. At these *unoptimized* catalyst loadings, the amount of tetra-acid produced by this large-scale reaction would provide enough ligand to convert over 30 kg of 6-methoxy-2-vinyl naphthylene into the naproxen aldehyde.

Figure 3.5: color changes during tetra-acid synthesis

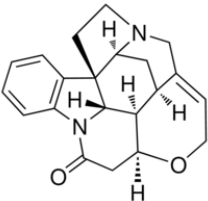
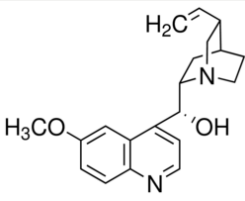
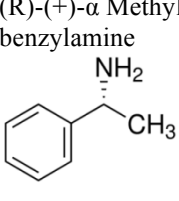
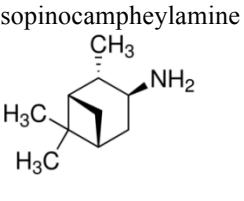
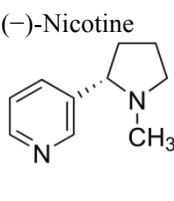
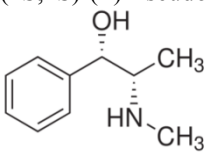
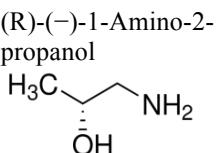
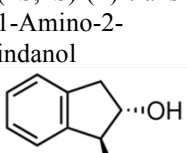
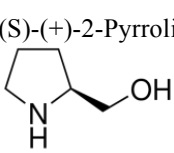
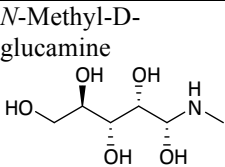
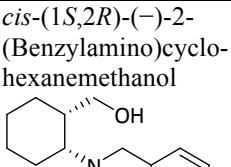
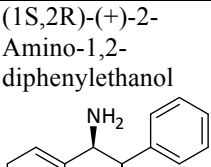
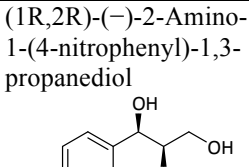
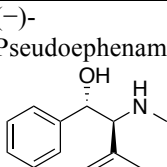
3.3. Classical resolution of racemic tetra-acid with chiral amine bases

The formation of diastereomeric salts with chiral amine bases can give rise to salts with differing solubilities. This property can be utilized to separate enantiomers of either an acidic or basic compound. However, the degree to which the diastereomeric salts differ in solubility is a difficult property to predict, and screening for the correct combination is usually necessary.

Scheme 3.2: Tetra-acid resolution by salt formation.

A library of nine structurally diverse amine bases was screened at Freeslate under a variety of solvent mixtures. The only hit from the initial screen was with pseudoephedrine. Because this is a controlled substance, a follow-up screen was performed with four additional amino alcohols, and later with Myers' analog of pseudoephedrine, pseudoephedrine (Figure 3.6).⁹ None of these additional bases screened yield high selectivity.

Figure 3.6: Chiral amine bases screened for resolution.

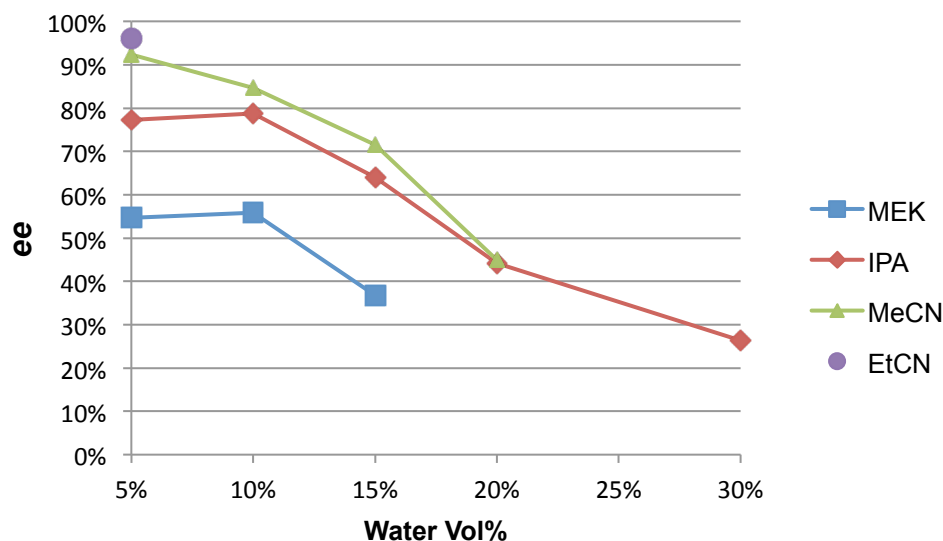
Alkaloids		Chiral Amines		
B1-Strychnine 	Quinine 	(R)-(+)- α Methyl benzylamine 	(1S,2S,3S,5R)-(+)-Isopinocampheylamine 	(-)-Nicotine 
Chiral Amino Alcohols				
(1S,2S)-(+)-Pseudoephedrine 	(R)-(-)-1-Amino-2-propanol 	(1S,2S)-(+)-trans-1-Amino-2-indanol 	(S)-(+)-2-Pyrrolidine methanol 	
Follow-up screen				
N-Methyl-D-glucamine 	cis-(1S,2R)-(-)-2-(Benzylamino)cyclohexanemethanol 	(1S,2R)-(+)-2-Amino-1,2-diphenylethanol 	(1R,2R)-(-)-2-Amino-1-(4-nitrophenyl)-1,3-propanediol 	(-)-Pseudoephedrine 

Screens performed by Freeslate as part of a collaboration with Eli Lilly.

A variety of conditions were also examined by screening. In this secondary screen the equivalents of amine:tetra-acid are determined to give most efficient resolution at a 4:1 ratio (one amine per carboxylic acid). At a 1:1 or 3:1 ratio, no solids form under the screen conditions. At a 2:1 ratio, the solids that crash out are racemic. The solvent mixture is optimized to 5% (v/v)

water in acetonitrile. In all solvent mixtures in the secondary screen, increasing water percentage decreases the *ee* of the isolated solids (Figure 3.7).

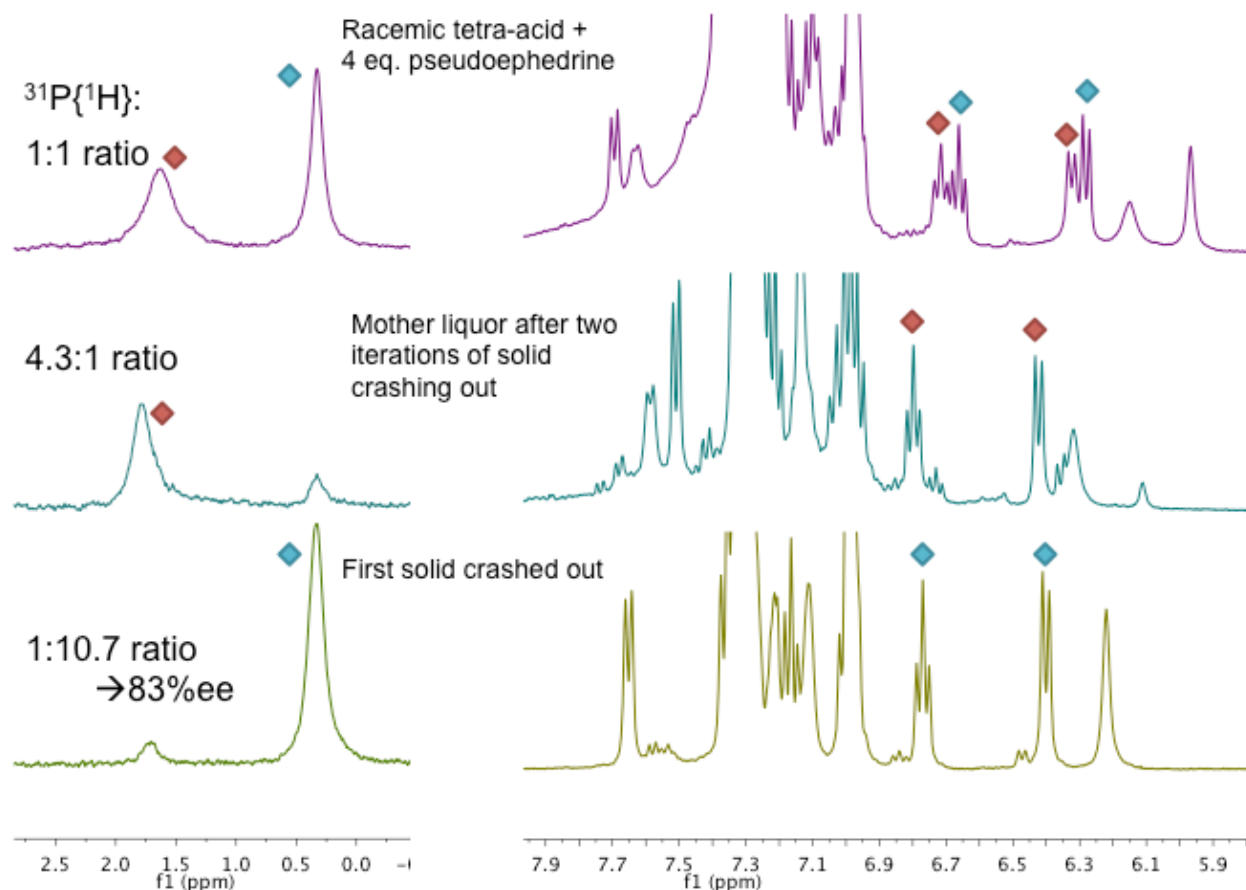
Figure 3.7: *ee* comparison with increase in water % of crystallization solution.



Graph reproduced from a screen by Freeslate. ©2013, Freeslate, Inc.

Compared to the original solvent mixture (10% water in 2-propanol), which gave 80% *ee* after a single crystallization, the optimized solvent mixture gives only one enantiomer within the detection limits of both NMR (of the diastereomeric salt) and HPLC. This avoids further recrystallization steps and simplifies the procedure. Further recrystallizations have little effect on the enantioselectivity of the isolated salt, but washing the crystals obtained in the first crystallization is crucial for the highest *ee*. To confirm this, the purity of material in each fraction of a resolution is examined. The second crop of crystals obtained from resolution are isolated by washing with cold solvent, and this wash material was isolated and found to be only 38% *ee*. The extent of enantioenrichment is easily observed by NMR, as the diastereomers exhibit distinct peaks in the aryl region of the proton and in the ^{31}P NMR (Figure 3.8).

Figure 3.8: ^{31}P and ^1H NMR spectra of diastereomers at each step in a resolution.

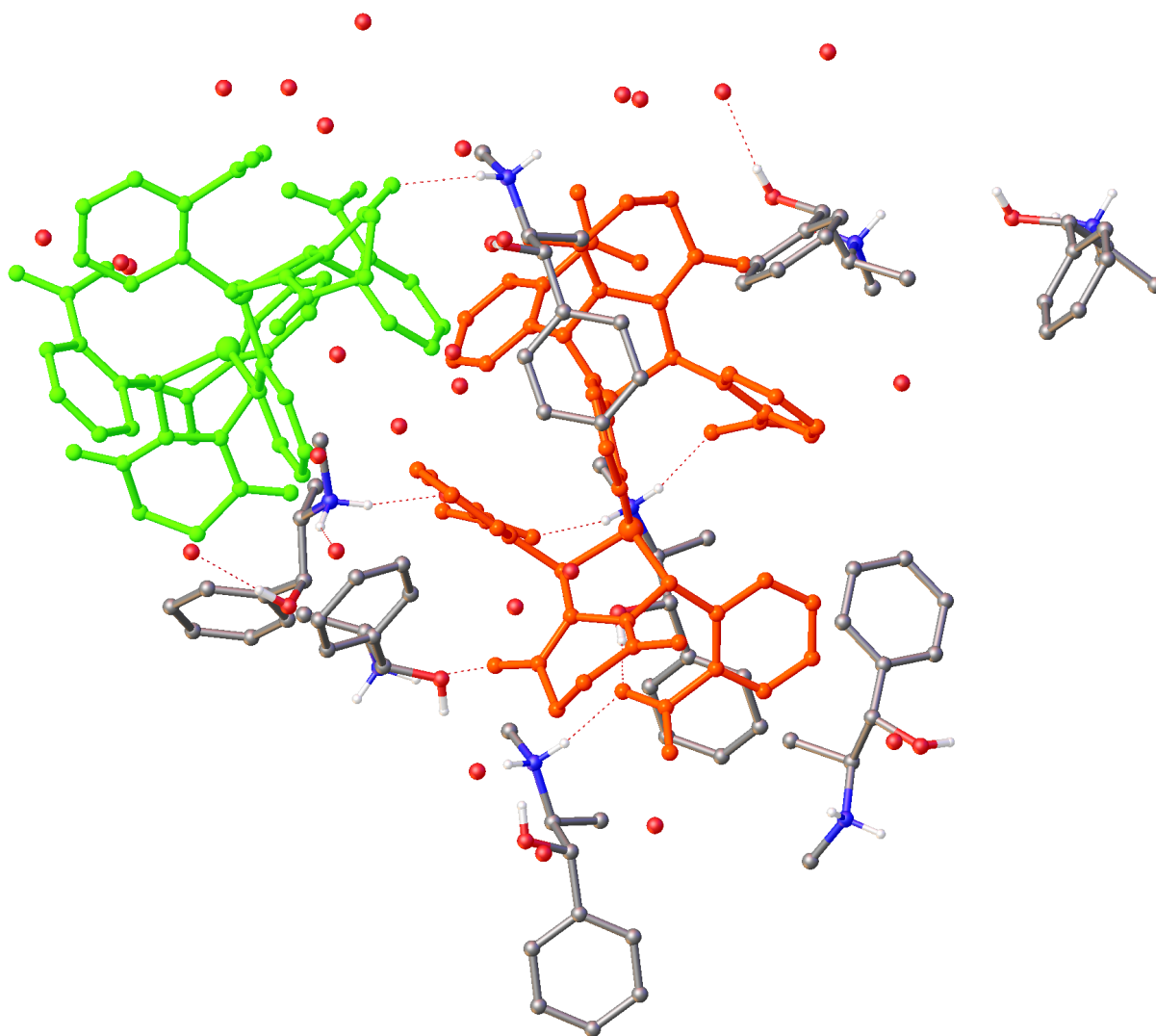


Once the salt of one enantiomer is isolated, a simple dissolution in methanol followed by addition of aqueous 3 M HCl and filtration returns the enantiopure tetra-acid, usually as a hydrate. The potency of this isolated material is typically high (93%), compared to the racemic starting material, which is usually about 75% potent.

We hoped that the crystal structure would provide a model that would allow us to predict the structural motifs needed for enantioenrichment, and thus allow for rational choice of resolving agents to avoid regulated substances. While the crystals formed are large and appear high-quality, even with numerous recrystallizations and multiple data collections on several crystals at different temperatures the data and refinement quality is substandard. The atomic

connectivity and composition of the main molecules have been reliably established, and two independent refinements—one by a macromolecular crystallographer (K. Satyshur) and one by a small molecule crystallographer (I. A. Guzei)—produced the same absolute configuration of the tetra-acid molecules, which also matches the chirality determined by HPLC. However, the refinements were done with numerous restraints and constraints, and it is not possible to identify and properly refine solvent molecules occupying lattice voids. In particular, there is a substantial amount of disorder that can be seen in the water molecules (Figure 3.9).

Figure 3.9: Crystal structure with disordered waters (orange spheres) visible.

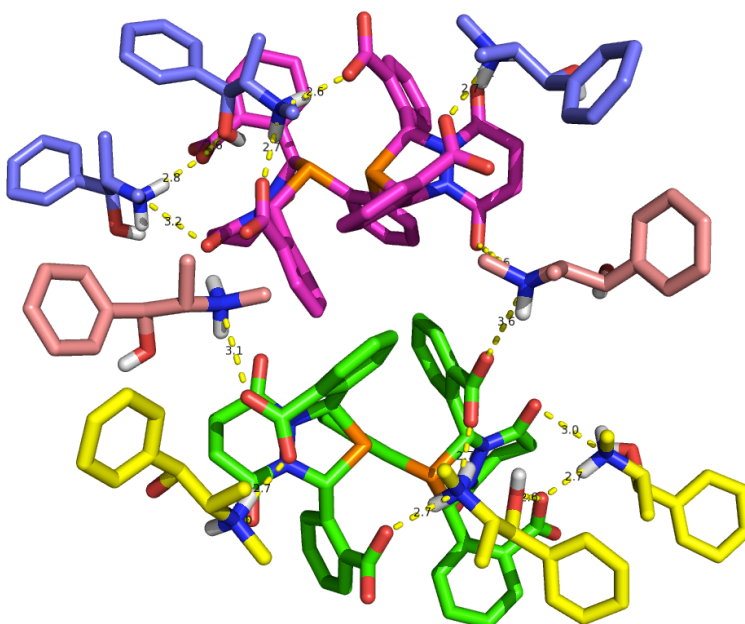


The crystal structure consists of two tetra-acid anions and eight protonated pseudoephedrine cations (Figure 3.10.A). A number of interesting features are worth noting. Each tetra-acid anion has one pseudoephedrine with two hydrogen bonds to the amine moiety, from carboxylates on opposite “arms” of the ligand (Figure 3.10.B). There are also two pseudoephedrine molecules that bridge between tetra-acid molecules, shown in dusty pink in Figure 3.10.A.

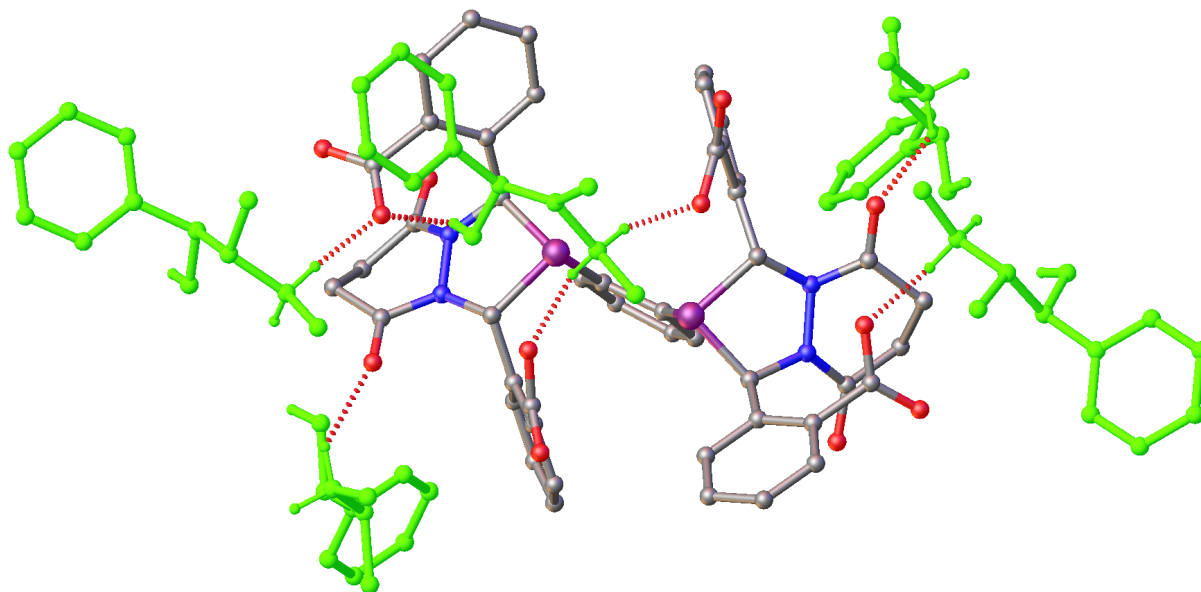
The low data quality and the complexity of the structure led us to abandon the crystal structure as a way to identify other bases that may be viable resolving agents. However, the structure supports the chirality determined by HPLC.

Figure 3.10: Simplified structure of the tetra-acid pseudoephedrine 1:4 salt.

3.10.A: Unit cell (disordered solvent molecules omitted)



3.10.B: detail of hydrogen bonding in a single tetra-acid.

**3.4a. Issues with ligand potency and revised synthesis of ligand**

During the development of AHF in a flow reactor we conducted a number of studies at much lower catalyst loadings than much of our previous work ($S/C > 10,000$). In the course of reducing the catalyst loading, we found that the rate of hydroformylation was far slower than we expected. The origin of the slow reactivity was determined to be the ligand, which is established to be only 32% ligand by mass by quantitative NMR with an internal standard. The problem of “low potency” ligand is widespread, as established by quantitative NMR of all available ligand samples in our group at the time of the discovery (Table 3.3). Multiple batches prepared by identical routes give routinely low potencies (entries 2-4, 6, 9), the racemic tetra-acid precursor is not totally potent (entry 7), but resolved tetra-acid is of high purity (entry 8). Values were originally acquired using standard decoupling (always-on), select values were re-acquired using more accurate inverse-gated (zgig30) decoupling, and are reported here for comparison.

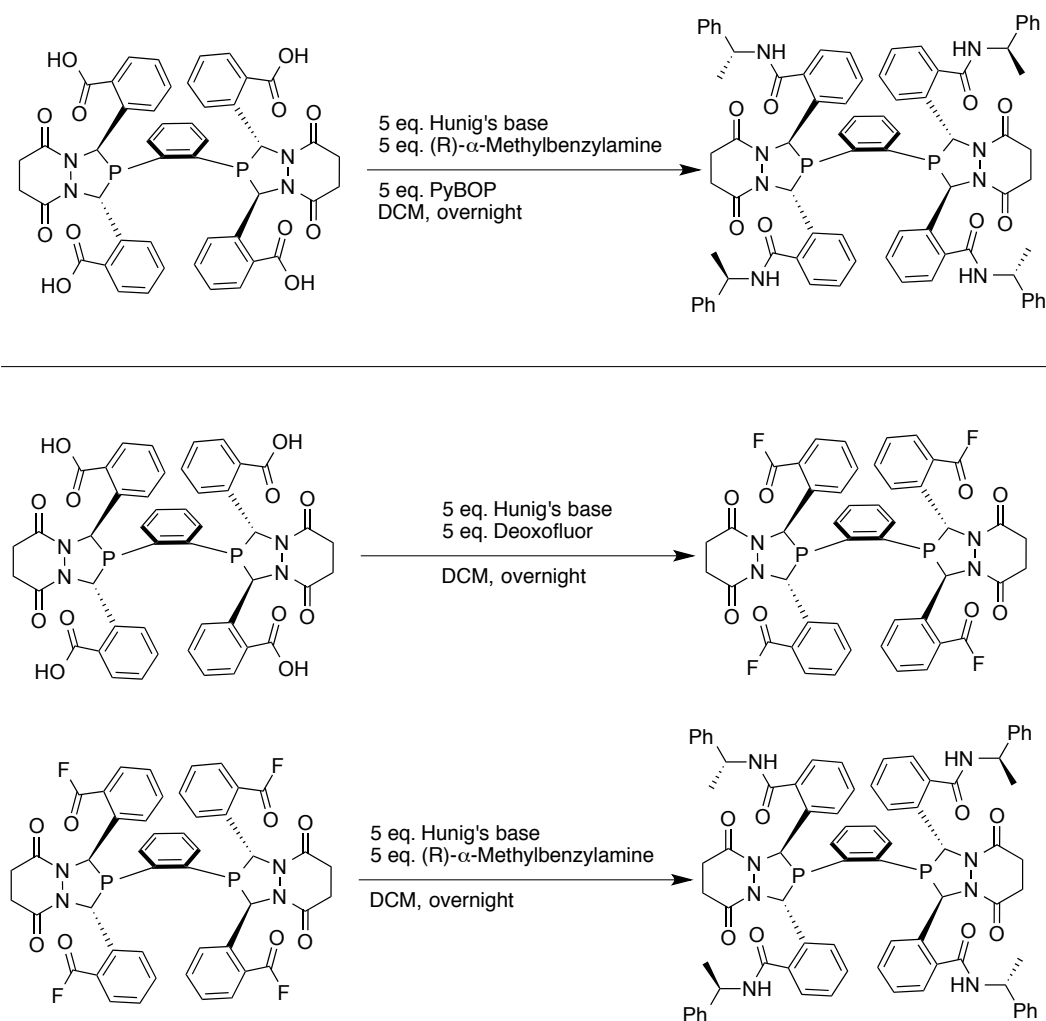
Table 3.3: Potency of ligand samples

Entry	Compound	Notes	NMR ratio / mass ratio (zgpg30)	NMR ratio / mass ratio (zgig30)
1	dppe	97% purity, Alfa control for internal standard	130	96.7
2	R,R,R-BRJ-D	Synthesized by Deoxofluor method	52.4	
3	R,R,R-BRJ-L	Synthesized by Deoxofluor method	45.5	
4	R,R,R-MLA2293	Synthesized from hydrated tetra-acid (Deoxofluor)	56.3	55.0
5	R,R,R-MLA1272	Synthesized from PyBOP coupling method	57.1	53.7
6	Rac tetra-amide, FFA	Synthesized by Deoxofluor method	52.3	
7	Rac t-acid	92.0 wt% based on solvent	53.5	
8	Resolved t-acid Batch 2 (BRJ)	95.9 wt% based on solvent	86.6	90.5 93.0
9	R,R,R-MLA3041	Measured at Lilly	--	34.3
10	MLA3042- Rh cat	Measured at Lilly	29.1 (at WI)	32.6

Beyond the fact that the low potency of the ligand means that reactions run with it may have variable results depending on the batch of ligand, the synthesis (in which we report quantitative yields) is inefficient and costly. To improve the supply of ligand available, we examine various coupling reactions for the ligand to find a high-yielding one and developed a reliable way to purify the ligand.

The original report of ligand synthesis is a coupling using the peptide coupling agent PyBOP.¹ This has recently been improved upon by moving to a synthetic route with an intermediate tetra-acyl fluoride,⁴ which avoids the purification step by column chromatography and allows for coupling of bulkier amides to the tetra-acid backbone, as well as providing higher yields of ligand (Scheme 3.3).

Scheme 3.3: Synthetic routes to bisdiazaphospholane tetra-amide ligands.



Because the improved reactivity of the tetra-acyl fluoride intermediate makes a broad range of bulky substrates accessible, improvement of this synthesis was first examined. The reaction as it was run prior to this study gave quantitative yield by mass but potency values in the

30-55 % range (Table 3.3). As this is a two-step procedure, determination of which step is low-yielding is crucial to understanding how to improve it. Therefore, reaction conditions were modified to attempt improvements in the potency of the final product (Table 3.4). A standard set of conditions based on routine synthesis of the ligand was chosen, and modifications to these conditions were applied to see if they effected any changes in yield and potency. The intermediate tetra-acyl fluoride is also examined in greater detail than during routine synthesis to determine which step is problematic.

This screen of reaction conditions provides little insight into how to modify the synthesis of ligand. There are no major improvements to the previously reported synthesis with any of the modifications made in Table 3.4. However, the potency of intermediate materials suggests that the formation of the tetra-acyl fluoride is the problematic step in the reaction. The yield (by mass) of tetra-acyl fluoride is typically quantitative. However, the potency of this isolated material is in the 40-58% range, much lower than the potency of the initial tetra-acid (top entry). The potency of ligand isolated after the coupling to amine is 42-54%, a much smaller decrease than that seen in the first step. By NMR, an unidentified set of peaks appears at 3.5 ppm, which may be due to byproducts from Deoxofluor®.

Table 3.4: Modifications to acyl fluoride coupling:

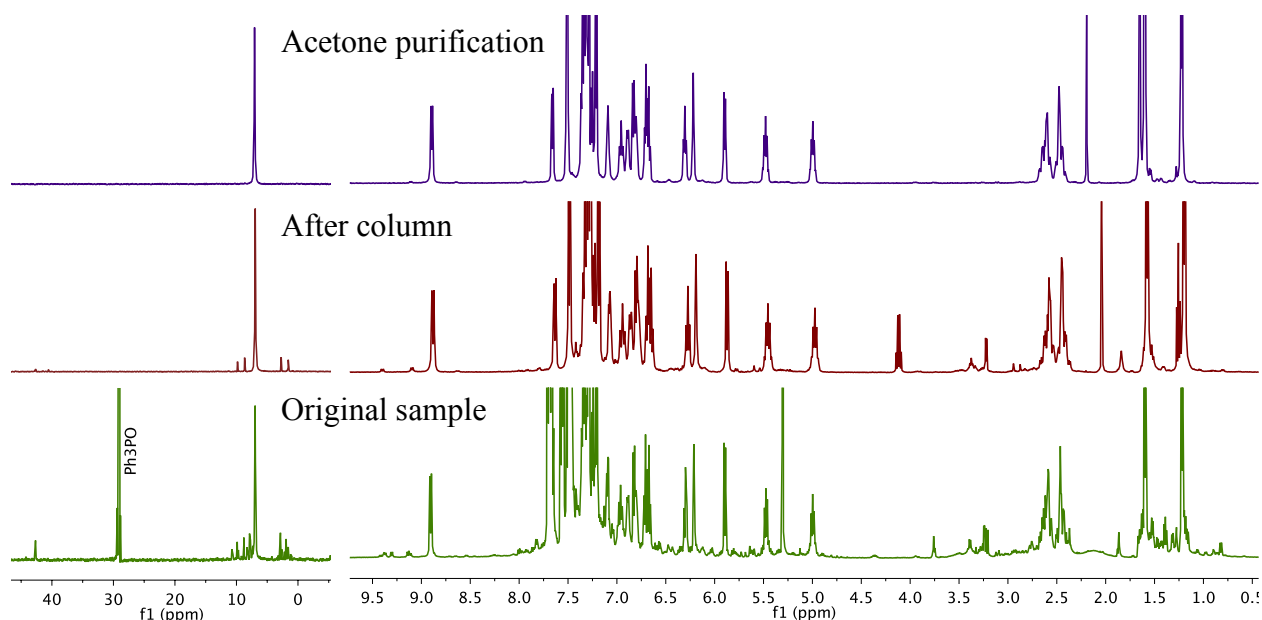
Batch	Condition modified	% Yield Acyl F (by mass)	% Yield Ligand ^a	% Potency Acyl F	% Potency ^b Ligand	Yield x potency
tetra-acid	batch for 1 and 2				88.8	
1-MLA	0 °C	100.4	86.7	54.5	53.5	46.4%
2-BRJ	6.8 mg/mL	96.8	83.2	57.8	48.2	40.1%
3-FFA	8 eq. deoxofluor + amines	89	60.4	47.2	42.5	25.7%
4-JW	dry tetra-acid overnight, extra washes in extraction	97.7	81.8	40.9	43.4	30.3%

^aBased on initial mass of tetra-acid. ^bAdjusted for coordinated solvent.

3.4b. “The acetone trick”: isolation of high-potency ligand

While working on the development of an improved ligand synthesis, our group still needed a source of clean, potent ligand for ongoing research in the field of AHF. Initially, column chromatography was relied on since ligand obtained from PyBOP coupling had previously been purified this way. However, with the improved sensitivity of the routine NMR instruments available in the past few years, we find that ligand purified in this way often contains multiple other phosphine species that were previously unnoticed due to the sensitivity of our routine instruments. After column chromatography, ligand with 52% potency is only upgraded to about 72% potency, and separation of the desired product is incomplete (Figure 3.11).

Figure 3.11: $^{31}\text{P}\{^1\text{H}\}$ and ^1H NMR of ligand sample after various workup techniques.



The limited success of column chromatography led us to search for a different method of purification: crystallization. Earlier work investigating AHF of 1,1-disubstituted olefins required higher catalyst loadings and therefore stock solutions of ligand at higher concentrations. At 55 mM in acetone the ligand was found to crash out of the stock solution after a short period of time. When attempting a recrystallization in a mixed acetone-hexane system, small crystals form on the side of the flask after acetone addition. Afterward, the entire solution becomes homogeneous briefly before crashing out a flocculent white solid, which is pure ligand. This technique is repeated with just acetone as the recrystallization solvent, and works best with a concentration of about 20 mg/mL of impure ligand in acetone. Recovery in the first two crops of crystals is 81% of the mass expected based on potency of the starting material. The isolated material is typically 90-95% pure. Recrystallizations that are too concentrated lead to some impurities crashing out, and more dilute leads to lower recovery. In addition, this method is effective for purification of

the crude material from ligand synthesis via T3P coupling and for purification of the racemic tetrabenzylamide ligand analog.

The original impetus for this project was difficulty in creating a large supply of ligand to support development of large-scale AHF. The difficulty encountered in providing this stockpile of ligand led to a number of improvements and insights into the ligand synthesis. In particular: the NMR of the azine starting material is more fully characterized, the synthesis of tetra-acid has been re-optimized for improved yield and demonstrated on a 300 mmol scale, the enantiomers of C_2 -symmetric tetra-acid can be resolved by classical resolution instead of preparative SFC, the purity of ligand and precursors can be quantitatively assessed by potency, and the purification of ligand can be simplified by a recrystallization. New, higher-yielding routes for the synthesis of tetra-amide ligands are under development as a result of these studies.

3.5. Experimental.

General considerations.

All reactions carried out in Schlenk flasks are performed under an atmosphere of nitrogen and open to an oil bubbler. THF is purchased from Aldrich and distilled from Na^o/benzophenone prior to use. DCM is purchased from Aldrich and purified by house-built solvent columns packed with alumina prior to use. HCl solutions were prepared from deionized tap water and conc. hydrochloric acid. Succinyl chloride is vacuum distilled prior to use. All other reagents were purchased from the suppliers listed below and used as received. NMR spectra were recorded at ambient temperature unless otherwise noted on Bruker AC-300, Avance III 400, or Avance III 500 spectrometers. ¹H and ¹³C NMR chemical shifts were referenced to tetramethylsilane if present or residual solvent. ³¹P and ¹⁹F NMR chemical shifts were referenced to TMS in the proton spectrum using the unified scale. ¹H NMR splitting patterns were designated as singlet (s), doublet (d), triplet (t), quartet (q), doublet of doublets (dd), apparent (ap), broad (br). First-order splitting patterns were assigned on the basis of the multiplet. Splitting patterns that could not be interpreted are designated as multiplet (m) or broad (br).

Reagent	CAS	Small Scale	Large Scale
Ethanol	64-17-5	Pharmco-Aaper (95%)	Decon (200 proof)
2-carboxybenzaldehyde	119-67-5	Aldrich	TCI (>98%)
Hydrazine monohydrate	7803-57-8	Aldrich	Acros (35% hydrazine, 55% hydrate)
THF	109-99-9	Aldrich	Fisher
1,2-bis(phosphino)benzene	80510-04-9	Strem	Strem
Succinyl chloride	543-20-4	Aldrich	Acros (95%)
Acetonitrile	75-05-8	Aldrich	N/A
Water	7732-18-5	Deionized tap	N/A
(S,S)-pseudoephedrine	90-82-4	Aldrich	N/A

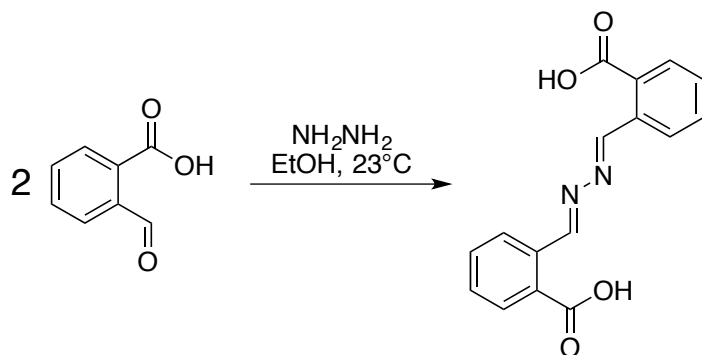
Methanol	67-56-1	Macron Fine Chemicals	N/A
HCl (3 M)	7647-01-0	Aldrich	N/A
DCM	75-09-2	Aldrich	Fisher (99.9%)
Diisopropylethylamine	7087-68-5	Aldrich	Aldrich
Propyl phosphonic acid anhydride (T3P)	68957-94-8	Aldrich	Aldrich
(R)- α -methylbenzylamine	3886-69-9	Aldrich	Fluka
(S)- α -methylbenzylamine	2627-86-3	Aldrich	Fluka
HCl (1 M)	7647-01-0	Aldrich	Red Bird Services
Acetone	67-64-1	Aldrich	Mallinkrodt (99.5%)
Triphenylphosphine oxide	791-28-6	Aldrich	Aldrich (99.8%)

Safety.

1,2-*Bis*-(phosphinobenzene) is highly pyrophoric. This compound should be left in the ampule until immediately before use, where it should be loaded into a syringe inside a glovebox or glovebag. Remaining material should be stored under inert atmosphere. All items coming in contact with the phosphine should be placed into a bleach bath.

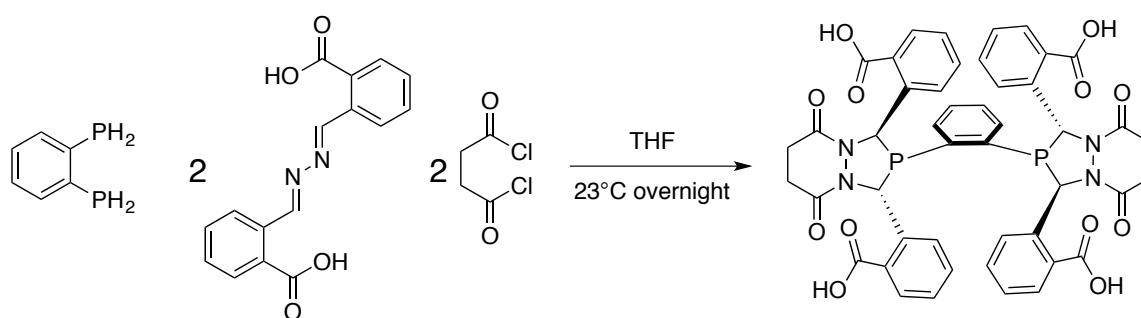
Pseudoephedrine is a List 1 substance under the Title 21 Code of Federal regulations.

Synthesis of 2,2'-(Azinodimethylidyne)bis-benzoic acid.



2-Carboxybenzaldehyde (31.63 g, 210.7 mmol) was dissolved in 300 mL of 95% ethanol in a large beaker. Hydrazine monohydrate (5.1 mL, 5.2g, 105.1 mmol) was added dropwise to the stirred solution and the resulting yellow suspension was stirred 1 hour at room temperature (21 °C). The reaction mixture was vacuum filtered through qualitative filter paper using a Buchner funnel connected to an aspirator. The filter cake was dried under vacuum (60 mtorr) for one hour to yield the azine as a yellow solid (29.70 g, 95%).

Revised bench-scale synthesis of tetra-carboxylic acid (rel-2,2',2'',2'''-(1,2-phenylenebis((1*R*,3*R*)-tetrahydro-5,8-dioxo-1*H*-(1,2,4)diazaphospholo(1,2-*a*)pyridazine-2,1,3(3*H*)-triyl))tetrakis-benzoic acid).



2,2'-(Azinodimethyldiyl)bis-benzoic acid (Note 1) (20.88 g, 70.47 mmol) was added to an oven-dried single-necked 1 L round-bottom Schlenk flask equipped with a Teflon-coated stirbar, glass stopcock and a rubber septum. The flask was then subjected to three cycles of evacuation followed by refilling with nitrogen to remove air (Note 2). Dry, inert THF (500 mL) (Note 3) was added via cannula transfer from an inert bomb flask, then the bis(phosphino)benzene (5.0 g, 35.2 mmol) was added via syringe (Note 4). The flask was submerged in a 0 °C ice-water bath and allowed to cool at least 20 minutes. Succinyl chloride (11.7 mL, 16.4 g, 106 mmol) (Note 5) was then added dropwise via syringe, slowly, over 50 minutes to control the resulting exotherm

(Note 6). Reaction mixture turns directly from a yellow suspension to a white suspension, usually by the end of this step but always within a few hours after addition is complete. The reaction was stirred under N₂ overnight at room temperature (Note 7), allowed to settle 1-2 hours, then vacuum filtered through qualitative paper on a large Buchner funnel, rinsed with additional THF, and dried under vacuum (60 mtorr) to yield a white solid (14.4489 g, 45.7%; 12.365 g (39.1%) tetra-acid when solvate accounted for) (Note 8, 9).

Note 1: Prepared by above procedure.

Note 2: The evacuation/refill cycles should be done slowly because the solid azine is very powdery.

Note 3: The THF was purchased from Aldrich Chemical Co. and distilled over Na^o/benzophenone in a nitrogen atmosphere prior to use. The concentration of the reaction influences the yield: the optimized concentration is 100 mL THF for every gram of phosphine used.

Note 4: Bis(phosphino)benzene was purchased from Strem, neat, and the full contents of the 5 g ampoule were pulled into a syringe inside a nitrogen-filled glovebox (a glovebag can also be used but any remaining phosphine stored in a glovebag will deteriorate more quickly). The ampoule was then rinsed with THF (2x1 mL) and the resultant solution pulled into the same syringe as the rest of the phosphine. The use of a sealed secondary carrying container to transfer the phosphine to the fume hood in which the reaction is set up is highly recommended because of the stench of the phosphine.

Note 5: Succinyl chloride (95%) was purchased from Aldrich, vacuum distilled, and degassed prior to use. It should be stored in a bomb flask covered in tinfoil, and appear as a colorless liquid. Using 3 equivalents of succinyl chloride tends to give higher, more reproducible yields.

Note 6: The addition of succinyl chloride is highly exothermic and should be done more slowly at the beginning of the addition time period. For example, the first mL of succinyl chloride should be added over the first 15 min, the next 3 mL over the next 15 min, then the remainder over the last 20 min. Alternatively, the use of a syringe pump and the addition procedure described in the large-scale synthesis can be employed.

Note 7: "Overnight" is typically 16-24 hours. Leaving the mixture for longer has no known deleterious affect, provided the flask is still air-free.

Note 8: Yields (after drying under vacuum) are in the 30-46% range for this synthesis. However these numbers do not account for the THF (or other solvent) that remains coordinated to the product. After two rounds of drying there is typically about 1.6 equivalents of THF (observed by NMR).

Note 9: If the ligand becomes oxidized, the phosphine oxide shows up at δ 55.78 ppm in the ^{31}P NMR spectrum (in DMSO).

Large-scale synthesis of tetra-acid (rel-2,2',2'',2'''-(1,2-phenylenebis((1*R*,3*R*)-tetrahydro-5,8-dioxo-1H-

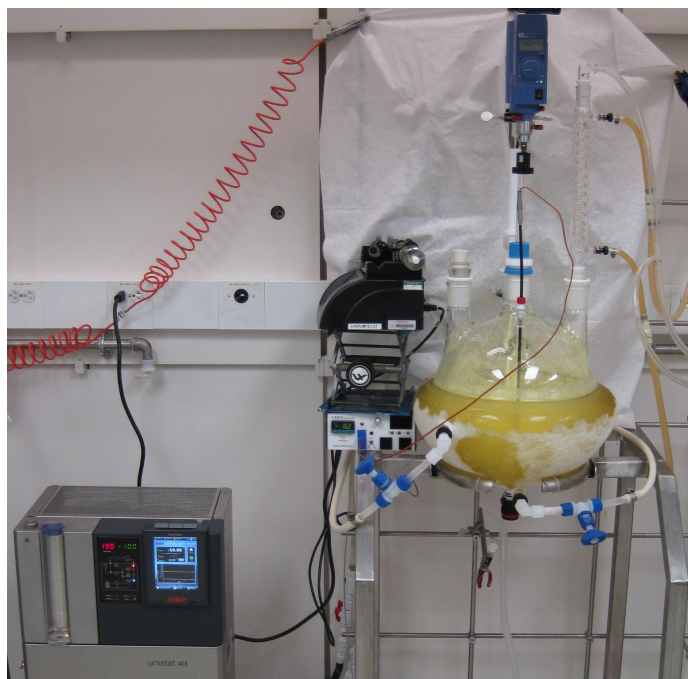
(1,2,4)diazaphospholo(1,2-*a*)pyridazine-2,1,3(3H)-triyI))tetrakis-benzoic acid).

Note: Performed at Eli Lilly

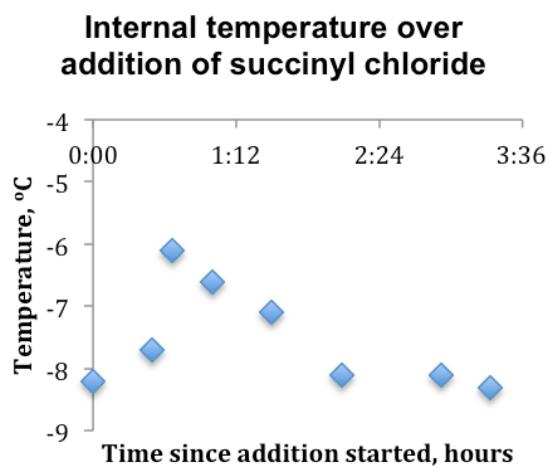
The reaction is run in a 22 L, half-jacketed flask with a bottom valve, four necks and a thermocouple port. The four necks are equipped with an Ika Werke overhead stirrer, a baffle for

improved stirring, a nitrogen inlet on top of a condenser, and a reducing adapter with a septum (Note 1). 2,2'-(Azinodimethyldiynyl)bis-benzoic acid (179.9 g, 607 mmol) was suspended in 4700 mL THF (10% additional volume was added to account for solvent loss overnight) and the resulting yellow suspension was allowed to stir at 160 rpm under nitrogen overnight (20 h) at room temperature to degas. In the morning the reaction was cooled to -8.2 °C with a Huber Unistat 405 chiller connected to the jacket and set to -10 °C. Bis(phosphino)benzene (43.02 g, 303 mmol) was added to the stirring slurry dropwise over 5 minutes with no temperature change. The syringe was then rinsed with 15 mL of degassed THF and this was added to the reaction. Succinyl dichloride (100 mL, 897.5 mmol) is added via syringe pump, set to add at 25 mL/hour and actually added at 28.6 mL/hour (3.5 hour addition). Temperature is maintained within the range of -8.2 to -6.1 °C over the course of the addition (Note 2). As succinyl chloride is added, the reaction remains heterogeneous but changes from a yellow suspension to a white suspension. Upon complete addition of succinyl chloride, the rate of stirring is increased to 267 rpm to wash down solids stuck on the wall of the flask above the liquid level. An hour after succinyl chloride addition was complete, the rate of stirring was reduced to 150 rpm, the chiller was turned off, and the temperature allowed to rise to room temperature overnight. After stirring for 20 hours, the solid was drained through the bottom port on the reaction flask, and the flask was rinsed with THF (500 mL). The solids were vacuum filtered on a polypropylene pad and rinsed with 2 x 1.6 L THF. The solids were allowed to dry on the filter for 45 min with vacuum pulling air through the filter cake. The product was broken up to yield a granular powder and dried in a vacuum oven set to 40 °C and 88.9 mmHg for 24 hours. Yield = 105.2 g (39.5%) of a white solid (96.4 g (36.2 %) yield when THF solvate mass (1.2 molar equivalents) seen by NMR is subtracted).

Note 1: Large scale tetra-acid synthesis reaction setup



Note 2: Temperature changes over succinyl chloride addition are graphed below. No temperature change is observed during the first 20 minutes.



Screens of bases and solvent conditions for classical resolution of tetra-acid (run by Freeslate).

Screening procedure:

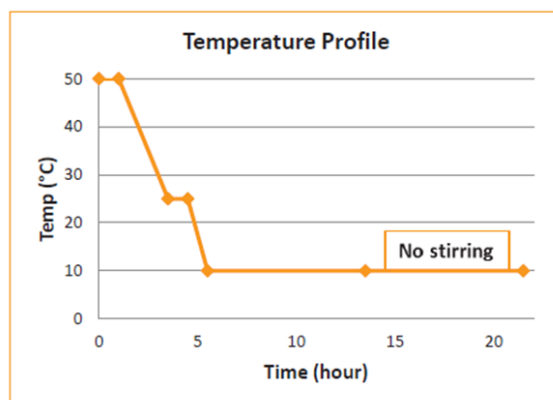
Salt formation (Day-1):

- Powder dispense Racemic tetra-acid in appropriate vials of 8x12 array (96-1mL vials) using Powdernium according to the library design.
 - The targeted amount of material in each vial is 20 mg, 22.25 μmol ;
- Add stir bars;
- Dispense counter ion (amine) solutions, 1.0 eq., in 500 μL of MeOH;
 - Strychnine did not dissolve in MeOH and was added manually as a slurry.
- Seal the plate and stir at 50 $^{\circ}\text{C}$ for 2 h;
- Remove the solvents under Genevac, followed by high vacuum.

Solvent Dispense and Solubility Study (Day-2):

- Dispense resolution solvents according to the library design (500 μL / well);
- Seal the plates and run the temperature profile.

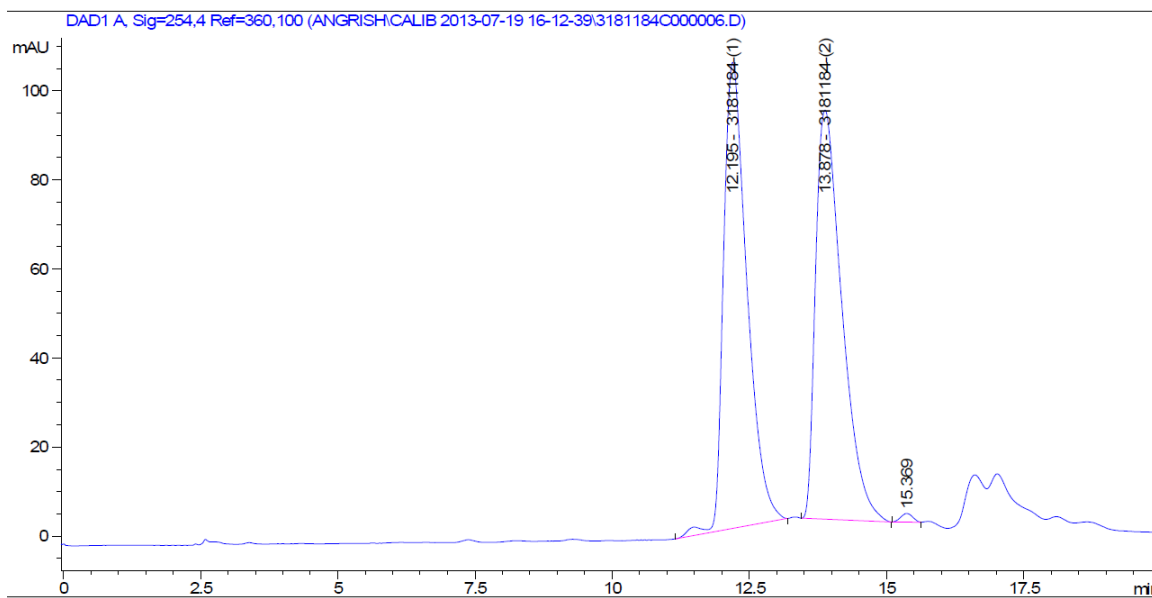
Temperature profile for screen of bases for classical resolution:



Graph reproduced from a screen by Freeslate. ©2013, Freeslate, Inc.

Filtration and Visual Observation (Day 3):

- Centrifuge the plates briefly and place back on the deck at the equilibration temperature for 5 minutes without stirring;
- Using a four-tipped needle assembly transfer supernatant to a sealed filtration assembly;
 - After filtration, Master plate opened and visual observation noted;
- Remove aliquots of filtrate (40 μ L) and diluted to an appropriate concentration for HPLC analysis. Prepare two dilution plates (10x and 100x) by serial dilution using Reagent alcohol.
- Visually observe the master plate.
 - If crystalline: analyze supernatant by HPLC. Chiralpak AD-RH (4.6 x 150mm, 5.0 μ m) Mobile Phase: A: H₂O (+0.08% TFA), B: MeOH (+0.08% TFA), ramp 30% B to 50% B over 15 min, hold at 50% B for 3 min. 0.8 mL/min, Column Temp: 30 °C, Injection volume of 5 μ L, Detection at 254 nm. Peaks at 12.2, 13.9 min.

**Screen 1:**

- **8 Different Solvents/Solvent Mixtures (S)**

- A. MEK
- B. MEK: H₂O (9:1)
- C. EtOH: Heptane (3:1)
- D. IPA: H₂O (9:1)
- E. THF: H₂O (9:1)
- F. THF: MeOH (1:1)
- G. EtCN: H₂O (9:1)
- H. EtOAc

- **9 Different Chiral Amines**

- 1. Strychnine
- 2. Quinine
- 3. (R)-(+)- α -Methylbenzylamine
- 4. (1S,2S,3S,5R)-(+)-Isopinocampheylamine
- 5. (-)-Nicotine
- 6. (1S,2S)-(+)-Pseudoephedrine
- 7. (R)-(-)-1-Amino-2-propanol
- 8. (1S,2S)-(+)-trans-1-Amino-2-indanol
- 9. (S)-(+)-2-Pyrrolidinemethanol

- Screening Conditions:
- Racemic tetra-acid: 20 mg, 22.25 μ mol
- Chiral amine: 2.0 - 4.0 eq., 44.5 - 89 μ mol
- MeOH: 500 μ L (salt formation)
- Solvents/Solvent Mixtures: 500 μ L Concentration: 40 mg/mL, 0.045 M

To read the following tables, compare the relative concentrations of peak 1 (first table) with those of peak 2 (second table). A large difference indicates the resolution conditions will produce enantioenrichment.

Key:

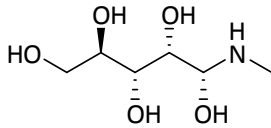
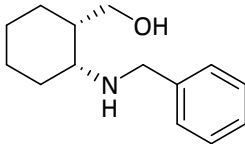
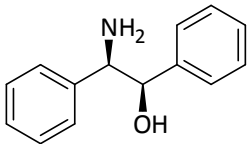
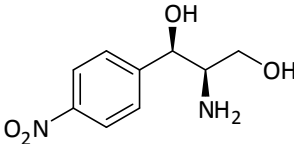
Acid: Base ratio		1:4									1:2		
Chiral Resolving Agents		B1	B2	B3	B4	B5	B6	B7	B8	B9	B1	B4	B8
		1	2	3	4	5	6	7	8	9	10	11	12
8-Solvents	A												
	B												
	C												
	D												
	E												
	F												
	G												
	H												

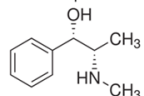
Concentration of 3181184-(1) Retention time 13 min													
	Solvent(s)	1	2	3	4	5	6	7	8	9	10	11	12
A	MEK	0.9	18.0	1.4	9.0	0.8	2.2	0.3	ND	ND	1.0	6.7	0.4
B	MEK: H ₂ O (9:1)	4.1	19.0				4.7						
C	EtOH: Heptane (3:1)	1.2				1.5					1.1		9.8
D	IPA: H ₂ O (9:1)	3.8				5.5	1.8				3.6		20.7
E	THF: H ₂ O (9:1)	11.5				1.1	4.7						
F	THF: MeOH (1:1)	9.1				0.6							
G	EtCN: H ₂ O (9:1)	2.0	12.2		21.6		ND				4.8		
H	EtOAc	0.3	5.0	ND	2.2	ND	0.6	ND	ND	ND	0.4	1.0	ND

Concentration of 3181184-(2) Retention time 14 min													
	Solvent(s)	1	2	3	4	5	6	7	8	9	10	11	12
A	MEK	0.8	17.6	1.1	10.9	0.8	1.9	ND	ND	ND	0.9	7.9	0.4
B	MEK: H ₂ O (9:1)	4.1	19.8				20.7						
C	EtOH: Heptane (3:1)	1.2				1.5					1.0		10.9
D	IPA: H ₂ O (9:1)	3.8				5.7	21.7				3.3		21.5
E	THF: H ₂ O (9:1)	8.4				1.6	13.6						
F	THF: MeOH (1:1)	1.3				0.7							
G	EtCN: H ₂ O (9:1)	1.8	10.4		21.9		4.0				4.0		
H	EtOAc	0.3	4.4	ND	2.4	ND	0.4	ND	ND	ND	0.4	1.2	ND

Hits

Screen 2:

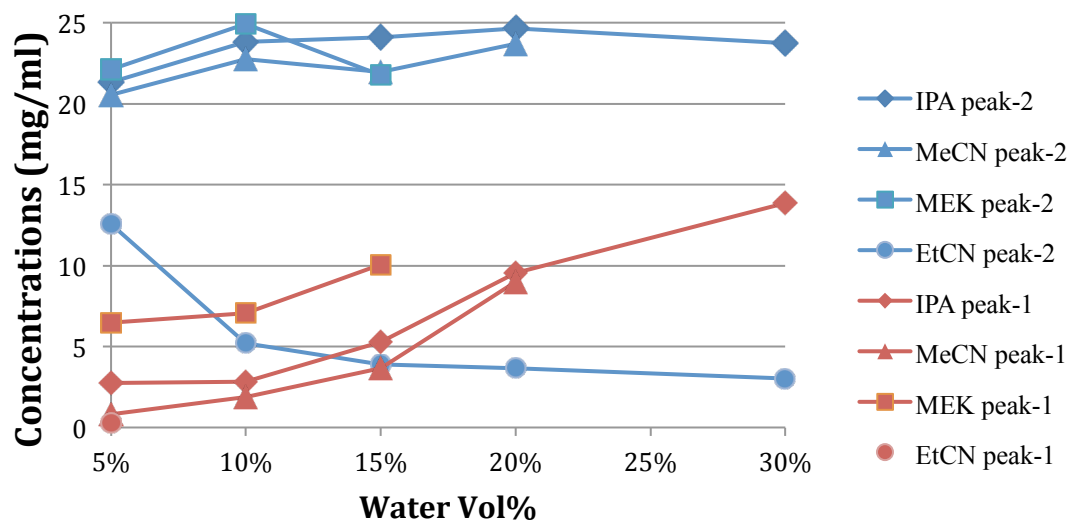
Amine 1	Amine 2	Amine 3	Amine 4
			
<i>N</i> -Methyl-D-glucamine	<i>cis</i> -(1 <i>S</i> ,2 <i>R</i>)-(-)-2-(Benzylamino)cyclohexanemethanol	(1 <i>S</i> ,2 <i>R</i>)-(+)-2-Amino-1,2-diphenylethanol	(1 <i>R</i> ,2 <i>R</i>)-(-)-2-Amino-1-(4-nitrophenyl)-1,3-propanediol

		1	2	3	4	5	6	7	8	9	10	11	12
		Water vol%					(1S,2S)-(+)-Pseudoephedrine eq.			Resolving Agents			
		5%	10%	15%	20%	30%	1:1	1:2	1:3	Amine 1	Amine 2	Amine 3	Amine 4
A	Acetone	<div>1:4 TetraAcid : (1S,2S)-(+)-Pseudoephedrine</div> <div></div>					10 vol% Water			1:4 TetraAcid : Amine; 10 vol% Water			
B	MEK												
C	MeOH												
D	EtOH												
E	IPA												
F	MeCN												
G	EtCN												
H	THF												
Concentration of 3181184-2 Retention time 14 min													
	Solvent	3	2	3	4	5	6	7	8	9	10	11	12
A	Acetone						4.05			ND			1.02
B	MEK	22.13	24.91	21.75			13.98						2.52
C	MeOH						8.66						
D	EtOH						8.19			1.50			1.43
E	IPA	21.33	23.82	24.10	24.67	23.76	2.98			ND		21.79	1.94
F	MeCN	20.55	22.77	21.95	23.69					ND			
G	EtCN	12.56	5.20	3.90	3.67	3.01	7.38		14.79	ND			ND
H	THF						1.47	2.98		ND			
Concentration of 3181184-(1) Retention time 13 min													
	Solvent	1	2	3	4	5	6	7	8	9	10	11	12
A	Acetone						4.16		ND				1.26
B	MEK	6.48	7.05	10.06			14.10						2.21
C	MeOH						8.63						
D	EtOH						8.24			1.41			1.64
E	IPA	2.73	2.84	5.30	9.53	13.85	3.03			ND		21.24	1.80
F	MeCN	0.82	1.89	3.64	9.00					ND			
G	EtCN	0.25	ND	ND	ND	ND	7.36		0.68	ND			
H	THF						1.97			ND			

Blank wells = Fully soluble

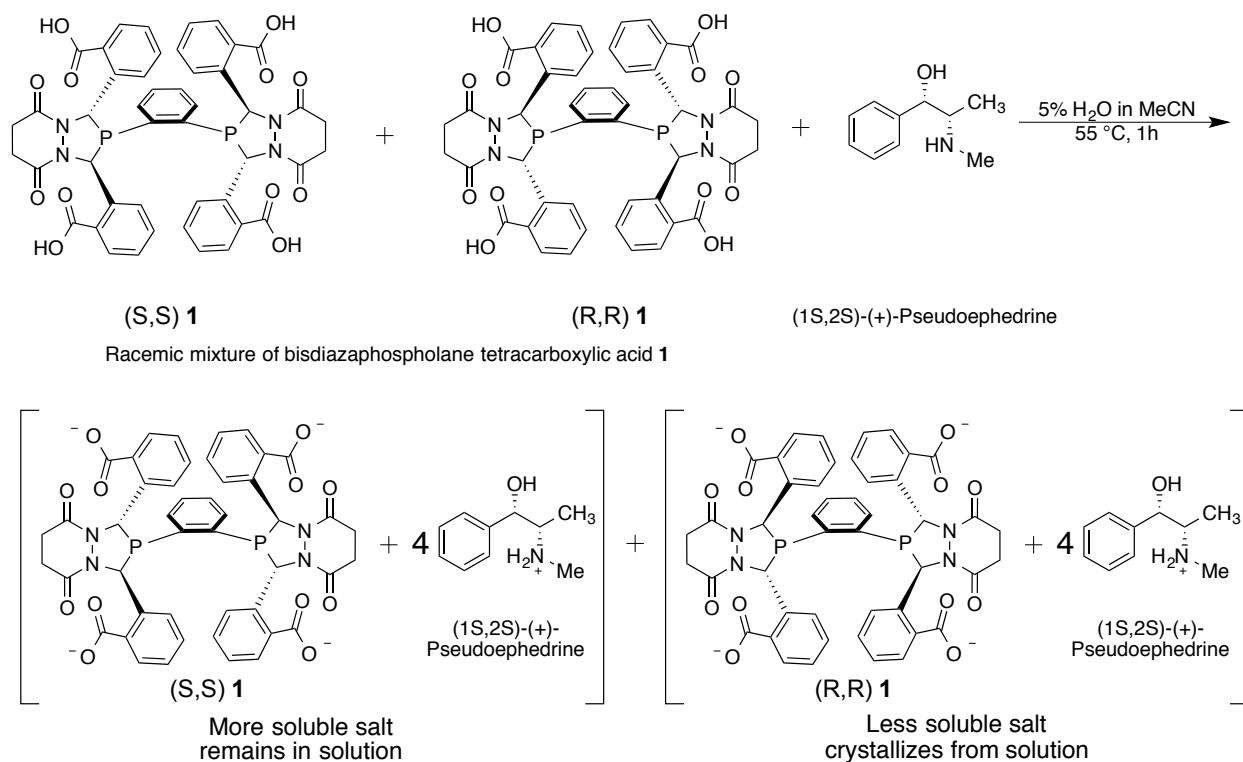
Role of water in separation efficiency:

HPLC peak area vs. % water in resolution solvent



Graph reproduced from a screen by Freeslate. ©2013, Freeslate, Inc.

Classical resolution of *rac* tetra-acid with pseudoephedrine.



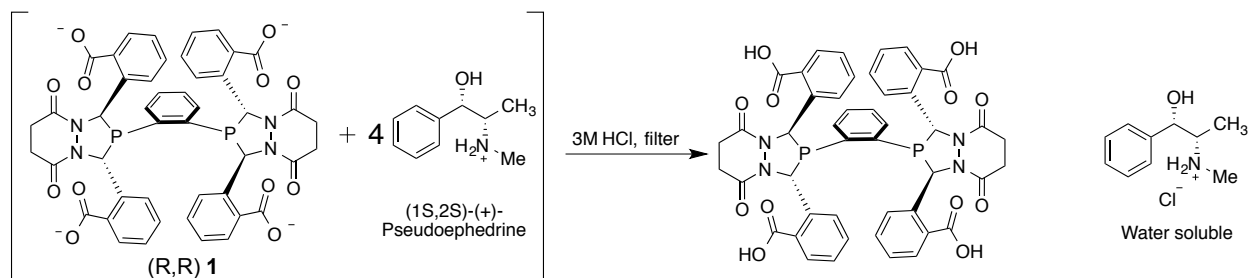
Rac tetra acid (10.02 g, 11.15 mmol) and (+)-(S,S)-pseudoephedrine (7.309 g, 44.24 mmol) were combined in a 1 L Erlenmeyer flask. 432 mL of a solution of 5% H₂O in MeCN was added and the mixture was heated in a warm water bath to 55 °C and swirled until a clear yellow solution formed. Once the solution was fully homogeneous, it was allowed to stand at 55 °C with occasional swirling for one hour, then the heater to the water bath was switched off and it was allowed to stand undisturbed and cool to room temperature overnight (16 h). Clumps of crystals (see below) form overnight, and are isolated by decanting the mother liquor and rinsing the solids with 5% H₂O in MeCN cooled to 0 °C (2 x 10 mL). The crystals are dried under a gentle stream of N₂ to yield a first crop of 4.715 g (60.4% yield) white crystals. The mother liquor is allowed to stand for an additional 3 days in the fridge (5 °C), during which a second batch of

smaller, discrete crystals form. The mother liquor is also decanted from these, and they are washed with cold 5% H₂O in MeCN (2 x 10 mL) to yield an additional 0.583 g (6.7%, 67.1% overall yield) of (R,R)-tetra-acid salt. The mother liquor is retained for isolation of the other enantiomer of salt.

Crystal morphology in the first crop, isolated from 5% H₂O in MeCN.



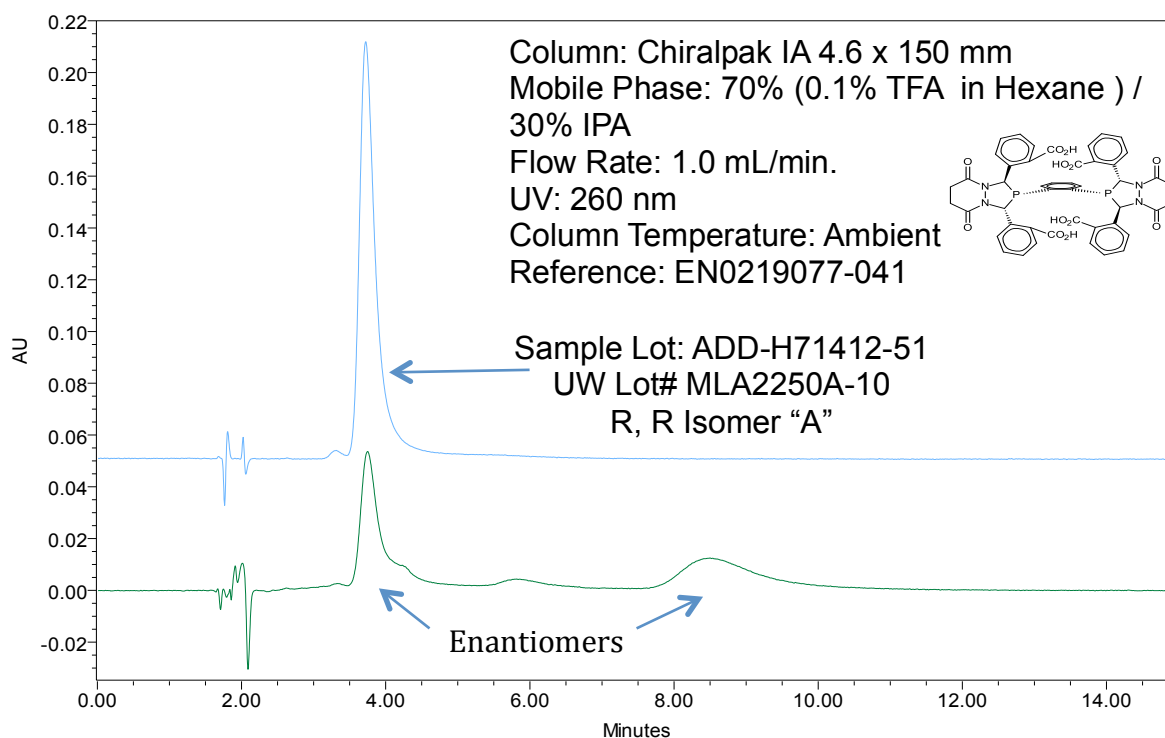
Isolation of free (R,R) tetra-acid.



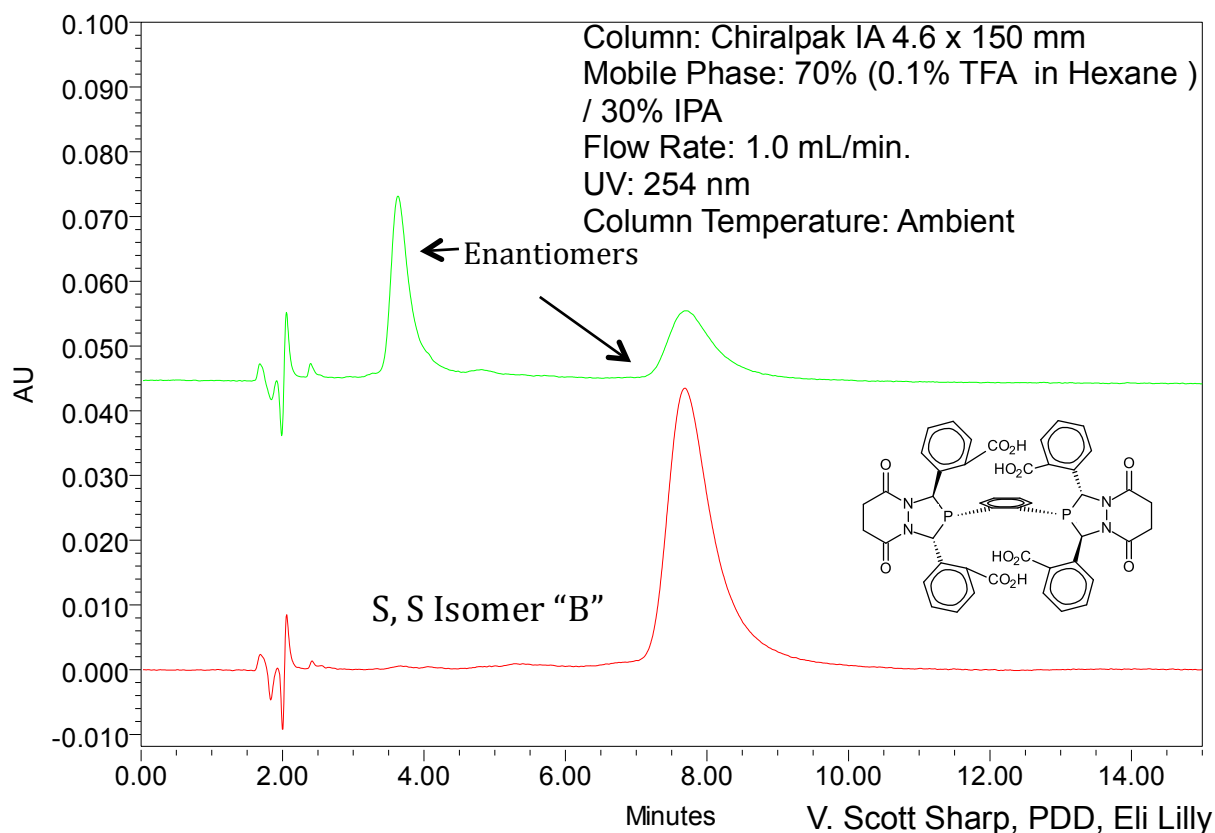
The diastereomeric salt from above (1.964 g, 1.26 mmol) was dissolved in a minimal amount of methanol. To this solution 3 M aq. HCl is added (300 mL), and a white solid forms. The solid is vacuum filtered through qualitative paper two times, washed with water (3 x 100 mL), and dried under vacuum to yield a white solid (0.982 g, 86.5%).

By NMR, no pseudoephedrine remains. HPLC shows only the (R,R) enantiomer of tetra-acid.

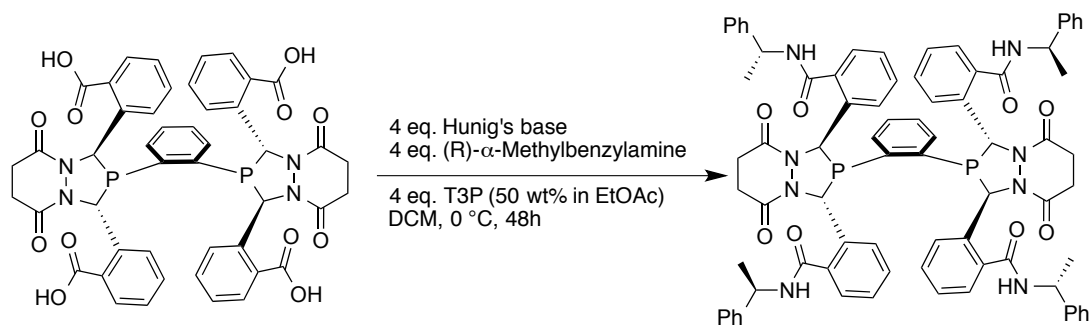
HPLC of classically resolved tetra-acid:



vs. a sample of known chirality:



Synthesis of (R,R,R) tetramethylbenzylamide (BisDiazaphos) with T3P.



2.99 g (3.33 mmol) of tetra-acid is placed in a 250 mL round-bottom Schlenk flask and the flask is subjected to three evacuation/N₂ refill cycles. Degassed DCM (100 mL) is added, followed by diisopropylethylamine (4.63 mL, 26.6 mmol), then benzylamine (2.18 mL, 20.0 mmol) as a solution in 10 mL DCM. The flask is cooled in a dry ice/ethylene glycol bath, to an external temperature of -15 ± 5 °C, and T3P solution (11.88 mL, 50 wt% in EtOAc, 20.0 mmol) is added dropwise over a 20 minute period. The reaction is moved to a 0 °C ice water bath and allowed to warm to room temperature with the bath. After 48 hours, the reaction mixture is washed with 2 x 100 mL H₂O, 2 x 100 mL 1M HCl, and 1 x 100 mL H₂O. The aqueous layer was back-extracted with 10 mL DCM after each wash. The combined organics were dried over Na₂SO₄ and concentrated to yield 4.042 g crude product (150% yield). The crude material is dissolved in 50 mL acetone (12.5 ml/g) and placed in the freezer. Solids that crash out overnight are vacuum filtered, washed with cold acetone, and the filtrate is put back in the freezer for an additional crop. The acetone recrystallization is performed four times to yield a combined mass of 1.52 g (56.3%).

Purification of BDP ligands by “the acetone trick”.

Crude ligand (1.15 g, 52% potent, 0.456 mmol) is placed in a vial and diluted to a concentration of 20-60 mg/mL, until all solids disappear. This can be done open to air. Upon standing a few minutes, white solids begin to crash out. The mixture is left to stand at least an hour, then vacuum filtered through qualitative paper, rinsed twice with a small portion of acetone, and dried under vacuum (60 mtorr) to yield 189 mg (31.6%) clean ligand. The filtrate is placed in a -33 °C freezer overnight, which yields a second crop of solid (293 mg, 49.0% yield), isolated by the same procedure as the first crop. The mother liquor is concentrated to yield a solid then redissolved in a minimal amount of acetone and left to stand. Occasionally a third crop crashes out. Overall yield clean material 482 mg (0.368 mmol, 80.6 % yield based on potency of initial material).

Determination of potency of ligand and precursors.

In the same vial, at least 10 mg of triphenylphosphine oxide (to get 3 significant figures) and approximately 20-30 mg of the ligand compound to be analyzed are weighed out. An appropriate NMR solvent is added and the entire mixture is transferred to a NMR tube. ^1H and $^{31}\text{P}\{^1\text{H}\}$ spectra are acquired and the molar ratio of standard to analyte by ^{31}P NMR is compared to the molar ratio by mass to determine the potency:

$$\frac{\text{Moles ligand based on phosphorus NMR}}{\text{Moles ligand by mass}} * 100 = \% \text{ potency}$$

The ^{31}P NMR should be acquired with inverse gated decoupling and a d1 of at least 15 seconds. The proton NMR can be used to adjust for coordinated solvent in cases where only the mass balance of phosphorus nuclei is of interest (e.g. in determining the quality of tetra-acyl fluoride

synthesis). This is done by calculating the weight percent of analyte by proton NMR then using this value to adjust the molar ratio in ^{31}P NMR:

$$\frac{\text{Mass of analyte weighed}}{\text{FW ligand}} * \text{proton weight \% analyte} = \text{adjusted moles ligand by mass}$$

3.6. References.

- ¹ Clark, T. P.; Landis, C. R.; Freed, S. L.; Klosin, J.; Abboud, K. A. *J. Am. Chem. Soc.* **2005**, *127*, 5040–5042.
- ² Wong, G. W.; Adint, T. T.; Landis, C. R. *Org. Synth.* **2012**, *89*, 243-254.
- ³ See Chapter 2 and the following: (a) Watkins, A. L.; Hashiguchi, B. G.; Landis, C. R. *Org. Lett.* **2008**, *10*, 4553-4556. (b) McDonald, R. I.; Wong, G. W.; Neupane, R. P.; Stahl, S. S.; Landis, C. R. *J. Am. Chem. Soc.* **2010**, *132*, 14027-14029. (c) Watkins, A. L.; Landis, C. R. *Org. Lett.* **2011**, *13*, 164-167. (d) Risi, R. M.; Burke, S. D. *Org. Lett.* **2012**, *14*, 1180 – 1182. (e) Risi, R.M.; Burke, S. D. *Org. Lett.* **2012**, *14*, 2572 – 2575. (f) Ho, S.; Bucher, C.; Leighton, J. L. *Angew. Chem., Int. Ed.* **2013**, *52*, 6757-6761.
- ⁴ Adint, T. T.; Wong, G. W.; Landis, C. R. *J. Org. Chem.* **2013**, *78*, 4231–4238.
- ⁵ Adint, T. T.; Landis, C. R. *J. Am. Chem. Soc.* **2014**, *136*, 7943-7953.
- ⁶ B. R. Jones, Landis Group, unpublished results.
- ⁷ Clark, T. P.; Landis, C. R. *J. Am. Chem. Soc.* **2003**, *125*, 11792. Hencoch, F. E.; Hampton, G.; Hauser, C. R. *J. Am. Chem. Soc.* **1969**, *91*, 676-681.
- ⁸ Timothy D.W. Claridge, Chapter 8 Correlations through space: The nuclear Overhauser effect, In: Timothy D.W. Claridge, Editor, *Tetrahedron Organic Chemistry Series*, Elsevier, 2009, Volume 27, Pages 247-302.
- ⁹ Mellem, K. T.; Myers, A. G. *Org. Lett.* **2013** *15*, 5594-5597.

Chapter 4

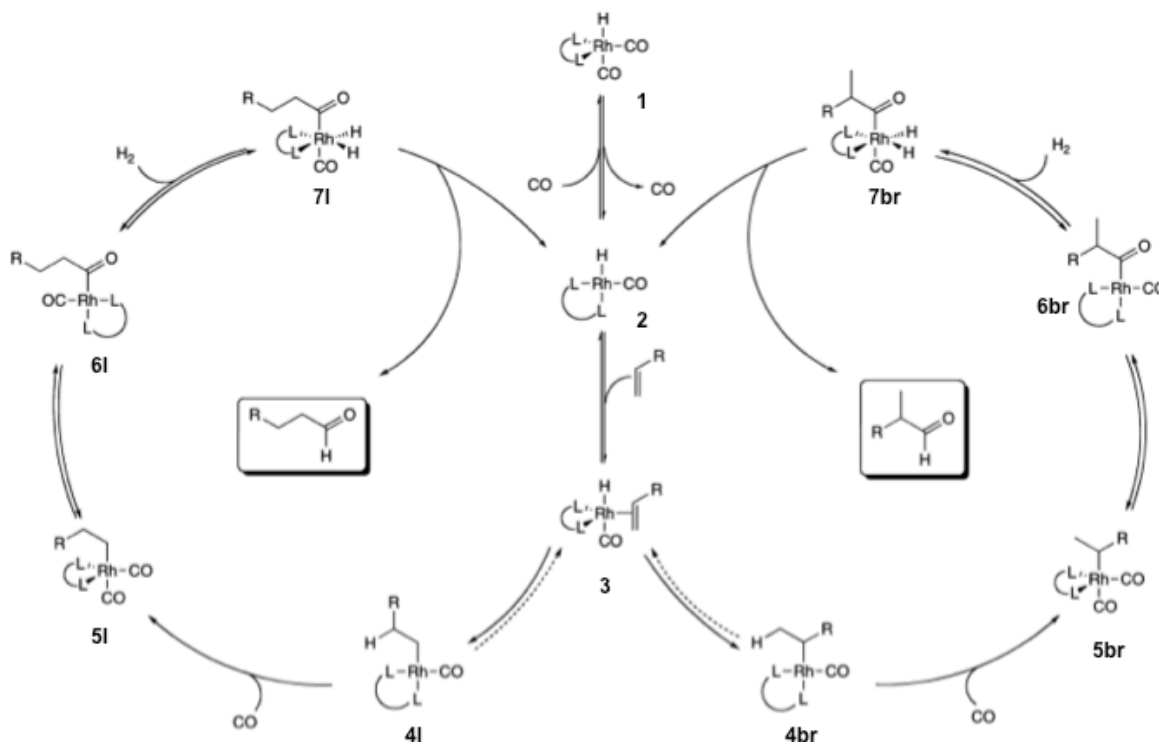
High-pressure, circulating NMR apparatus as a tool to study asymmetric hydroformylation: Observation of reaction timecourses and catalyst speciation under realistic reaction conditions

Portions of the work contained in this chapter were done in collaboration with Dr. Nicholas J. Beach, who constructed the apparatus and solved many design issues. All modifications to the apparatus described herein were implemented by him.

4.1 Introduction

The mechanism of hydroformylation first proposed by Heck and Breslow in 1961 remains relevant to studies today.¹ The catalyst resting state is the off-cycle species **1**, the hydrido dicarbonyl (Figure 4.1). Under normal reaction conditions, this species loses one CO ligand to generate the postulated active catalyst **2** and enter the catalytic cycle. Observation of the intermediates along the cycle is typically only done under conditions that deviate greatly from those used for asymmetric hydroformylation (AHF). Detailed kinetic and mechanistic studies have elucidated the role of many of these intermediates,^{2,3,4} but the direct observation of their formation and equilibria *during* catalysis has not been accomplished.

Figure 4.1: Mechanism of hydroformylation.



To be able to conduct NMR studies of hydroformylation under more realistic reaction conditions, a number of issues must be addressed. First, studies done with routine septum-capped NMR tubes are limited to pressures close to atmospheric, and the pressure changes with the course of a reaction cannot be either monitored or controlled. This severely limits the ability to perform kinetic studies with this type of equipment. In addition, pressure plays an integral role in the kinetic profile of a hydroformylation, and pressures well above atmospheric are required to replicate the kinetics seen in batch reactions.

To address these limitations in hydroformylation and in other reactions using reagent gasses, high-pressure NMR has been implemented in a number of cases.⁵ Initial reaction designs were simply sealed tubes that had only diffusion-controlled mass transfer. Development of sapphire NMR tubes with a titanium spin collar that were compatible with commercially available NMR instrumentation led to greater interest in these methods.⁶ More recent designs are even more advanced, including features such as circulation of gas through the reaction mixture⁷ and of circulation of the pressurized reaction mixture through a specialized NMR cell and other online analyses like IR.⁸ Mechanistic studies of hydroformylation with iridium triphenylphosphine complexes are a recent focus of a research study that employed one of the most sophisticated of these examples.⁹ Efficient mass transfer and sample mixing is accomplished by bubbling gas through a micro-drilled capillary using a circulating pump. A similar apparatus based on the U. Rostock LIKAT design⁷ has recently been constructed in our group by Dr. Nick Beach (Figure 4.2). Further elaborations on the design to improve throughput capabilities are ongoing.

One of the goals of this work is to observe changes in the catalyst speciation with changes in reaction conditions during active hydroformylation. As an ideal, we envision the

ability to run a single reaction in the HP-NMR apparatus and acquire both rate data and catalyst speciation under multiple step changes in conditions (e.g. temperature, pressure). This would provide a complete kinetic picture of the reaction in a single experiment and allow for nuanced understanding of how the relative rates of each product differ with reaction conditions. Initially, substrates that were of significance to our collaboration with Eli Lilly were examined, styrene and a precursor to naproxen, 6-methoxy-2-vinyl naphthalene. These aryl alkene substrates are advantageous as test compounds since they exhibit highly pressure-dependent selectivity in hydroformylation and the observation of regioselectivity over the course of the reaction can provide a probe for the effective gas concentrations in solution. Later studies focused on hydroformylation of *Z*-1-(benzoyloxy)-1-hexene.

Figure 4.2: High-pressure, circulating NMR apparatus with injection capability (HP-NMR).

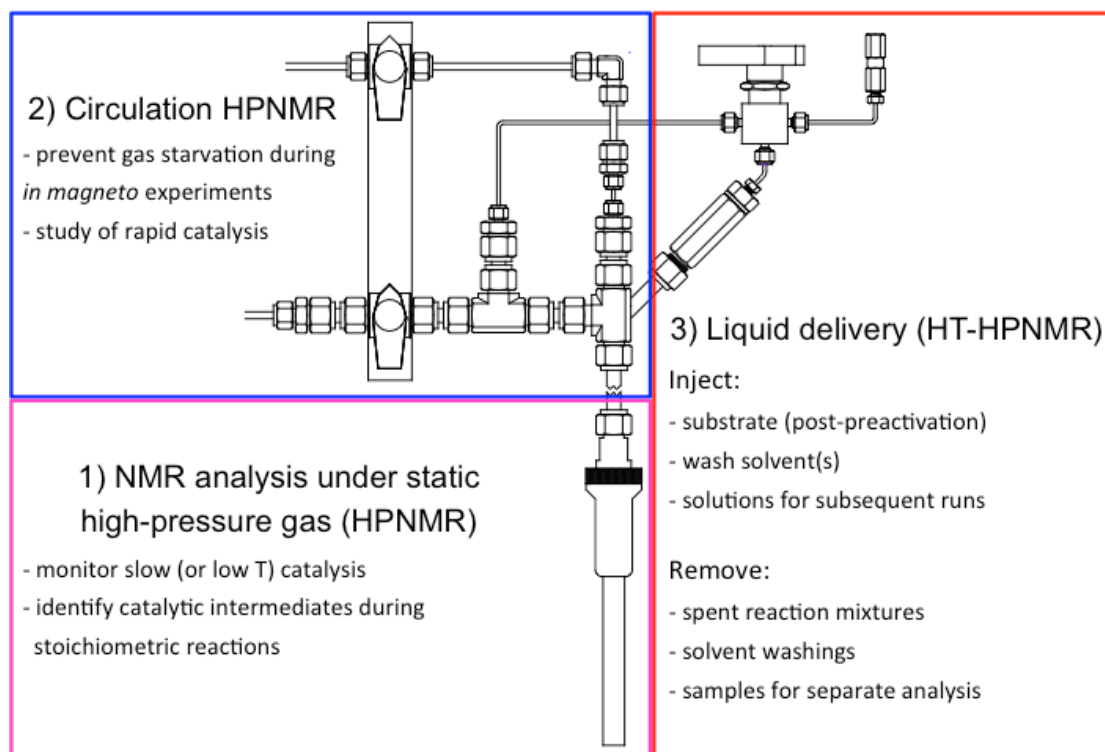


Figure courtesy of Dr. Nick Beach.

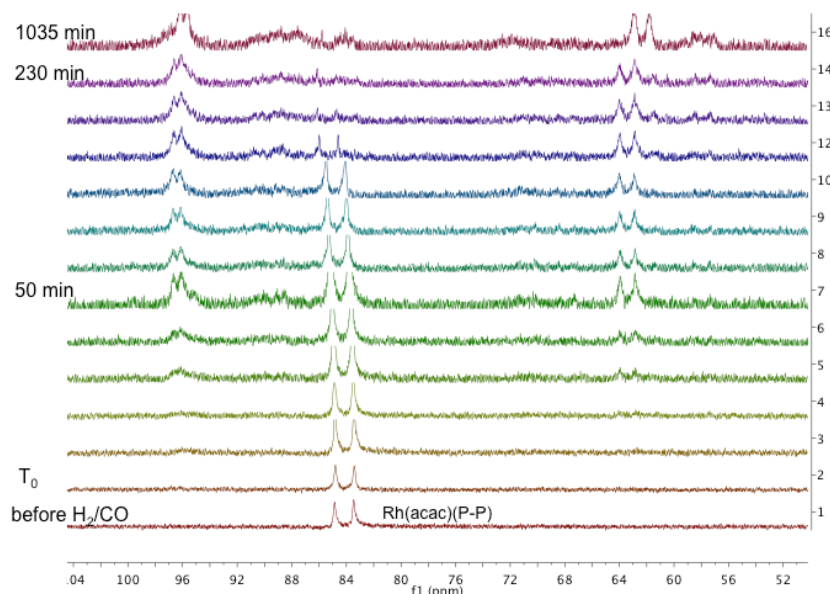
Much of this work involved the simultaneous development of the HP-NMR apparatus and determination of kinetic and mechanistic parameters. We began with an unoptimized apparatus and a research goal of observing a timecourse of the AHF of styrene to determine the kinetics and catalyst speciation in a single experiment. In trying to fulfill this research goal the limitations of the apparatus were put in context, and many of the components were improved by Dr. Nick Beach. Many later experiments build upon results from earlier work on an unoptimized apparatus, and this chapter is organized to describe the back-and-forth process of developing the apparatus and acquiring meaningful data on it.

4.2 Equipment setup and design issues

4.2.a: Starvation

The initial experiments were done without circulation, and as expected, the hydroformylation of styrene was slow. ^{31}P NMR showed that the resting state was not the hydride species (Figure 4.3), and instead was one or more uncharacterized alkyl or acyl species. This is a hallmark of a starved reaction, where the mass transfer of gas into the liquid phase plays a role in the rate law. Once the circulation pump was incorporated into the apparatus, circulation through a 700 μ single-pore glass capillary greatly increased the mass transfer, and consequently the rate of the reaction.

Figure 4.3: Catalyst speciation under static (starved) conditions.



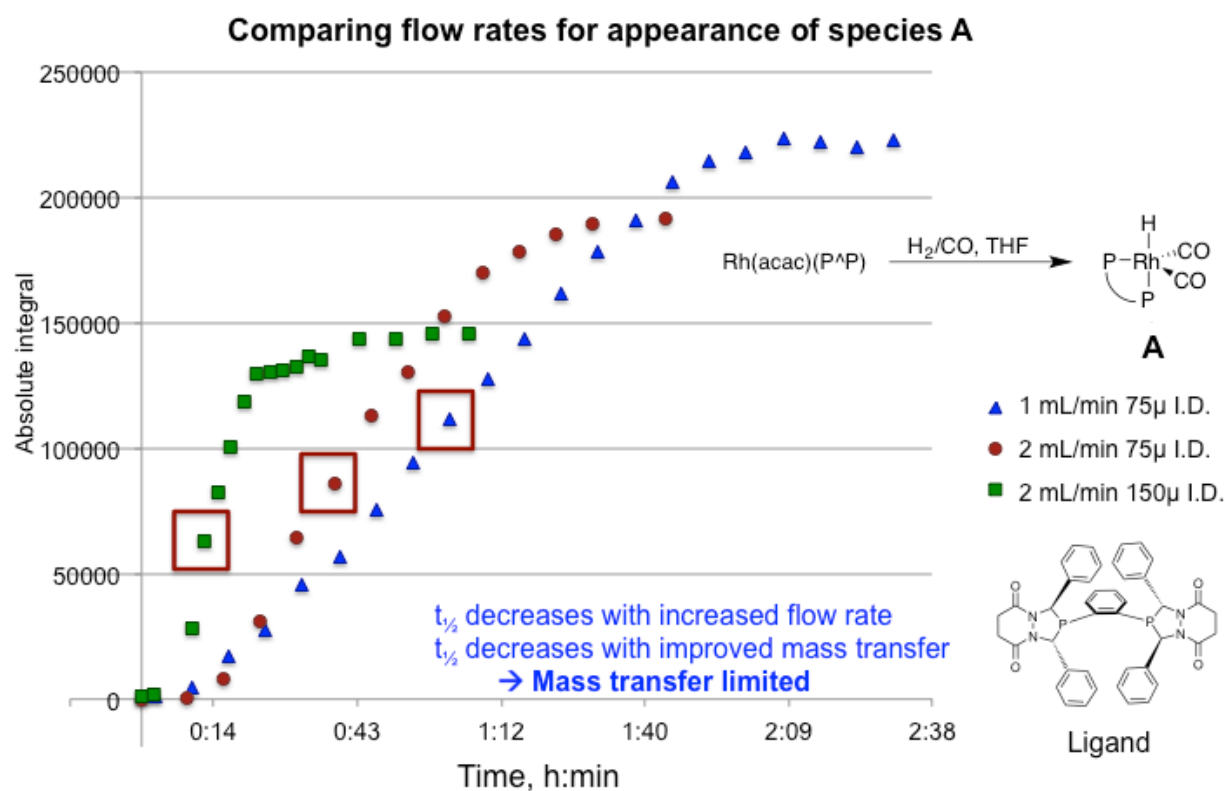
4.2.b: Lineshape

As predicted, the lineshape deteriorates during circulation, to the point where determination of integrals is no longer possible due to broadening of peaks into the baseline. We first aimed to combat this by creating custom-designed capillaries that would provide small, champagne-like bubbles to provide high mass transfer. Moving to a smaller pore size (28-75 μ inner diameter) restricted the flow to the point where pressure buildup in the pump was observed. In addition, initial experiments run with the goal of determining the rate of pre-activation demonstrated that the observed rates were dependent upon gas flow, and mass transfer limited (Figure 4.4). Increasing both the flow rate and the capillary diameter increased the rate of formation of species **A**, which is most easily quantified by looking at the half-life of the reaction (boxed in red in figure 4.4). Alleviating the high mass transfer requirement by reducing the concentration of the catalyst was not possible because of the limits of detection in the apparatus at the time. A minimum concentration of 10 mM was needed to obtain high-quality signal with

the tetraphenyl ligand in Figure 4.4, a more soluble analog of the typical bisdiazaphospholane ligands employed in AHF.

Observation of a fast reaction at high catalyst concentrations proved to be beyond the reach of the apparatus at this point in its development. This research problem was left until we had a more optimized setup. The acquisition of a complete ^1H timecourse of AHF in the HP-NMR for determination of reaction rates became the new focus.

Figure 4.4: Monitoring pre-activation of tetraphenyl catalyst at different flow rates.

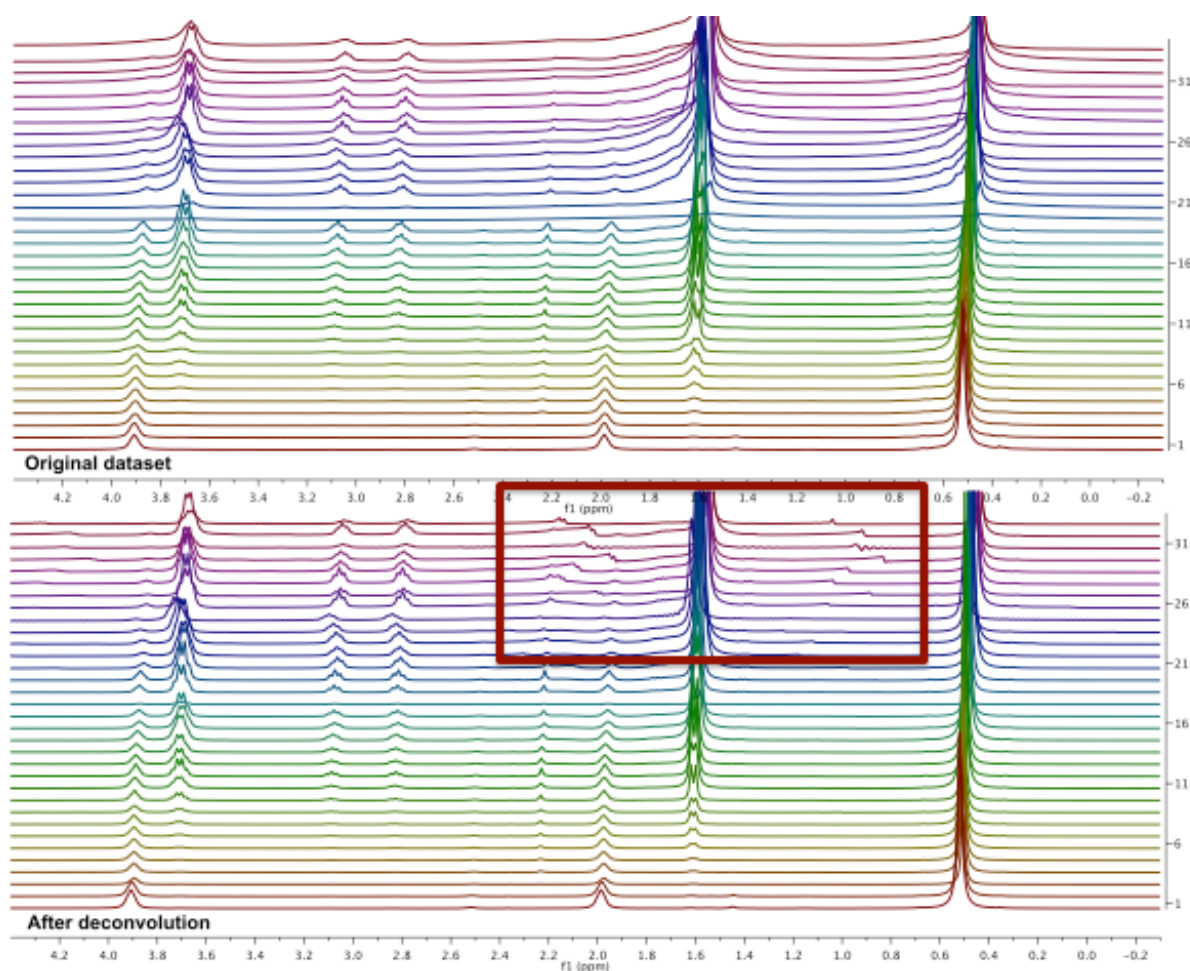


4.2c: Post-acquisition deconvolution to improve lineshape and sample autoshimming:

As mentioned above, the lineshape deteriorates during circulation, to the point where determination of integrals is no longer possible due to broadening of peaks into the baseline. A single scan spectrum shows that the origin of this is the averaging of many different,

nonhomogeneous scans. Additionally, at later points in the reaction the linewidth would increase substantially because of solvent loss and changes in the shimming. This led us to attempt post-acquisition enhancement of the data set by reference deconvolution. The major problem with this strategy is that the broadness of the peaks leads to poor baseline resolution. Without complete baseline resolution of the singlet chosen for deconvolution, significant errors get built into the deconvolved spectra, seen as additional “choppiness” in the baseline.

Figure 4.5: Reference deconvolution to improve lineshape.



Timecourse before (top) and after (bottom) reference deconvolution using *bis*-TMS benzene internal standard peak. Problematic baseline is highlighted in the red box.

Beyond the problems with lineshape during circulation, the static lineshape was also broad, and tended to change every time the apparatus was removed from the NMR instrument. Reshimming tended to be tedious and time-consuming, with only mediocre results. To combat this, autoshimming was implemented using the “ed tune” command. With overnight shimming on a mock sample, lineshape could be improved by over a Hz width at half height. This is now implemented as a routine procedure for experiments in the HP-NMR.

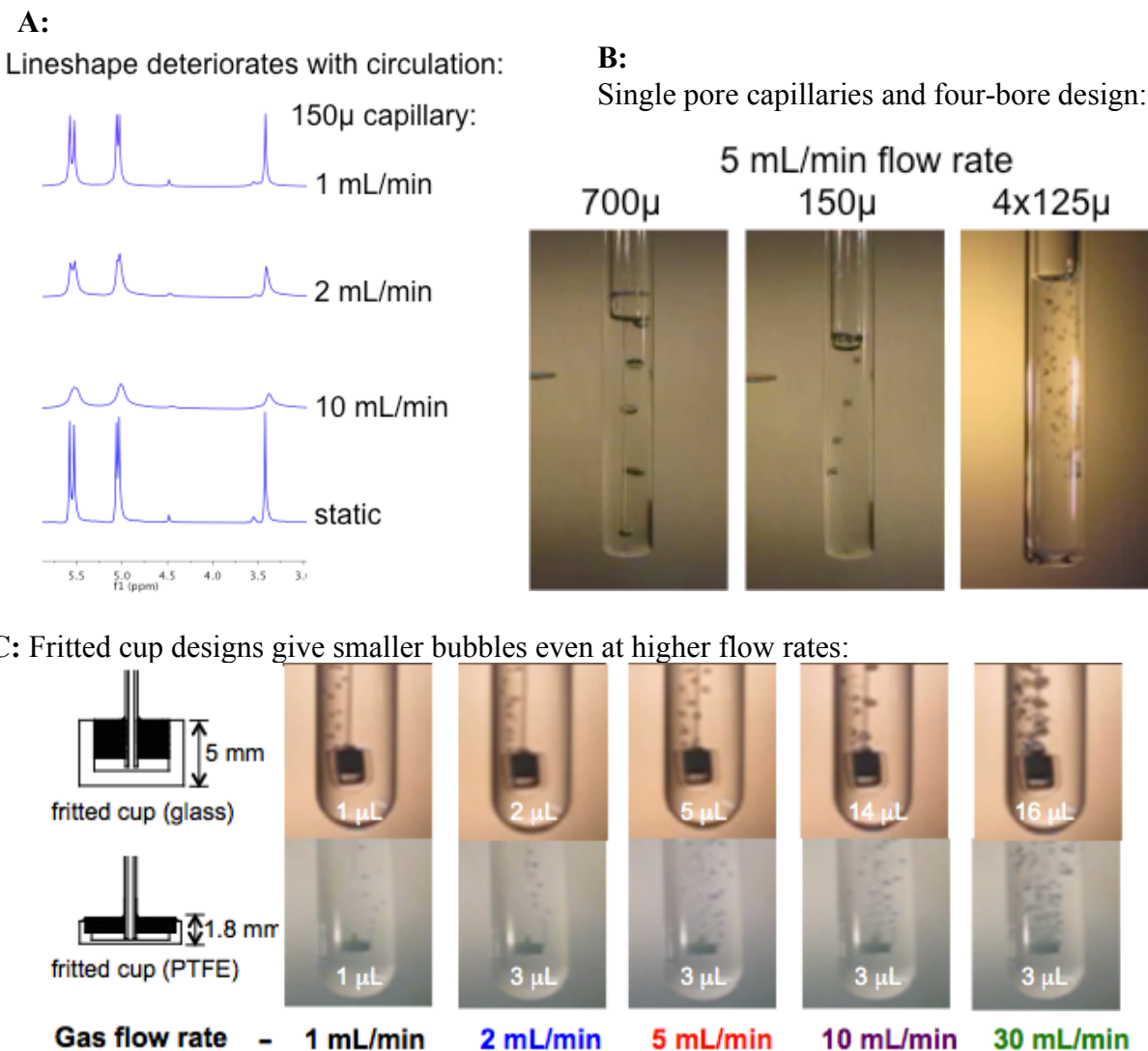
4.2d: Circulation rate vs. lineshape and capillary design

One of the distinct advantages of AHF with bisdiazaphospholane catalysts is the extraordinarily high rates conferred by the catalyst. However, when attempting to maintain saturation concentrations of syngas in the reaction solvent, this feature of the catalyst became a challenge. In particular, we were interested in determining reaction kinetics at 80 °C and a variety of syngas pressures in conditions similar to those envisioned for flow studies at Eli Lilly (Chapter 5). This elevated temperature increased the rate of the reaction and made efficient mass transfer a primary concern with the apparatus. To improve mass transfer, more complex capillary designs were developed. For some designs, acceptable lineshape could be maintained at low flow rates (<5 mL/min), but for all designs the use of higher flow rates led to signal deterioration beyond useful levels (Figure 4.6).

Reducing the catalyst concentration further and halting circulation during acquisition, then circulating in the delays between spectra circumvented the issue of poor lineshape. This method is only truly effective for acquiring proton timecourse data, as the amount of time under static pressure that the sample requires to acquire a ^{31}P spectrum leads to starvation and changes in speciation over the course of a single NMR acquisition. Reducing the number of scans and

the delay times as much as possible can mitigate this issue, and with sufficiently concentrated reaction mixtures spectra can even be acquired with a single scan.

Figure 4.6: Lineshape with different flow rates and bubble size changes with different capillary designs and flow rates



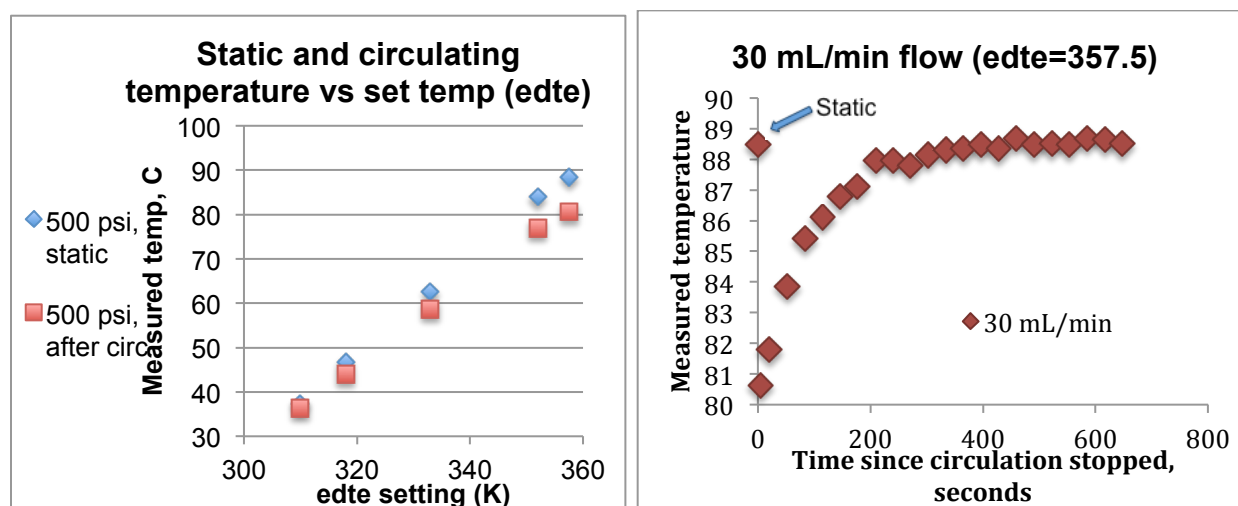
Dr. Nick Beach

4.2.e Temperature calibration and variation with flow

One variable that had not been accounted for previously was an understanding of the temperature drop during circulation vs static pressure. We wanted to know how far the

temperature dropped upon circulation, how quickly it recovered, and to confirm the temperature we expected based on an old calibration file. To measure this, the liquid feed capillary is replaced with a melting-point tube filled with ethylene glycol as a temperature standard. The temperature does drop upon circulation; at 80 °C the drop is about 8 °C at the first data point (Figure 4.7).

Figure 4.7: Temperature profile after circulation



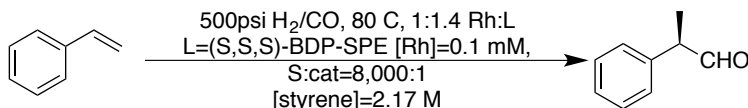
4.3 HP-NMR runs with styrene

In determining many of the above reactor issues and modifying the experimental design, many of the intermediate spectra were from the AHF of styrene but under starvation kinetics. The best of these experiments are reproduced in this section.

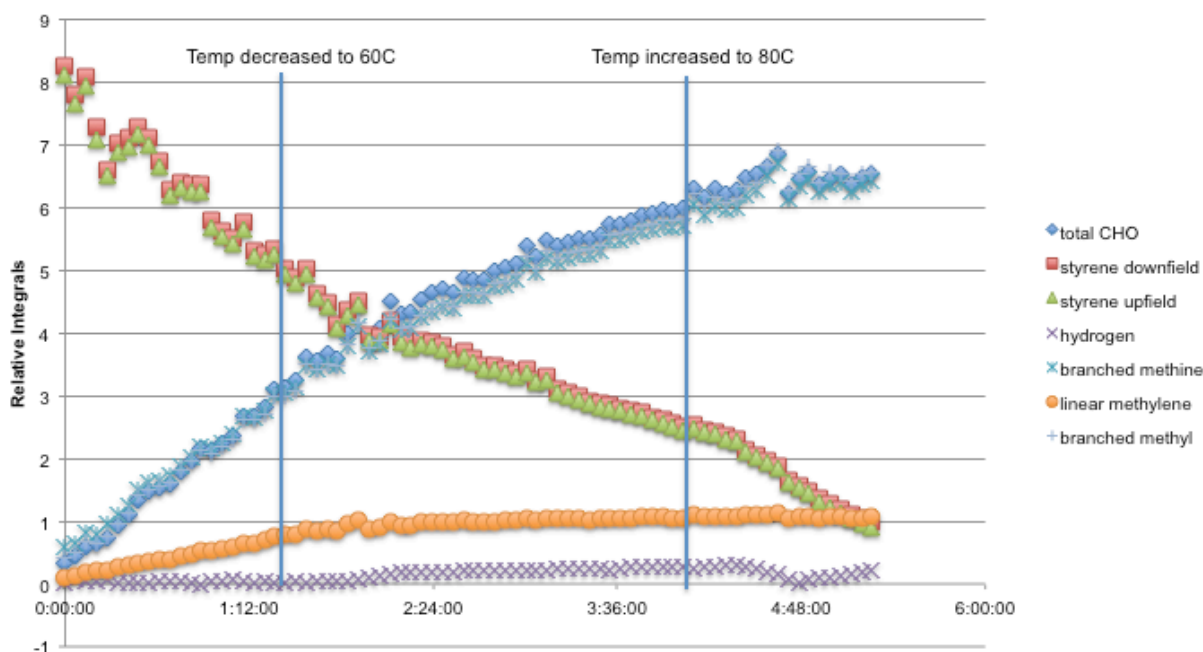
In Figure 4.8, the hydroformylation of styrene was run with circulation at 30 mL/min through a 150 μ single-pore capillary. The reaction is starved, and this is observed in the low b:l at the end (6.2). However, the step change from 80 to 60 °C and back again illustrates the role of temperature on selectivity, with the minor pathways (linear and minor branched) slowing down at lower temperature. In addition, in the lower temperature regime hydrogen appears in the

spectrum, indicating that the reaction has slowed enough to keep up with mass transfer. One other feature of note is the lag between a step change in temperature and the response in the data. Similar step changes will be made in the next section, but with pressure instead.

Figure 4.8. AHF of styrene with step changes in temperature (starved)



Styrene AHF at 80C, 500psi, 8000:1 s:cat [styrene]=2.17M



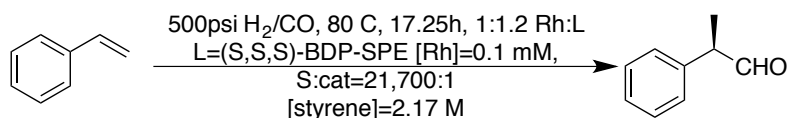
Circulating 30 mL/min through 150 μ single-pore capillary

Expanding on the result in Figure 4.8, the concentration of catalyst was lowered in a series of runs until the reaction began to exhibit a non-linear rate of consumption of styrene (Figure 4.9). The results in Table 4.1 summarize the two runs presented in Figure 4.9, and suggest that this is nearly a non-starved AHF in the HP-NMR, after moving to the new fritted

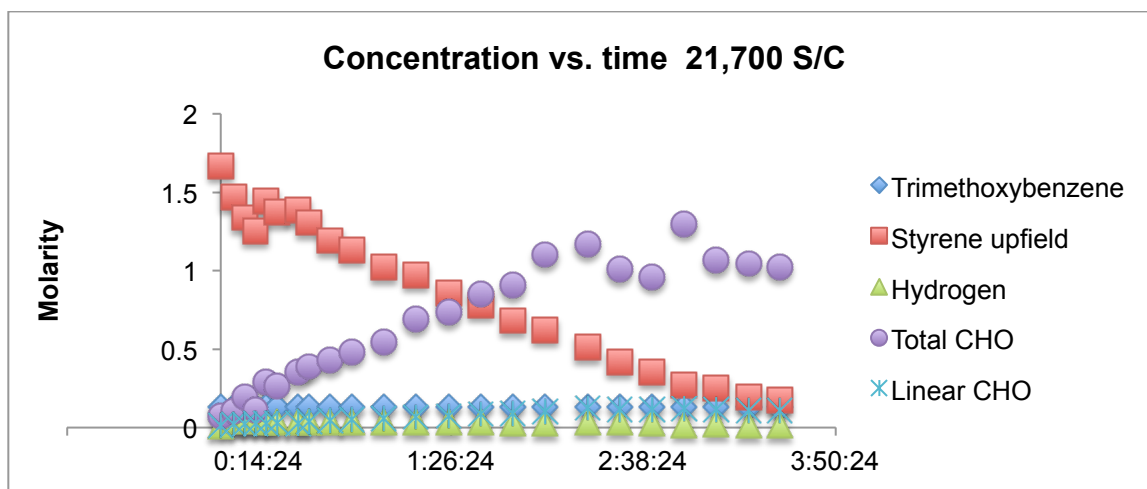
cup capillary design and reducing the catalyst loading further. The factors used to assess this are the b:l and enantioselectivities, which are for the first time nearing levels of selectivity seen in batch reactions.¹⁰ In addition, the consumption of olefin is starting to appear non-linear.

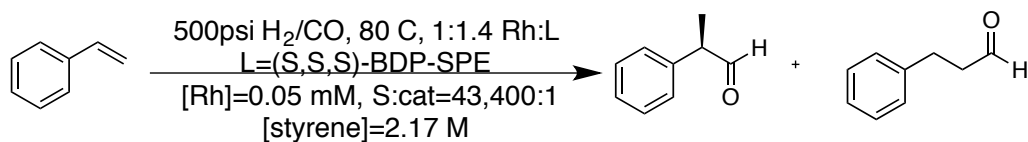
While these results are not yet completely consistent with those found in batch, and require feed rates that preclude observation of the reaction by ³¹P NMR, the ability to monitor this system with a steady-state concentration of hydrogen is in itself remarkable. With a desired run temperature of 80 °C and an extraordinarily fast catalyst, these reaction conditions represent some of the most challenging in terms of maintaining sufficient mass transfer. Many analogous reactions will have less forcing conditions, and be amenable to study in the HP-NMR.

Figure 4.9: AHF of styrene at 80 °C and lower catalyst loadings: starved vs. non-starved behavior.

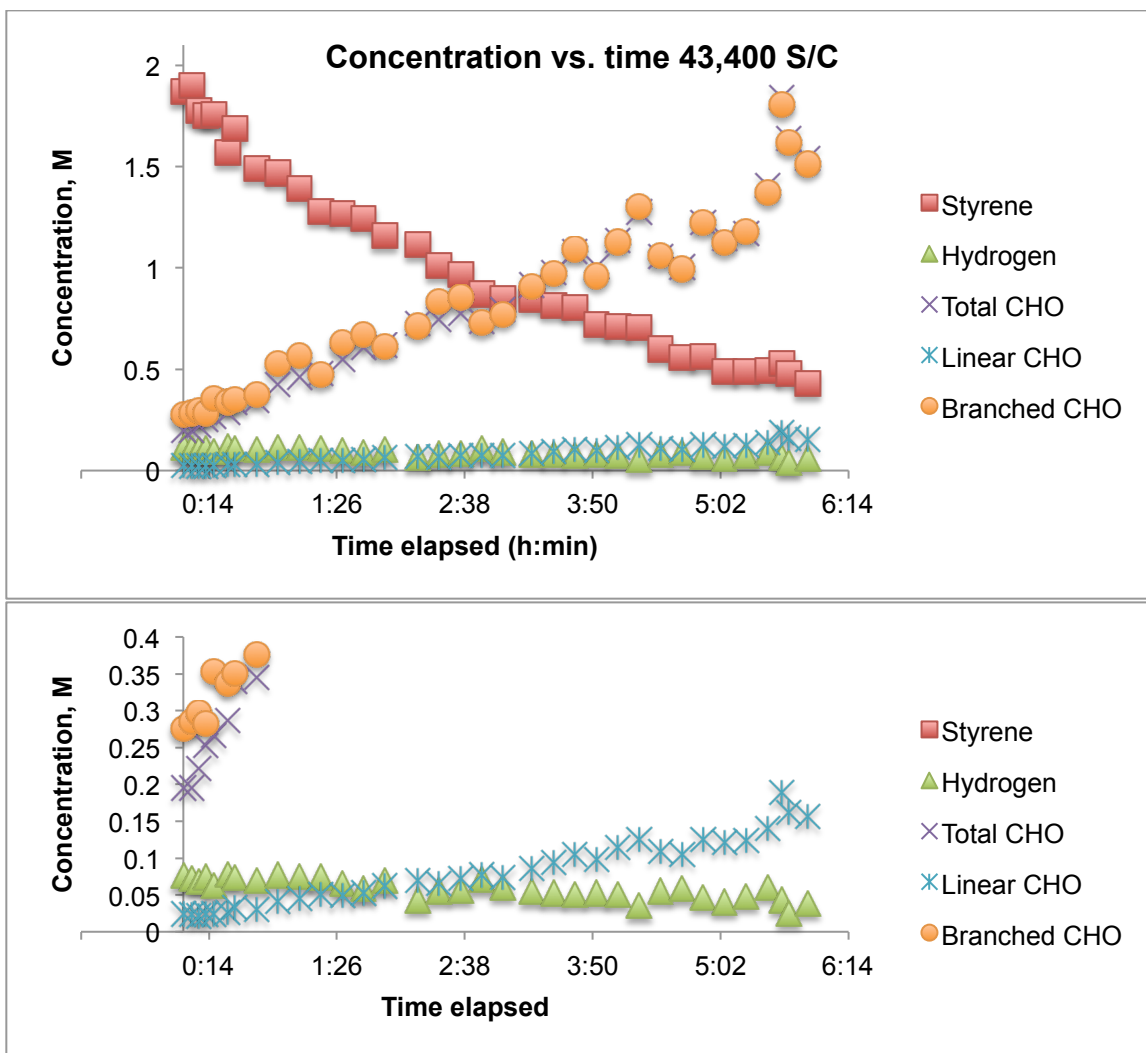


A: starved reaction:





B:non-starved reaction:



A: Circulating 30 mL/min through 4x150 μ four-bore capillary, average 29 mM H₂.

B: Circulating 30mL/min through glass fritted cup capillary, average 83mM H₂

Table 4.1: Comparing HP-NMR runs of styrene

Parameter	4-bore, 21,700:1 Sub:Cat	fritted cup, 43,400:1 Sub:Cat
Styrene TOF	69 min ⁻¹	91 min ⁻¹
Branched CHO TOF	58 min ⁻¹	83 min ⁻¹
Linear CHO TOF	5.7 min ⁻¹	7.4 min ⁻¹
Average H ₂ conc.	29.3 mM	83.0 mM
b:l ; <i>ee</i>	12.7:1 ; 89%	10.2:1 ; 92%

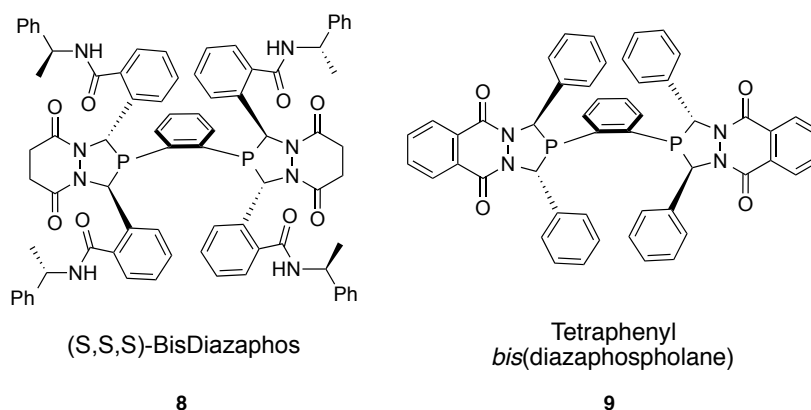
4.4 HP-NMR studies with *Z*-1-(benzoyloxy)-1 hexene

All the developments in reactor design and reaction setup discussed above had only led back to the original, unsolved issue of efficient mass transfer to prevent starvation. In particular, observation of the catalyst by ³¹P NMR requires higher catalyst loading to attain reasonable sensitivity and short data acquisition times. Yet higher catalyst loadings increase the rate of the reaction to the point that it exceeds the rate of mass transfer of syngas into the reaction.

To accomplish simultaneous observation of catalyst speciation and non-starved kinetics, we chose to investigate the hydroformylation of a disubstituted olefin instead. The increased steric bulk of disubstituted olefins means they undergo hydroformylation at lower rates, which should help mitigate the mass transfer issues of running at high catalyst loading. In addition, the catalyst was switched to one derived from *rac* tetraphenyl bisdiazaphospholane **9** instead of the standard tetra-amide ligand **8** used in the Landis group. The tetraphenyl ligand is more soluble than **8** but far less enantioselective and also slightly slower. More importantly, the ³¹P{¹H} NMR of the hydrido complex **1** made with the tetraphenyl ligand **9** is a simple doublet as

opposed to two broad dd. The simplified and sharp NMR spectrum means that slightly lower concentrations of catalyst can be employed, to help further reduce the rate of the reaction.

Figure 4.10: Ligands for asymmetric hydroformylation.

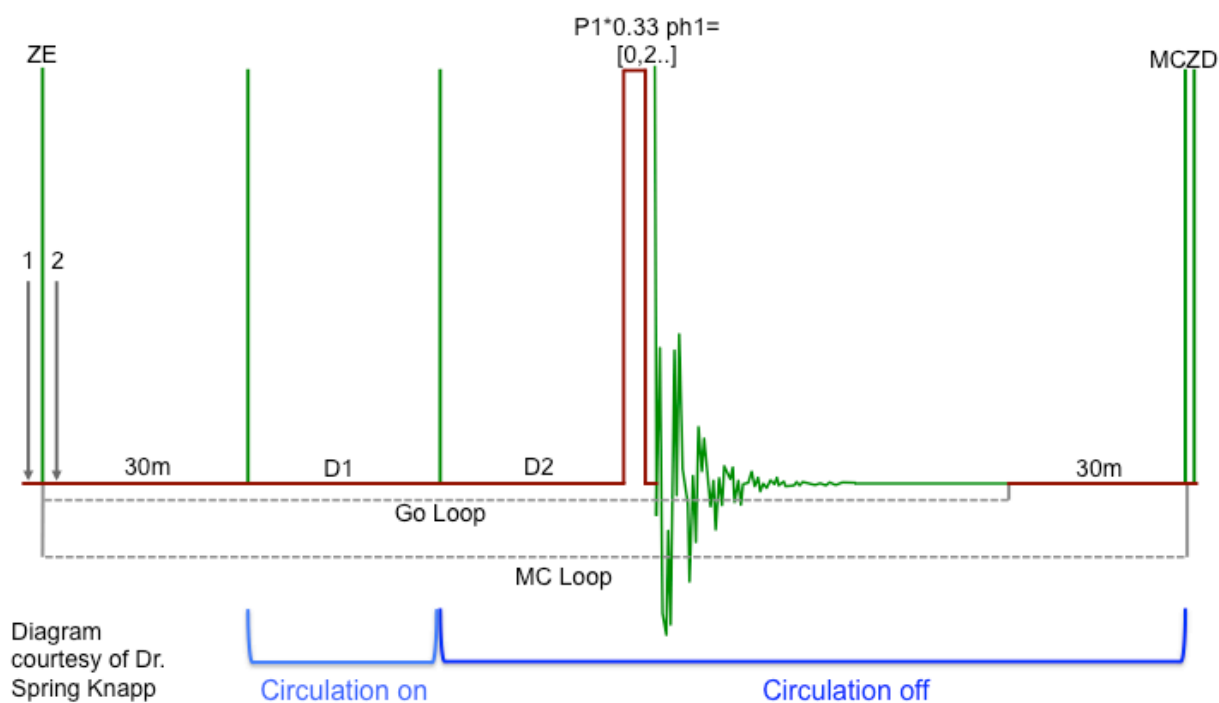


4.4.a Development of pulse program for circulation during d1 delay

In addition to the above modifications to the experimental design, a new strategy was employed to maximize mixing time. The pulse program is modified to include a TTL command that interfaces with the bypass valve on the circulation pump. If the pump is left constantly circulating, when this valve is open, no gas flows through the capillary. When the valve closes, circulation resumes. This is written into the pulse program to allow for circulation during the delay between scans (d1) in a given experiment (Figure 4.11). This does two things: it makes longer experiments that require more scans possible without starvation, and it removes the need to decide between short experiment times and sufficiently long d1 values for high-quality data. There are a few additions to the pulse program: the TTL channel control and an additional delay, d2. d2 is the delay between when the circulation pump is shut off and when the acquisition begins; it needs to be sufficiently long to allow for bubbles to stop flowing through the reactor (4

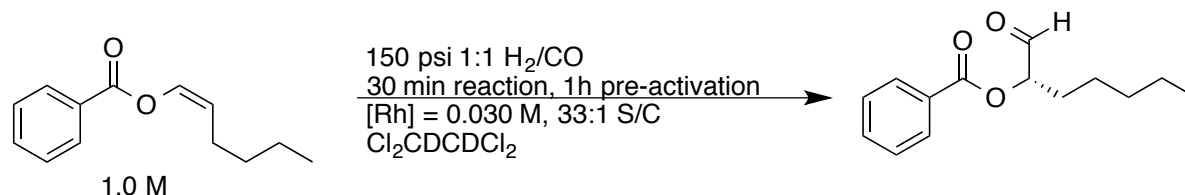
seconds was the value used in these experiments, but later tests indicated that even 1 second is sufficient).

Figure 4.11: Modified pulse program with circulation during the inter-scan delay.



4.4.b Batch and HP-NMR studies with *Z*-1-(benzoyloxy)-1 hexene

The tetraphenyl ligand **9** displays lower selectivities with many other substrates, but had never been evaluated with the enol ester substrate selected for these studies. Batch reactions at 150 psi were run to determine baseline values for reaction rate and selectivity with this substrate, and are summarized in table 4.2. The tetraphenyl ligand produces slightly lower regioselectivity than **9**, but the rates are fast enough that there would only be about two data points per half life for the reaction run at 50 °C.

Table 4.2: Batch AHF of Z-1-(benzoyloxy)-1-hexene.

Entry	Temperature	TON	[Rh] mM	Conversion	Branched:Linear
1	40	6	30.0	18.2%	36
2	53	16	30.0	47.7%	38
Ligand 12	60 (24h)	333	4.50 (0.3% cat)	100%	>50; <i>ee</i> 97%

Based on these initial data a run in the HP-NMR apparatus was performed with a set temperature of 300K (actual temperature 22.5 °C) to allow enough time between data points (acquiring 4 proton and 4 phosphorus spectra every hour) for good kinetic modeling (Figure 4.12). After acquiring a sufficient number of data points under the first set of conditions, a step change is made to a lower pressure. The pressure is then further lowered after a second set of data points were acquired. Throughout the course of the run a steady-state concentration of H₂ was apparent in the proton spectrum and varied linearly with changes in pressure (Figure 4.13). In good agreement to this, the rate of the reaction under different pressure regimes was calculated from a single data set, and the data exhibit a linear dependence on 1/P_{syngas}.

Figure 4.12: Proton NMR stacked plot and timecourse of the AHF of Z-1-(benzoyloxy)-1-hexene under three pressure regimes.

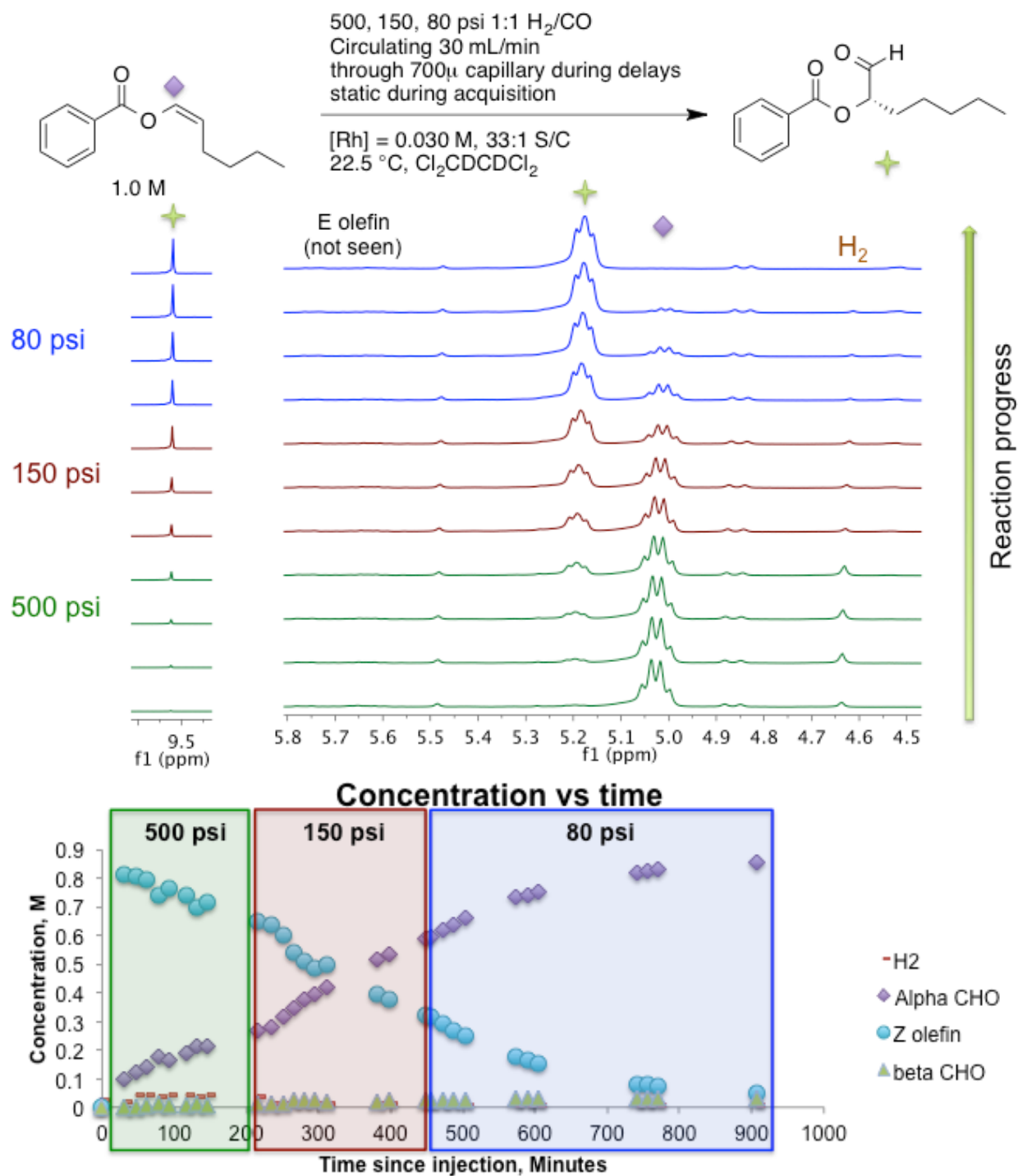
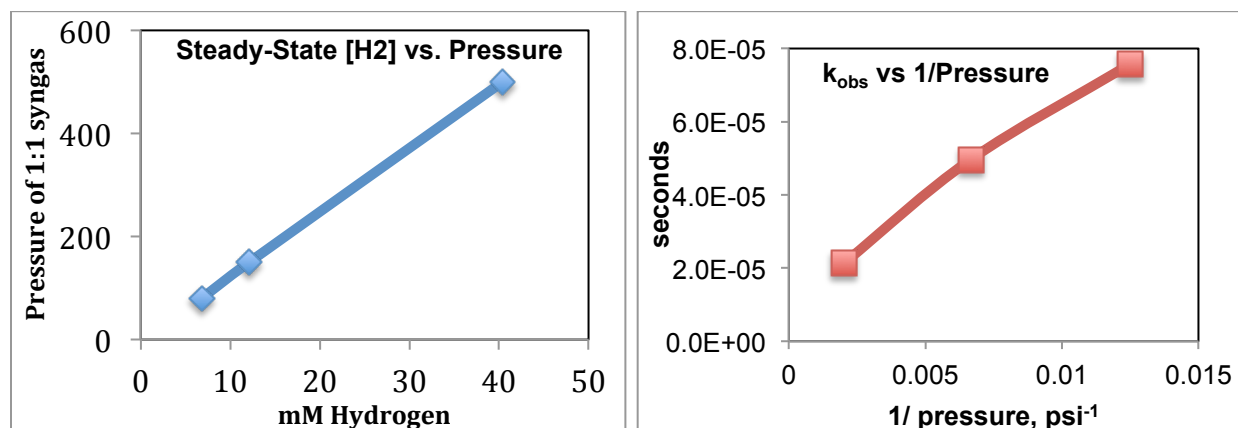
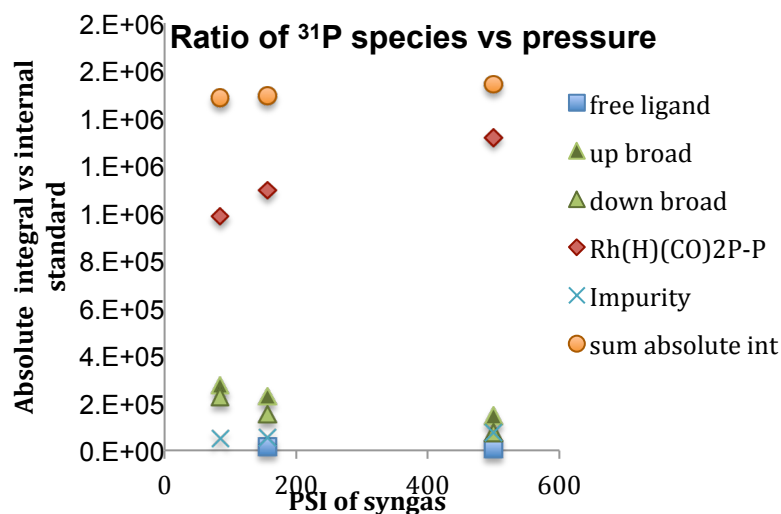
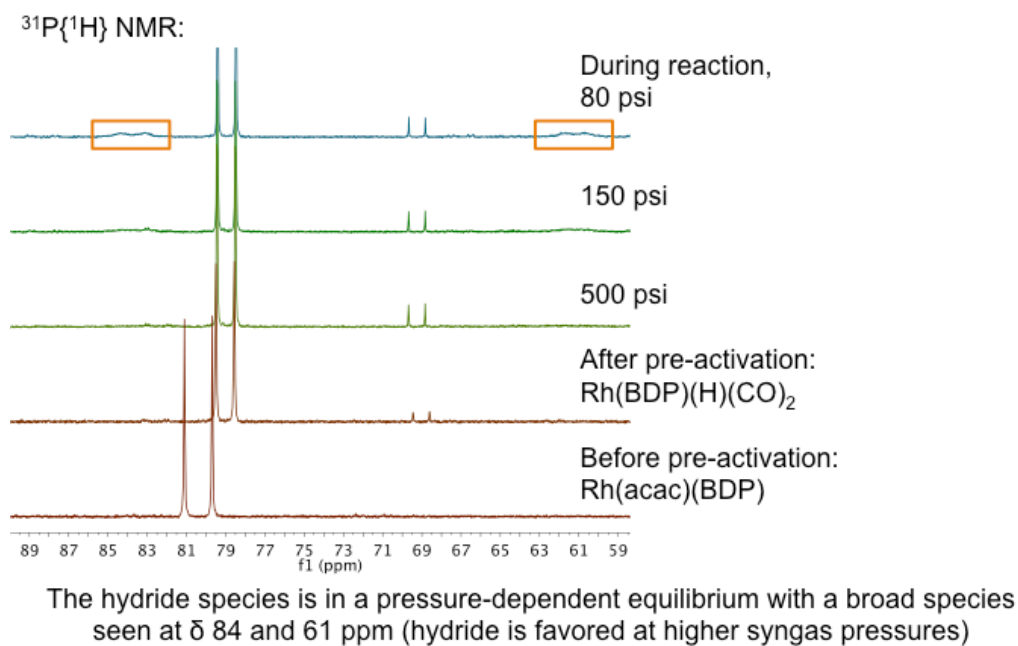


Figure 4.13: Average H_2 concentration and observed rate constant varies with pressure during the AHF of Z-1-(benzoyloxy)-1-hexene.



In addition to the rate data derived from the proton spectra, the ^{31}P spectra show that the majority of the catalyst is in the hydrido-dicarbonyl form **1**, the resting state (Figure 4.14). This supports the conclusion that the experimental redesign and modified pulse program allow for observation of catalyst speciation and non-starved kinetic data in a single experiment. Ongoing work in the Landis group will identify the minor species seen in the phosphorus spectra and continue to use the high-pressure NMR to observe real-time changes in selectivity with step changes in reaction conditions.

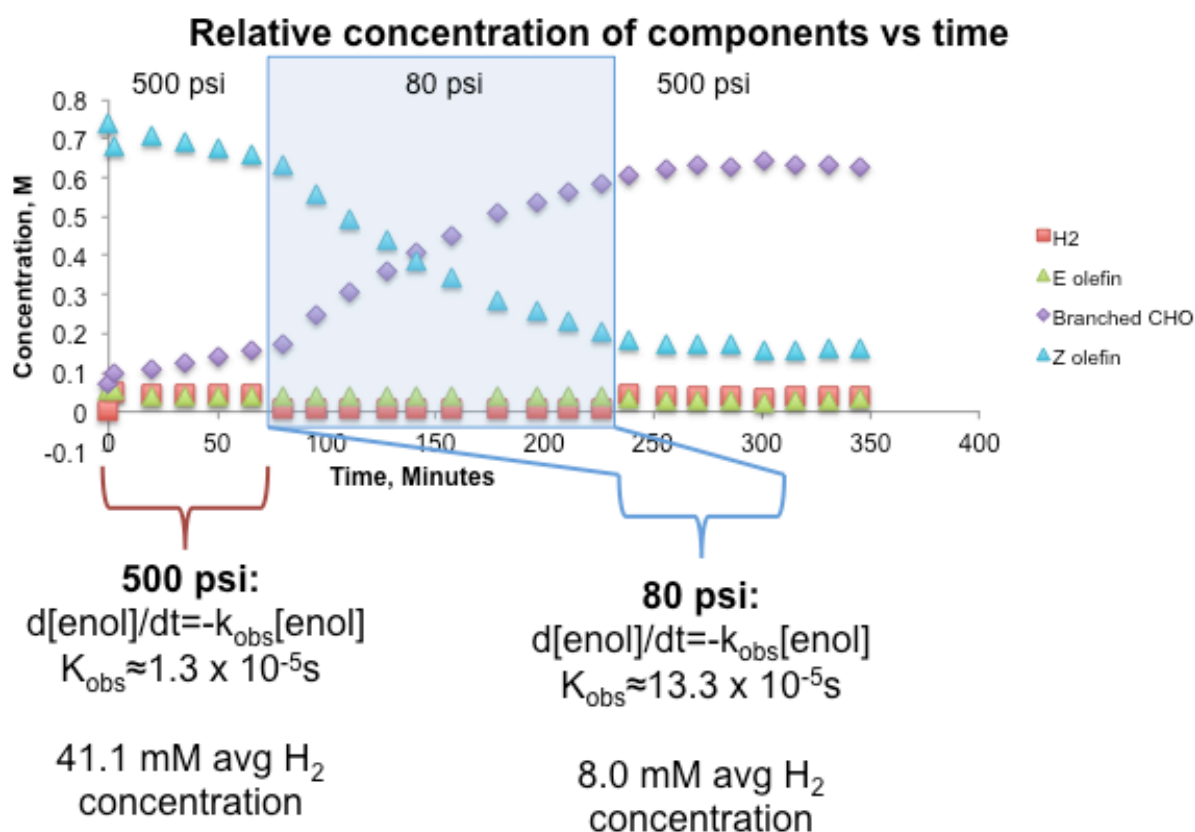
Figure 4.14: Observation of catalyst species by ^{31}P NMR and speciation with pressure changes.



The reaction was repeated with similar conditions, but the catalyst loading was slightly lower due to impurity formation during the pre-activation. The k_{obs} values derived from these data are in reasonably good agreement with those from the run in Figure 4.12 (Figure 4.15). Additionally, there is a clear break in the graph at about 70 minutes in, when the first step change is made.

Further work will continue with this substrate and catalyst and investigate the affects of other step changes. In addition, moving to a non-chlorinated solvent may provide more reproducible behavior by limiting catalyst degradation.

Figure 4.15: AHF of enol ester substrate with step changes between 80 and 500 psi.



4.5 Experimental.

All manipulations were carried out under nitrogen using standard Schlenk, high vacuum, and glovebox techniques. Bisdiazaphospholane ligands and their Rh complexes were prepared by the methods described in Nelsen, E. R.; Landis, C. R. *J. Am. Chem. Soc.* **2013**, *135*, 9636 – 9639 and Adint, T. T.; Wong, G. W.; Landis, C. R. *J. Org. Chem.* **2013**, *78*, 4231–4238. $[\text{Rh}(\text{acac})(\text{CO})_2]$ was used as received from Dow Chemical and stored in a N_2 -filled glovebox. 1:1 $\text{CO}:\text{H}_2$ was purchased from Airgas. THF and toluene were obtained from Sigma-Aldrich and

either distilled from sodium/benzophenone ketyl under N₂ or dried by safety columns prior to use. Styrene, 1,3,5-trimethoxybenzene, 1-hexyne and benzoic acid were obtained from Sigma-Aldrich. 6-Methoxy-2-vinyl-naphthalene was prepared by J. Martinelli at Eli Lilly and used to prepare solutions in toluene, which were filtered through a PTFE filter before use. Z-1-(benzoyloxy)-1-hexene was prepared according to the previously reported method¹¹ Chiral HPLC analysis of the aldehyde from 6-methoxy-2-vinyl-naphthalene was performed on a Gilson analytical HPLC with a Chiralpak ID column: 3% 2-propanol / 97% hexanes with 0.1% TFA, ambient temperature, on a Chiralpak ID (0.46 cm x 25 cm), 0.7mL/min flow, detect at 220 or 254 nm. In an isolated sample (after silica gel chromatography), $t_{r(S)} = 15.3$ and $t_{r(R)} = 17.1$ minutes. In a crude sample, they appear at $t_{r(S)} = 16.2$ and $t_{r(R)} = 18.3$; $t_{r(olefin)} = 9.2$, $t_{r(linear)} = 26.7$ min. The relative responses of these compounds vary, depending on the wavelength measured at, and caution should be used in determining conversion or branched:linear ratios by HPLC. Gas chromatographic analysis was performed on a Varian Chrompack system using a β -DEX 225 capillary column from Supelco, 30 m x 0.25 mm ID x 0.25 μ m film thickness. Resolution conditions for the hydroformylation product of styrene have been reported in Watkins, A.L.; Hashiguchi, B.G.; Landis, C.R. *Org. Lett.* **2008**, *10*, 4553-4556.

A typical HP-NMR reaction:

Inside a nitrogen-filled glovebox, solid Rh(acac)(CO)₂ (31.1 mg), tetraphenyl bisdiazaphospholane ligand (114.9 mg) and 1,3,5-trimethoxybenzene (17.3 mg, as an internal standard) are weighed into a vial. To these solids are added tetrachloroethane-*d*₂ (0.880 mL) and a 100 mM stock solution of triphenylphosphine oxide in tetrachloroethane-*d*₂ (0.200 mL). The vial is swirled until all solids dissolve, then the solution is pulled into a 2.5 mL gas-tight valved

syringe. The vial is rinsed with 0.300 mL of tetrachloroethane- d_2 , then the rinse is pulled into the same syringe. Two additional syringes each loaded with 0.300 mL of tetrachloroethane- d_2 are also prepared at this time. The syringe plungers are pulled out to maximize the volume of nitrogen inside the syringes, and the valves closed.

The apparatus is left under vacuum from the previous use. Before injection, the valve to the vacuum is closed and nitrogen is reintroduced into the system up to approximately 50 psi. This is then purged through the exhaust port and the process repeated ~ 3 times to purge the exhaust port with N_2 . The reactor is filled to about 30 psi of nitrogen, which is then purged through the injection port. At the end of this purge, the exhaust valve is opened slightly. The syringe with catalyst solution is inserted into the injection port and the plunger depressed to inject all the solution and the nitrogen contained in the syringe. Nitrogen from the N_2 purge collar is drawn in until the syringe is about half full, then this is also injected into the injection port. The process is repeated with one of the chaser syringes of tetrachloroethane- d_2 , and the valve on the injection port is turned until it is open to the bypass. Syngas is introduced into the apparatus up to the reaction pressure, circulated for about 10 seconds to mix the sample, and the injection port is turned to closed (vertical) during this brief circulation. Pre-activation, if used, is set up. The circulation pump is typically set to 30 mL/min for all experimental manipulations.

After pre-activation is complete, the valve between the reagent gas ante-bottle and the regulator is closed, and the reaction is vented down to atmospheric pressure. Injection of a syringe filled with the olefin (0.520 mL, 2.5 mmol) followed by the second syringe of chaser solvent is performed by the same method described above, pressurized, and briefly circulated to mix. The sample is tuned, shimmed, the gain is adjusted, and data acquisition is commenced.

Spectra are acquired as alternating proton and phosphorus experiments, using the “kinig1d.UW_HP NMR_new ” pulse program (for ^{31}P) and “zg30_1H_HP NMR_circulation” (for ^1H). A delay of 4 seconds is used for the bubble dissipation delay (d2), and d1 values of 16s for proton and 10s for ^{31}P (inverse gated) spectra. Timecourses are run with NS=8 for proton and NS=32 for ^{31}P , and occasionally longer ^{31}P (NS=256 or 512) experiments are interspersed to better observe minor catalyst peaks. For these longer experiments, a TR command is done at $\text{NS}_{\text{timecourse}}-1$ and the result saved by typing the command “wra XX” where XX is the current experiment number+900. In this way a data point that is consistent with the rest of the timecourse can be acquired at the same time as the longer experiment.

Temperature calibration experiments:

To measure the temperature upon circulation in the reaction solvent, the liquid feed capillary was replaced with a melting-point tube filled with ethylene glycol and sealed to the end of the stainless steel capillary with heat-shrink tubing. All pressurization and depressurizing were done through the bypass side, and pressure in the capillary was maintained by doing all manipulations with the liquid bypass valve open to the liquid feed side.

2 mL toluene- d_8 with 12 mM trimethoxybenzene was placed in the instrument with a capillary filled with neat ethylene glycol attached in place of liquid feed capillary. For higher flow rates (>1 mL/min), took an initial spectrum (static), then circulated for 10 min (5 min wasn't sufficient for full equilibration, 15 min gave same temp as 10 min) at reported flow rate to equilibrate. Set temperature (“edte”) and measure actual temperature after circulation stopped (1 scan spectra, with a 30s interval).

4.6. References.

-
- ¹ Heck, R. F.; Breslow, D. S. *J. Am. Chem. Soc.* **1961**, *83*, 4023-4027.
- ² Watkins, A. L.; Landis, C. R. *J. Am. Chem. Soc.* **2010**, *132*, 10306– 10317.
- ³ Nelsen, E. R.; Landis, C. R. *J. Am. Chem. Soc.* **2013**, *135*, 9636 – 9639.
- ⁴ Brown, J. M.; Kent, A. G. *J. Chem. Soc., Chem. Commun.* **1982**, 723 – 725. Brown, J.; Kent, A. *J. Chem. Soc. Perkin Trans. 2* **1987**, 1597.
- ⁵ (a) Horvath, I. T.; Miller, J. M. *Chem. Rev.* **1991**, *91*, 1339 – 1351. (b) Gaemers, S.; Luyten, H.; Ernsting, J. M.; Elsevier, C. J. *Magn. Reson. Chem.* **1999**, *37*, 25-30. (c) Diebolt, O.; van Leeuwen, P. W. N. M.; Kamer, P. C. J. *ACS Catal.* **2012**, *2*, 2357–2370. (d) Schulz, T.; Färber, C.; Leibold, M.; Bruhn, C.; Baumann, W.; Selent, D.; Porsch, T.; Holthausen, M. C.; Siemeling, U. *Chem. Comm.* **2013**, *49*, 6834-6836.
- ⁶ Roe, D. C. J. *J. Magn. Reson.* **1985**, *63*, 388.
- ⁷ (a) Selent, D.; Baumann, W.; Boerner, A. Eur. Patent DE10333143, **2005**. (b) Walther, A. Köckritz. A. Martin, D. Selent, Eur. Patent DE102011007527, **2012**.
- ⁸ Buser, J. Y.; McFarland, A. D. *Chem. Commun.* **2014**, *50*, 4234-4237.
- ⁹ Kubis, C.; Baumann, W.; Barsch, E.; Selent, D.; Sawall, M.; Ludwig, R.; Neymeyr, K.; Hess, D.; Franke, R.; Börner, A. *ACS Catal.* **2014**, *4*, 2097–2108.
- ¹⁰ Watkins, A. L.; Hashiguchi, B. G.; Landis, C. R. *Org. Lett.* **2008**, *10*, 4553-4556. Watkins, A. L.; Landis, C. R. *J. Am. Chem. Soc.* **2010**, *132*, 10306– 10317.
- ¹¹ See chapter 2 and Gooßen, L. J.; Paetzold, J.; Koley, D. *Chem. Commun.* **2003**, 706-707.

Chapter 5

Asymmetric hydroformylation in a flow reactor for industrial-scale applications

This work was performed in collaboration with Eli Lilly and Co. and substantial contributions were made by Scott A. May, Martin D. Johnson, Joel R. Calvin, James R. Stout, and Joseph R. Martinelli.

Other contributors to this project include (in alphabetical order): Jonas Y. Buser, Alison N. Campbell, Richard F. Cope, Brian D. Haeberle, Gordon R. Lambertus, and Michael E. Laurila. Paul Milenbaugh, Todd Maloney.

Specific work performed at Eli Lilly is recognized within the text.

5.1 Introduction.

5.1.a Advantages to developing asymmetric hydroformylation as a continuous flow process.

While commodity scale linear-selective hydroformylation is an expansive industrial process that produces billions of pounds of aldehydes annually, the industrial application of asymmetric hydroformylation (AHF) with catalyst-controlled selectivity is unreported to date. There are a number of examples of fine chemicals produced by industrial hydroformylation, particularly in the fragrance industry, but direct, cost-effective synthesis of chiral aldehydes has not been demonstrated.¹ The main barriers to development of an industrial-scale asymmetric hydroformylation are the control of selectivity, cost, and safety. Selectivity relies upon gas pressure and efficient mass transfer, conditions that can be difficult to achieve in larger batch reactions. Performing AHF in a continuous flow reactor alleviates the safety concerns by limiting the volume of gas in the reaction, allows for rapid scalability of the process in a small footprint, and additionally reduces cost. Combining the high rates and selectivities of bisdiazaphospholane ligands developed in the Landis group with continuous flow technology developed at Eli Lilly and Co. produces a safe, scalable asymmetric hydroformylation technology, which we applied to the synthesis of naproxen as an initial demonstration.

On the fine chemicals scale, a number of examples of linear-selective hydroformylation have been employed to generate intermediates for pharmaceuticals, fragrances, and agrochemicals. In particular, BASF and Roche both produce vitamin A by rhodium-catalyzed hydroformylation.¹ Celanese also uses a process for hydroformylation of limonene to produce fragrance intermediates.² Hydroformylation of norbornene has been demonstrated on a 10 kg scale with a rhodium dppf catalyst that produces only the *exo* product, though this process relies on the stereochemical information in the substrate, not the catalyst, to induce

diastereoselectivity.³ While these examples demonstrate the potential for applying hydroformylation to synthesis of fine chemicals, none of them utilize a chiral catalyst and *asymmetric* hydroformylation to induce chirality during the process. In order for it to become a commercially viable process, asymmetric hydroformylation must compete with other routes to chiral aldehydes. We believe that the development of an economical, scalable asymmetric hydroformylation technology will help transform the state of the art by addressing cost and safety concerns.

The adaptation of AHF to pharmaceutical synthesis has been hindered by safety concerns related to the use of large amounts of syngas and the requirement of specialized high-pressure reactors that are costly and incompatible with current infrastructure. Synthesis of APIs (active pharmaceutical ingredients) is most commonly done in multipurpose production facilities. This is due to the transient nature of pharmaceutical synthesis, where the peak output and duration of a particular process is not known when designing the first production-scale run, and the equipment will often be repurposed for different processes when a particular production run is complete. Flow chemistry provides some key advantages specific to performing high-pressure reactions in the pharmaceutical industry.⁴

First, flow reactors are scalable, which reduces the financial risk of capital investment in testing out a new drug candidate that may not perform well enough to reach commercialization. The types of homogeneous, continuous flow reactors used in this work are a simple, flexible design, which minimizes the overhead cost of implementation and allows for re-use of equipment for later studies. In addition, this type of reactor design is mostly liquid-filled during operation, which minimizes the amount of hazardous gas to levels below those required for running the same scale reaction in a batch reactor.⁵ This means that the reactions can be

performed in shared facilities instead of specialized plants, which further decreases the overhead and the risk of catastrophic accidents. Finally, the time and cost of scale-up of continuous reactions tends to be less than that for current processes, and the conditions are more easily scaled from those developed on the experimental laboratory scale.⁴

When running in a flow reactor, there are a few key terms for understanding what is happening in flow. First, in a batch reactor the material all goes in and out of the reaction at the same time. The analogous value in a flow reactor is the residence time, τ , which is the average time that the material spends in the reactor. Residence time is defined as $\tau = \frac{V}{Q}$, where V is the volume of the reactor and Q is the volumetric feed rate. In an ideal system, all material would experience the exact same amount of time in a reactor. However, mixing along the length of the reactor occurs and leads to non-ideal behavior, which is quantified as the axial dispersion number. When a reagent gas is involved in the reaction, a determination of the $k_L a$, the gas-liquid volumetric mass transfer coefficient, allows for quantification of the ability of the system (either in a batch or flow reactor) to provide gaseous reagents to the chemical reaction occurring in the liquid phase.

Hydroformylation in flow is not a new concept, with numerous examples in a variety of systems, including immobilized catalysts in biphasic systems with ionic liquids or in reactors with scCO_2 , jet-loop reactors with nanofiltration, among others.⁶ However, in recent reports of asymmetric synthesis in flow, asymmetric hydroformylation is notably absent.⁷ The process development group at Eli Lilly has developed expertise in flow technology, highlighted by some of their recent publications in the field.^{5, 8} We embarked upon a collaboration to expand this technology to include asymmetric hydroformylation.

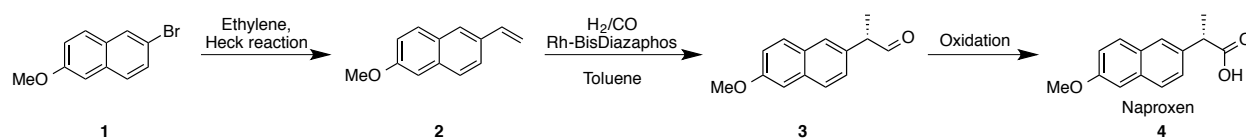
5.1.b Highlighting AHF in flow by performing the continuous asymmetric synthesis of naproxen

A three-step, enantioselective synthesis of naproxen is envisioned as a demonstration of the viability of asymmetric hydroformylation in continuous flow. This synthesis starts with a Heck reaction with ethylene to form the vinyl naphthalene **2** (Scheme 5.1). This substrate is then pumped into the continuous flow reactor (Figure 5.1), where it undergoes asymmetric hydroformylation. The final step is oxidation of the product aldehyde to the corresponding acid, naproxen. This scheme is ideally envisioned as three sequential reactions telescoped together, each using a different reagent gas. Demonstrating this multi-step synthesis in a flow reactor provides the chance to carry the intermediate aldehyde directly on to a more stable product. Previously, the product aldehyde has been avoided in synthesis because it is sensitive to epimerization.⁹ The same rationale can be used for preventing accumulation of the vinyl naphthalene precursor **2**, which can be sensitive to polymerization. Telescoping the reactions together not only minimizes waste associated with work-up, it also avoids byproduct formation.

The proposed synthesis of naproxen is not intended to disrupt the current commercial synthetic method—it is instead envisioned as a way to highlight the work herein with a molecule that was one of the first pharmaceuticals to be sold as a single enantiomer.¹⁰ The straightforward synthesis proposed includes the formation of the chiral center by asymmetric hydroformylation. AHF has been employed in the synthesis of enantiopure (*S*)-naproxen previously, but the cost of the reaction as employed exceeded the currently established route, via the Syntex synthesis.^{9,11,12} In addition, the platinum-catalyzed AHF gave high *ee* (>96%) but relatively poor regioselectivity with a branched:linear ratio of 3:1.^{9,13} Other routes to enantiopure (*S*)-naproxen include Noyori's asymmetric hydrogenation¹⁴ and the Zambon synthesis.¹⁵ Noyori's ruthenium-catalyzed

asymmetric hydrogenation produced high *ee* and quantitative yield, but was avoided because of the process safety concerns with high pressures of hydrogen gas (135 atm) and the expense of the precursor unsaturated acid.¹⁰ AHF in a flow reactor instead should allow for lower catalyst loading than the previously reported AHF, and will avoid the process concerns of having large amounts of hazardous gasses. Combining the Heck synthesis from the bromonaphthalene starting material **1** will reduce the effective cost of olefin **2** by minimizing workup procedures and preventing impurity formation in the sensitive intermediates. All of the advantages to a continuous flow AHF are highlighted in the synthesis of an enantiopure API like naproxen.

Scheme 5.1: Synthesis of naproxen highlighting the use of reagent gasses.



5.1.c Equipment setup

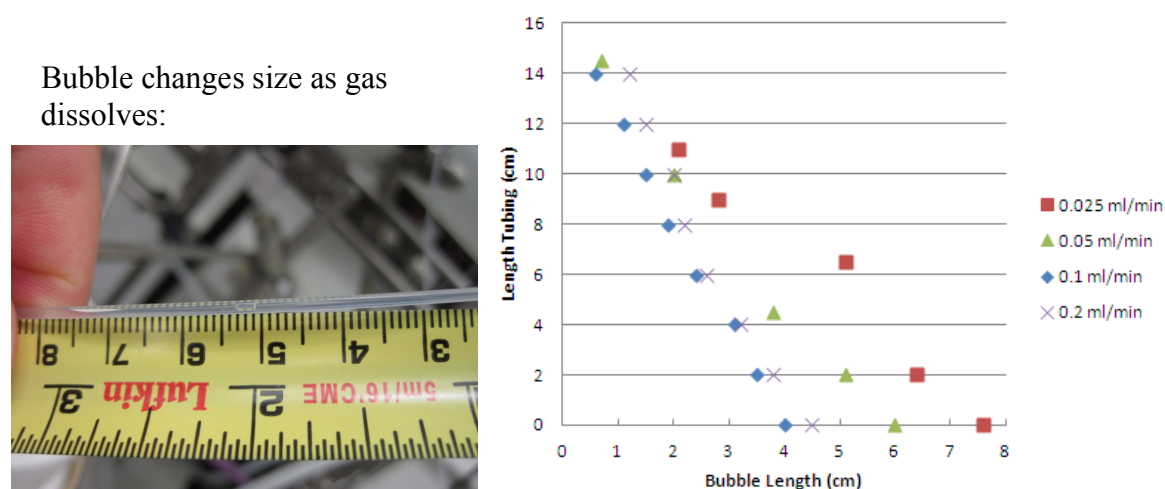
Batch runs at the University of Wisconsin-Madison were run in a CAT24 Hastelloy or stainless steel autoclave, in glass pressure bottles,¹⁶ or in a high-pressure NMR apparatus (see Chapter 4).

Batch runs at Eli Lilly are run in an Endeavor parallel reactor, which provides excellent gas-liquid mixing and efficient mass transfer. Unless otherwise noted, these runs were performed with the same solutions used in the flow runs for more direct comparison. Typical reactions are set up on a 2 mL volume scale.

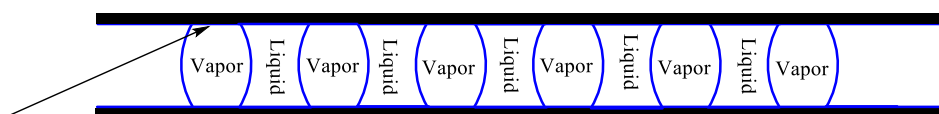
All flow runs were conducted at Eli Lilly. These were initially conducted in a 13 mL segmented flow reactor. The pipes in series reactor described below ultimately surpassed this

design. The segmented flow reactor design is limited by the lack of control of the gas and liquid fill levels across the entire reactor. This is evident when part of the reactor was replaced with PFA tubing and the size of gas and liquid segments is observed over the course of the reactor. Moving to a pipes-in-series design allows for independent adjustment of the gas and liquid flow rates, allowing for more flexibility in the range of available running conditions.

Figure 5.1: Segmented flow in 13 mL tubular reactor.



Ideal state where vapor and liquid segments are equal



Thin film of liquid coats the reactor walls
resulting in high v/l mass transfer

Where we operate gas pulses result in different vapor segment size

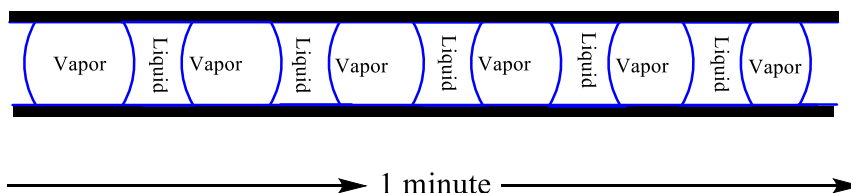
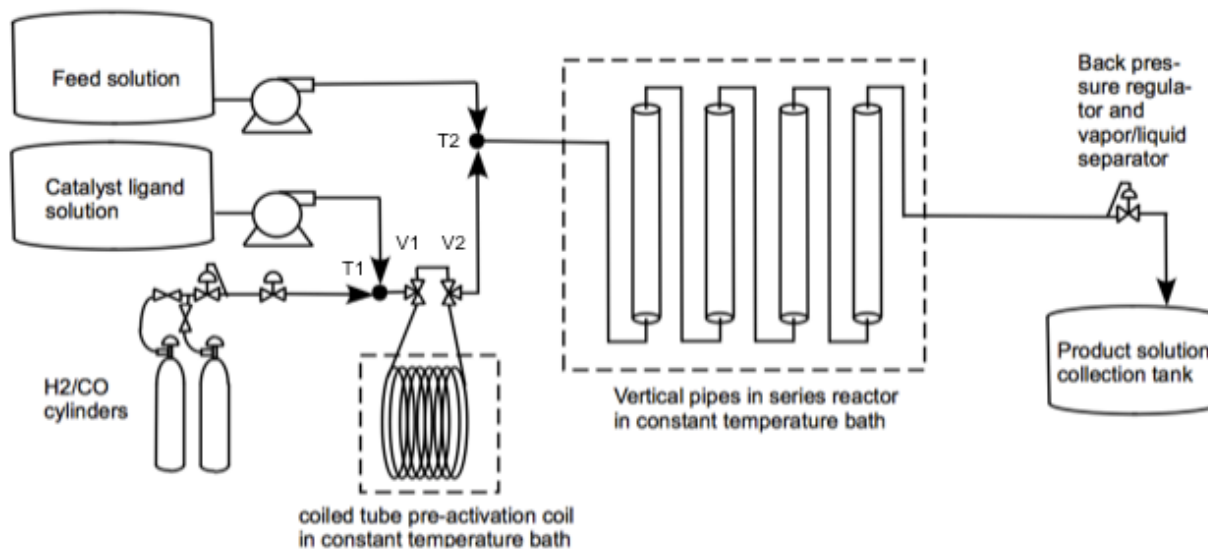


Figure 5.2: Flow system overview

Flow system designed, built and tested at Eli Lilly.

The optimized reactor design involves a 23.8 mL pipes in series reactor consisting of twenty 0.3 mL pipes connected with 10' jumpers of 1/16" stainless steel tubing (Figure 5.3). A pre-activation coil for the catalyst is included, which can be incorporated into or isolated from the flow path by a valve control (Figure 5.2, V1&V2). This allows for premixing of the catalyst feed solution with the reagent gas in a separate, heated zone prior to introduction of the olefin feed solution. The olefin and catalyst/reagent gas lines then combine at T2 prior to entering the reactor. A back-pressure regulator maintains constant pressure over the entire reactor to prevent zones where starvation may occur.

Figure 5.3. A similar 38 mL pipes in series reactor.

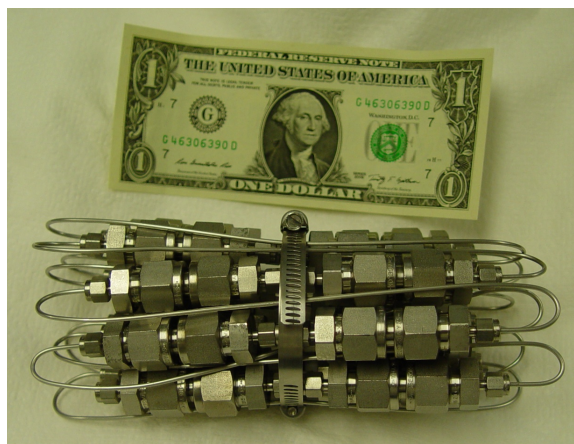


Photo provided by Eli Lilly

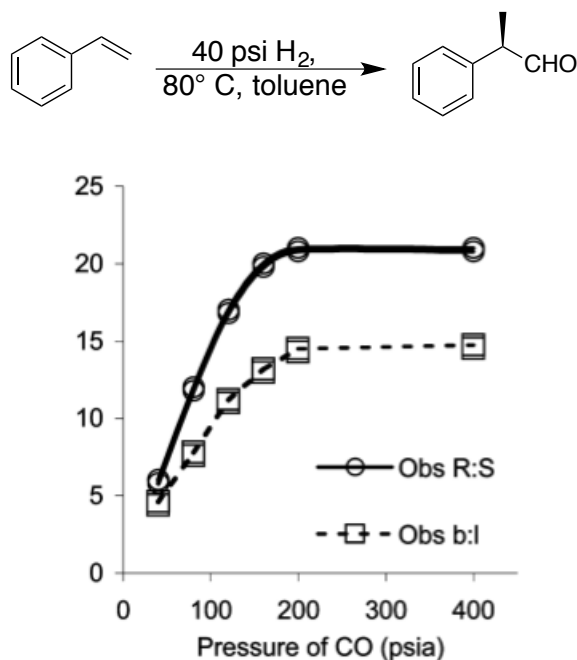
As discussed above, while application of flow technology to asymmetric reactions has been expanding, relatively little work has been done on systems which involve reagent gasses. To develop selective hydroformylation, control of gas to liquid mass transfer is crucial, as the effective concentration of syngas in the solution determines selectivity. Pipes in series type reactors are particularly advantageous for independent control of the gas and liquid flow rates and therefore the control of mass transfer efficiency. The studies in this chapter are a mixture of batch studies to estimate rates and selectivities before moving into a continuous flow apparatus, flow studies, and batch studies that are intended to reproduce the flow studies to demonstrate that the flow system is well controlled.

5.2.a Batch studies to establish flow rates: Styrene

Much of the preliminary work in the flow system and on determining the rates of AHF for aryl alkenes under different conditions were done with styrene as an analog for the more costly 6-methoxy-2-vinyl naphthalene **2**. Styrene is an attractive substitute because much of the work done to determine the kinetics of AHF uses styrene as a model system.¹⁷ In addition,

styrene, like other aryl alkenes including **2**, exhibits CO pressure dependent selectivities, which this study aims to control (Figure 5.4).

Figure 5.4: Selectivity of styrene AHF changes with pressure.



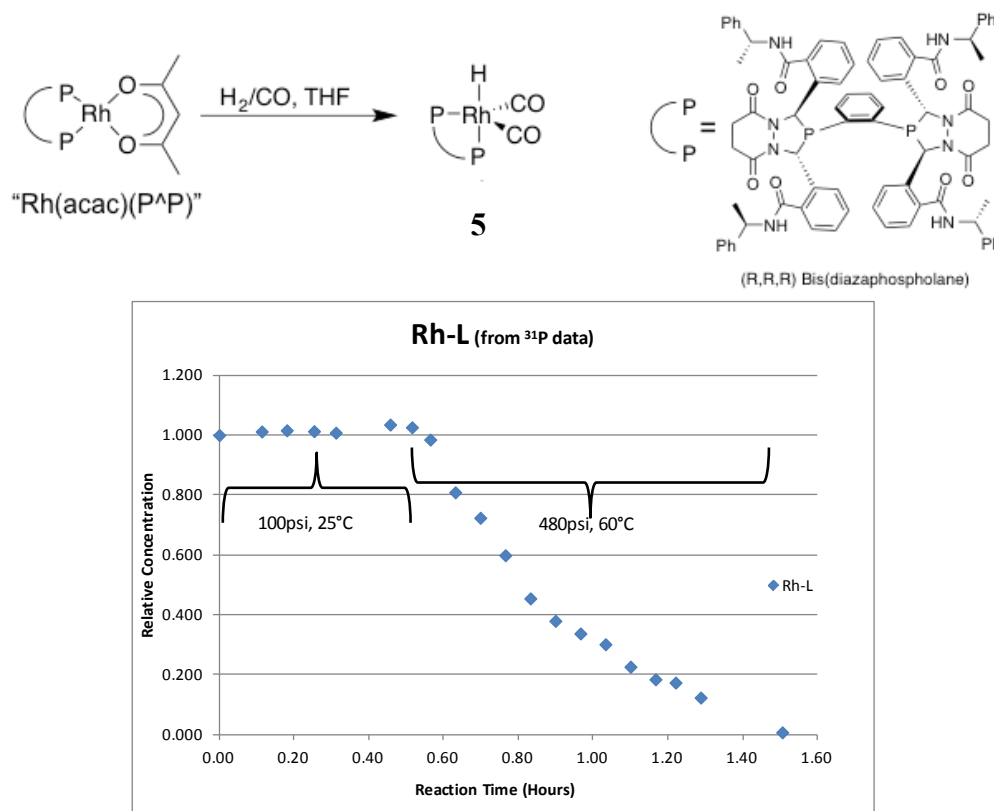
While control of this additional parameter is challenging, the use of aryl alkenes like styrene and **2** also provides data about mass transfer in the reaction, which we used as a probe of actual reaction conditions over the course of the reaction. If the hydroformylation of pressure-sensitive aryl alkenes occurs in an apparatus with high selectivities, the reactor is producing a high $k_L a$ value and will provide efficient gas-liquid mass transfer.

5.2.b React-NMR at Lilly and reaction timecourses.

React-NMR studies on the AHF of styrene were done at Lilly with the help of Jonas Buser. These studies helped elaborate some of the kinetic details observed in batch reactions previously, and suggested that elevated temperatures and extended pre-activation times (at least one hour) were necessary for complete conversion of the catalyst precursor to the

hydridodicarbonyl species **5** (Figure 5.5). Reactions were carried out in the React-NMR apparatus described recently.¹⁸

Figure 5.5: Decay of Rh(acac)(bis(diazaphospholane)) during pre-activation of the catalyst.

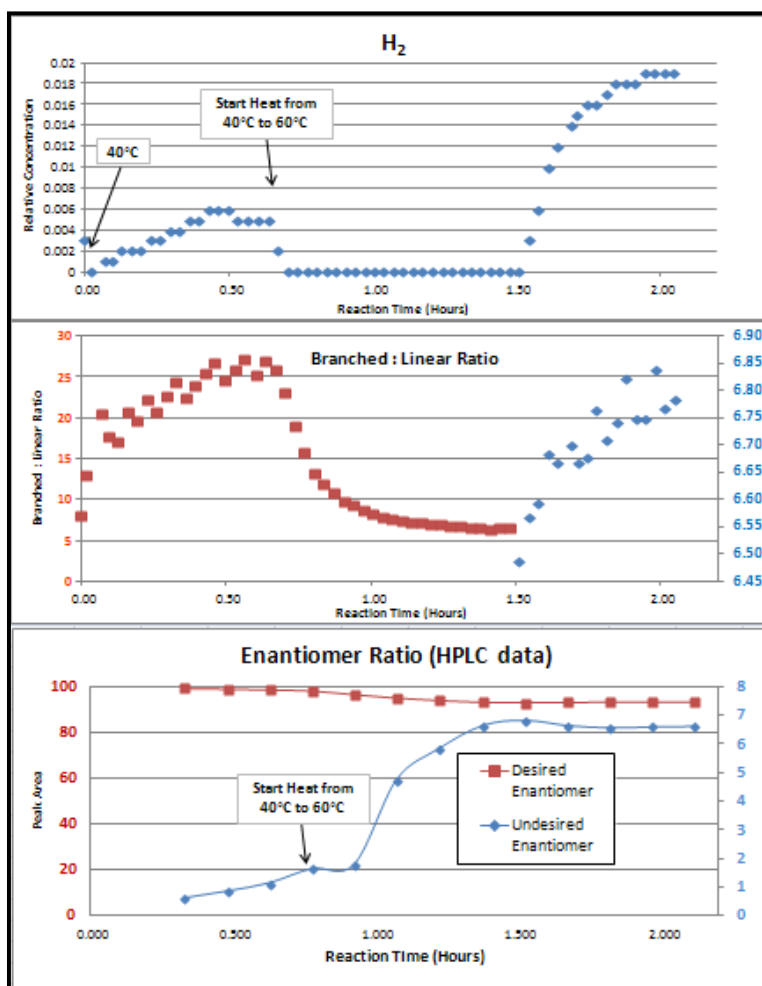
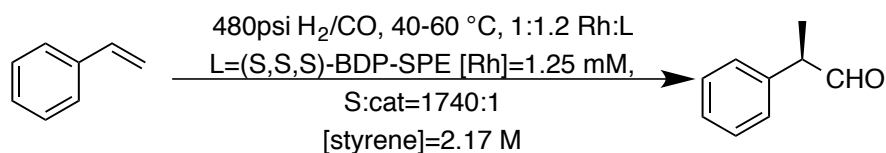


Jonas Buser, Eli Lilly

However, the AHF rapidly undergoes starvation at such high catalyst loadings, and further examination of the rate data will require modification of the experimental setup (Figure 5.6). This experiment does, however, provide direct observation of the dependence of selectivity on mass transfer. When the concentration of H₂ is low (and, by extrapolation the concentration of CO is low), the selectivity of the reaction decreases rapidly. As the reaction reaches completion and H₂ reappears in the spectrum, the selectivity returns to a high level. Particularly telling is the third chart in Figure 5.6, where starvation conditions lead to rapid formation of the minor

enantiomer. More work on direct observation of the AHF of styrene was performed on the circulating high-pressure NMR (HP-NMR) apparatus built at Wisconsin, which is designed to mitigate mass transfer issues (see Chapter 4). In this apparatus, the catalyst species were also observed by ^{31}P NMR, and the hydridodicarbonyl **5** reappears at the same time as H_2 reappears, indicating a change in resting state under starvation conditions.

Figure 5.6: Selectivity under starvation kinetics in the React-NMR.



Jonas Buser, Eli Lilly

5.2.c Flow runs with styrene

Flow studies run with styrene were also run with a commercially available analog of the bisdiazaphospholane catalysts, Ph-BPE (Figure 5.7). Unfortunately, many of these studies are compromised because of the strong dependence on catalyst age that reactions run with Ph-BPE exhibited. Since the flow runs were done with different ages of catalyst (and the catalyst ages while the reaction is reaching steady state), the data collected are of limited use for optimization of flow conditions. Select studies that highlight these problems are reported in Figure 5.8.

Figure 5.7: Ligands used for AHF flow studies

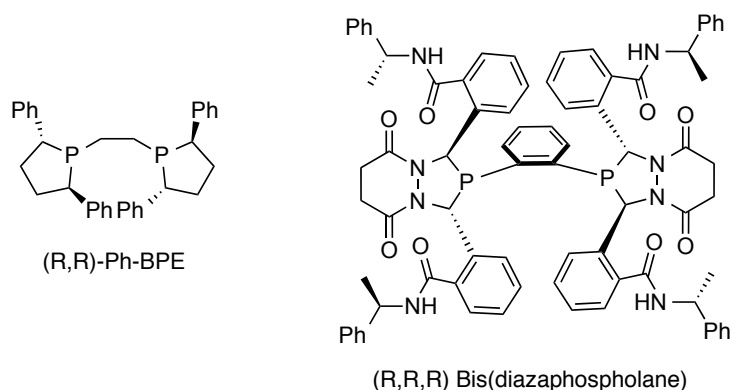
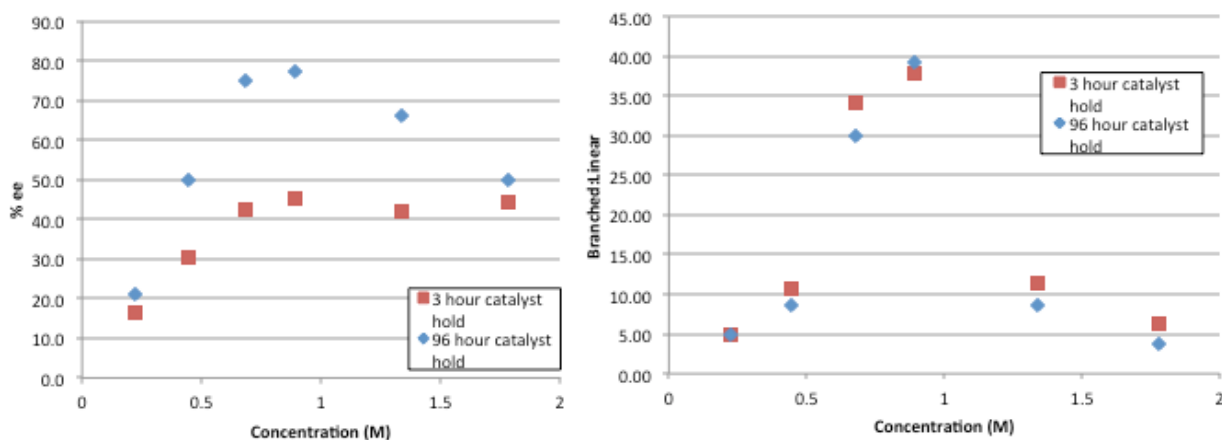


Figure 5.8: AHF with Ph-BPE: effect of catalyst age on selectivity.

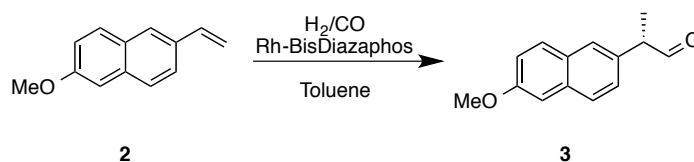


Alison Campbell, Eli Lilly

5.3.a Batch studies with naproxen olefin

The AHF of the naproxen olefin **2** was performed in glass pressure bottles initially to set benchmarks for the rate and selectivity of the reaction. While none of these preliminary results match those reported previously,¹⁹ the selectivities appear promising, and the rates at the given conditions suggest that the naproxen olefin will exhibit a similar rate to styrene.

Table 5.1: Initial runs at UW: batch runs in glass pressure bottles.



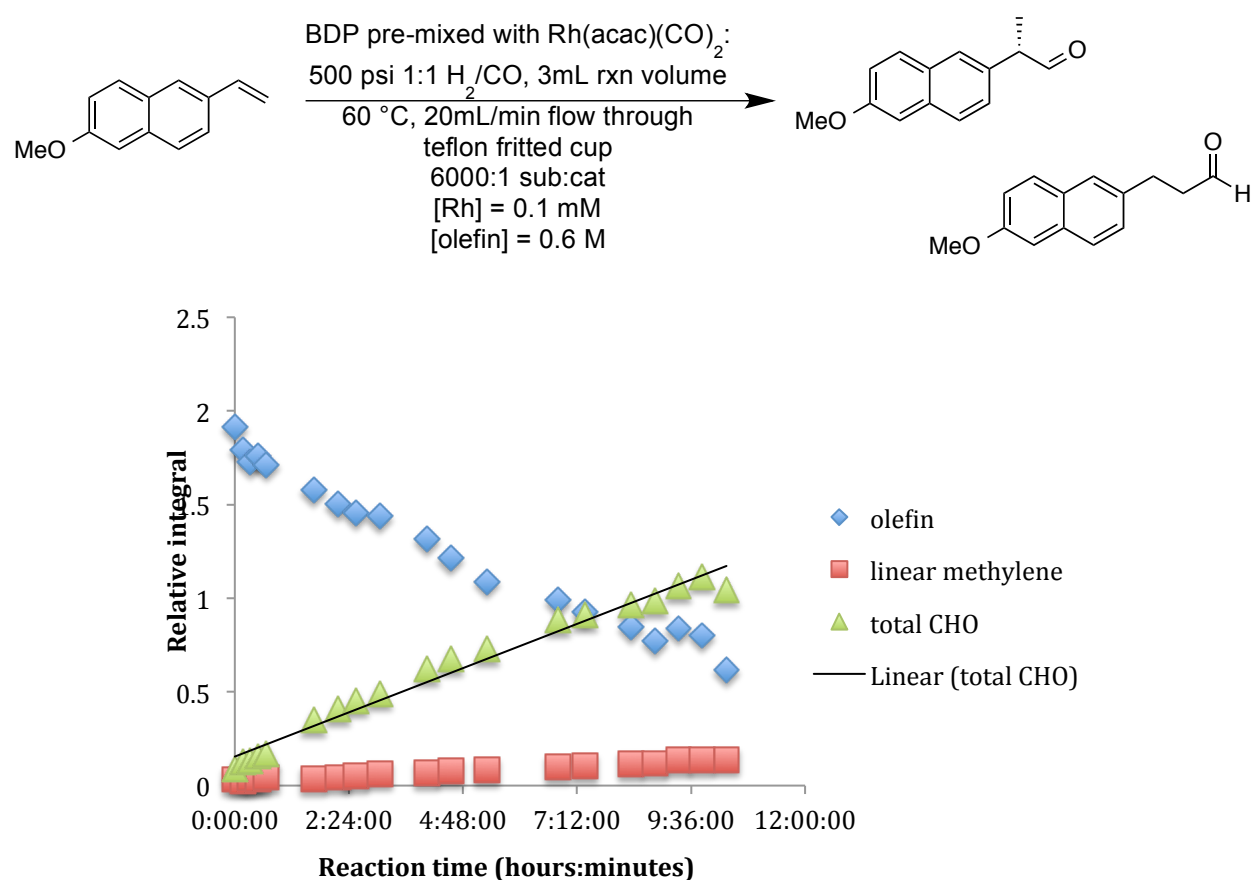
Entry	[olefin]	time, h	S/C	Conv.	b:l	ee
1 rac	1 M	40	500	100	20.7	n.d.
2 S,S,S	0.8 M	1	6400	3	>30	n.d.
3 S,S,S	0.8 M	4	6400	16	27	n.d.
4 S,S,S	0.8 M	13.5	6400	60	29.5	71%
5 R,R,R*	0.8 M	1	2000	9.5	20.7	n.d.
6 R,R,R*	0.8 M	22	2000	97.4	29.2	n.d.
7 R,R,R (Endeavor)	0.54 M	3	1350	29	26.3	n.d.
8 Previously published [#]	1 M	8	500	100	>50	96%

Reactions run at 150 psi H₂/CO, 40 °C. * Ligand is of high potency, and shows little change in rate or selectivity from previous ligand (S,S,S) obtained from Aldrich. [#]Previous published result was at 120 psi CO / 40 psi H₂.

With the initial results in Table 5.1 in hand, the AHF was investigated in the HP-NMR apparatus at 80 and 60 °C under a number of different S/C loadings. In all cases, the reaction appears

starved, where the rate of olefin decay and aldehyde growth are best fit to linear regressions. This gives a zero-order dependence on olefin, a hallmark of the resting state changing and the reaction being mass-transfer limited. When run at lower catalyst concentrations to prevent starvation, the solvent in the reaction is lost and data quality deteriorates before enough of the reaction timecourse is complete. Because of these data quality issues, initial rates and selectivities were studied by reactions at varying concentrations in the CAT24 multi-well Parr screening apparatus.

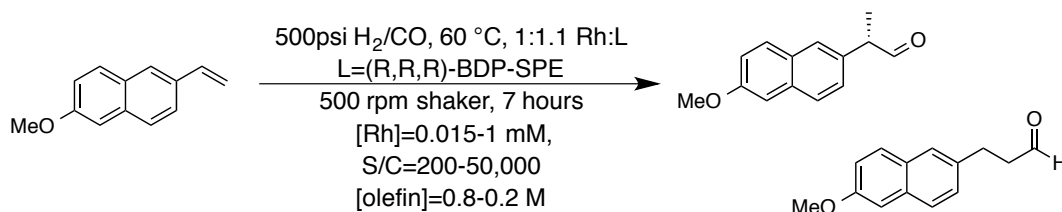
Figure 5.9: HP-NMR timecourse of Naproxen hydroformylation showing starvation kinetics



End results of HPNMR run were 70% conversion, 15:1 b:l, 86% *ee*.

Parallel reactions in the CAT24 are limited to screening at a single set of pressure and temperature conditions. The concentration of catalyst and olefin were varied over a range of values to develop an initial set of conditions for the flow reactor. Target results were to achieve about 87% conversion in a 6 h batch run, so that if the reaction were to go 12 h (12 h τ) in a flow reactor it would reach essentially complete conversion. Unfortunately the utility of these screening runs is limited because the reactions are not well mixed, even at 500 rpm, and the observed selectivities appear mass-transfer limited. This is seen most in the low values of branched:linear and enantioselectivity across all reactions, including control wells that were run with styrene to be able to compare to previous rate data. The most use these data can be is as a rough prediction of rate. To get selectivity numbers and true rate data, a reactor with a much higher $k_L a$ is needed.

Tables 5.2-5.5: Screening catalyst loading at two temperatures to observe approximate rate.



Conversion with varying [Rh] and [olefin]

[olefin]	[Rh] →	0.4 mM		0.1 mM		0.03 mM		0.015 mM		1 mM	
	0.8 M	0.962	0.355	0.531	0.082	0.145	0.018	0.074	0.011	1.000	0.750
	0.6 M	0.975	0.465	0.535	0.123	0.167	0.025	0.029	0.013	1.000	
	0.4 M	0.987	0.590	0.625	0.160	0.213	0.035	0.107	0.014	1.000	
	0.2 M	1.000	0.885	0.803	0.237	0.265	0.058	0.174	0.004	1.000	
	0.6 M styrene	1.000	0.612	0.803	0.187	--		0.091	0.004	--	

60 °C 40 °C

TON with varying [Rh] and [olefin]

[olefin]	[Rh] →	0.4 mM		0.1 mM		0.03 mM		0.015 mM		1 mM	
	0.8 M	1923	709	4244	655	3874	468	3950	599	800	600
	0.6 M	1462	697	3209	736	3333	496	1165	514	600	
	0.4 M	986	590	2501	638	2834	463	2857	365	400	
	0.2 M	500	442	1605	473	1764	385	2314	55	200	
	0.6 M styrene	1500	918	4816	1122	--		3636	151	--	

B:L ratio with varying [Rh] and [olefin]

[olefin]	[Rh] →	0.4 mM		0.1 mM		0.03 mM		0.015 mM		1 mM	
	0.8 M	13.22	16.2	11.89	18.3	9.85	28.4	10.21	34.4	12.59	21.4
	0.6 M	10.83	19.2	11.96	17.2	8.29		5.26		8.55	
	0.4 M	9.11	14.8	10.65	18.1	8.55		8.91		9.78	
	0.2 M	6.78	15.4	7.56	13.6	6.96		6.28		8.43	
	0.6 M styrene	8	19.8	8.06	17.6	--		9.08		--	

60 °C 40 °C

% ee with varying [Rh] and [olefin]

[olefin]	[Rh] →	0.4 mM		0.1 mM		0.03 mM		0.015 mM		1 mM	
	0.8 M	74.7	56.7	75.2	58.8	69		69.6		66	
	0.6 M	70.7	53.6	73.3	51.7	62.4		43.6		63.5	
	0.4 M	57.9	45.9	68.2	38.7	58.7		61.7		53	
	0.2 M	40.5	19.7	54.6	26.4	48.7		28.4		41.43	
	0.6 M styrene	36.1		41		--		44.6		--	

Table 5.6: Endeavor screens at Eli Lilly compared to batch work at Wisconsin.

	Time	[Rh]	S/C	conv.	B:L	ee
Styrene	6 hours	0.06 mM	10,000	33	4.5	27
	6 hours	0.1 mM	6,000	54	4.47	33
	6 hours	0.4 mM	1500	97.8	6.82	54
	12 hours	0.06 mM	10,000	60.8	4.64	24
Naproxen	6 hours	0.06 mM	10,000	10.8	9.8	77
	6 hours	0.1 mM	6,000	32.5	7.61	80
	6 hours	0.4 mM	1500	91.5	12.01	82
	12 hours	0.06 mM	10,000	27.2	11.39	78
CAT24 Naproxen	7 hours	0.1 mM	6,000	53.3	12.0	52
	7 hours	0.4 mM	1500	97.5	10.8	54

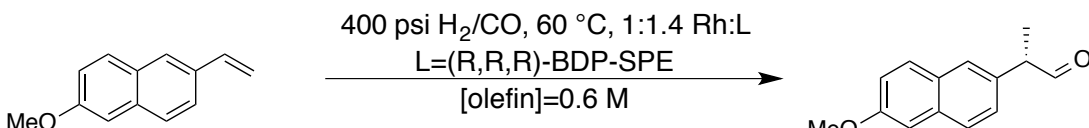
[olefin] = 0.6M, 60 °C, using Rh(acac)(bisphosphine) for solutions.

5.3.b Flow studies with naproxen olefin:

Upon moving to the finalized pipes in series reactor design and using the *bis*(diazaphos) catalyst with the naproxen olefin **2**, our initial estimate to reach three half-lives in a 6 h τ was a S/C loading of 10,000, 60 °C, 400 psi, and an olefin concentration of 0.6 M. This was based on the values determined by screening in the CAT24 (Tables 5.2-5.5, above). We estimated that while the above reactions were starved, the overall rate may not change substantially, only the selectivity would change. However, the initial flow run progressed to only 7% conversion at a 6 h τ . We assumed the catalyst solution was compromised, but after a number of modifications to the system (Table 5.7, entries 2-4) to test the integrity of the catalyst solution and the reaction setup, low conversion remained problematic. This was eventually determined to be the result of a dilution error that led us to run at lower catalyst loadings than intended, a problem that was

exacerbated by discovering that the catalyst being used was of low potency. The potency and dilution were accounted for in the final two runs, and accordingly we saw high conversion and good selectivity in these runs. The pre-activation coil was bypassed for run 6, but no change in the reaction resulted. Further experiments are needed to determine the role of pre-activation.

Table 5.7: Flow studies with naproxen olefin: Adjusting catalyst source and loading



Flow run (change made)	[Rh] feed	S/C*	τ (hrs)	% conv.	b:l	ee
1: Preformed catalyst in THF	0.5 mM	10,000 28000	6	7	9	85
2: (cat solution prepared in THF, diluted in toluene)	0.06 mM	10,000 85,000	6	0	-	-
3: (same catalyst, preactivation coil bypassed)	0.06 mM	85,000	6	0	-	-
4 (increase S/C by changing flow rates, same solutions)	0.06 mM	1500 12,500	6	0	-	-
5 (adjusted dilution error from runs 2-4)	5 mM	1500 4300	6	87	13.7	88
6 (preactivation coil bypassed)	5 mM	1500 4300	6	87	12	86

*Numbers with a strikethrough were the intended catalyst loadings, the actual loadings adjusted for dilution and potency are given below.

After the runs in Table 5.7, a few modifications were made to the reaction setup. First, the catalyst pre-activation coil was separated so that its temperature can be independently controlled from that of the pipes in series reactor. Second, the ligand was evaluated to ensure accurate catalyst loadings and no side reactions due to minor isomers present in the low potency ligand samples used in Table 5.7 (details of this purification are in Chapter 3). All experiments after this point in the chapter are run with purified ligand.

We began the next set of flow conditions by reproducing the final conditions from the previous run. While the catalyst loading is slightly higher, the conversion and selectivities in the initial conditions of the new run (Table 5.8, entry 3) are similar to those from the previous set of flow runs (Table 5.8, entries 1 and 2). In addition, the data from the batch run are consistent with the flow studies (Table 5.9, entry 2). After establishing steady state at this baseline set of conditions, we switched to flowing the catalyst and syngas feed through the preactivation loop. Unfortunately, the amount of time to reach steady state was underestimated, and delayed analysis of samples from the reactor led us to believe we had compromised the catalyst in some way, since the conversion dropped in the samples we had examined. In retrospective, this drop was due to the gap where olefin feed was flowing but catalyst had not reached full strength in the reactor. No data at full steady state is available therefore, but the selectivities appear to be excellent. This set of conditions will be repeated once a more accurate measure of τ is known.

Table 5.8: Flow studies with naproxen olefin: Probing the effect of pre-activation, running longer to reach steady state.

Flow run (change made)	S/C	% conv.	b:l	ee
1-Previous run set	4300	87	13.7	88
2-Previous run set (preactivation coil bypassed)	4300	87	12	86
3-Reproducing conditions (preactivation coil bypassed)	1350	97.9 \pm 0.3	18.9 \pm 0.7	90.2 \pm 0.5
4-pre-activation coil in line ^a	1350	n.d.	20 \pm 4	93 \pm 1
5-repeat of 3 (preactivation coil bypassed)	1350	97.4 \pm 0.2	20.9 \pm 0.7	93.4 \pm 0.2
6-raised temp. to 70 C	1350	99.07 \pm 0.01	14.7 \pm 0.5	91.5 \pm 0.1

60 °C, 400 psi, s/c = 1350, [cat] = 0.37 mM, [olefin] = 0.50 M, 6h tau predicted.

^aRun 4 did not reach steady state.

Returning to the original set of conditions demonstrated that the results in entry 3 were reproducible (Entry 5). The slightly higher selectivities in this run may be ascribed to the steady state being fully reached for these samples, as the sampling used to calculate the values in Table 5.8 were taken starting 24 hours after the flow run started, whereas those in entry 3 were taken starting 17 hours after the run had started, which may not have been steady state.

Table 5.9: Endeavor batch studies: matching flow studies in table 5.8 and determining the role of temperature and pressure

Well	SM (%)	ee (%)	B/L	T (°C)	P (psi)	S/C	Catalyst/olefin age
1	3.6	89.9	16.2	60	400	1350	preact., new/new
2	3.3	86.3	14.1	60	400	1350	new/new
3	8.5	91	17.3	60	400	1350	new/old
4	5.3	91	15.9	60	400	1350	old/new
5	5.8	91.2	10.8	60	150	1350	new/new
6	48.8	89.7	18	40	300	1350	new/new
7	55.2	84.8	15.6	40	400	1350	new/new
8	57.8	91.5	18.2	40	150	1350	new/new

6 hours, [cat] = 0.371 mM, [olefin] = 0.487, data from HPLC.

The large temperature dependence when switching from 40 to 60 °C reactions in the Endeavor suggests that we may be able to run at higher temperatures without a decrease in selectivity in the flow reactor. Assessment of the temperature dependence was previously unavailable because of limitations to the mass transfer efficiency in the reaction setup at Wisconsin. A series of Endeavor runs were set up to probe the temperature dependence of AHF of the naproxen olefin (Table 5.10). The enantio- and regioselectivity of the reaction are maintained at temperatures of 39-70 °C. This suggests we will be able to run at 70 °C in the

flow reactor with no negative effect on the selectivity of the reaction, and a substantial gain in the reaction rate, so that tau may be reduced. When this change in temperature was implemented in the flow reactor, the conversion increased from 97.4 to 99.1% (Table 5.8, entry 6). However, modest drops in the enantioselectivity and larger drops in the branched selectivity were observed.

Table 5.10: Endeavor batch studies with naproxen olefin at different temperatures.

Temp (set)	T (°C) actual	SM (%)	ee (%)	B/L
100	100	0.8	28.6	5.3
80	80	0.8	73	9.3
70	70	0.8	89	11.2
60*	60	47.1	79	8.1
60	60	6.8	85	11.9
50	45	100	-	-
40	42	51.3	79	14.2
30	39	58.4	81	13.8

6 hours, [cat] = 0.371 mM, [olefin] = 0.487 M, S/C = 1343, 400 psi, data from HPLC. *S/C = 5983, [olefin] = 0.487 M.

A series of Endeavor runs at lower conversion were run to determine the role of preactivation of the catalyst at different temperature and pressure regimes. Reactions were run for 3 hours with conditions analogous to those run previously. Two wells were reserved to run catalyst without pre-activation as a control and a test of the stability of the Rh(acac)(bisphosphine) precatalyst. The rest were run with catalyst that was pre-activated by subjecting the Rh(acac)(bisphosphine) toluene stock solution to a 150 psi atmosphere of syngas at 60 °C overnight. ³¹P NMR of this stock solution after preactivation showed 74% of the Rh(H)(CO)₂(Bisdiazaphospholane), 10% unbound ligand, and about 10% of the Rh(acac)(bisphosphine) precatalyst species (which may be present because the catalyst reverts to

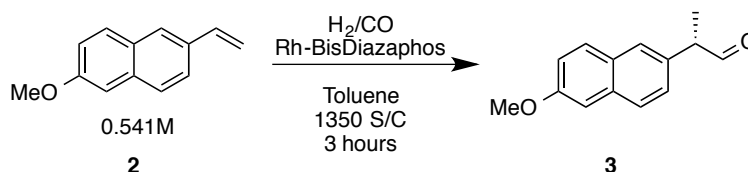
this form under conditions of low syngas pressure), the remainder being an unidentified species (5.5%, at 128 and 92 ppm) and an oxide of the ligand (0.5%). This solution was used to set up Endeavor runs 1h, 6h, and 24h after the preactivation was complete.²⁰ The solution was stored under a nitrogen atmosphere at room temperature as it aged. As shown in table 5.11 and figure 5.10, there appears to be no substantial change in the activity or selectivity of the catalyst between 1 and 24 hours after pre-activation.

Additionally, this study provides additional data about the temperature and pressure dependent selectivity of the reaction to better suggest conditions for future flow runs. The temperature has a profound affect on the rate of the reaction, but the selectivity changes little between 40 and 60 °C (Figure 5.10). At 70 °C, both the branched and the enantioselectivity drop slightly. This effect is larger when the experiment is run with 150 psi of syngas, suggesting that the reaction may become mass-transfer limited under these conditions.

Increasing syngas pressure has previously been shown to inhibit the overall reaction rate, but improve the selectivity of the reaction.¹⁷ The origin of this effect is that the rate of the major, branched pathway is independent of CO concentration, but the minor branched and linear pathways are inhibited by CO. This can be seen in these Endeavor studies as well, with lower pressure leading to higher conversion. When a single case is examined (70 °C, Figure 5.11), it is apparent that the rate of the linear pathway increases most with decreased syngas pressure, while the rate of formation of the major, desired product is essentially unchanged. This is entirely consistent with past results. However, at 40 °C the rate of formation of the major, branched product is increased under lower syngas pressure, leading to substantially higher conversion at 150 psi (compared to 400 psi) but similar selectivities. However, the lower overall rate at 40 °C

is undesirable when trying to minimize the residence time. Running at 150 psi appears to confer few advantages, and further optimization will be done at higher pressures.

Table 5.11: Endeavor batch studies with naproxen olefin to determine stability of pre-activated catalyst under a N₂ atmosphere.



Entry	Conditions T (°C) / P (psi)	1h after preactivation			6h after preactivation			24h after preactivation		
		SM (%)	ee (%)	B/L	SM (%)	ee (%)	B/L	SM (%)	ee (%)	B/L
1	60/400*	21.0	92.3	17.8	23.5	91.6	15.2	20.7	90.4	15.9
2	60/400*	22.9	92.1	17.4	22.9	91.6	14.9	21.9	91.2	16.8
3	60/400	27.3	91.8	15.4	14.1	90.3	11.8	15.5	91.1	14.0
4	60/150	10.4	90.9	10.4	27.3	90.9	11.0	11.0	90.8	10.4
5	70/400	2.4	90.4	11.1	3.8	89.3	11.7	6.9	90.0	11.3
6	70/150	1.7	86.4	6.8	1.8	86.2	7.0	1.8	86.8	6.5
7	40/400	64.9	91.2	20.4	64.1	91.7	11.3	66.4	90.2	26.3
8	40/150	49.4	93.1	18.1	48.8	91.6	14.3	53.6	93.4	22.0

All reactions run for 3h, with a S/C = 1343:1, [olefin] = 0.487 M. *Not pre-activated catalyst (as a control) Aged 24 (entry 1) or 72 (entry 2) hours.

Figure 5.10: Graphical representations of table 5.11.

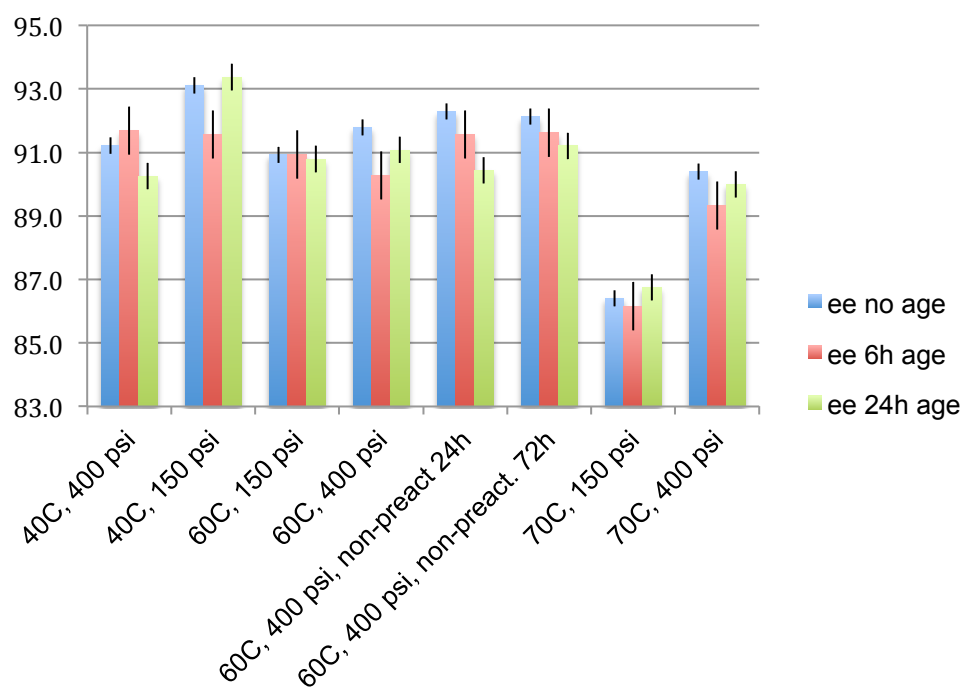
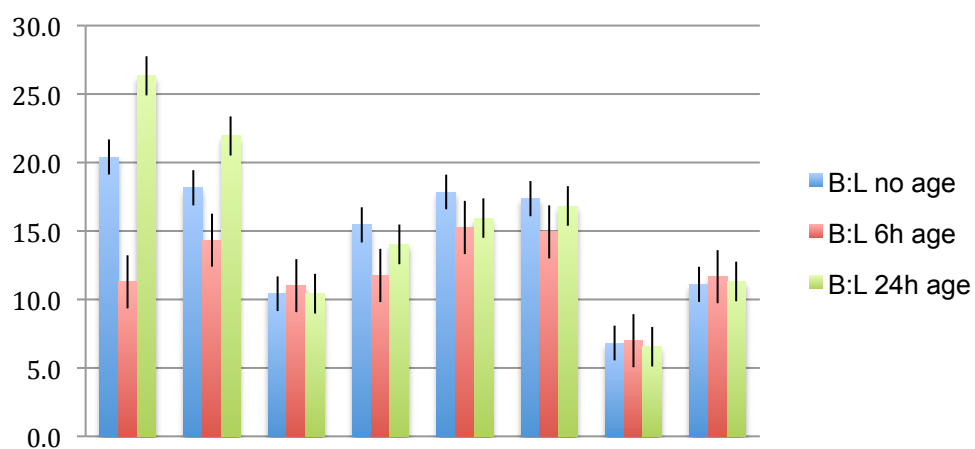
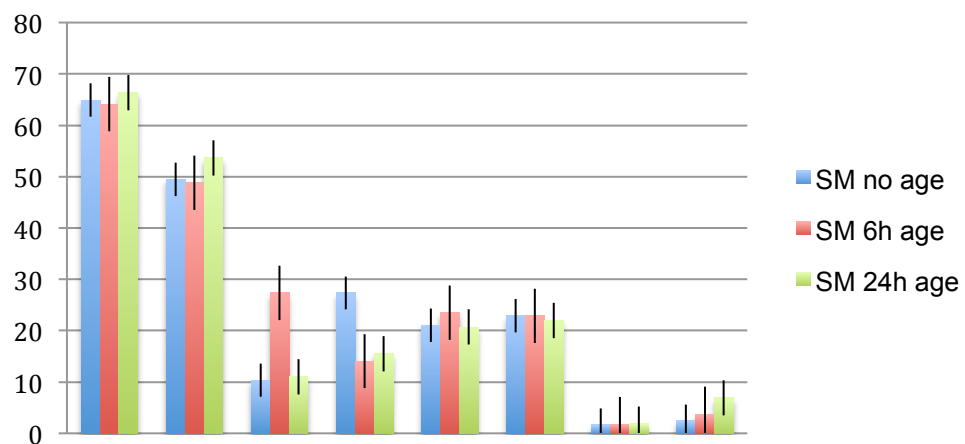
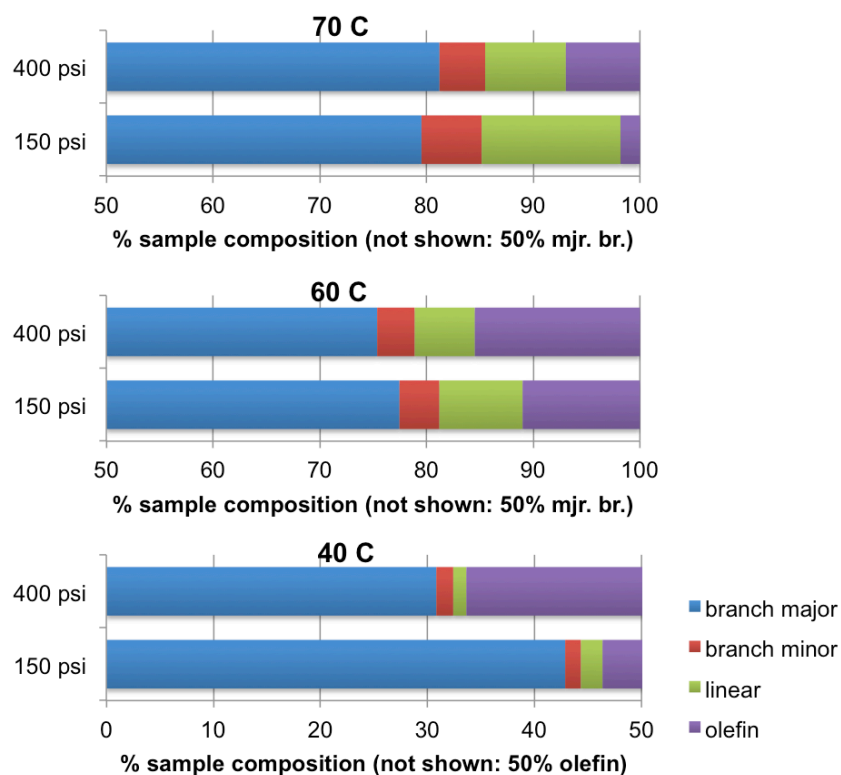


Figure 5.11: Pressure and temperature effects on sample composition.



3h reaction, pre-activated catalyst after 24 h, S/C 1343, [olefin] = 0.487 M.

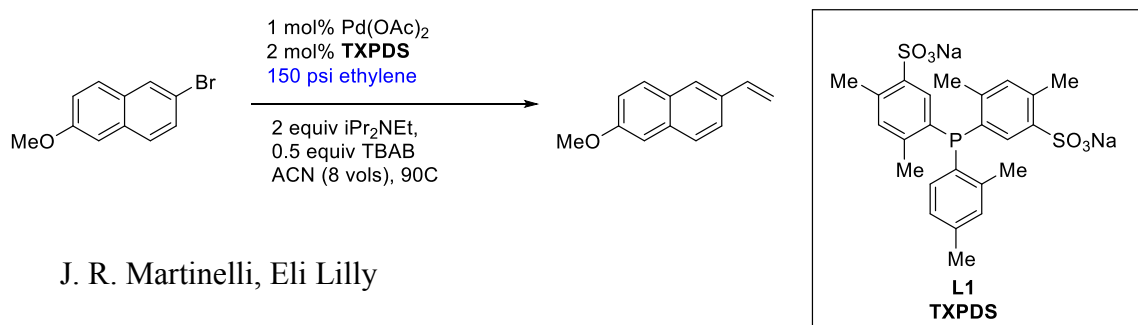
These flow and batch studies have mapped out an initial set of conditions that will serve as a baseline for further optimization of the selectivity and conversion in a given residence time. Further work is ongoing.

5.4 Heck reaction and oxidation for completion of synthesis.

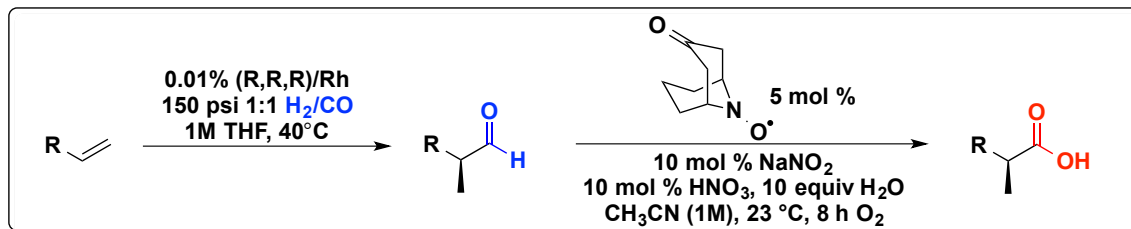
To complete the proposed synthesis of naproxen, formation of the starting 6-methoxy-2-vinyl naphthalene via a Heck reaction and oxidation of the aldehyde to the carboxylic acid were investigated.

The synthesis of the starting naphthalene is accomplished by a Heck reaction with ethylene using the TXPDS ligand, developed based on a Japanese patent.²¹ The reaction proceeds to >99% conversion and yields 86% isolated material after extraction and filtration. Further work with this reaction may incorporate it into a flow process that can be run in series with the hydroformylation.

Scheme 5.2: Heck reaction with ethylene.



The oxidation of the aldehyde product to a carboxylic acid was initially explored as a homogeneous, aerobic oxidation that would be amenable to flow using a catalyst system developed in the Stahl lab.²² This oxidation employs a nitroxyl radical as the catalyst and is an attractive alternative to other oxidations that are known to epimerize the chiral center (Scheme 5.3). Unfortunately, the limitation of this chemistry is arene rings with a methoxy substituent, and the reaction gives none of the desired product under all conditions screened. Instead, a preliminary screen of oxidation methods was performed, and the Pinnick oxidation was selected as a good alternative for its mild reaction conditions, relatively few byproducts, and retention of stereochemical information. Optimization of this oxidation is ongoing.

Scheme 5.3: Oxidation of chiral aldehydes developed by the Stahl lab.

Screening and oxidation performed by Kelsey Miles

Overall, the development of a rudimentary continuous flow AHF has been accomplished. What remains is to fully characterize the important features of the reaction in flow to better optimize the results by lowering tau, improving the selectivity, and isolating material at full conversion. Further work will also describe the role of pre-activation in the outcome of AHF reactions, as well as the role of the number of gas equivalents (gas flow rate). The research-scale flow reactor developed in this project provides a design that accounts for the high mass transfer required by AHF, and provides flow results that match those obtained in analogous batch reactions. These features describe a well-behaved reactor that is ready for optimization.

The reactor design presented here also has the advantage of being a readily scalable design, allowing for rapid progress from research to pilot scale. Further work will center on understanding the interplay between various conditions to provide a model for scaling up AHF of other substrates in flow. The development of this reactor contributes to Eli Lilly's continuous flow toolkit and establishes the parameters needed to realize a safe, cost-effective, process scale asymmetric hydroformylation.

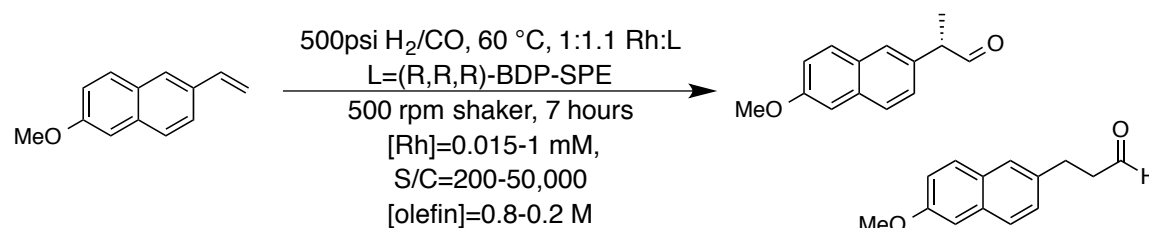
5.5 Experimental.

General considerations.

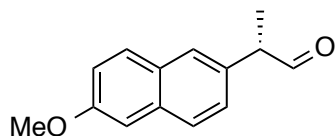
Reactions at Wisconsin: All manipulations were carried out under nitrogen using standard Schlenk, high vacuum, and glovebox techniques. Bisdiazaphospholane ligands were prepared as reported in chapter 3 via the tetra-acyl fluoride intermediate. $[\text{Rh}(\text{acac})(\text{CO})_2]$ was used as received from Dow Chemical and stored in a N_2 -filled glovebox. 1:1 $\text{CO}:\text{H}_2$ was purchased from Airgas. THF and toluene were obtained from Sigma-Aldrich and either distilled from sodium/benzophenone ketyl under N_2 or dried by safety columns prior to use. 6-Methoxy-2-vinyl-naphthalene was obtained from Sigma-Aldrich or prepared by J. Martinelli at Eli Lilly and used as received. Chiral HPLC analysis was performed on a Gilson analytical HPLC with Chiralpak IA, IB, IC, and ID columns.

Catalyst stock solutions were prepared inside a nitrogen-filled glovebox and transferred to the reaction vessel with Eppendorf micropipettors. Solutions were typically prepared as 20 mM then diluted down to the desired concentration to ensure accurate weighing. Occasionally the 6-methoxy-2-vinyl-naphthalene substrate would appear hazy after dissolution in toluene, for NMR and flow experiments the solution was filtered through a PTFE syringe filter prior to use; for CAT24 experiments the solution was used without filtering. The effect of filtering was determined to be negligible through control reactions run in the Endeavor.

CAT24 reactions.



Reactions in the CAT24 were set up in the glovebox by adding solutions of $\text{Rh}(\text{acac})(\text{CO})_2$ and the ligand in an appropriate solvent. Wells not in use contain an empty test tube to prevent the condenser fingers from falling off during the course of the reaction. Olefin is then added, followed by the reaction solvent to rinse the sides of the tube and dilute all wells to the same total volume, 1 mL. The reactor is sealed, brought out of the glovebox, and set in an orbital shaker. Water lines are connected to the condenser ports. The reactor is heated to the reaction temperature (40 or 60 °C) for 20 minutes before syngas is added, using 5 purge-fill cycles to replace the entire reactor volume with syngas, then pressurizing to 500 psig. Reactions are shaken at 500 rpm for seven hours, then the temperature controller is turned off and the bomb is allowed to cool for 30 minutes. Once cooled, the shaker is turned off and depressurized. With no workup, each reaction well is sampled for NMR and HPLC analysis.



HPLC method for naproxen aldehyde: The (*R,R,R*) ligand gives rise to *S*-naproxen aldehyde as the major enantiomer. 3% 2-propanol / 97% hexanes with 0.1% TFA, ambient temperature, on a Chiralpak ID (0.46 cm x 25 cm), 0.7 mL/min flow, detect at 220 or 254 nm. In an isolated sample (after silica gel chromatography), $t_{\text{r}(\text{S})} = 15.3$ and $t_{\text{r}(\text{R})} = 17.1$ minutes. In a crude sample, they appear at $t_{\text{r}(\text{S})} = 16.2$ and $t_{\text{r}(\text{R})} = 18.3$; $t_{\text{r}(\text{olefin})} = 9.2$, $t_{\text{r}(\text{linear})} = 26.7$ min. The relative responses of these compounds vary, depending on the wavelength measured at, and caution should be used in determining conversion or branched:linear ratios by HPLC. Data collected at Lilly with an analogous method reports *lower* branched:linear than actual (by NMR) and *higher* conversion than actual (by NMR).

Flow runs:

Flow runs were performed at Eli Lilly, on a research-scale continuous flow reactor described in Section 5.1.c. Solutions were prepared in a nitrogen-filled glovebox and transferred to the flow reactor in bottles with a dip-tube attachment. At the end of the reactor, samples were collected every 24 minutes using an automated sampler. The solutions used for flow runs were also used for Endeavor batch runs to ensure consistent loadings and better agreement between batch and flow results.

Endeavor runs:

Batch screening at Eli Lilly was performed in an Endeavor parallel reactor. Solutions were transferred using micropipettors and diluted as necessary to the same total reaction volume (2 mL).

The pre-activated catalyst used in Table 5.11 was generated by transferring enough of the catalyst stock solution (5 mM) to a single endeavor well, weighing it, then the well was sealed and stirred at 60 °C, 150 psi for 18h. At the end of the pre-reaction, the well was cooled to room temperature, re-weighed, and solvent was added to obtain the original mass. The unused solution was stored in a vial in the glovebox until needed.

HP-NMR reactions: See Chapter 4. The equipment set used for naproxen runs was manual injection with valved gas-tight Hamilton syringes, circulation 30 mL/min using U. Rostock circulator and Teflon fritted cup design. Total reaction volume of 3 mL. Catalyst feed was prepared in the glovebox as a single solution with an excess of ligand.

5.6 References.

-
- ¹ Whiteker, G.T.; Cobley, C. J. *Top. Organomet. Chem.* **2012**, 42, 35–46.
- ² Hagen, J.; Bruns, K. (1980) German Patent 2849742, May 22, 1980.
- ³ Gu, J.; Storz, T.; Vyverberg, F.; Wu, C.; Varsolona, R. J.; Sutherland, K. *Org. Process Res. Dev.*, **2011**, 15, 942–945.
- ⁴ Poechlauer, P.; Colberg, J.; Fisher, E.; Jansen, M.; Johnson, M. D.; Koenig, S. G.; Lawler, M.; Laporte, T.; Manley, J.; Martin, B.; O’Kearney-McMullan, A. *Org. Process Res. Dev.* **2013** 17, 1472-1478.
- ⁵ Johnson, M. D.; May, S. A.; Calvin, J. R.; Remacle, J.; Stout, J. R. Diserod, W. D.; Zaborenko, N.; Haeberle, B. D.; Sun, W.; Miller, M. T.; Brennan, J. *Org. Process Res. Dev.* **2012**, 16, 1017–1038.
- ⁶ Previous reports of hydroformylation in a flow reactor: Güven, S.; Hamers, B.; Franke, R.; Priske, M.; Becker, M.; Vogt, D. *Catal. Sci. Technol.*, **2014**, 4, 524. Janssen, M., Wilting, J., Müller, C. and Vogt, D. *Angew. Chem. Int. Ed.* **2011**, 49, 7738–7741. Riisager, A.; Fehrmann, R.; Flicker, S.; van Hal, R.; Haumann, M; and Wasserscheid, P. *Angew. Chem. Int. Ed.*, **2005**, 44, 815–819. van Leeuwen, P. W. N. M.; Jongsmas, T.; Challa, G. *Macromol. Symp.*, **1994**, 80, 241–256. Webb, P. B.; Murielle F. Sellin, M. F.; Kunene, T. E.; Williamson, S.; Slawin, A. M. Z.; Cole-Hamilton, D. J. *J. Am. Chem. Soc.*, **2003**, 125, 15577–15588.
- ⁷ (a) Webb, D.; Jamison, T. F. *Chem. Sci.* **2010**, 1, 675. (b) Tsubogo, T.; Ishiwata, T.; Kobayashi, S. *Angew. Chem. Int. Ed.* **2013**, 52, 6590. (c) Xiao Yin Mak, X.; Laurino, P.; Seeberger, P. H. *Beilstein J. Org. Chem.* **2009**, 5, No. 19.

-
- ⁸ May, S. A.; Johnson, M. D.; Braden, T. M.; Calvin, J. R.; Haeberle, B. D.; Jines, A. R.; Miller, R. D.; Plocharczyk, E. F.; Renner, G. A.; Richey, R. N.; Schmid, C. R.; Vaid, R. K.; Yu, H. *Org. Process Res. Dev.* **2012** *16* (5), 982-1002.
- ⁹ Stille, J. K.; Su, H.; Brechot, P.; Parrinello, G.; Hegedus, L. S. *Organometallics* **1991** *10*, 1183-1189.
- ¹⁰ Harrington, P. J.; Eric Lodewijk, E. *Org. Process Res. Dev.* **1997**, *1*, 72-76.
- ¹¹ Brown, J. M.; Cook, S. J. *Tetrahedron* **1986**, *42*, 5105-5109.
- ¹² Sonawane, H. R.; Bellur, N. S.; Ahuja, J. R.; Kulkarni, D. G. *Tetrahedron: Asymmetry* **1992**, *3*, 163.
- ¹³ Parrinello, G.; Stille, J. K. *J. Am. Chem. Soc.* **1987**, *109*, 7122-7127.
- ¹⁴ Ohta, T.; Takaya, H.; Kitamura, M.; Nagai, K.; Noyori, R. *J. Org. Chem.* **1987** *52*, 3174-3176.
- ¹⁵ Giordano, C.; Castaldi, G.; Cavicchioli, S.; Villa, M. *Tetrahedron* **1989**, *45*, 4243-4252.
- ¹⁶ Wong, G. W.; Adint, T. T.; Landis, C. R. *Org. Synth.* **2012**, *89*, 243-254.
- ¹⁷ Watkins, A. L.; Landis, C. R. *J. Am. Chem. Soc.* **2010**, *132*, 10306-10317.
- ¹⁸ Buser, J. Y.; McFarland, A. D. *Chem. Commun.* **2014**, *50*, 4234-4237.
- ¹⁹ Watkins, A. L.; Hashiguchi, B. G.; Landis, C. R. *Org. Lett.* **2008**, *10*, 4553-4556.
- ²⁰ See experimental details for the pre-activation method.
- ²¹ Mori, H.; Kitahara, M. (ADCHEMCO Corp., Japan) Method for producing 4-tertiarybutoxystyrene. Japanese Patent JP2002167350, June 11, 2002.
- ²² Miles, K.; Abrams, M. L. Landis, C. R. Stahl, S. S. *Org. Lett.* in preparation.

Appendix A

**Expanding the scope of asymmetric hydroformylation:
various novel substrates**

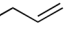
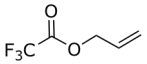
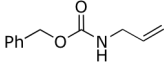
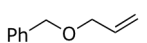
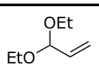
A.1: Asymmetric Hydroformylation of *Z*-Alkenes Produced by Metathesis

Abstract. Asymmetric hydroformylation with BisDiazaphos produces α -branched aldehydes from terminal olefins with excellent regio- and enantioselectivity. Recently, we have investigated hydroformylation to disubstituted olefins. Based on preliminary results, we hypothesize that *Z* disubstituted olefins will give higher rates and selectivity than the *E* isomers. *Z*-selective alkene metathesis constitutes the most general and practical route to these substrates. Herein we report our initial results for *Z*-selective alkene metathesis as catalyzed by $W(NAr)(C_3H_6)(Pyr)(OHIPT)$ and the subsequent hydroformylation of the products using $Rh(BisDiazaphos)$ catalysts.

Results of homocoupling reactions

Reactions previously reported. The reactions replicated in our lab were consistent with the results published by the Schrock group. The homocoupling of 1-octene was performed at lower temperatures, which produced higher *cis* selectivity (~95%) with a moderately lower conversion. The homocoupling of allylbenzene tended to be lower yielding than that reported, but the *cis* selectivity remained excellent.

Table 1. Homocoupling reactions.

Substrate:	conc.	% catalyst	temp	Time (hours)	% conversion	E:Z (method)
1-Octene	4.8 M	0.4%	70 C	48	57	1:25.7 (¹³ C)
	5.6 M	0.3%	87 C	24	64	1:17.9 (¹³ C)
Allylbenzene	5.4 M	0.3%	110 C	6/24	36/36	n.d.
	5.9 M	0.2%	120 C	24	14	1:12.3 (GC)
	6.5 M	0.3%	110 C	24	34	1:14.4 (GC)
Phenyl 1,4-pentadiene	0.6 M	4%	22 C/80 C	7/22	13/90	n.d.
Phenyl 1,3-butadiene	1.6 M	4%	RT	3/24	35/99	7:1/1:1.4 (¹ H) ^a
	2.3 M	2.4%	RT	2.5/5.5	58/91	1:3.2 /5.9:1 (¹ H)
PinB 	4.7 M	0.2%	100 C	24H	0	--
	2.7 M	0.75%	100 C	16H	52	1:23.5 (¹³ C)
	3.9 M	1%	40 C	24 H	0	
	4.6 M	1.26%	90 C	17 H	0	
	3.2 M	1%	110 C	24 H	0	
	2.5 M	2%	110 C	24 H	0	
	3.9 M	1.5%	110 C	17 H	0	
	2.6 M	2%	40 C	24 H	0	

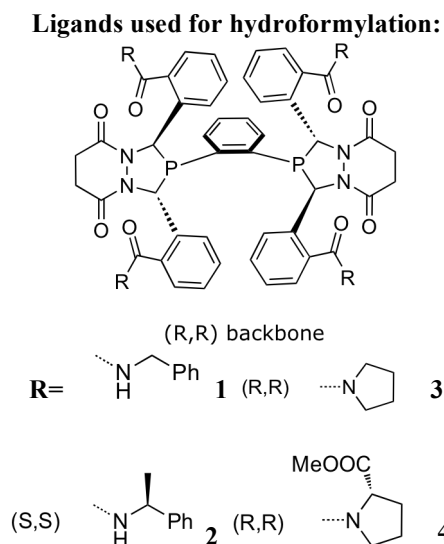
^aUpon workup, isomerized to 86% (*E,E,E*) isomer.

The homocoupling of phenyl 1,3-butadiene proceeded as reported, but we were unable to prevent the concurrent isomerization to the (*E,E,E*) isomer of 1,6-diphenyl-1,3,5-hexatriene. One notable difference in our reaction setup is that our reaction is more concentrated (1.6-2.3M) than the experiment reported in the Schrock group's supporting information (0.6M). The reaction was repeated with the exclusion of light, but in both cases a significant portion of the sample was isomerized to the (*E,E,E*) form either before an initial NMR could be taken (~10 min), or during the course of the reaction itself. The addition of CDCl₃ may also be responsible for isomerization, since the NMR of a reaction aliquot showed far lower *Z* selectivity (5.9:1 *E:Z*) than the bulk material worked up subsequently without the addition of CDCl₃ (1:3.2 *E:Z*).

Homocoupling of substrates not previously reported. In general, the homocoupling of substrates that were not reported by the Schrock group (allyl trifluoroacetate, CBz protected allylamine, acetals) gave no conversion. Based on the substrates for which the particular catalyst we used performs best, this is not entirely unexpected. However, phenyl 1,4-pentadiene converts to the homocoupled product when the reaction is carried out at elevated temperatures, though the E:Z selectivity was not determined.

Hydroformylation results

Z-7-tetradecene hydroformylation. The hydroformylation of Z-7-tetradecene is slow, with complete conversion requiring 4-5 day reaction times and higher catalyst loadings than other Z olefins we have studied. At higher temperatures, the hydroformylation of Z-7-tetradecene is



preceded by isomerization of the double bond to give an essentially statistical mixture of aldehyde isomers. Lowering the temperature to 40°C affords one major isomer with our standard methylbenzylamine ligand **2**, though reactions run to incomplete conversion indicate

isomerization to the *E* isomer still occurs. A few bulkier amide ligands were screened, with the hypothesis that these may provide less isomerization (as seen with other substrates). In other substrates we have seen a trend of faster, more selective hydroformylation of internal olefins with *Z* geometry, so limiting the isomerization to the *E* olefin could also improve the conversion. However, bulkier amide ligands give similar selectivity, and still result in isomerization of the double bond from *Z* to *E*. There is no apparent hydrogenation with these substrates. The aldehyde products of this hydroformylation are so similar that determination of enantioselectivity is challenging, and has not yet been accomplished.


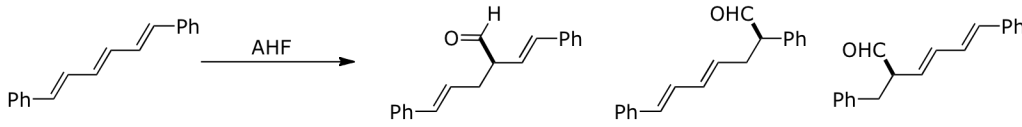
Table 2. Hydroformylation of *Z*-7-tetradecene.

Major isomer

Minor isomers

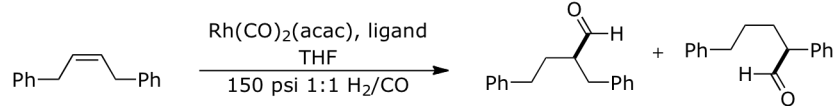
ligand	temp (°C)	time (hours)	Conc.	catalyst loading	% <i>Z</i> remaining	% isomerized to <i>E</i>	% converted to aldehyde (% major isomer)
1	70	21	1.3M	0.5%	50.6	45.8	3.6 (87.1)
1	110	40	0.7M	2%	0	minimal	100 (34.5)
1	40	48	1.0M	1.4%	17.2	35.0	47.8 (99.3)
2	40	113	0.7M	2.0%	3% (both isomers)		97 (92.3)
3	40	69	0.8M	1.0%	9.1	49.8	40.7 (94.9)
4	40	69	0.8M	1.0%	14.4	51.3	34.3 (93.6)

Table 4. Other hydroformylation reactions.

Ligand	temp (°C)	time (hours)	syngas pressure (psi)	cat loading	% Z remaining	% isomerized to E	% converted to aldehyde
 <p>Approximately 2:1 Z:E; also contains 59% allyl Bpin.</p>							
1	50	48	150	~2%	0	0	11.6
 <p>3.2:1 Z:E; also contains 30% in phenyl 1,3-butadiene.</p>							
1	50	40	150	~2%	0 isom.	64 remaining	36

Z-1,4-diphenyl-2-butene hydroformylation. The hydroformylation of diphenylbutene under reaction conditions analogous to those used for *Z*-7-tetradecene proceeds poorly (less than 3% conversion). The effect of bulky amide ligands was also screened, with low conversions and isomerization similar to that found with ligand **2**. The amount of isomerization to the *E* olefin remains consistent regardless of the ligand used. The low reactivity of this substrate may be due to the steric bulk of the phenyl rings, and the unactivated double bond. For comparison, the hydroformylation of *cis*-stilbene under the same pressure and temperature conditions gives 67% conversion in 24 hours with 0.2% catalyst loading.¹

Table 3. Hydroformylation of Z-1,4-diphenylbutene.

							
ligand	temp (°C)	time (hours)	Conc.	catalyst loading	% Z remaining	% isomerized to E	% converted to aldehyde
2	40	69	0.8M	1.0%	78.9	17.9	< 3%
3	40	69	0.8M	1.0%	86	11	< 3%
4	40	69	0.8M	1.0%	--	--	< 3%

Hydroformylation of other substrates. The hydroformylation of other homocoupling products was performed on crude mixtures from the homocoupling, which contained some of the uncoupled terminal olefin. In these examples, hydroformylation went to low enough conversion to suggest that these homocoupled substrates are also slow to undergo hydroformylation, similar to the results of 1,4-diphenyl-2-butene. For both substrates, at least part of the conversion to aldehyde as reported is due to the hydroformylation of the monosubstituted olefin.

A crude mixture of (*E,E,E*) and (*E,Z,E*) 1,6-diphenyl-1,3,5-hexatriene undergoes hydroformylation to give two main aldehyde isomers in a 63:37 ratio along with a number of minor isomers. The coupling constant of the aldehydes suggests that neither major isomer is a conjugated aldehyde, so no isomerization occurs after hydroformylation.

The product of allyl Bpin homocoupling was hydroformylated as a crude mixture (41.3% 1,4-bis(Bpin)-2-butene in allyl Bpin). There was 11.6% conversion to aldehyde products from both olefins, but little appears to be from the internal olefin. The balance of olefin was lost due to a leaky reactor.

Experimental details

All homocoupling reactions were run in C₆H₆ or C₆D₆ (distilled from Na/benzophenone and stored over mol sieves), or neat. Substrates were purified by vacuum transfer or distillation, degassed, and passed through activated alumina in the glovebox. The catalyst used for all homocoupling reactions was W(NAr)(C₃H₆)(Pyr)(OHIPT), as provided by the Schrock group. Reactions were carried out in oven-dried Teflon-sealed J-Young tubes, Schlenk flasks, or in vials

in an N₂ filled glovebox. Reactions carried out on a Schlenk line were left open to nitrogen and a mineral oil bubbler to help remove ethylene.

Homocoupling of phenyl-1,3-butadiene. Combined 0.30 mL of 80mM W(NAr)(C₃H₆)(Pyr)(OHIPT) with 0.130mL (1 mmol) of phenyl 1,3-butadiene in a 20 mL vial wrapped in tinfoil in an N₂ filled glovebox. The vial was loosely capped and allowed to stir at RT. An aliquot removed after 2.5 hours showed 64% conversion, at 5.5 hours the reaction proceeded to 91% conversion. After 6 hours the reaction mixture was passed through a plug of silica in a pipet using C₆D₆ and the solution was used directly for hydroformylation.

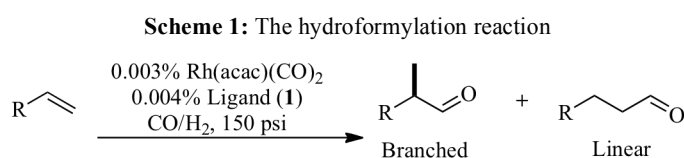
Typical hydroformylation procedure. Solutions of Rh(CO)₂(acac) (100mM) and ligand (20mM) in THF were combined in a pressure bottle in the glovebox. The reactor head was attached, and the apparatus removed from the glovebox and pressurized, after doing 5 purge/fill cycles of 1:1 syngas. The ligand and rhodium were allowed to pre-react at the reaction temperature for 30 min-2 hours. After pre-reaction, reactor was cooled 5 min and depressurized to ~1atm syngas. The substrate was injected using a gas-tight syringe, and the reaction was then re-pressurized after a few fill/purge cycles of syngas and replaced in the oil bath. Upon completion of the reaction, the reactor was cooled to room temperature, depressurized, and a small amount of CDCl₃ was added for a crude NMR of the reaction.

A.2 Asymmetric hydroformylation of 1,1-disubstituted olefins

Asymmetric Hydroformylation of 1,1-Disubstituted Olefins

Asymmetric hydroformylation (AHF) research to date has been focused on monosubstituted substrates. The goal of this research is to develop asymmetric variants of hydroformylation of disubstituted olefins. In particular, this is an attractive transformation because of the increased synthetic utility of chiral aldehydes that contain more complex motifs, beyond the methyl branches afforded by AHF of monosubstituted olefins. In addition, this research is intended as a way to make AHF more accessible to bench-scale chemists, so demonstration of a general procedure that applies to a broad scope of functionalized olefins is another goal. With these goals in mind, improving our understanding of the mechanistic details should also provide insight into how to best accomplish these challenging transformations.

The challenge in modern organic chemistry is to synthesize complex structures with less waste using reactions that are effective on the industrial scale as well as the bench scale. Catalysis

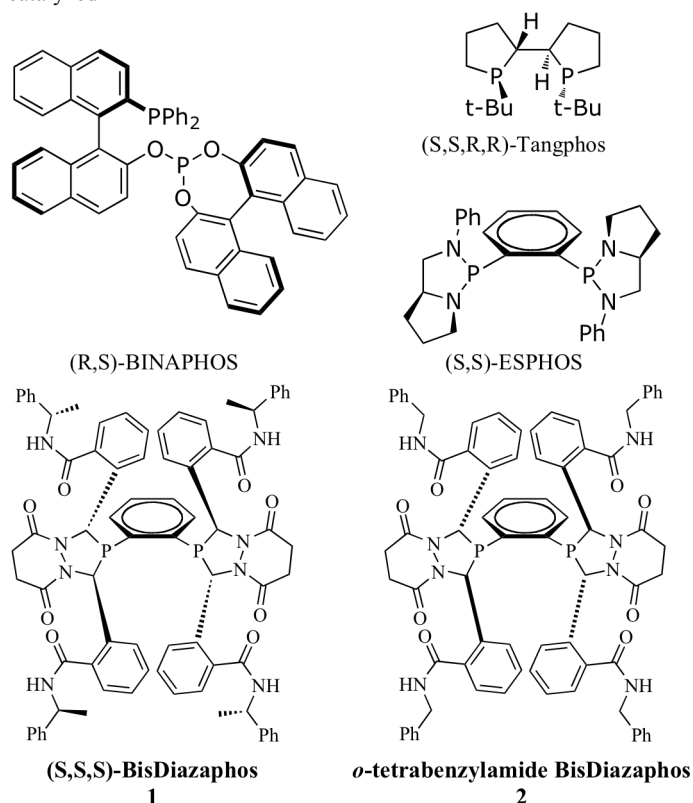


addresses these goals, enabling highly enantioselective and atom economical processes with very low amounts of catalyst. Hydroformylation on the industrial scale is one such process that transforms olefins and synthesis gas (a 1:1 mixture of hydrogen and carbon monoxide) into nine million pounds of aldehydes per year.¹ Hydroformylation is an attractive process because it has perfect atom economy and the gaseous reagents are easily separated from the products, streamlining purification.

The vast majority of industrial hydroformylation products are the achiral, linear aldehyde (Scheme 1). Asymmetric hydroformylation (AHF) is a variation of this process that forms the chiral, branched regioisomer. A number of ligands have been developed to catalyze AHF, including BINAPHOS, TANGPHOS, and ESPHOS.² The bis-3,4-diazaphospholane ligands (**1**, **2**) developed in our group induce a high level of regio- and enantioselectivity (40:1 b:l and 96% ee for vinyl acetate) in AHF with consistently high turnover frequencies (as high as 20,000 turnovers per hour). Additionally, these catalysts are efficient at low temperatures (<100°C) and pressures (150 psi), which renders AHF at the bench-scale accessible without as much specialized equipment.

Despite the general utility of chiral aldehydes in organic synthesis, AHF is underutilized. One reason is that hydroformylation research and development is largely focused on commodity production of linear aldehydes. The majority of AHF literature focuses on simple monosubstituted

Figure 1: Representative ligands for branch-selective rhodium catalyzed AHF



alkenes,¹ such as styrene and vinyl acetate, which have limited use in more complex syntheses. Monosubstituted olefins can only produce a methyl branch, which limits the structural motifs that AHF can be applied to. Hydroformylation of disubstituted olefins has the potential to produce far more complex branching points, and may even provide access to chiral quaternary aldehydes (Scheme 2).

Scheme 2: Regiochemical outcomes of AHF with disubstituted olefins

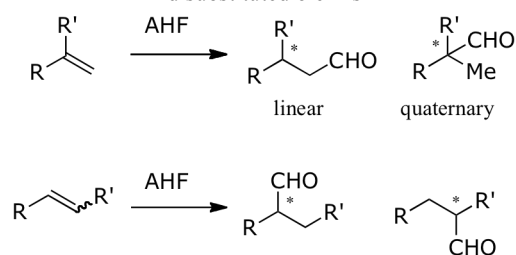
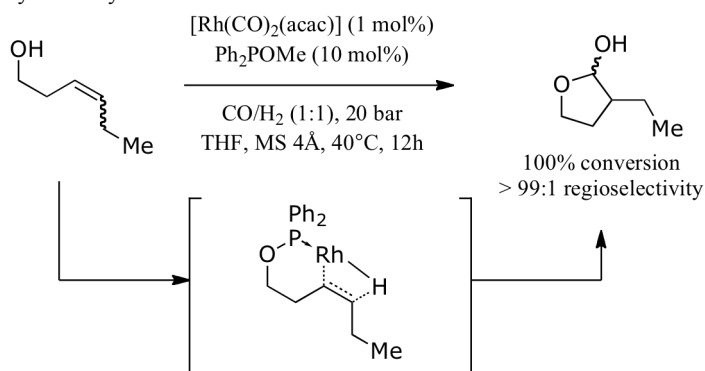


Table 1: Selectivity of the AHF of 1-acetamido-1-propene

Alkene	Conversion (%)	1-formyl: 2-formyl	% ee
	66	4.6:1	32
	99	32:1	90

Disubstituted olefins present a number of challenges in AHF not encountered with monosubstituted olefins. Regioselectivity control remains crucial, and may be more difficult to

Scheme 3: Catalytic directing group approach to regioselective hydroformylation

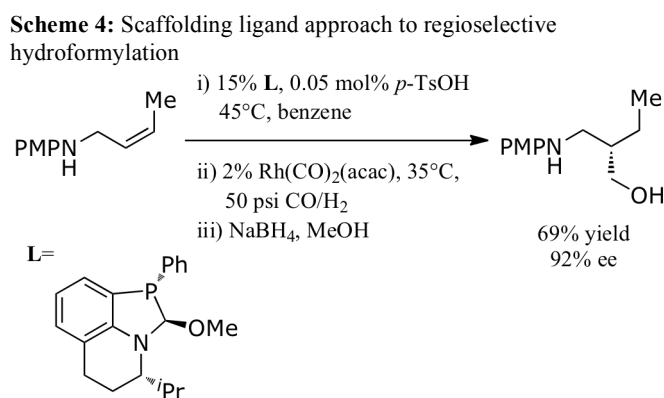


direct with internal olefins when there is less of an electronic preference for one substitution over another. Previous work in our group and others has also shown that the *E/Z* stereochemistry of the olefin affects the selectivity of the AHF reaction, with *E* olefins showing both lower regioselectivity and enantioselectivity than the corresponding *Z* olefins. Nozaki and coworkers reported lower enantioselectivities for the *E* isomers in the (R,S)-BINAPHOS/rhodium catalyzed AHF of simple symmetrical butenes (85% ee for the *Z*, 48% for *E*) and hexenes.¹ Our group recently reported that AHF of 1-acetamido-1-propene is not only more regio- and enantioselective, but also faster for the *cis* isomer (Table 1).³ The increased steric bulk of disubstituted olefins makes coordination to the rhodium center more disfavored, and thus slower reaction rates and lower conversions are common issues. Additionally, the rhodium can catalyze isomerization of the double bond to a different position if an α hydrogen is present, leading to either less reactive trisubstituted olefins or undesired hydroformylation products. Furthermore, much of the literature that does report hydroformylation of disubstituted substrates has not yet addressed the enantioselectivity of these transformations.

One strategy used with disubstituted olefins is directing hydroformylation using an external moiety that interacts with both the rhodium center and the substrate. Bernhard Breit and coworkers report a system using an *ortho*-diphenylphosphanylbenzoic acid (*o*-DPPB) stoichiometric directing group or a methyl-diphenylphosphinite catalytic directing group to achieve high regioselectivity with hydroformylation of allylic alcohols,^{4,5} as well as homoallylic and bishomoallylic alcohols.⁶ In these examples, a reversibly bound phosphinite catalyst-directing group binds covalently to the substrate alcohol. This complex then coordinates to the metal center and the olefin undergoes a highly regio- and diastereoselective hydroformylation⁷ (Scheme 3). A limitation to this approach is that the substrate scope is limited to substrates containing a nearby

alcohol functional group. In addition, while diastereoselectivity control has been achieved with this system, results with enantiocontrol have yet to be reported.

A similar strategy has been employed by K. L. Tan's group, which uses a scaffolding ligand to direct hydroformylation. In particular, this approach is exciting as the only report to date of enantioselective catalysis with such ligands,^{8,9} providing up to 92% ee (Scheme 4). Unfortunately, the substrate scope with this approach is also limited, in this case to allyl alcohols, amines and sulfonamides. These catalyst-directing group ligand systems are also capable of overriding the inherent preference for forming the linear product from hydroformylation of 1,1-disubstituted olefins, yielding quaternary aldehydes.^{10,11}

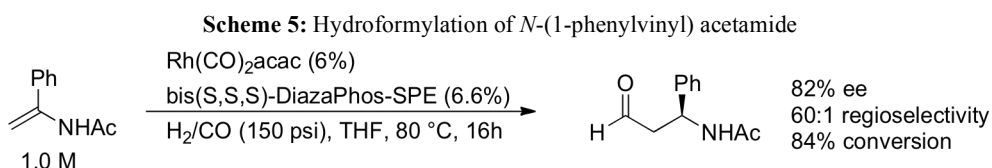


Other examples of hydroformylation to form quaternary centers are rare, as they violate the oft-cited Keuleman's rule, which states that the formyl group will add to an olefin to form the less-substituted aldehyde.¹² One major exception to this is α - β unsaturated esters, which exhibit a strong electronic preference to insert at the α -position, regardless of the substitution. Clarke and coworkers have demonstrated this with our ligand and others, for the hydroformylation of *N,N*-diethylacrylamide as well as a series of 1,1-disubstituted acrylate esters.^{13,14} Based on the high activity of our ligands with this class of substrates, we expect we should be able to form highly functionalized quaternary centers with high enantioselectivity and good conversion.

As is evident from the current literature, hydroformylation of more complex substrates is far from a solved problem. Few reports are for *asymmetric* hydroformylation, and even those that exhibit excellent regioselectivity have other limitations. Such scaffolding approaches as used by Tan and Breit necessarily limit the scope to specific functionalities. Many of the literature reports also use higher syngas pressures, which will inhibit the adaptation of these techniques by bench-scale chemists.

Hydroformylation of 1,1-disubstituted olefins.

Research in the Landis group has primarily focused on AHF of monosubstituted olefins thus far, with only a few examples of disubstituted olefins. Those examples have demonstrated the challenges associated with efficient hydroformylation of disubstituted olefins, in particular, the slower reaction rates and dependence on substrate regiochemistry (*E/Z* isomerism). With this in mind, the initial goal of this project is to explore the salient features of a successful reaction with an eye towards developing a generally applicable reaction methodology.



Neil Strotman at Merck & Co., Inc. found that the (3,4)-BisDiazaphos- ligands provide unique reactivity with *N*-(1-phenylvinyl) acetamide, giving good yield and selectivity (Scheme 5), whereas none of the other phosphine ligands screened afforded *any* product. This promising result is the impetus for our interest in expanding the scope of hydroformylation, with the aim to create a more general, selective and efficient route to chiral building blocks.

Based on results with monosubstituted olefins, we expect electron-withdrawing groups such as acetates to favor the branched product in hydroformylation, and substrates that contain

motifs that provide excellent branch-selectivity in AHF (styrene derivatives) should also provide branch-selective AHF for disubstituted olefins. However, this yields a notoriously inaccessible quaternary center, and this may result in lower yields of the linear product rather than the quaternary aldehyde. Keuleman's Rule does not always apply, particularly if the substrate has a strong enough electronic preference for one formyl insertion over the other. We anticipate that we will be able to form chiral quaternary centers via hydroformylation of α -substituted acrylates. More electron-rich olefins will likely have slower reaction rates, and it remains to be seen whether a synthetically useful hydroformylation of such substrates can be developed.

General considerations.

The first reactions (run with *N*-(1-phenylvinyl) acetamide) showed inconsistent conversions despite identical reaction conditions, and this was eventually attributed to differences in the distribution of catalyst species *in situ*, which was standardized by pre-reacting the rhodium catalyst precursor and ligand under 30-150 psi of syngas (1:1 mix of H₂ and CO) for 30-60 minutes, followed by injection of the substrate. Subsequent substrates all underwent this reaction regime. Increasing concentration of the substrate unsurprisingly improved the reaction rate as well; reactions were generally run at the highest possible concentration—given the requirement of pre-reaction of the catalyst, this tended to be around 1.7 M in substrate. Catalyst loadings of 1-2% were used, with the intention that this may be reduced to lower loadings once other conditions were optimized. This proved to be possible for some substrates, but is unlikely for others that react more slowly. While most substrates showed better conversion with increasing temperature, the competing hydrogenation reaction frequently becomes more pronounced at higher temperatures, which is problematic for some substrates. This fits with the findings of the Clarke group as well, who found that both the product distribution and regioselectivity of hydroformylation of methyl

cinnamate were highly temperature dependent.¹⁴ Other substrates we tested appear to heavily favor hydrogenation over hydroformylation, even under low pressures of hydrogen.

Reaction times.

Table 2: AHF of 2,3,3-trimethyl-1-butene.

Entry	psi (CO/H ₂)	Temp (°C)	Time (h)	% Conv. ^a	% Olefin lost ^a
1	70/70	120	6	18.3	47.7
2	15/15	120	6	4.4	51.9
3	15/15	60	6	7.2	37.5
4	70/70	60	6	10.5	39.3
5	70/70	35	21	4.6 ^b	n.d.
6	15/15	35	21	1-3 ^b	n.d.
7	70/70	75	48	28	47.4
8	70/70	40	48	10.6	29.6
9	105/35	120	7	minimal	n.d.

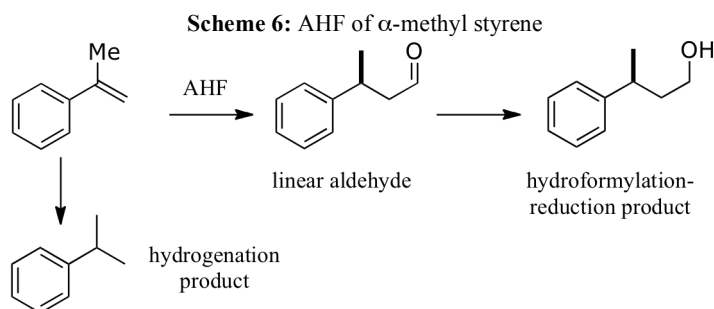
Reaction conditions: 2 mol% rac. benzylamide ligand **2**, THF, 1.8M in substrate, pre-reacted 30min. (a) ¹H NMR integration vs. mesitylene (b) internal standard peak not seen, conversion measured vs. remaining olefin.

In general, hydroformylation of disubstituted olefins is slower than that of monosubstituted olefins. One of the challenges in hydroformylation of disubstituted olefins is therefore to get good conversion with the shortest reaction time possible. The hydrocarbon substrate 2,3,3-trimethyl-1-butene demonstrates the inherent challenges to AHF of disubstituted substrates. Under optimized conditions, this substrate gives only 28% conversion (Table 2, entry 7). Increasing the syngas pressure from 30 to 140 psi improves the yield, and allowing the reaction to go for longer also improves conversion. The optimized conditions were obtained after noting that the low boiling point of the substrate (78-80°C) was causing significant loss of starting material into the gas phase. However, at low temperatures, the reaction becomes too sluggish to be synthetically practical (entries 5-6). Pairing a moderate reaction temperature with much longer reaction times allows for the best conversion. We predict that this low reactivity is due to the extreme steric bulk of the *t*-butyl group and the complete lack of electronic activation of the double bond.

Considering that the first hurdle to overcome in developing a synthetically practical AHF method is getting good conversion, reactions were generally run at least 24 hours, and most showed little change between being reacted 24 hours versus 48 hours. One notable exception to this is the hydroformylation of α -methyl styrene (at 120°C), which was complete in less than 3 hours. Fitting with our expectation that olefins with electron withdrawing groups would be easier to hydroformylate, all of the acrylates used show complete conversion within 24 hours, as does Z-1-(benzoyloxy)-1-hexene. One thing that remains to be seen is whether using forcing conditions (high temperatures) for less reactive substrates erodes the enantioselectivity beyond a synthetically useful point. This is a cause for concern with regard to the other pure hydrocarbon substrate studied, α -methyl styrene, which requires higher temperatures for complete conversion of the olefin.

α -Substituted styrenes: A study in undesired side reactions.

AHF of α -methyl styrene also demonstrates the potential for side reactions with longer reaction times and higher temperatures. The hydroformylation is fast compared to other α -substituted styrenes, but suffers from moderate conversion of 55% after optimization at 60°C (table 3, entry 2). However, at higher temperatures reduction of the formyl double bond to form an alcohol becomes a competing reaction (Scheme 6). This raised the question of whether it was possible to selectively favor formation of the aldehyde over the alcohol, and vice versa. This is possible, and at 120°C and 60psi of 1:1 syngas (entry 4), the linear aldehyde is obtained in 58% yield after 15 hours, with 19% of the starting material remaining, and 23% converted to either the hydrogenation or alcohol product.

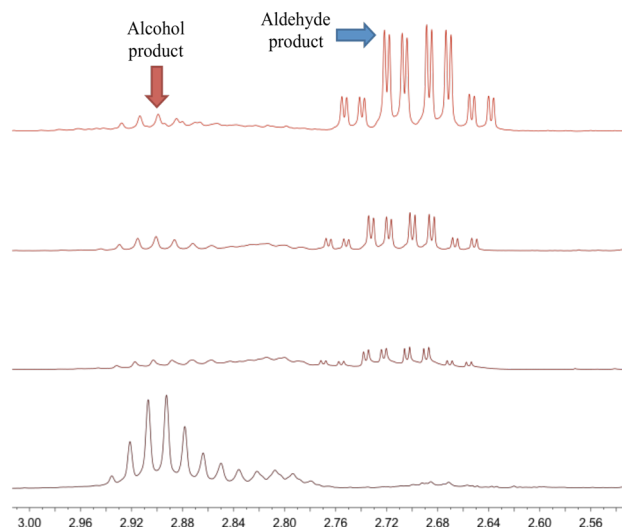
**Table 3:** Hydroformylation of α -methyl styrene.

Entry	Psi (CO/H ₂)	Temp (°C)	Time (h)	% Conv. ^c	CHO:OH product
1 ^a	70/70	60	6	17	1:0
2 ^a	70/70	60	20	55	1:0
3 ^b	30/30	60	6	14	1:0
4 ^b	30/30	120	15	81	1:0.4
5 ^b	70/70	120	6	67	1:0.44
6	105/35	120	6	86	1:0.26
7	70/70	120	24	100	0:1

Reaction conditions: 2 mol% ligand **2**, THF, 1.8-2.3M in substrate. ^aSolvent was a mixture of THF and acetone-d₆. ^bThe amount of substrate added may not have been accurate. ^cCalculated vs. integration of remaining starting material.

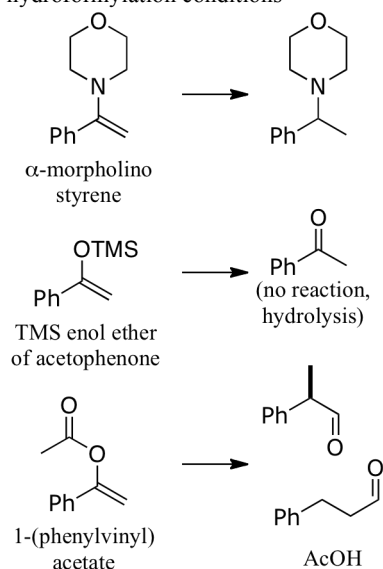
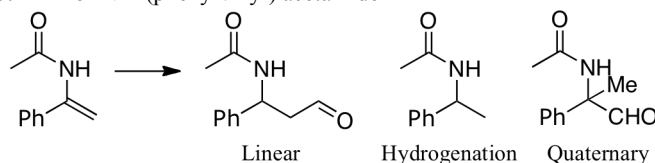
Raising the CO pressure seemed to improve results moderately. At 105psi CO and 35psi H₂ (entry 6), in 6 hours 74% of the linear aldehyde was obtained, with 14% of the starting material remaining and the remaining 16% converted to either the alcohol or hydrogenation byproduct. Conversely, at 120°C and 140psi of syngas, the aldehyde was completely converted to the alcohol reduction product after 24 hours (entry 7). Running the reaction for less time under these conditions did not prevent the isomerization reaction (see the NMR spectra after 3 hours in figure 2). Regardless of the conditions used, it appears that there will always be competition from the hydrogenation reaction, which appears insensitive to the temperature or pressure of either gas. The reduction reaction to form the alcohol can be completely suppressed by keeping the reaction temperature at 60°C or below, but this lowers the conversion. Thus the aldehyde can only be cleanly formed in 55% yield, whereas the alcohol can be formed in nearly 100% yield.

Figure 2: AHF of α -methyl styrene after 3 (top spectrum), 6, 9 and 24 hours.



Hydroformylation of many other α -substituted styrene derivatives was more problematic than the hydrocarbon α -methyl styrene. While some hydrogenation occurred with α -methyl styrene, α -morpholino styrene hydrogenates under hydroformylation conditions without producing any aldehyde. At 140 psi and 90°C, the hydrogenation goes cleanly to complete conversion; if either temperature or syngas pressure is reduced the reaction doesn't go to completion. Neither reducing the partial pressure of H₂ (to 20psi) or the temperature (to 30°C) prevents the hydrogenation reaction. This may be because the enamine is more electron-rich than other substrates attempted, and this slows the CO insertion step, allowing the rhodium alkyl to react with H₂ to hydrogenate.

The TMS enol ether of acetophenone was unreactive under hydroformylation conditions, and the only reaction seen was that of the enol decomposing to acetophenone in wet NMR solvent after sitting under hydroformylation conditions. The other oxygenated styrene derivative studied, 1-(phenylvinyl) acetate, decomposes under reaction conditions via a suspected β -acetoxy elimination from the rhodium center to give acetic acid and styrene, which then undergoes hydroformylation.

Scheme 7: Reactions of other α -substituted styrene derivatives under hydroformylation conditions**Scheme 8:** AHF of N-1-(phenylvinyl) acetamide**Table 4:** AHF of N-1-(phenylvinyl) acetamide

Entry	Ligand	Pressure (CO/H ₂)	Temp (°C)	Time (h)	% Conv.	Hydrog.
1 ^c	1	75/75	80	16	84	n.r.
2 ^{a,b}	2	37.5/112.5	80	24	100	36%
2 ^b	2	7.5/22.5	70	22	76	8%
3	1	15/15	70	44	63	None
4	1	35/35	70	44	46	None
5	1	70/70	70	44	30	None
6	2	15/15	30	44	0	None

Reaction conditions: 2 mol% ligand, 1-1.66M substrate, THF. ^aNot pre-reacted.

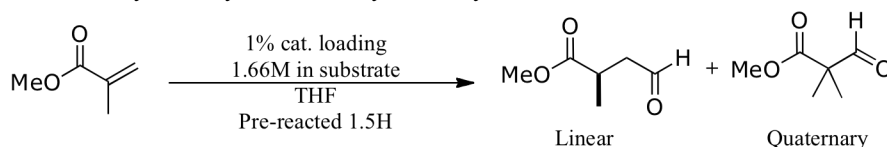
^bUsed toluene as a co-solvent. ^cResult found by Dr. Neil Strotman.

In comparison to the above substrates, the more electron-poor substrate N-1-(phenylvinyl) acetamide exhibits better behavior in hydroformylation. This substrate demonstrated good hydroformylation with our ligands under conditions for which it was unreactive with a screen of other phosphine ligands done by Neil Strotman (Scheme 5, above). When trying to reproduce this result in our own lab, we found difficulty getting a reasonable conversion with ligand **2**. Only under very low pressures of syngas were we able to get a reasonable conversion of 83% (including 8% hydrogenation), and frequently significant amounts of hydrogenation also occurred. When this reaction was revisited with ligand **1** instead, very different results were found (Table 4). No hydrogenation occurred, and complete regioselectivity was seen for the linear product. With ligand **2**, some formation of a singlet in the aldehyde region of the ¹H NMR spectrum occurs. This was hypothesized to be the quaternary regioisomer, however further NMR examples were unable to confirm this and the compound was not isolated. With ligand **1**, this substrate also shows a clear inhibition by CO, as the best conversion (63%) was seen for the lowest syngas pressure used (30

psi), and conversion decreases with increasing syngas pressure (Table 4, entries 3-5). This difference may also be attributable to using only THF as the solvent instead of a mix of THF and toluene, but inhibition by CO is a more likely cause for the changes in conversion.

Acrylate hydroformylation

Scheme 9: Hydroformylation of methyl methacrylate



Based on the expectation that olefins with electron-withdrawing substituents would be active in hydroformylation, a number of acrylate substrates were attempted. In general these showed complete conversion within 24 hours or less. Methyl methacrylate undergoes AHF to yield a mixture of the branched (quaternary) product and the linear product, the ratio of which shows a minor dependence on the syngas pressure used (Table 5). Higher syngas pressures favor formation of the quaternary aldehyde, as do lower temperatures.

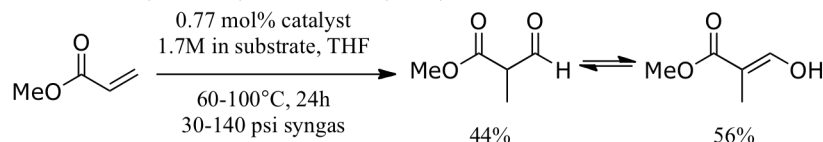
Table 5: Hydroformylation of methyl methacrylate

Entry	Temp. (°C)	CO/H ₂ (psi)	Time (h)	Conv. (%)	Linear:quat product
1	90	140	24	100	1:0.23
2	50	30	48	98	1:0.46
3	70	60	48	100	1:0.28
4	70	140	24	100	1:0.38
5a	90	60	24	100	1:0.07
5b	90	60	48	100	1:0.10

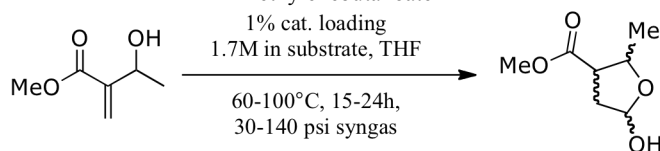
After finding the facile AHF of methyl methacrylate and the observed preference for insertion to form the branched product, the AHF of methyl acrylate was also attempted. The AHF can be run with low syngas pressures and catalyst loadings under 1%, and gives full conversion and perfect regioselectivity for the branched product, methyl 2-methyl-3-oxopropanoate. As expected, this

1,3-dicarbonyl product contains a much more acidic α proton, and exists as a mixture of tautomers (roughly 44% keto form and 56% enol form at room temperature), which will hinder any retention of enantioselectivity.

Scheme 10: Hydroformylation of methyl acrylate



Scheme 11: Hydroformylation of methyl-3-hydroxy-2-methylenebutanoate



One of the goals we have for demonstrating synthetic utility of AHF is in exploring the tolerance of the reaction for a number of functional groups. With this in mind, and encouraged by the high reactivity of acrylates in AHF, we tried the reaction with methyl-3-hydroxy-2-methylenebutanoate. This substrate has two new factors that were not yet explored: a free hydroxyl group that will demonstrate functional group tolerance, and a stereocenter that may show diastereoselectivity. This reaction gives complete conversion except when the syngas pressure is lowered to 30 psi. When run at 60 °C, the distribution of products is insensitive to changes in pressure in the 70-140 psi range, and at 140 psi there is no change with an increase in the temperature to 100 °C. The observed products are a mixture of hemiacetals with undetermined diastereoselectivity. This allows potential access to not only aldehyde products, but also lactones via a subsequent oxidation of the hemiacetal.¹⁰

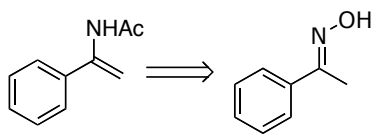
Experimental.

A. General considerations. All phosphines were generated under N_2 using standard Schlenk line procedures. Workup and flash chromatography of ligands for hydroformylation was performed

open to air. *o*-Tetraacid Bisdiazaphos, *rac* C₂ symmetric *o*-tetrabenzylamide bisdiazaphos **1**, (*S*)-(-)- α -methylbenzyl *o*-tetraamide (*S,S*)-Bisdiazaphos **2**, and (*S*)-(-)- α -methylbenzyl *o*-tetraamide (*R,R*)-Bisdiazaphos were prepared as reported in literature.²⁰ (Acetylacetonato) dicarbonylrhodium(I) was recrystallized from toluene and hexanes (green crystals) prior to use. Benzoic acid was sublimed prior to use in hydro-oxycarbonylation reactions. THF and toluene were distilled from sodium/benzophenone ketyl under N₂ prior to use. CH₂Cl₂ was distilled from P₂O₅ under N₂ prior to use. THF and toluene used for hydroformylation reactions and hydro-oxycarbonylation reactions was additionally degassed by performing at least 3 freeze-pump-thaw cycles. Ethyl acetate, hexane, and dichloromethane were obtained from Sigma-Aldrich, CCI Chemical, and Mallinckrodt Chemical respectively. NMR spectra were recorded at ambient temperature on a Varian Mercury 300, Inova-500 or Unity 500 or a Bruker AC-300. ¹H and ¹³C NMR chemical shifts were referenced to tetramethylsilane if present or residual solvent. ³¹P NMR chemical shifts were referenced to an external standard of 85% H₃PO₄. Mass spectra were collected on a Bruker ULTRAFLEX[®] III for Matrix-assisted laser desorption/ionization (MALDI), or on a Waters (Micromass) LCT[®] for electrospray ionization experiments with a sample cone voltage of 20.

B. Synthesis of substrates for hydroformylation

α -Methyl styrene, methyl methacrylate, and methyl acrylate were purchased from Sigma Aldrich and used as received. 1-Phenyl-1-trimethylsiloxyethylene,²¹ α -morpholino styrene,²² 2,3,3-trimethyl-1-butene²³ 1-(phenylvinyl)acetate²⁴ and methyl-3-hydroxy-2-methylenebutanoate²⁵ were all synthesized by the literature procedure. Spectral data for all compounds matched the literature reports.



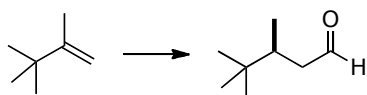
N-(1-phenylvinyl)acetamide was synthesized from acetophenone via the oxime²⁶ following a modified version of the literature procedure: Acetic anhydride (10.5 mL, 111.0 mmol) was added dropwise over 25 min to a solution of acetophenone oxime (5.0046 g, 37 mmol) in dry toluene (20 mL). Freshly distilled acetic acid (6.4 mL, 111.0 mmol) was added, and this solution was cannulated into a flask under N₂ containing iron powder (4.196 g, 74.0 mmol). The reaction mixture was heated to 70 °C for 4 h under nitrogen, then filtered through Celite and the residues washed with toluene until the filtrate ran colorless (60mL toluene). The filtrate was cooled in an ice bath and washed with 2M aqueous sodium hydroxide (2 × 15mL) and brine (1 × 25mL). The organic fraction was dried (MgSO₄) and concentrated *in vacuo* to yield 5.8g crude material. Purification by column chromatography, eluting with 1:1 ethyl acetate and hexanes, followed by crystallization from hot ethanol and water yields the pure title compound as cream colored crystals, 1.86g (31.2%): ¹H NMR: (300.1 MHz, CDCl₃) δ 7.411 (m, 5H), 6.790 (NH, br s, 1H), 5.891 (s, 1H), 5.100 (s, 1H), 2.147 (s, 3H), 1.599 (s, 3H). These spectral data match the literature report.²⁶

²⁷ We found better yields when the iron powder was freshly purchased and stored under nitrogen at all times.

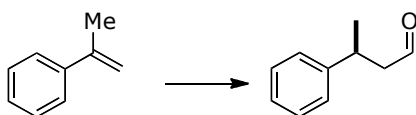
C. General method for hydroformylation.

Inside a N₂-purged glovebox, THF solutions of Rh(CO)₂(acac) and *o*-tetrabenzylamide bisdiazaphos **1** were measured using 1000μL and 200μL Eppendorf® pipets and combined in an

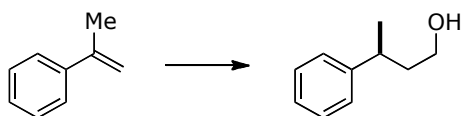
oven-dried 15mL Ace Glass pressure bottle equipped with a magnetic stir bar which was then sealed with a reactor head and brought out of the glovebox. The reaction vessel was subjected to 5 pressurization (140psi)/depressurization (15psi) cycles with syngas to ensure replacement of the dinitrogen atmosphere with syngas, then pressurized to 140 psi and allowed to stir for 30-60 min in an oil bath at the reaction temperature. The reaction vessel was then removed from the oil bath and allowed to cool for 5 minutes, then the pressure was reduced to just above atmospheric and the olefin was injected with a gas-tight syringe with a 12" needle. If used, the internal standard was added directly to the olefin, and an ^1H NMR spectrum was obtained to quantify the amount of standard. Solid olefins (e.g. N-vinyl acetamide) were injected as a solution in THF. The reaction was then re-pressurized to the reaction pressure after additional pressurization/depressurization cycles and replaced in the oil bath. Upon completion of the reaction, the pressure bottle was removed from the oil bath and allowed to cool to room temperature, then vented in a fume hood. NMR spectra are initially obtained of the crude reaction mixture by adding acetone- d_6 or CDCl_3 directly to the reaction mixture.



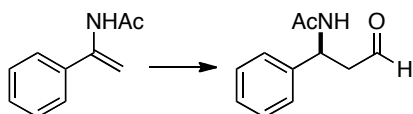
3,4,4-Trimethyl butanal. ^1H NMR: (299.9 MHz, acetone- d_6) δ 9.71 (dd, $J = 3.1, 1.2$ Hz, 1H), 2.06 (m, 2H), 1.89 (m, 1H), 0.88 (s, 9H), 0.86 (CH_3 , dd, $J = 6.7, 0.7$ Hz, 3H).



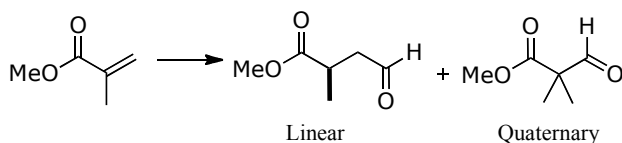
3-Phenyl butanal. ^1H NMR: (500.2 MHz, acetone- d_6) δ 9.58 (CHO, dd, $J = 2.4, 1.3$ Hz, 1H), 7.38-7.06 (m, 5H), 5.62 (PhCH, td, $J = 8.6, 5.8$ Hz, 1H), 2.79 (CH_2 , ddd, $J = 16.5, 8.8, 2.8$ Hz, 1H), 2.67 (CH_2 , ddd, $J = 16.2, 5.6, 1.3$ Hz, 1H), 1.36 (CH_3 , d, $J = 7.1$ Hz, 3H).



3-Phenyl butanol. From 0.85 mmol α -methyl styrene; purified by column chromatography on silica eluted with 30% ethyl acetate in hexane, colorless oil: ^1H NMR: (300.1 MHz, CDCl_3) δ 7.24 (Ph, m, 5H), 3.59 (CH_2OH , td, $J = 6.5, 4.1$ Hz, 1H), 3.51 (CH_2OH , td, $J = 6.8, 3.9$ Hz, 1H), 2.88 (CH, sextet, $J = 7.4$ Hz, 1H), 1.85 (CHCH_2 , q, $J = 6.8$ Hz, 2H), 1.28 (CH_3 , d, $J = 7.0$ Hz, 3H); ^{13}C NMR: (75.4 MHz, CDCl_3) δ 147.1, 128.7 (2C), 127.2 (2C), 126.3, 61.4, 41.2, 36.7, 22.6.

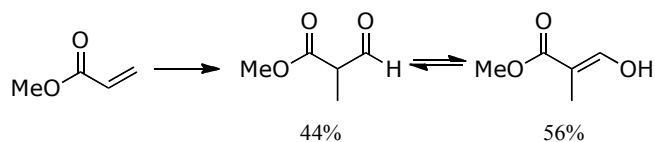


3-Acetamido-3-phenyl propanal. ^1H NMR: (299.7 MHz, CDCl_3) δ 9.68 (CHO, dd, $J = 2.6, 1.8$ Hz, 1H), 7.31 (m, 5H), 5.50 (td, $J = 8.0, 6.3$ Hz, 1H), 2.92 (ddd, $J = 16.4, 7.8, 2.6$ Hz, 1H), 2.83 (ddd, $J = 16.4, 7.6, 1.6$ Hz, 1H), 1.90 (s, 3H).



Methyl 2-methyl-4-oxobutanoate (linear product). ^1H NMR: (299.9 MHz, CDCl_3) δ 9.77 (CHO, t, $J = 1.0$ Hz, 1H), 3.70 (OMe, s, 3H), 2.95 (AB of ABX, m, 2H), 2.55 (X of ABX, m, 1H), 1.23 (CH_3 , d, $J = 7.1$ Hz, 3H).

Methyl 2,2-dimethyl-3-oxopropanoate (quaternary product). ^1H NMR: (299.7 MHz, CDCl_3) δ 9.65 (s, 1H), 3.75 (s, 3H), 1.34 (s, 6H).



Methyl 2-methyl-3-oxopropanoate²⁸. ^1H NMR: (500.2 MHz, CDCl_3) δ 11.24 (d, $J = 12.7$ Hz, 1H, enol form), 9.77 (d, $J = 1.3$ Hz, 1H, keto form), 7.00 (dq, $J = 12.5, 1.1$ Hz, 1H, enol), 3.78 (s, 3H), 3.68 (s, 3H), 3.42 (qd, $J = 7.3, 1.2$ Hz, 1H, keto), 1.68 (d, $J = 1.1$ Hz, 3H, enol), 1.35 (d, $J = 7.5$ Hz, 3H, keto).

References

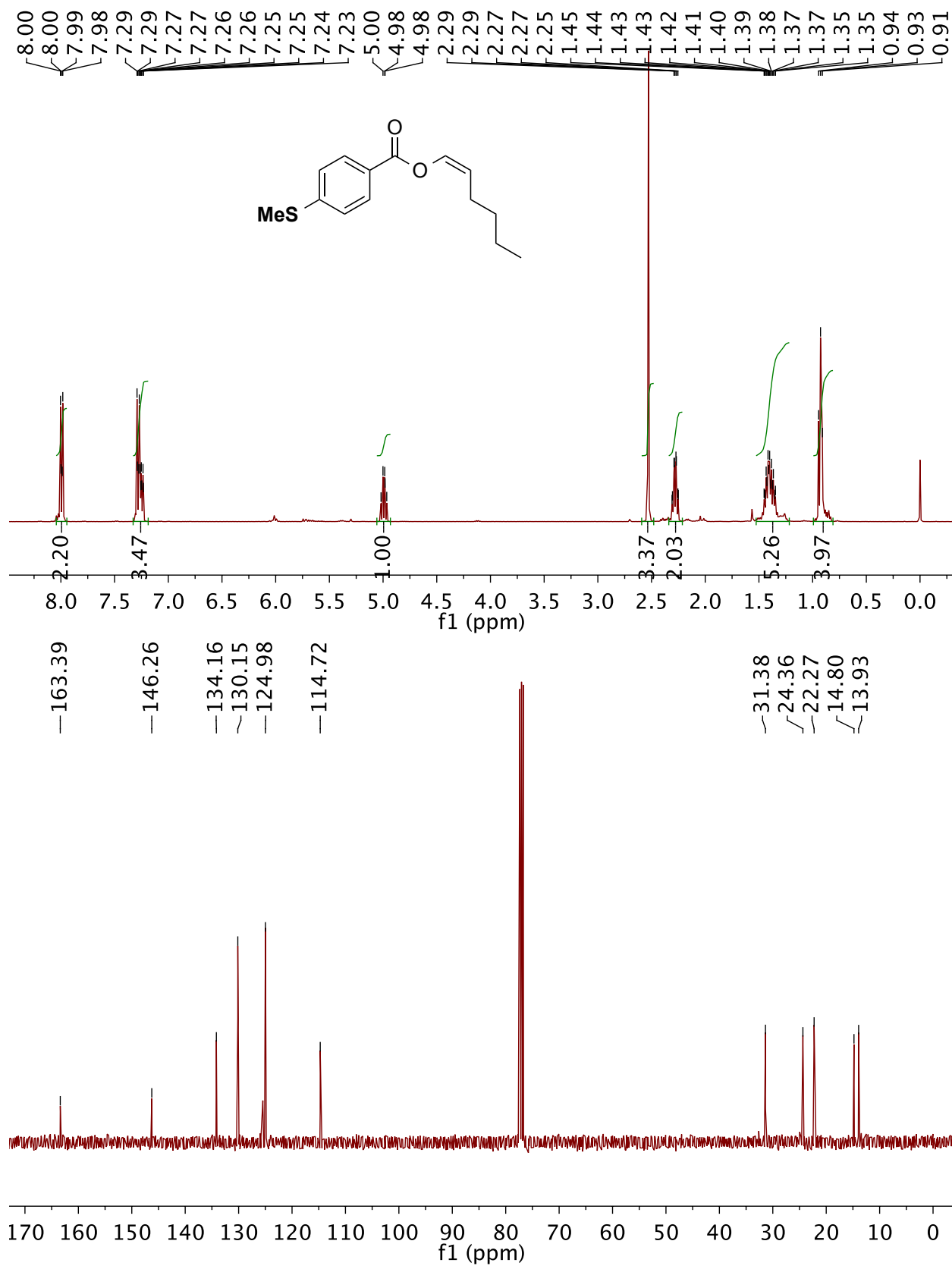
- (1) Gual, A.; Godard, C.; Castellón, S.; Claver, C. *Tetrahedron: Asymmetry* **2010**, *21*, 1135-1146.
- (2) Klosin, J.; Landis, C. R. *Acc. Chem. Res.* **2007**, *40*, 1251-1259.
- (3) McDonald, R. I.; Wong, G. W.; Neupane, R. P.; Stahl, S. S.; Landis, C. R. *J. Am. Chem. Soc.* **2010**, *132*, 14027-14029.
- (4) Grünanger, C.; Breit, B. *Angew. Chem. Int. Ed.* **2008**, *47*, 7346-7349.
- (5) Breit, B. *Acc. Chem. Res.* **2003**, *36*, 264-275.
- (6) Grünanger, C.; Breit, B. *Angew. Chem. Int. Ed.* **2010**, *49*, 967-970.
- (7) Rousseau, G.; Breit, B. *Angew. Chem. Int. Ed.* **2011**, *50*, 2450-2494.
- (8) Worthy, A. D.; Joe, C. L.; Lightburn, T. E.; Tan, K. L. *J. Am. Chem. Soc.* **2010**, *132*, 14757-14759.
- (9) Joe, C. L.; Tan, K. L. *J. Org. Chem.* **2011**, 7590-7596.
- (10) Ueki, Y.; Ito, H.; Usui, I.; Breit, B. *Chemistry, A European Journal* **2011**, *17*, 8555-8558.
- (11) Sun, X.; Frimpong, K.; Tan, K. L. Synthesis of Quaternary Carbon Centers via Hydroformylation. *J. Am. Chem. Soc.* **2010**, *132*, 11841-11843.
- (12) Keulemans, A. I. M.; Kwantes, A.; van Bavel, T. *Recl. Trav. Chim. Pays-Bas* **1948**, *67*, 298.
- (13) Noonan, G.; Newton, D.; Cobley, C.; Suárez, A.; Pizzano, A.; Clarke, M. *Adv. Synth. Catal.* **2010**, *352*, 1047-1054.
- (14) Clarke, M. L.; Roff, G. J. *Chemistry, A European Journal* **2006**, *12*, 7978-7986.
- (15) Lumbroso, A.; Vautravers, N. R.; Breit, B. *Org. Lett.* **2010**, *12*, 5498-5501.
- (16) Simaan, S.; Marek, I. *J. Am. Chem. Soc.* **2010**, *132*, 4066-4067.

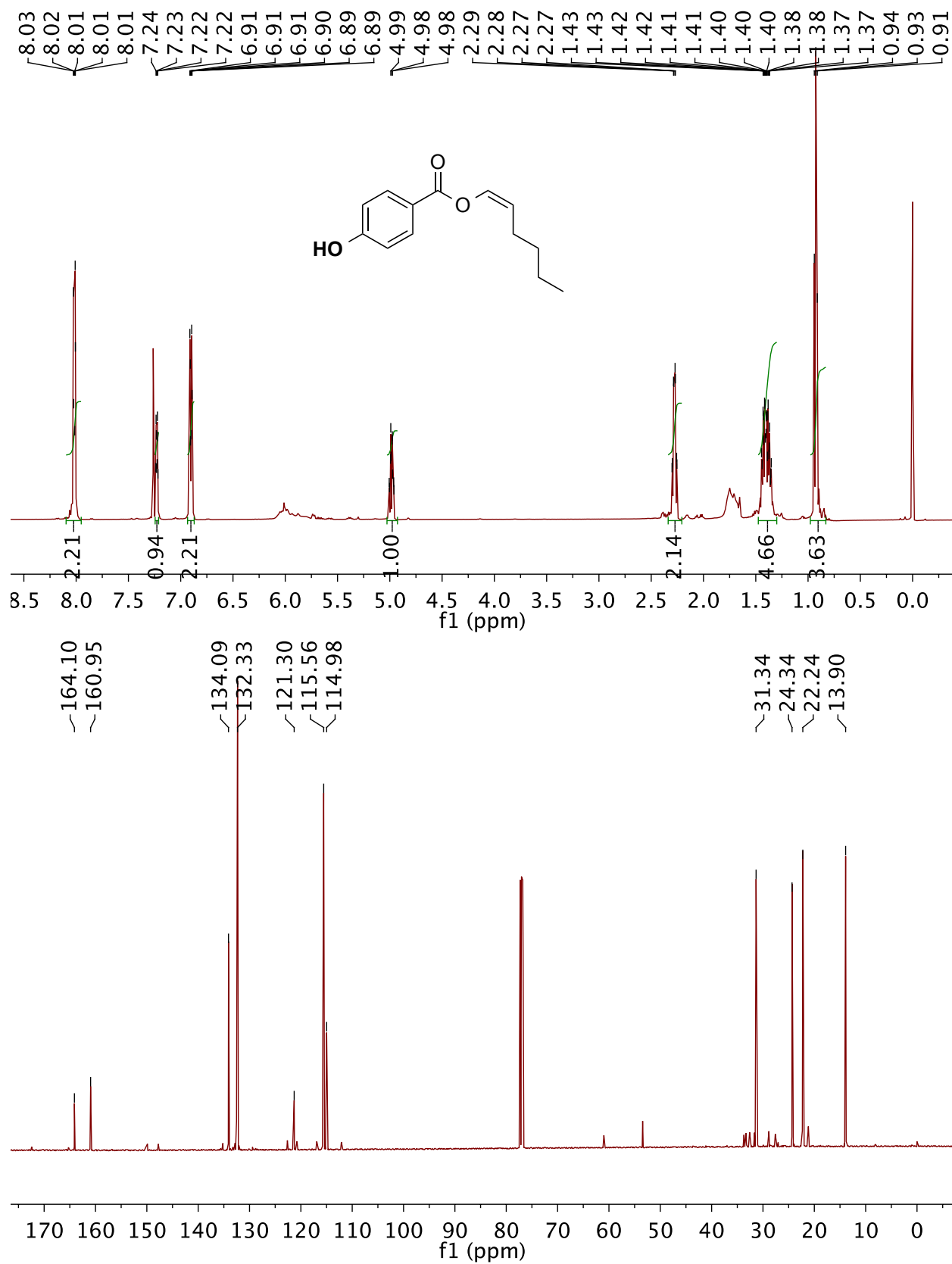
- (17) Doucet, H.; Martin-Vaca, B.; Bruneau, C.; Dixneuf, P. H. *J. Org. Chem.* **1995**, *60*, 7247-7255.
- (18) Goossen, L. J.; Paetzold, J.; Koley, D. *Chem. Commun.* **2003**, 706-707.
- (19) Chary, B. C.; Kim, S. *J. Org. Chem.* **2010**, *75*, 7928-7931.
- (20) Clark, T. P.; Landis, C. R.; Freed, S. L.; Klosin, J.; Abboud, K. A. *J. Am. Chem. Soc.* **2005**, *127*, 5040-5042.
- (21) Mukaiyama, T.; Narasaka, K. *Organic Syntheses, Coll. Vol.* **1993**, *8*, 323.
- (22) Noyori, R.; Yokoyama, K.; Hayakawa, Y. *Organic Syntheses, Coll. Vol.* **1988**, *6*, 520.
- (23) House, H. O.; Gaa, P. C.; Lee, J. H. C.; VanDerveer, D. *J. Org. Chem.* **1983**, *48*, 1670-1678.
- (24) Berkessel, A.; Sebastian-Ibarz, M. L.; Müller, T. N. *Angew. Chem. Int. Ed.* **2006**, *45*, 6567-6570.
- (25) Behrens, C.; Paquette, L. A. *Organic Syntheses, Coll. Vol.* **2004**, *10*, 41.
- (26) Burk, M. J.; Casy, G.; Johnson, N. B. *J. Org. Chem.* **1998**, *63*, 6084-6085.
- (27) Hughes, R. A.; Thompson, S. P.; Alcaraz, L.; Moody, C. J. *J. Am. Chem. Soc.* **2005**, *127*, 15644-15651.
- (28) Nakatsuji, H.; Nishikado, H.; Ueno, K.; Tanabe, Y. *Org. Lett.* **2009**, *11*, 4258-4261.

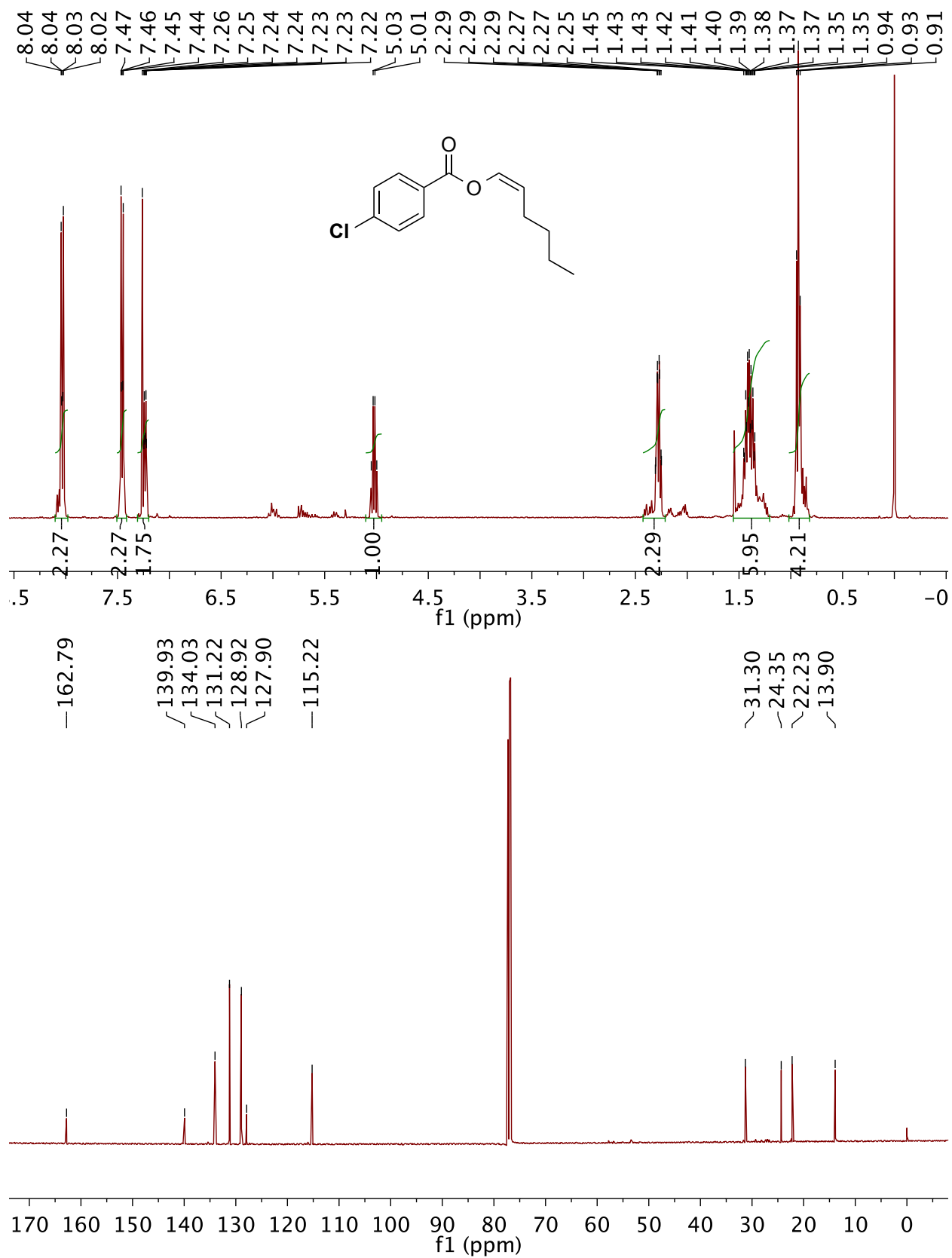
Appendix B

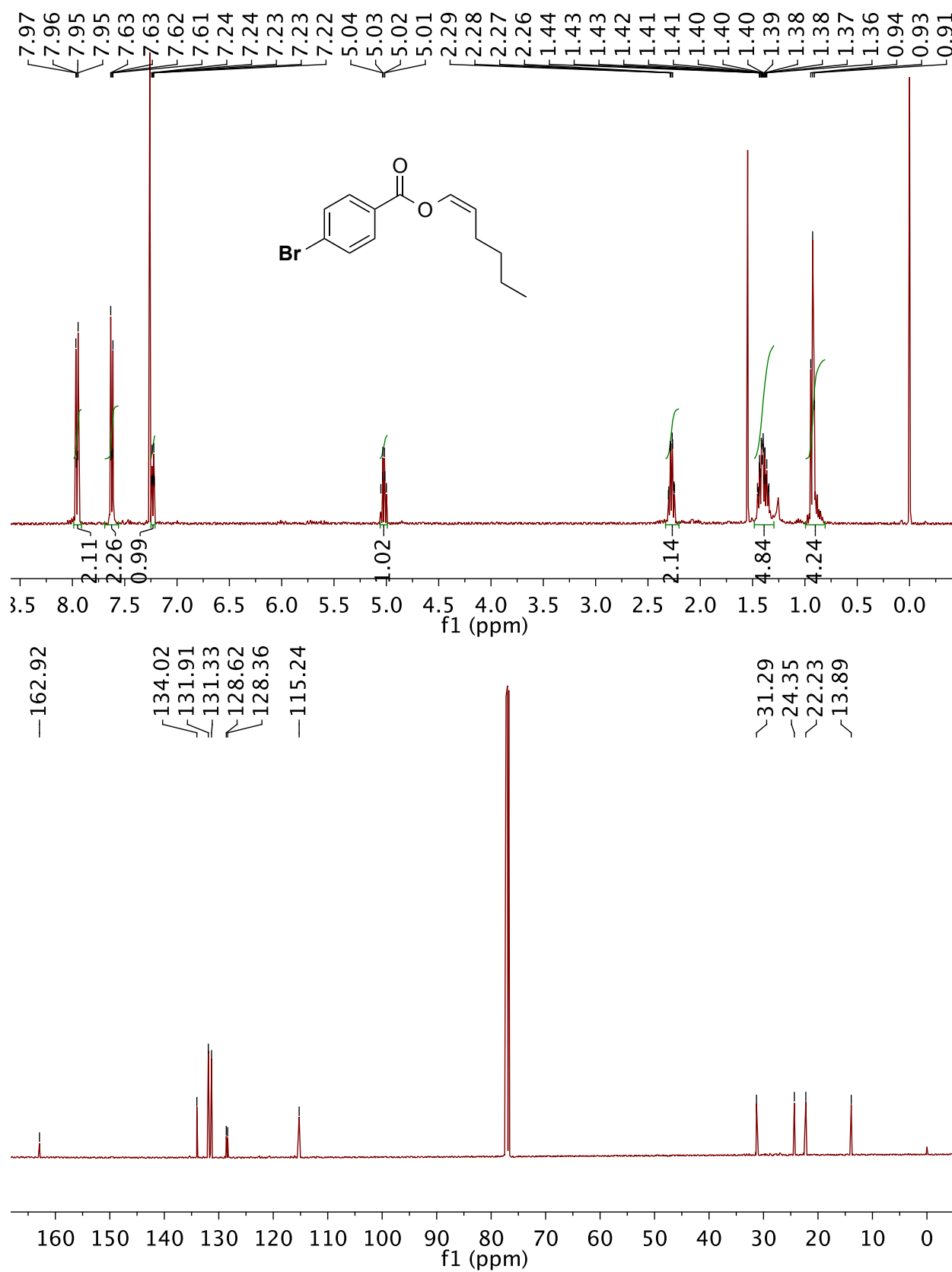
Spectra and supporting data for chapters 2-5.

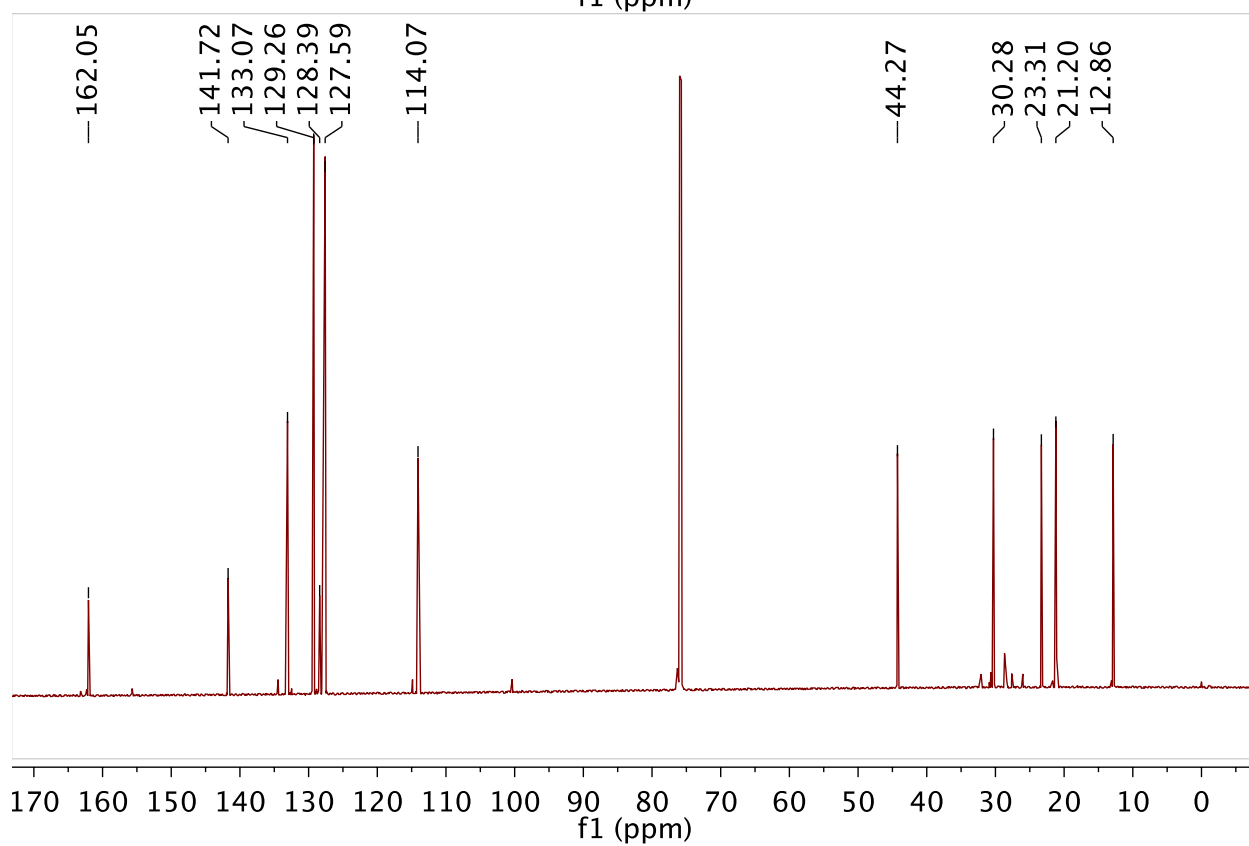
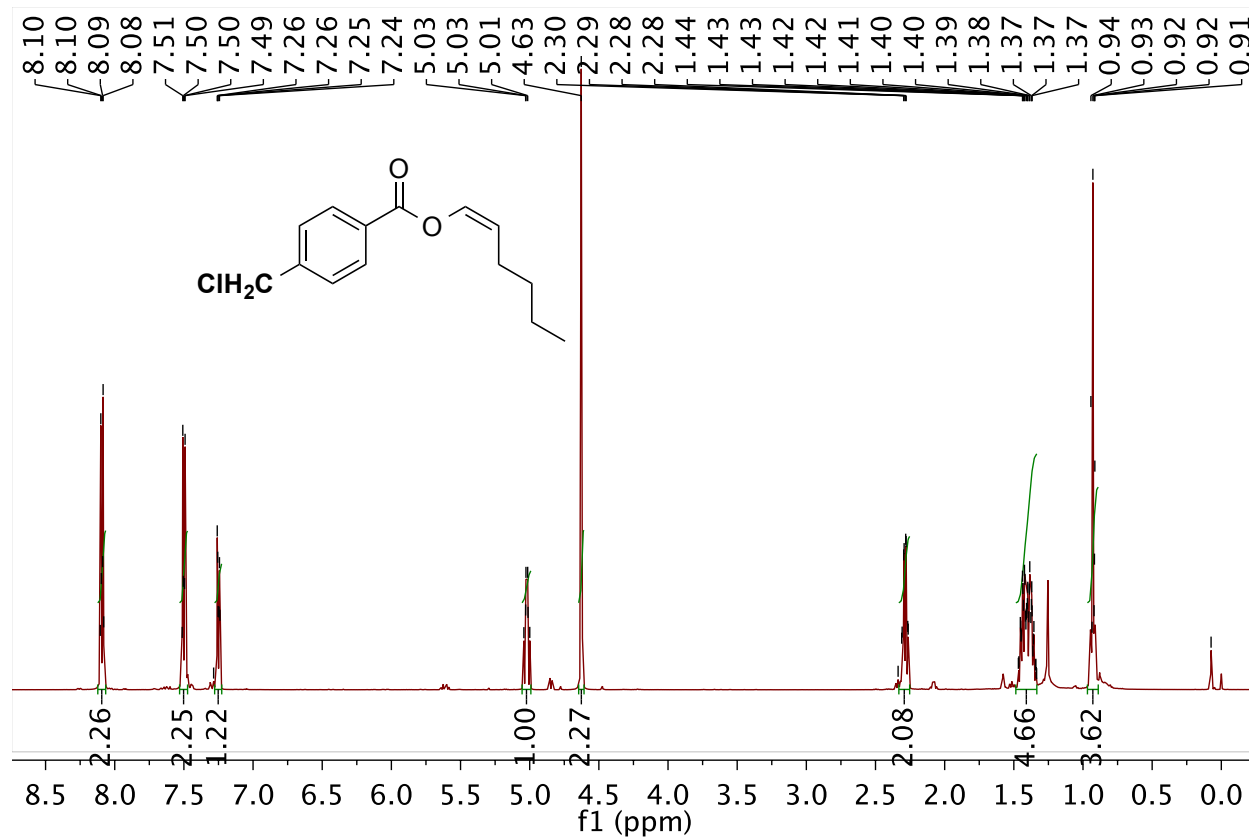
Chapter 2 Supporting data and spectra.

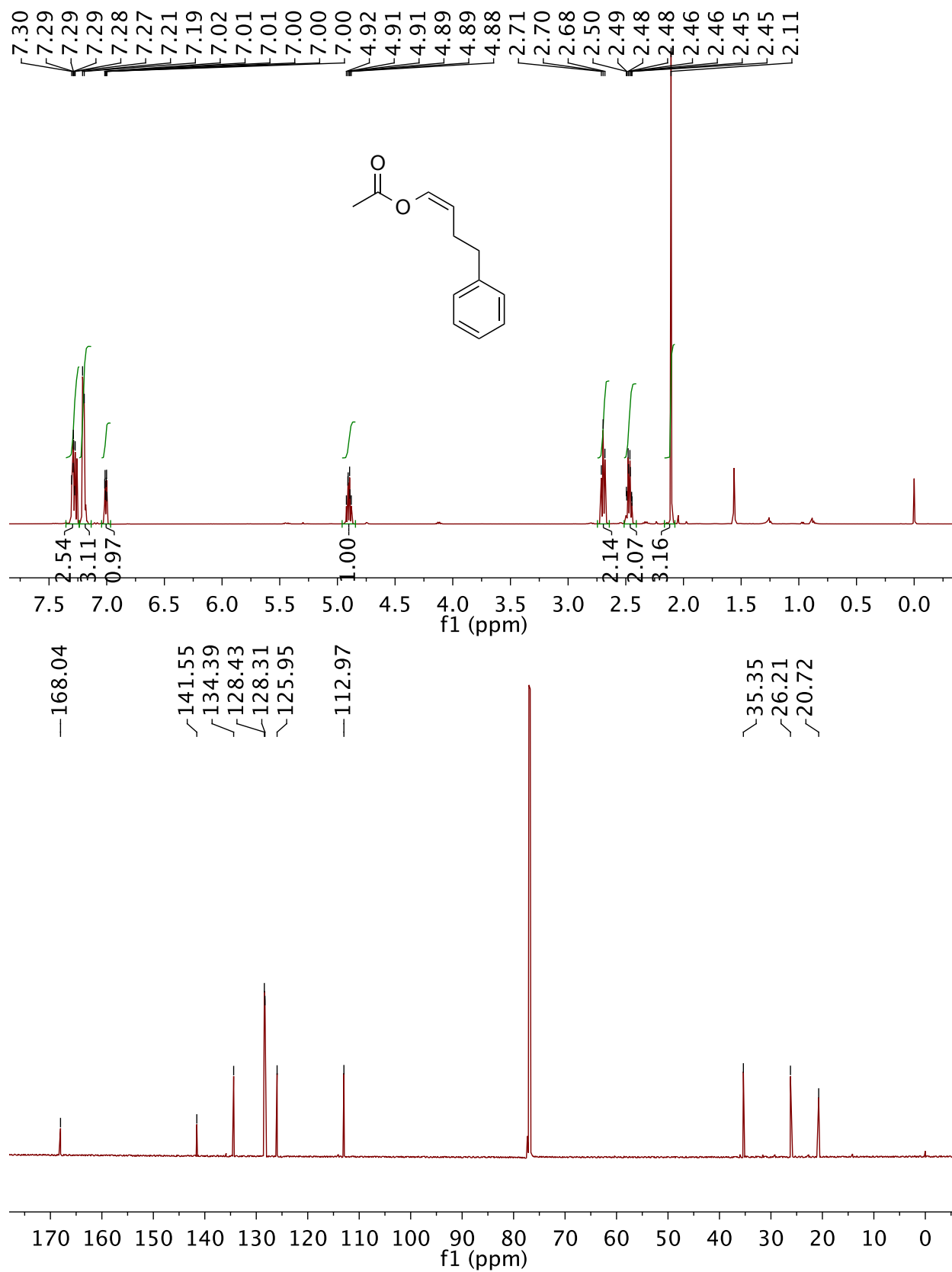


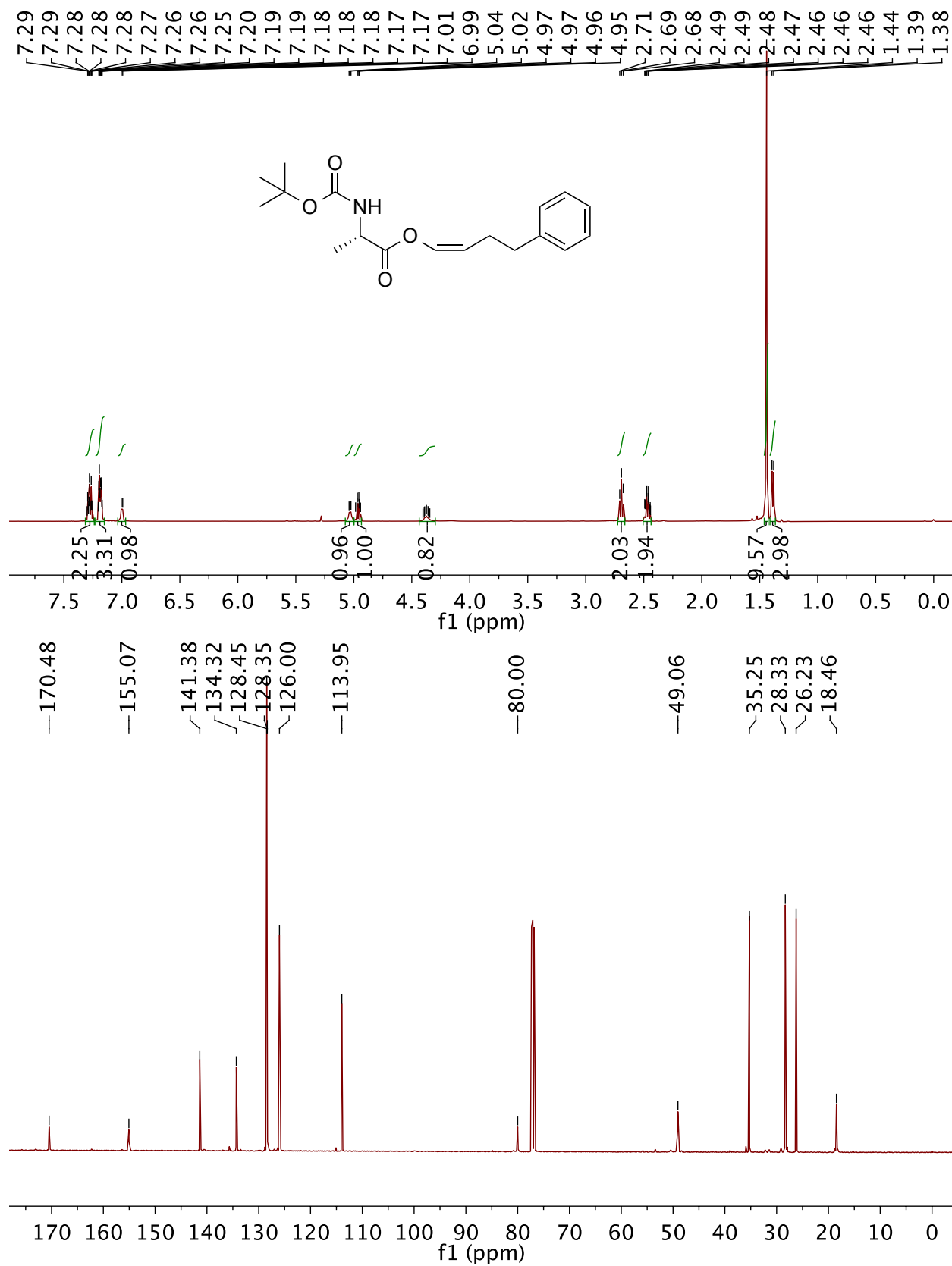


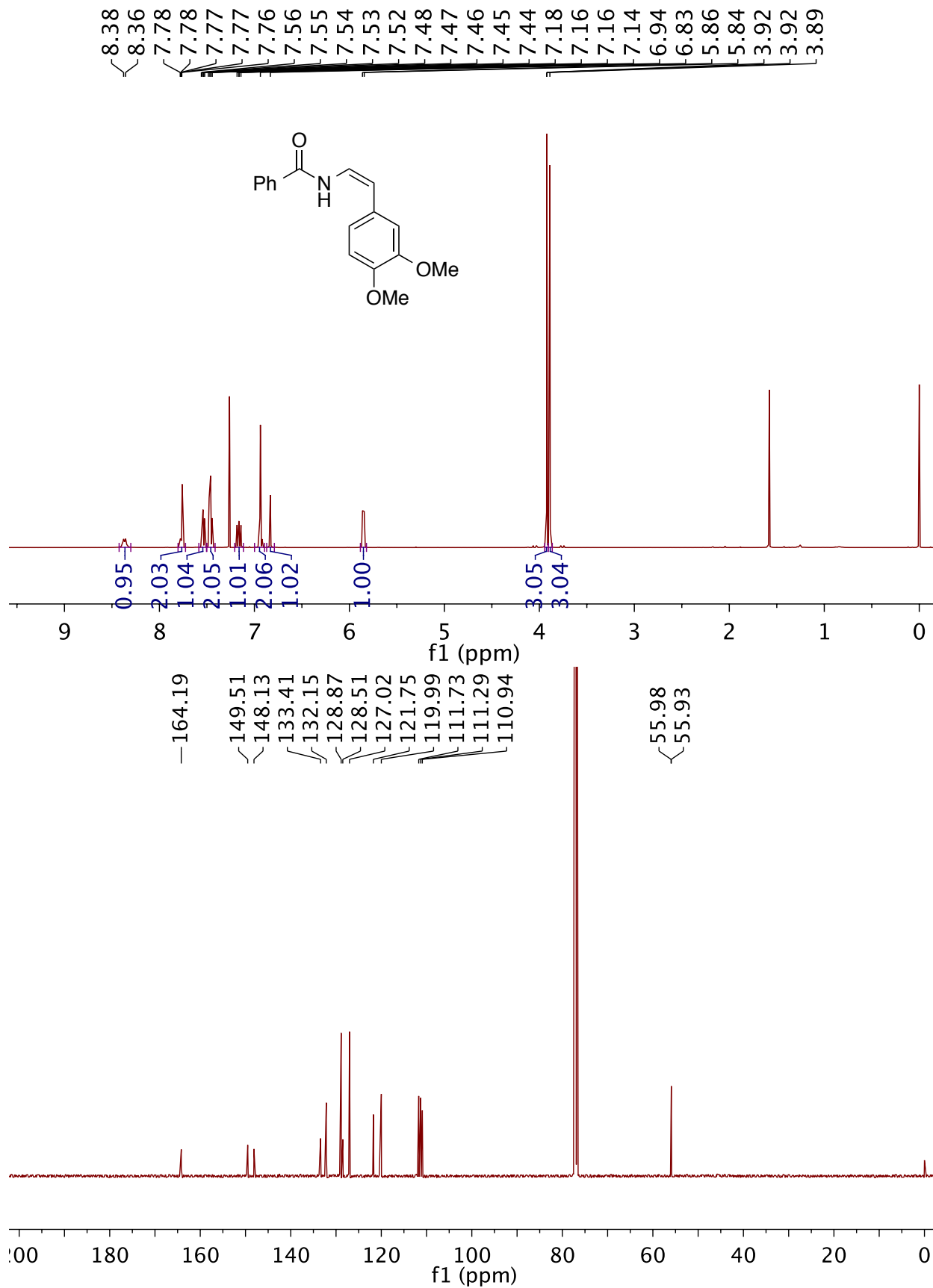


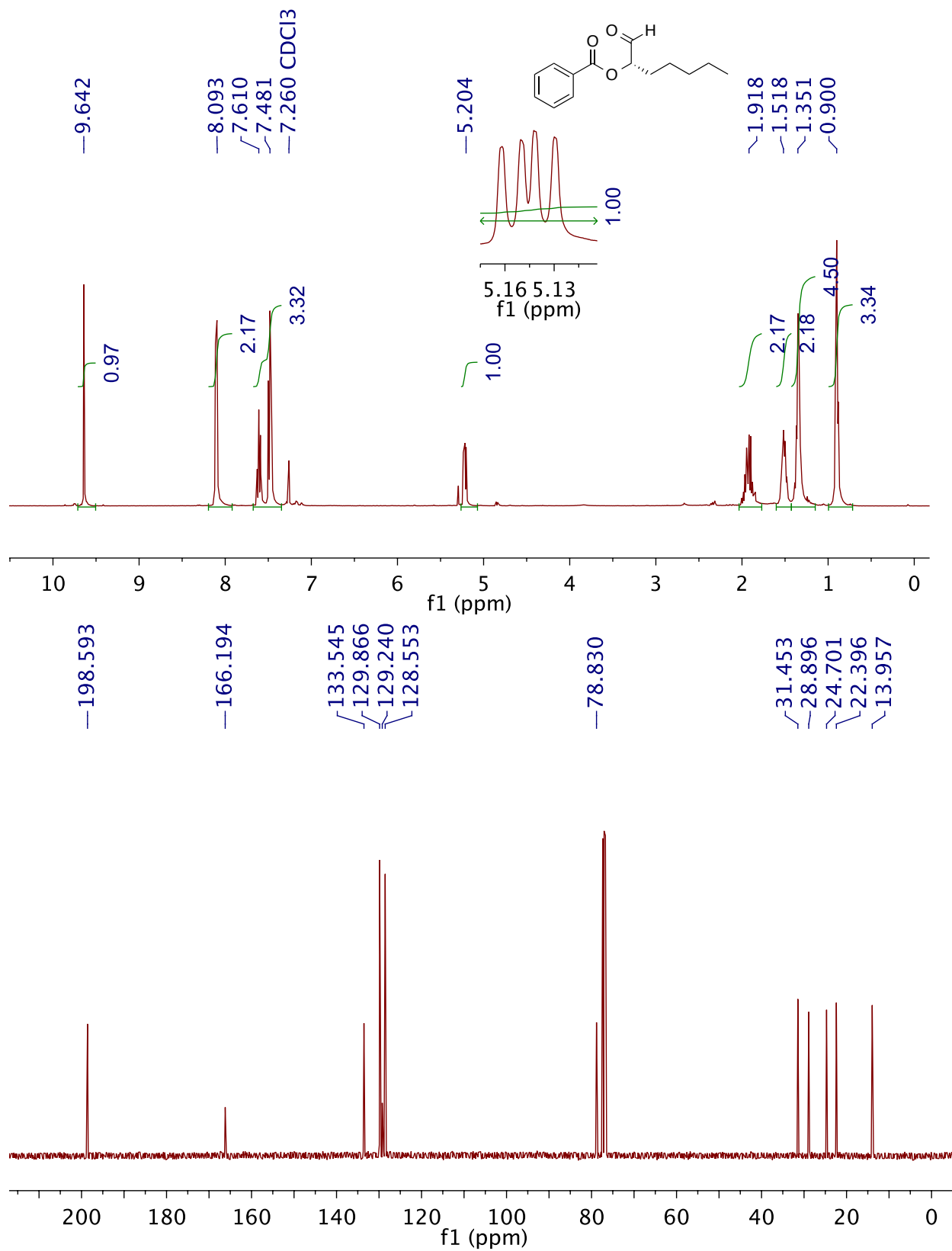


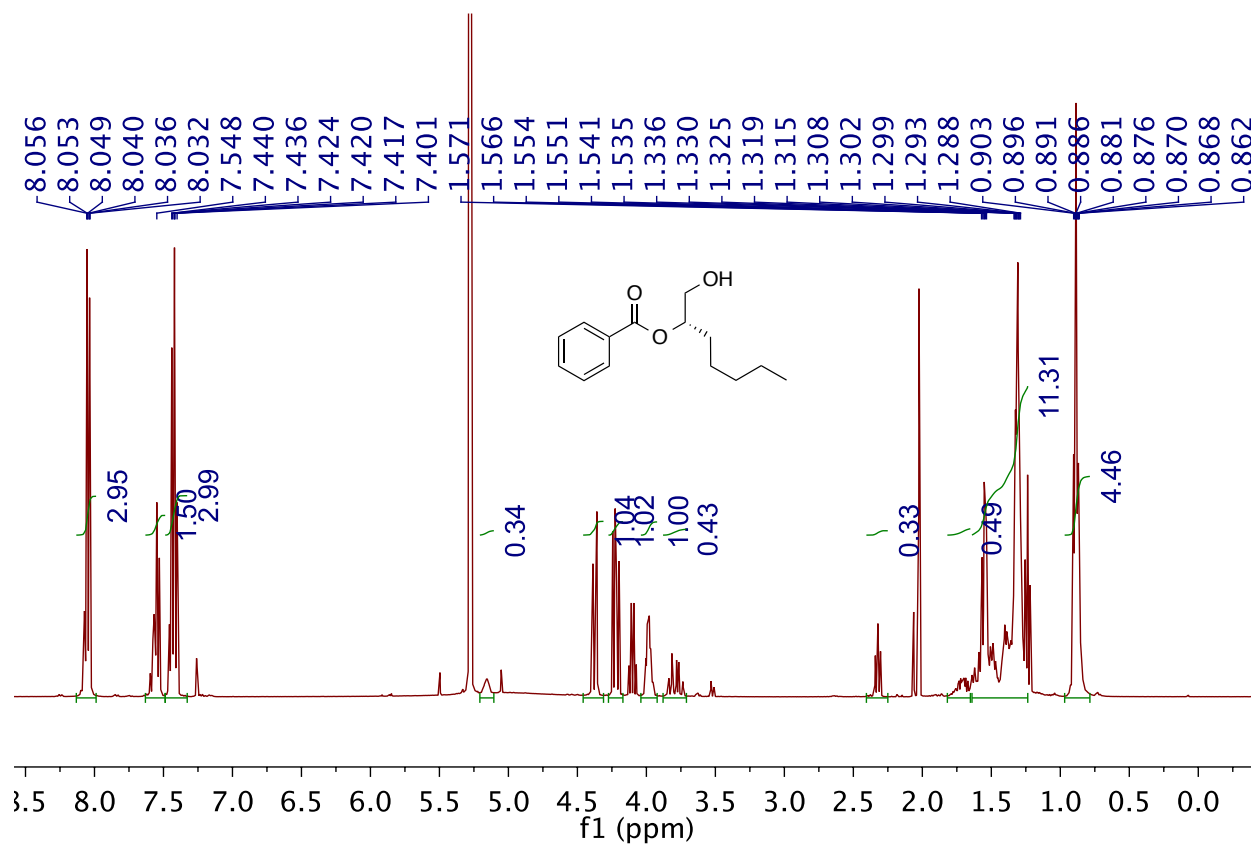




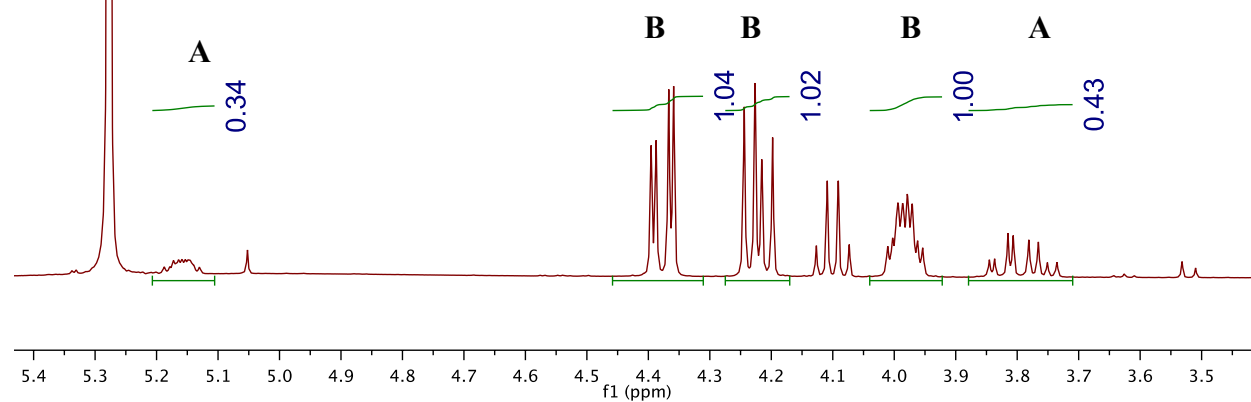
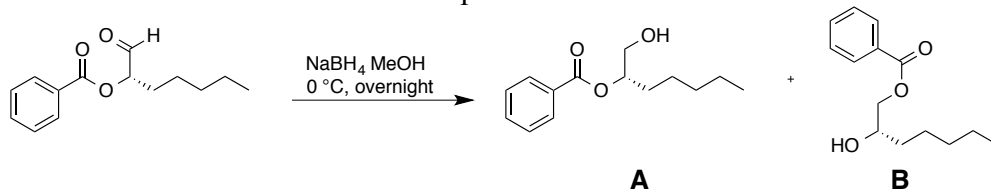


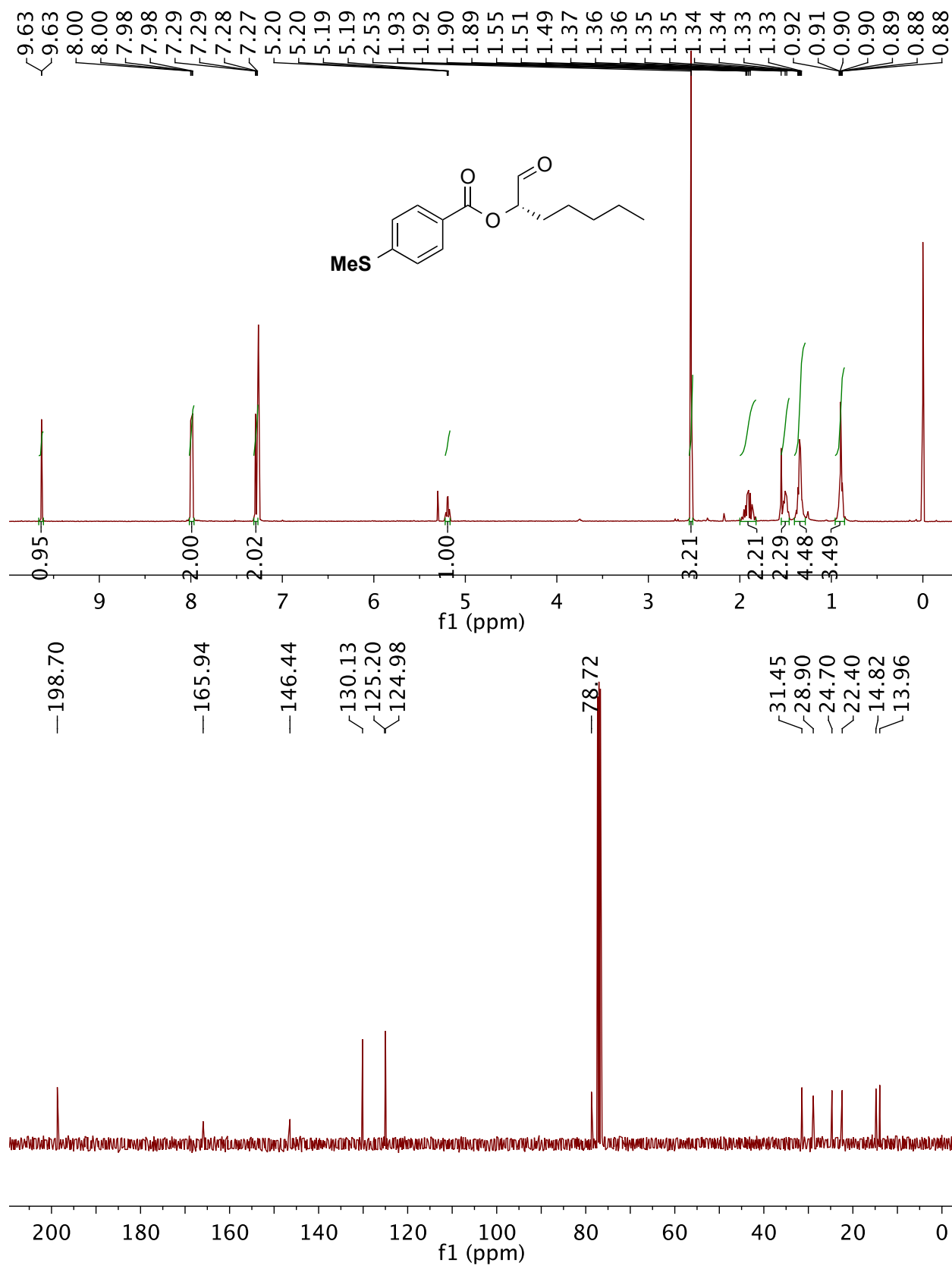


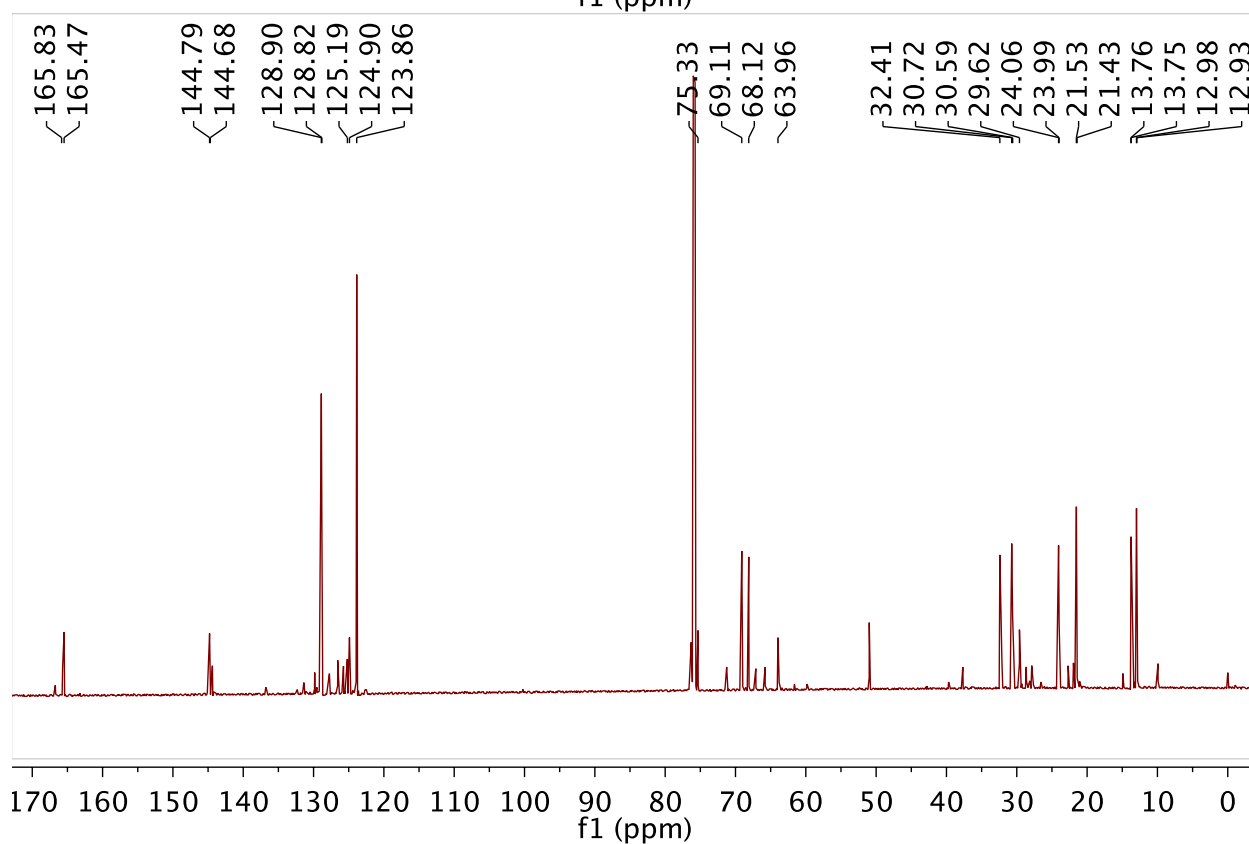
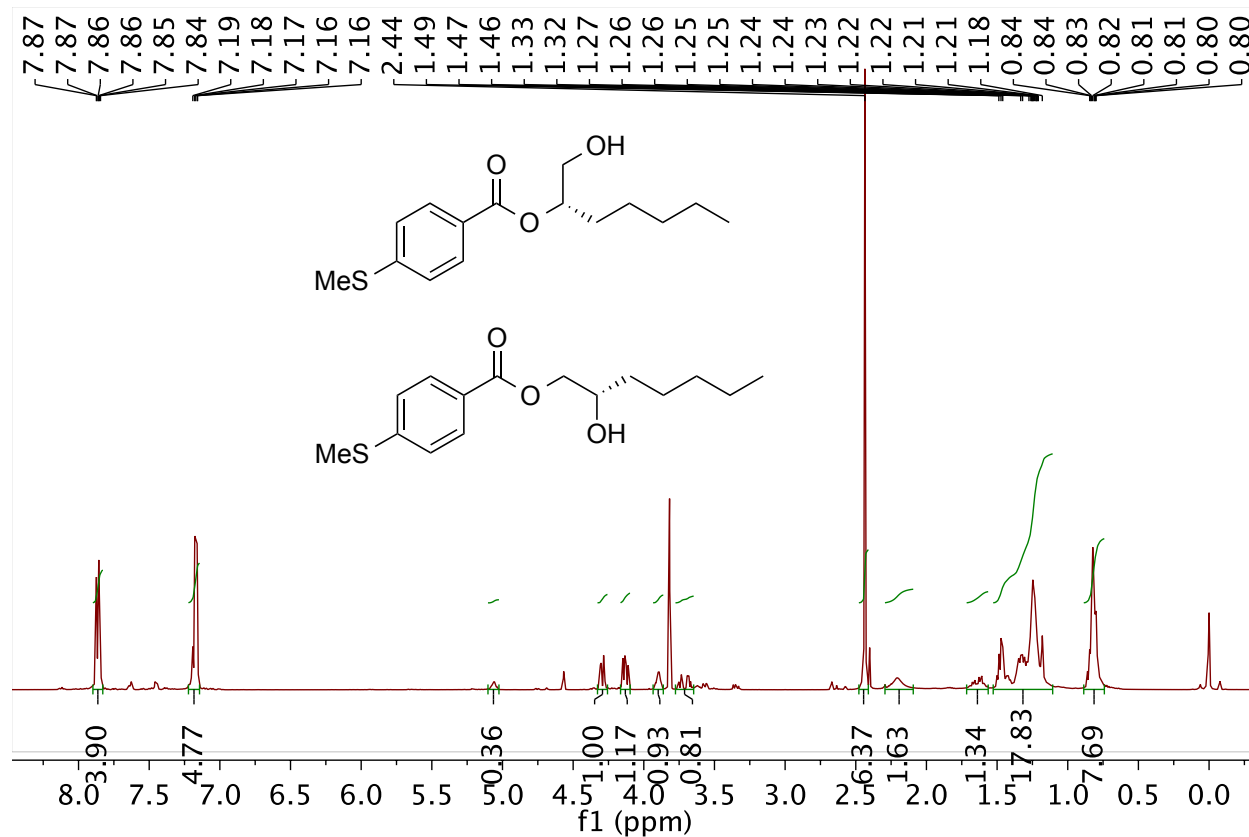


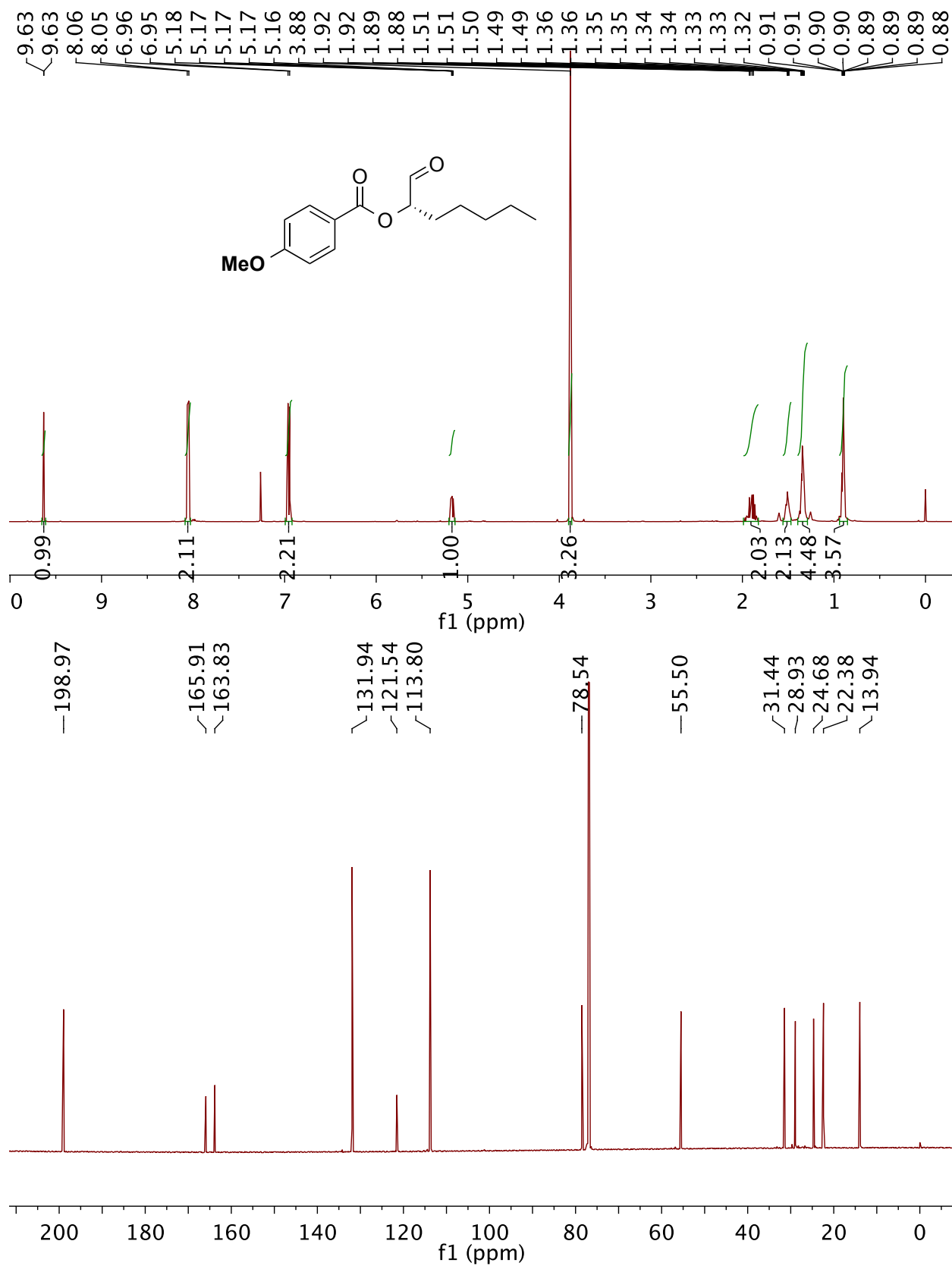


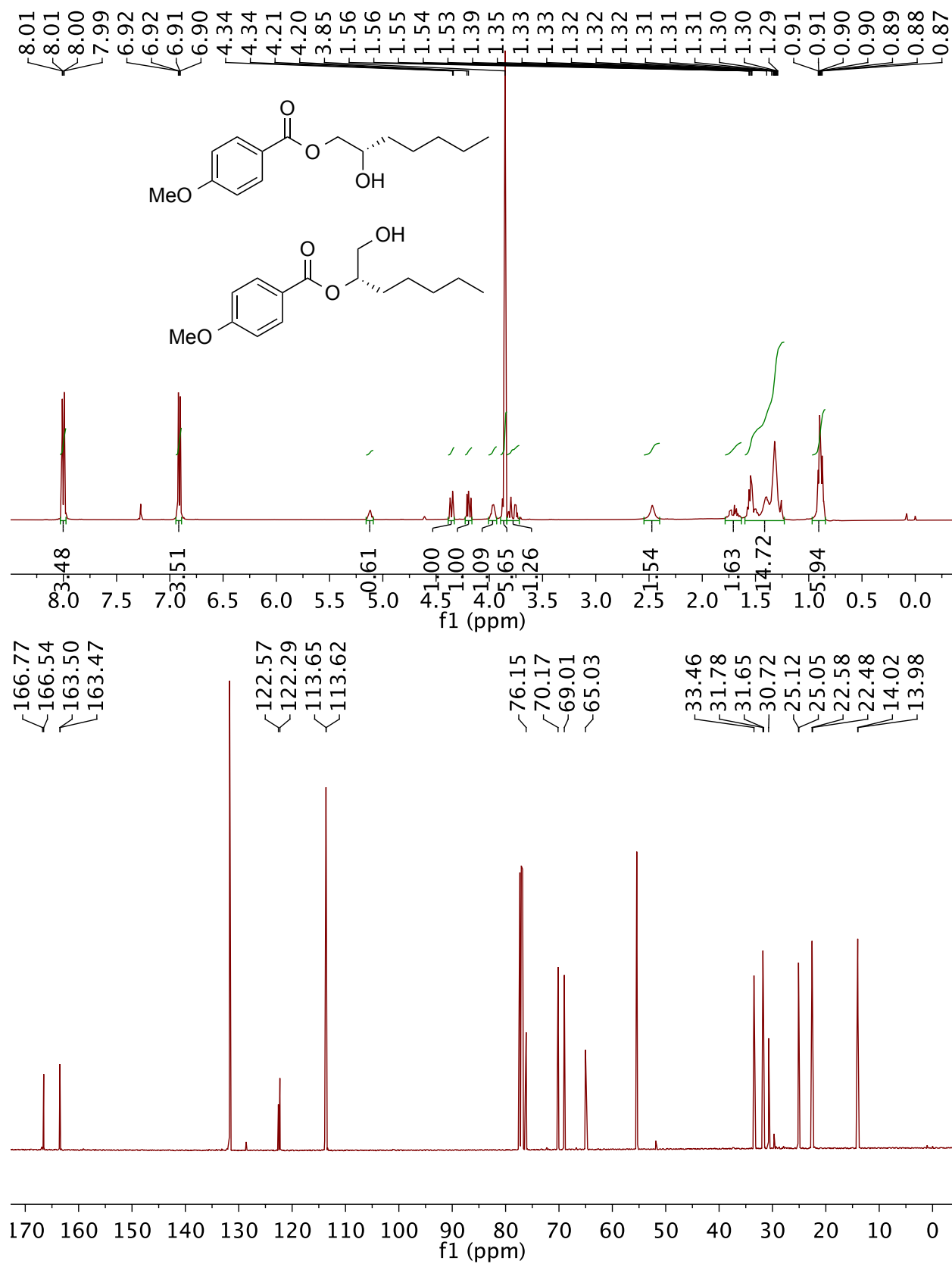
Detail of alcohol isomers in above spectrum:

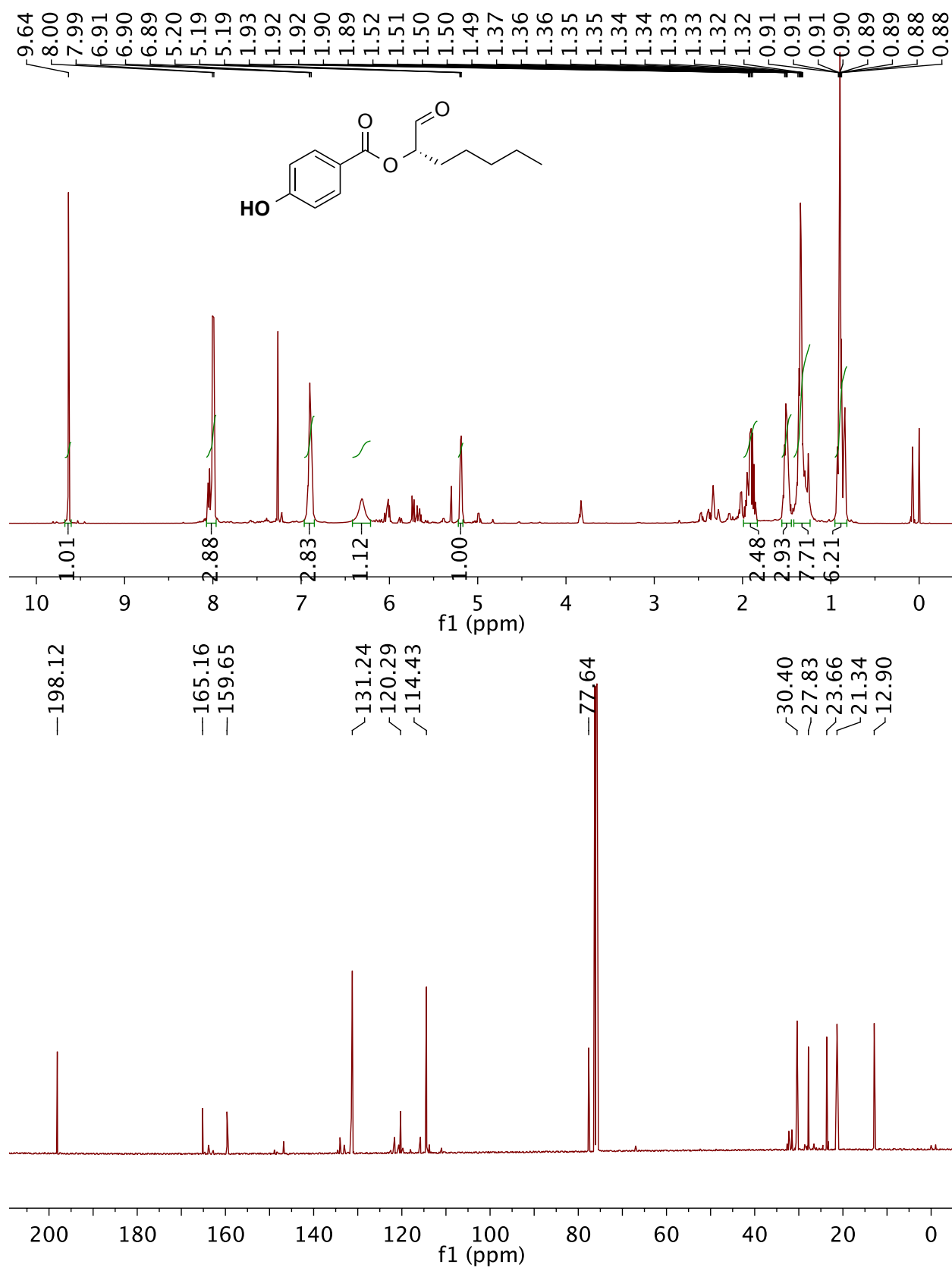


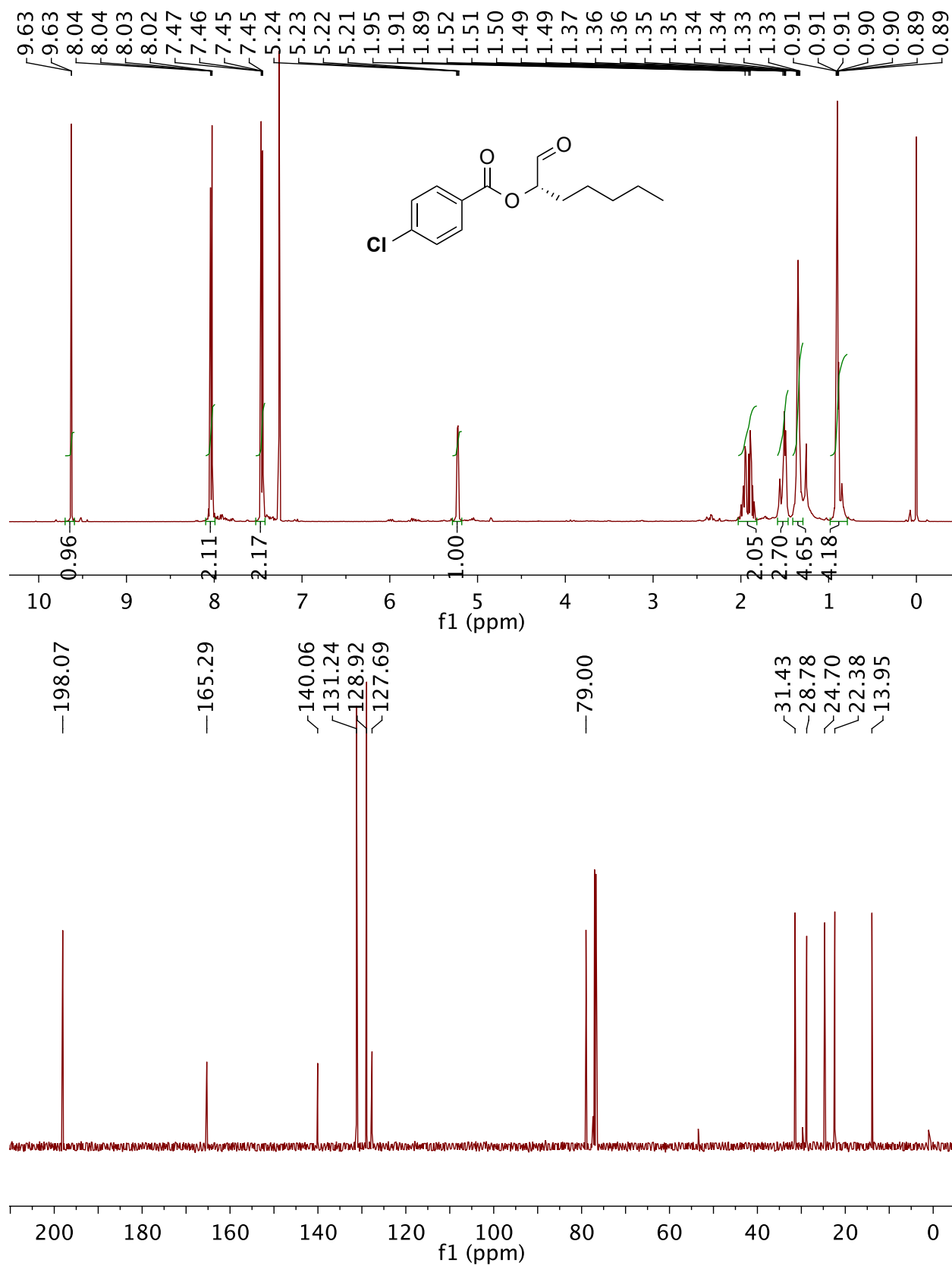


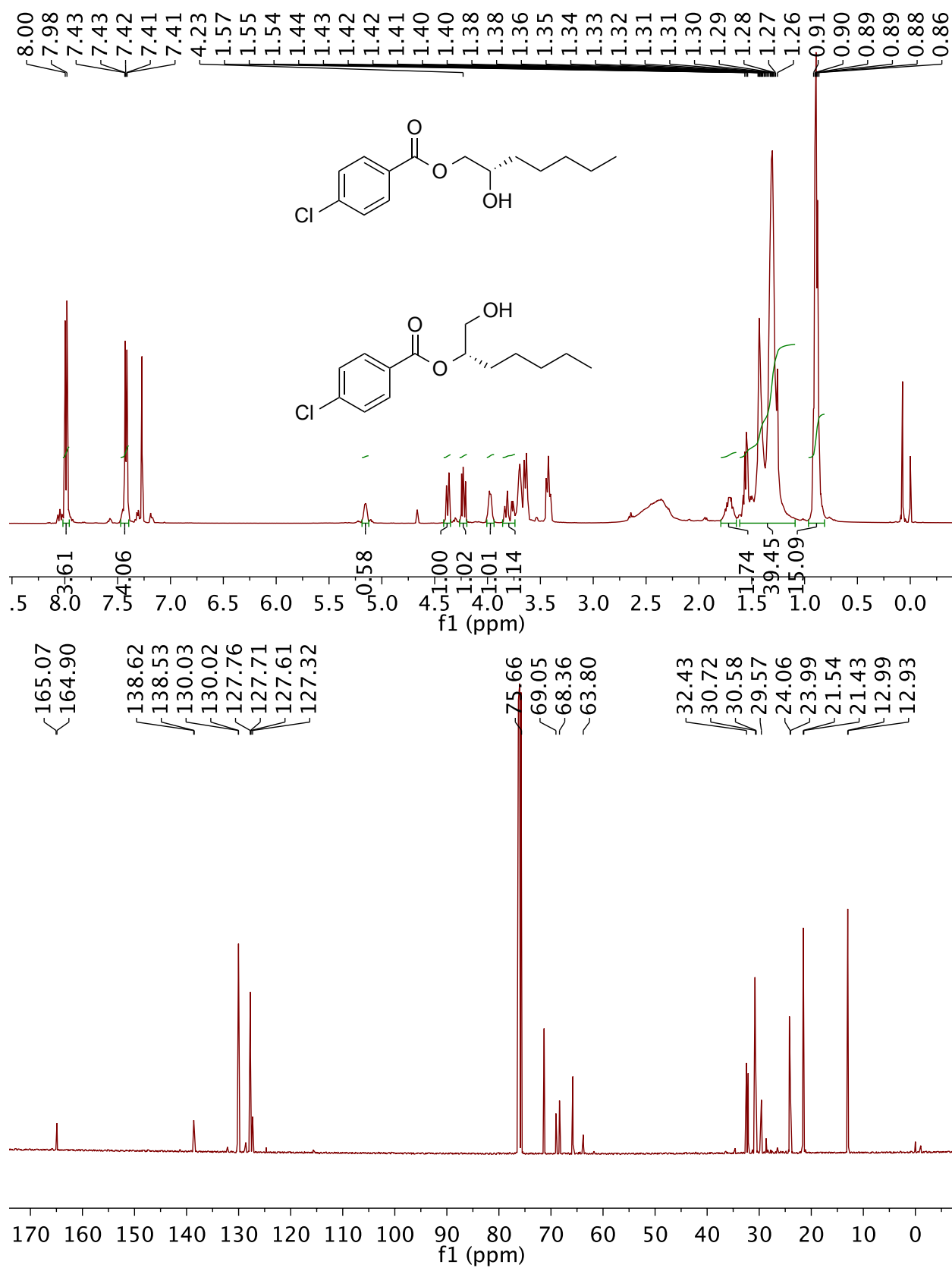


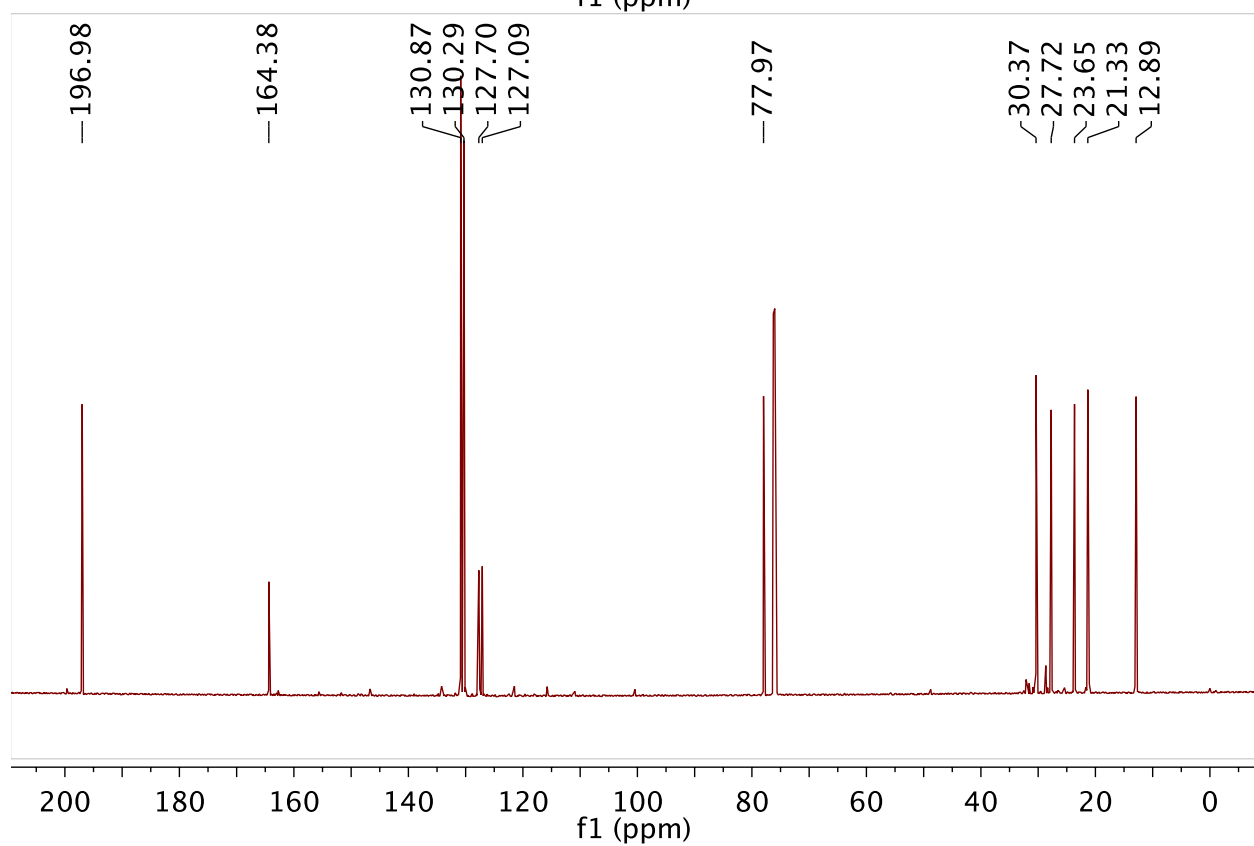
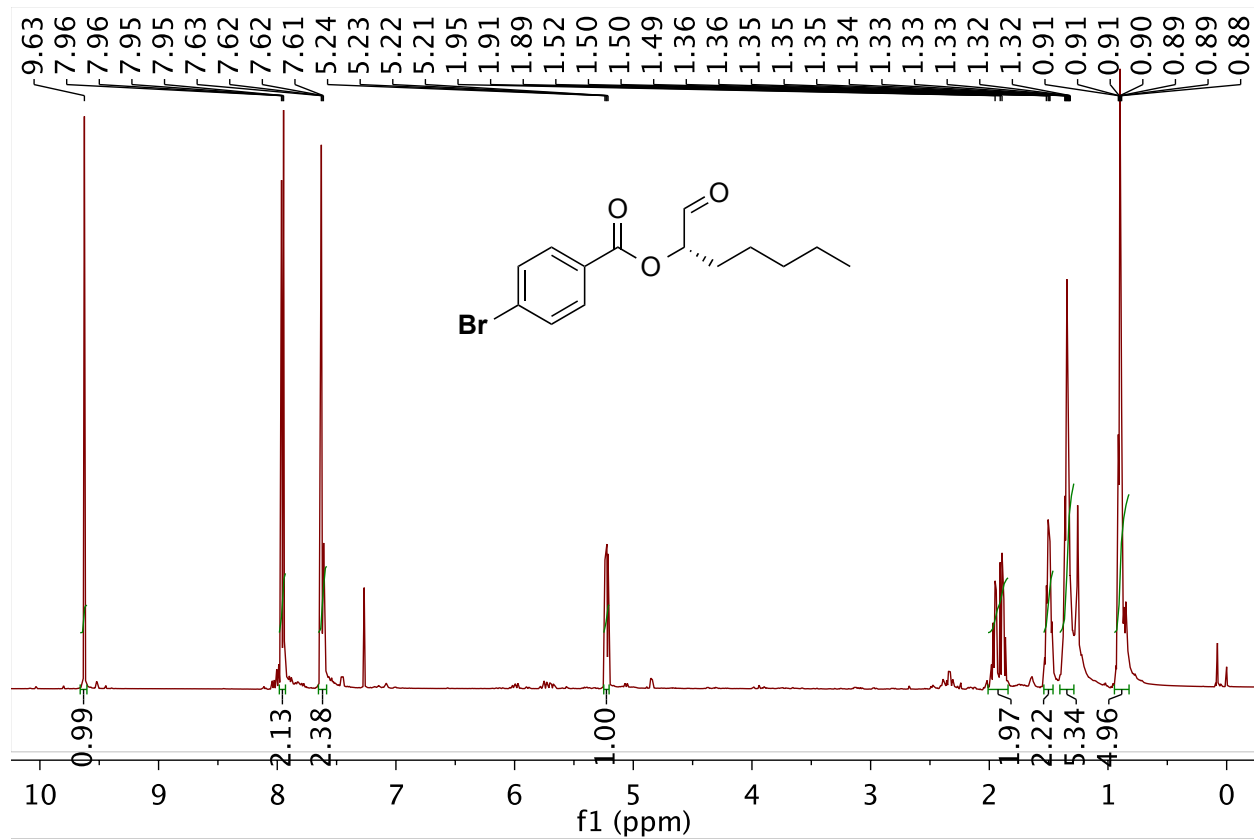


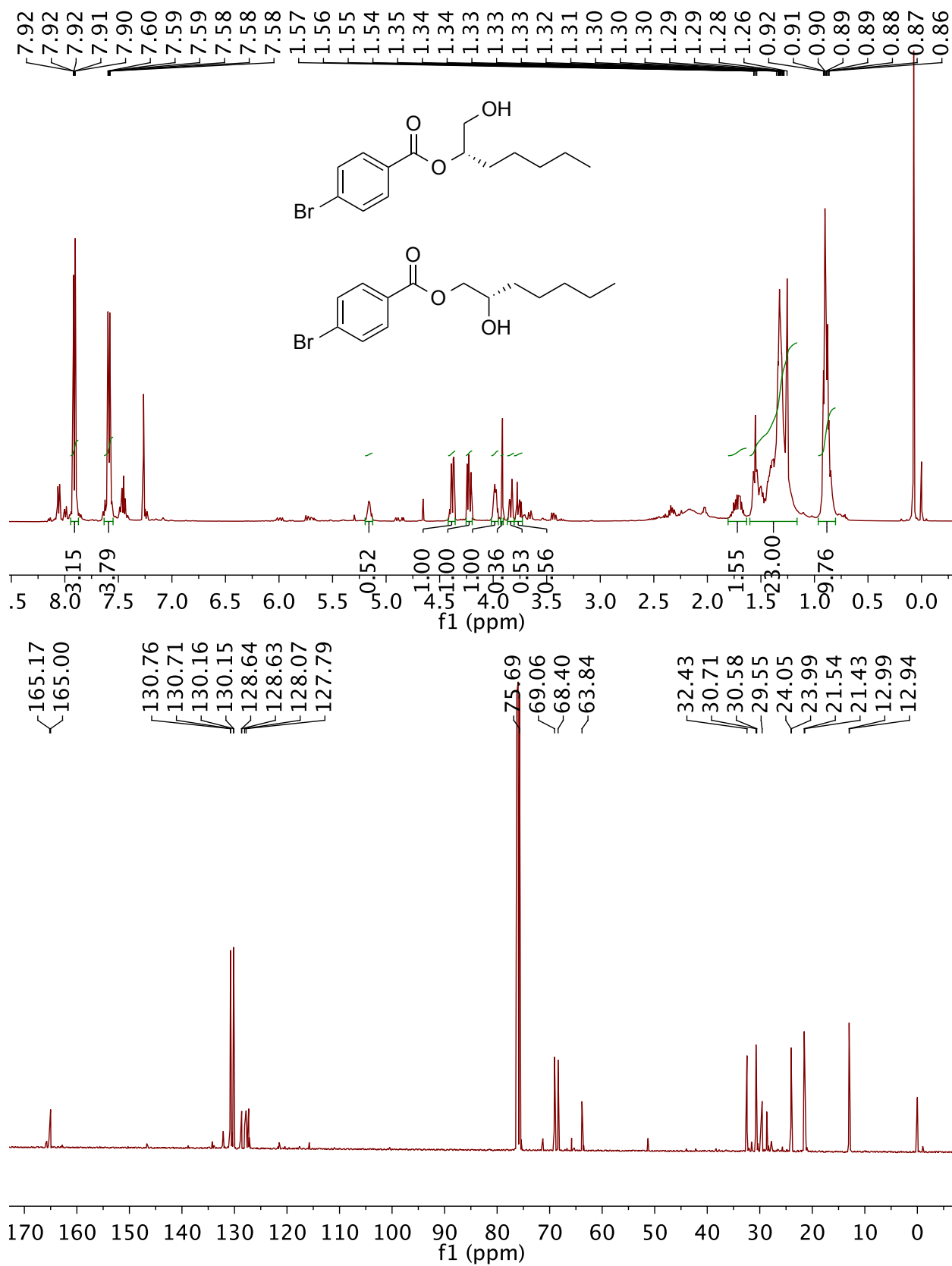


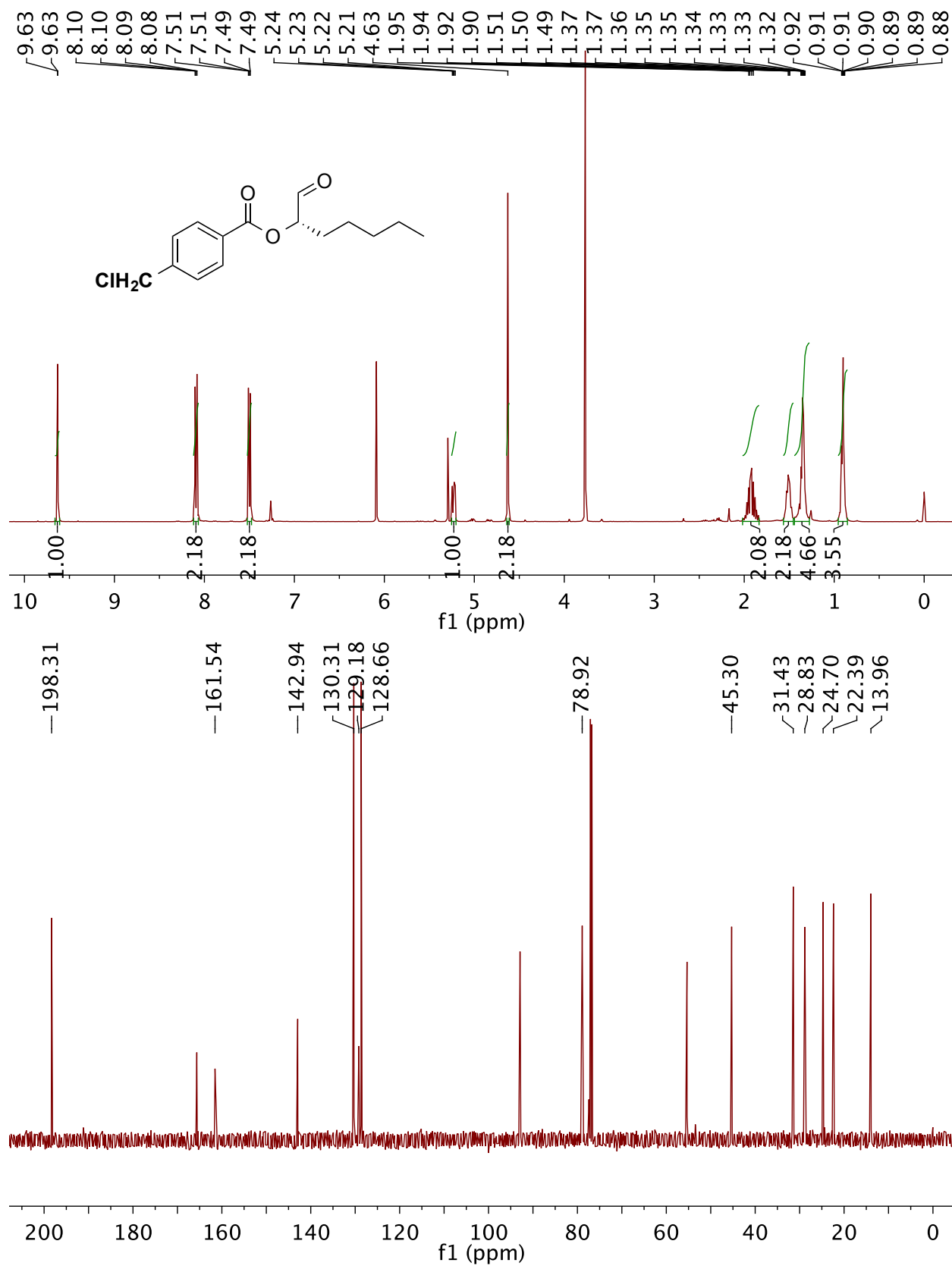


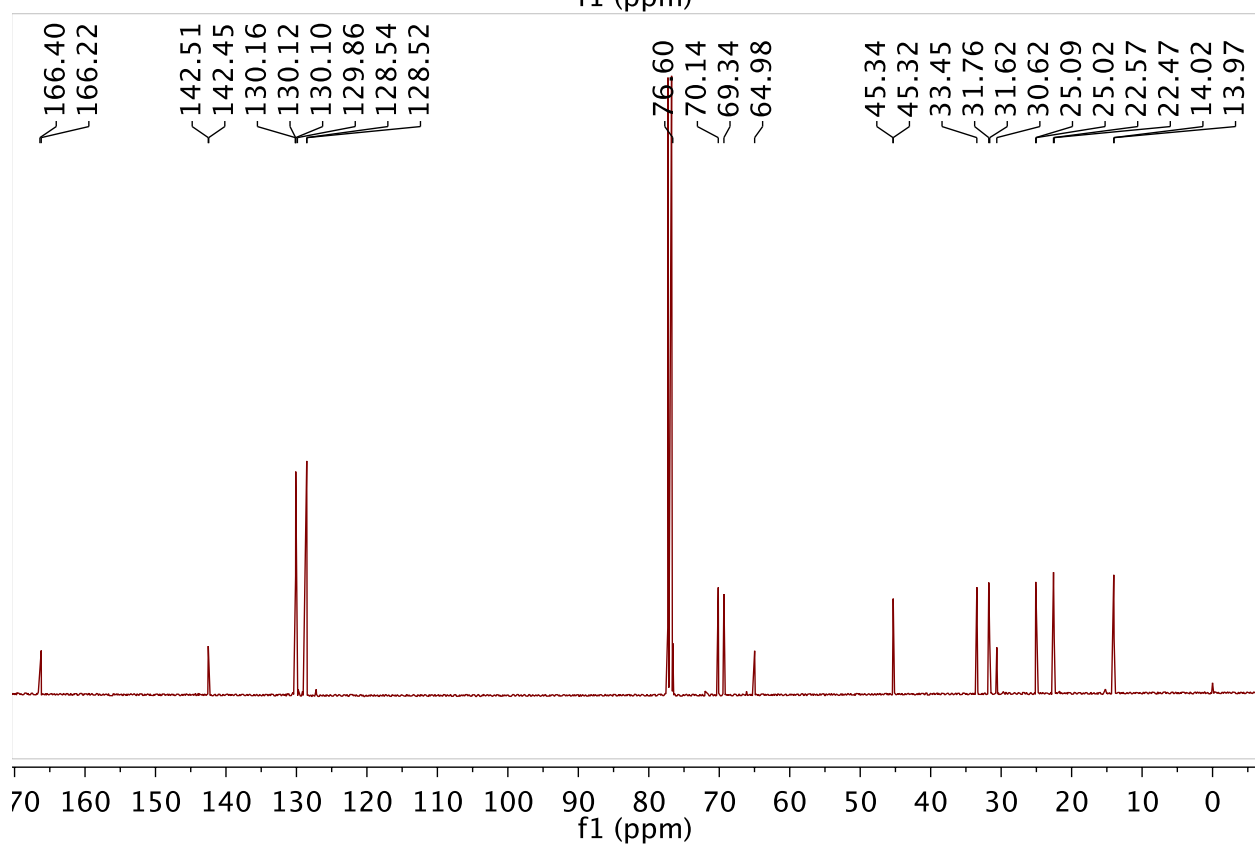
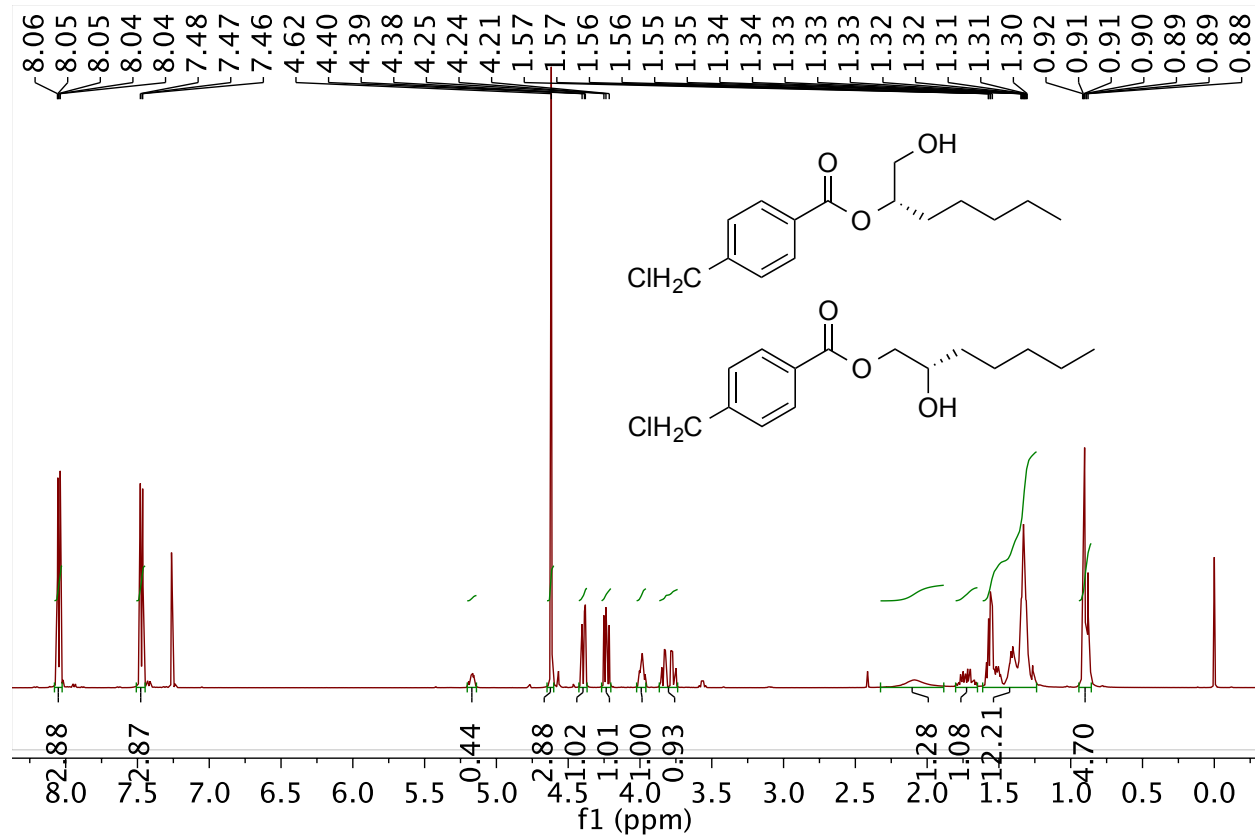


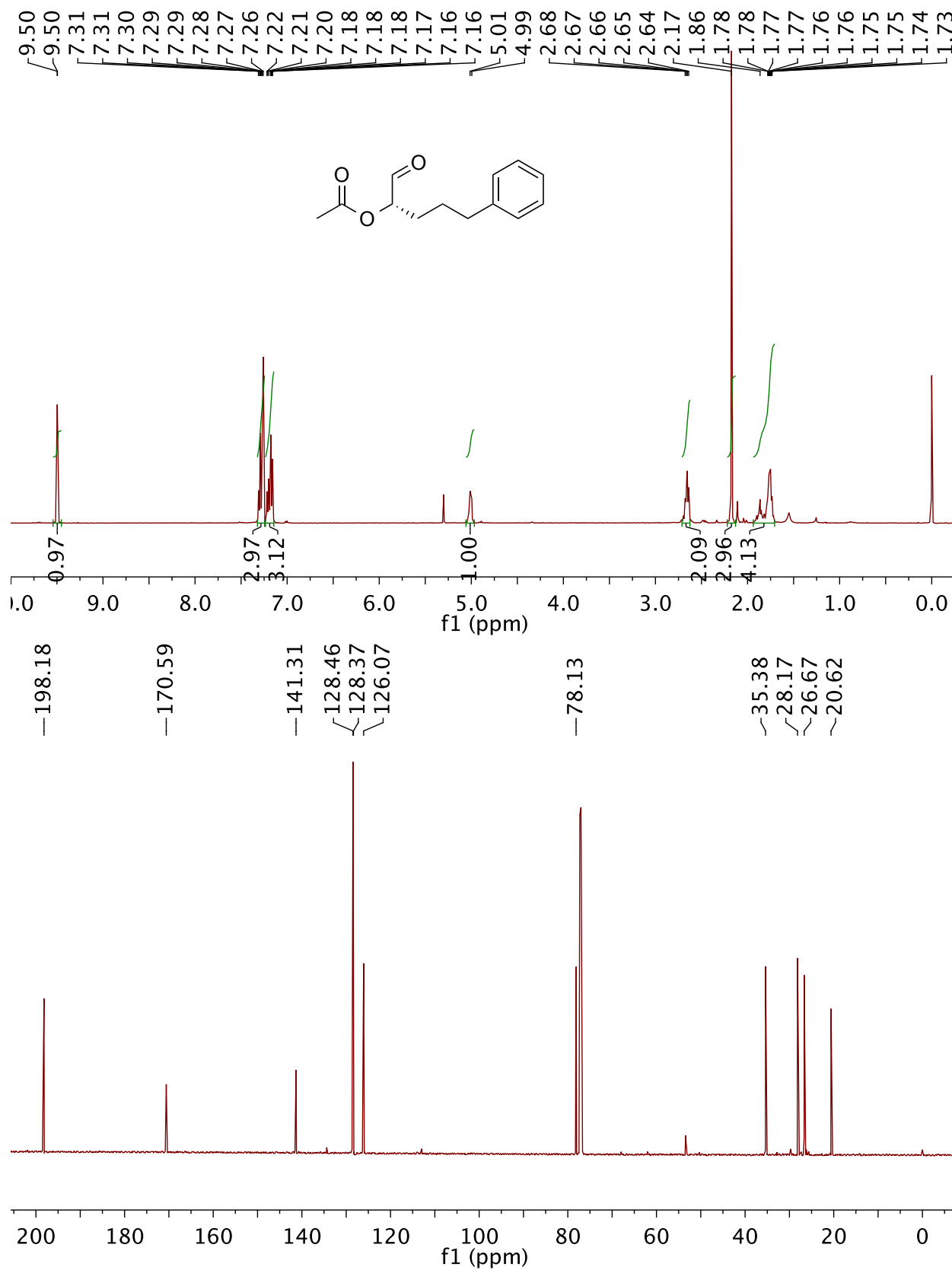


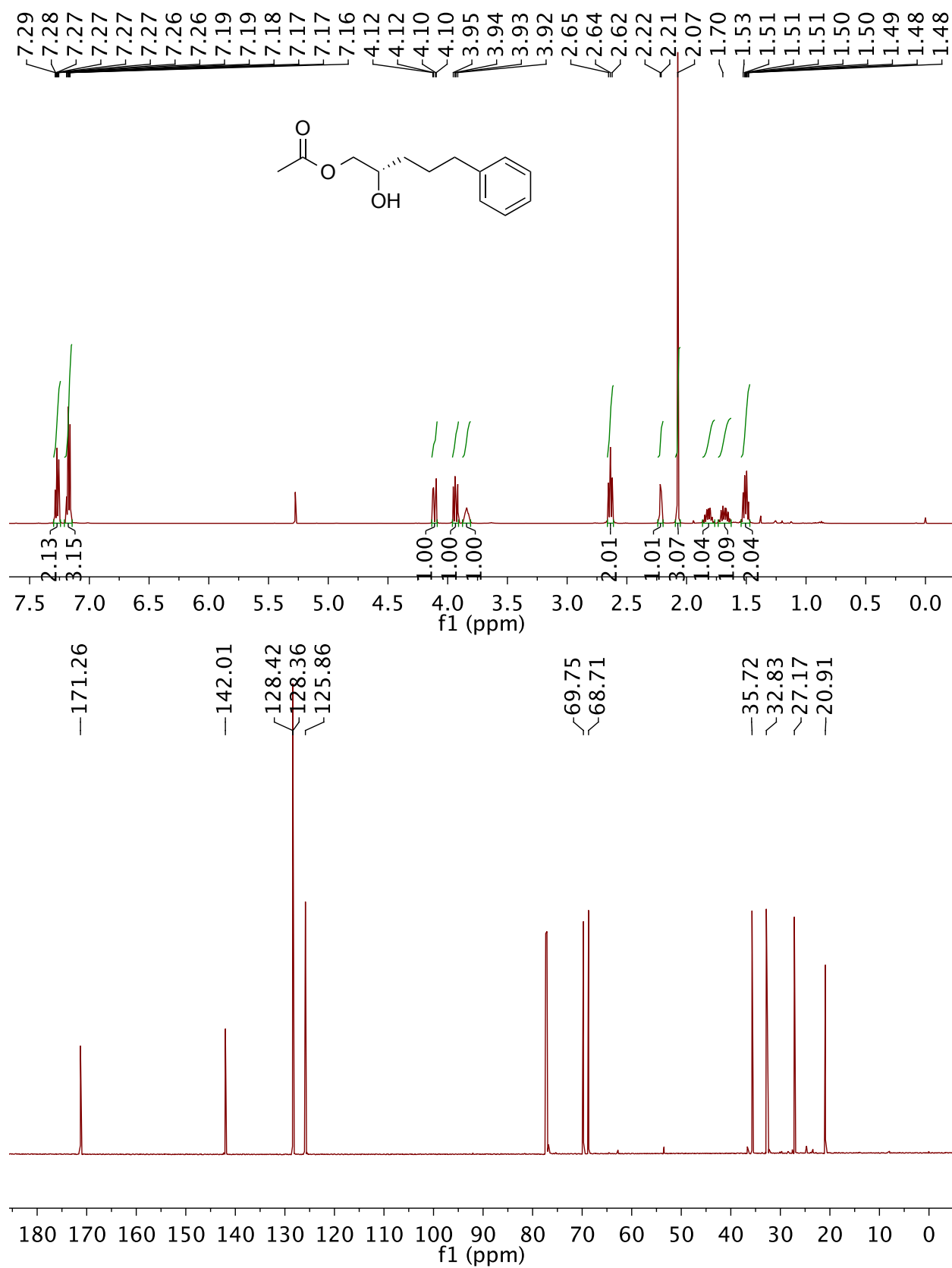


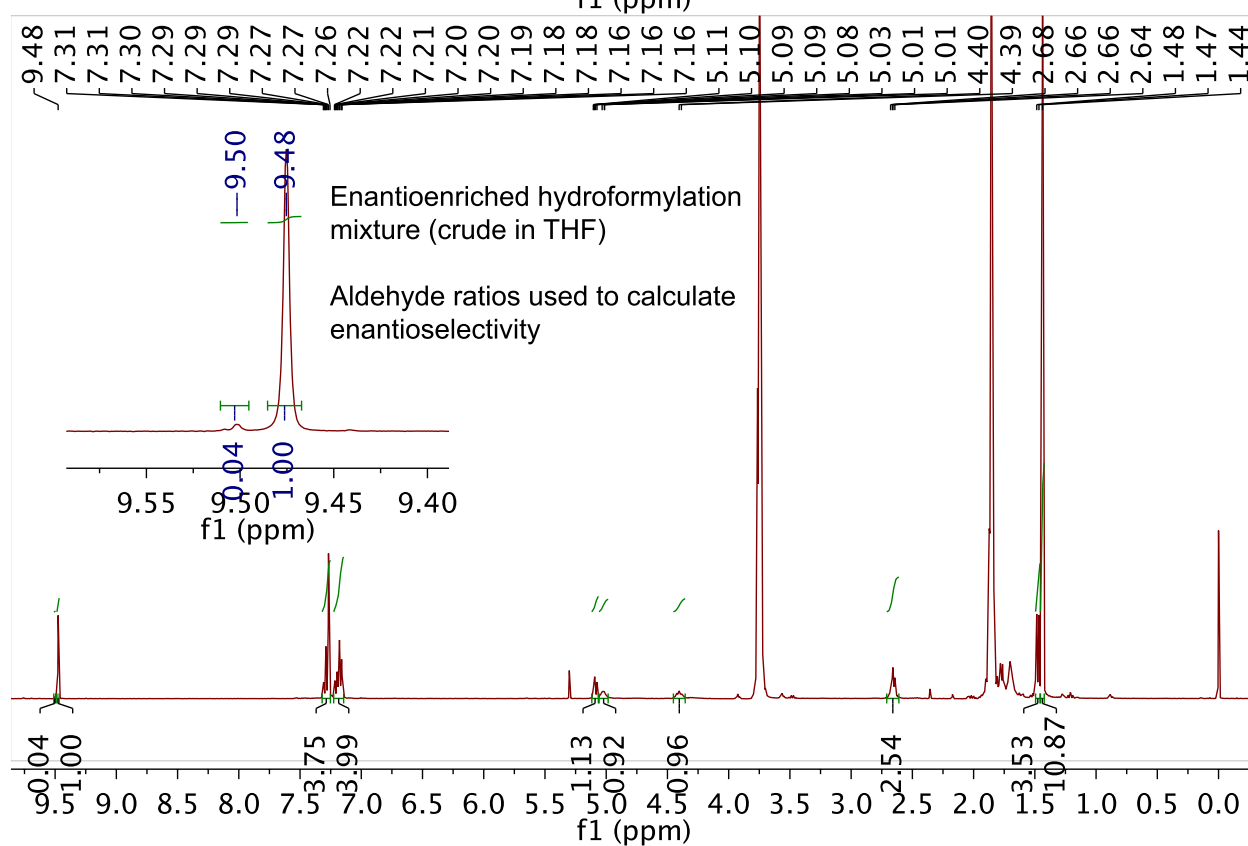
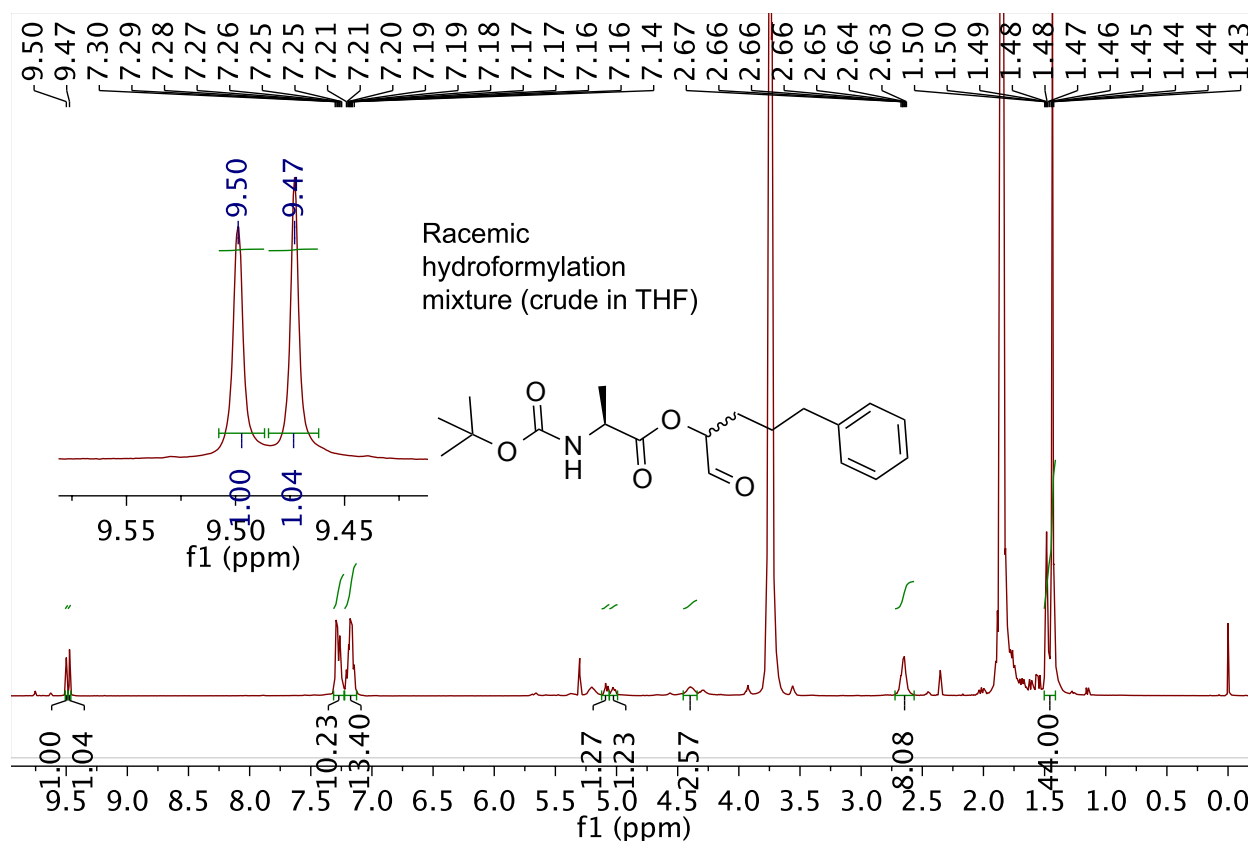


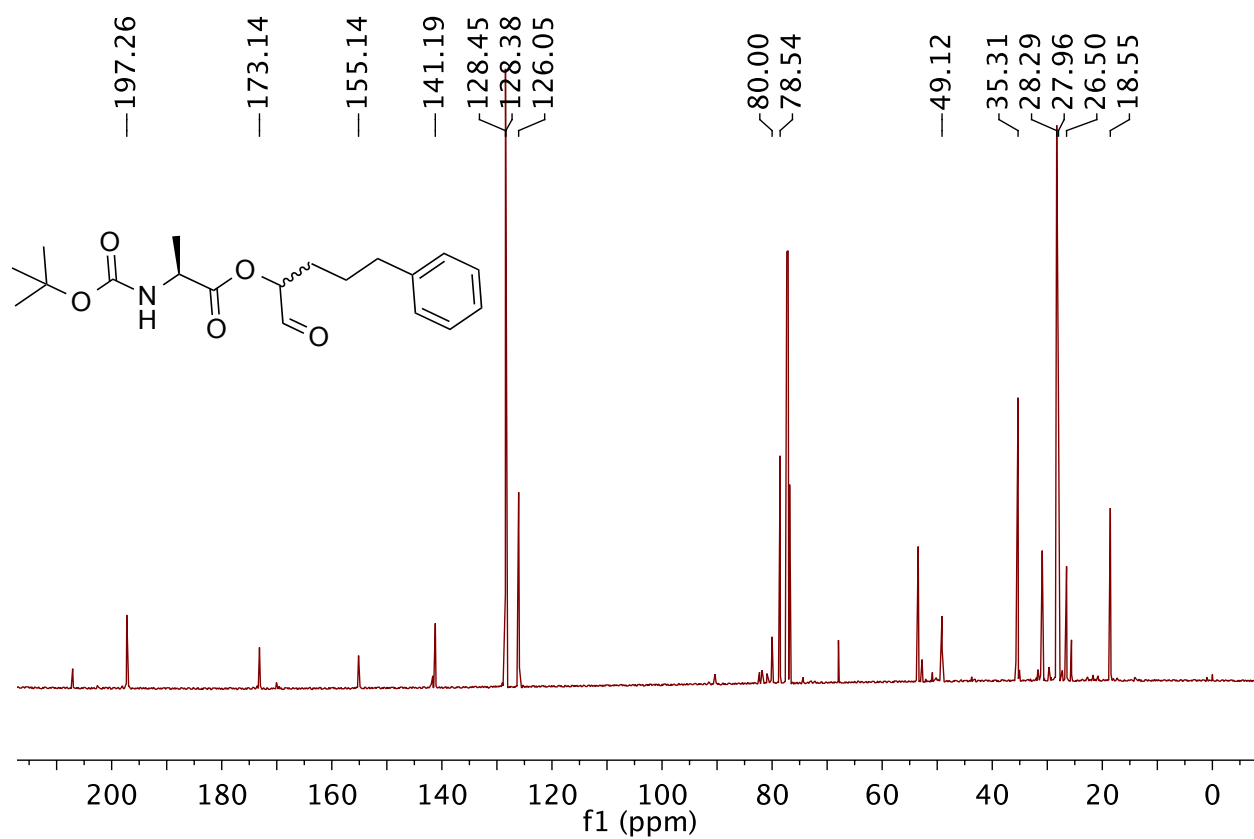


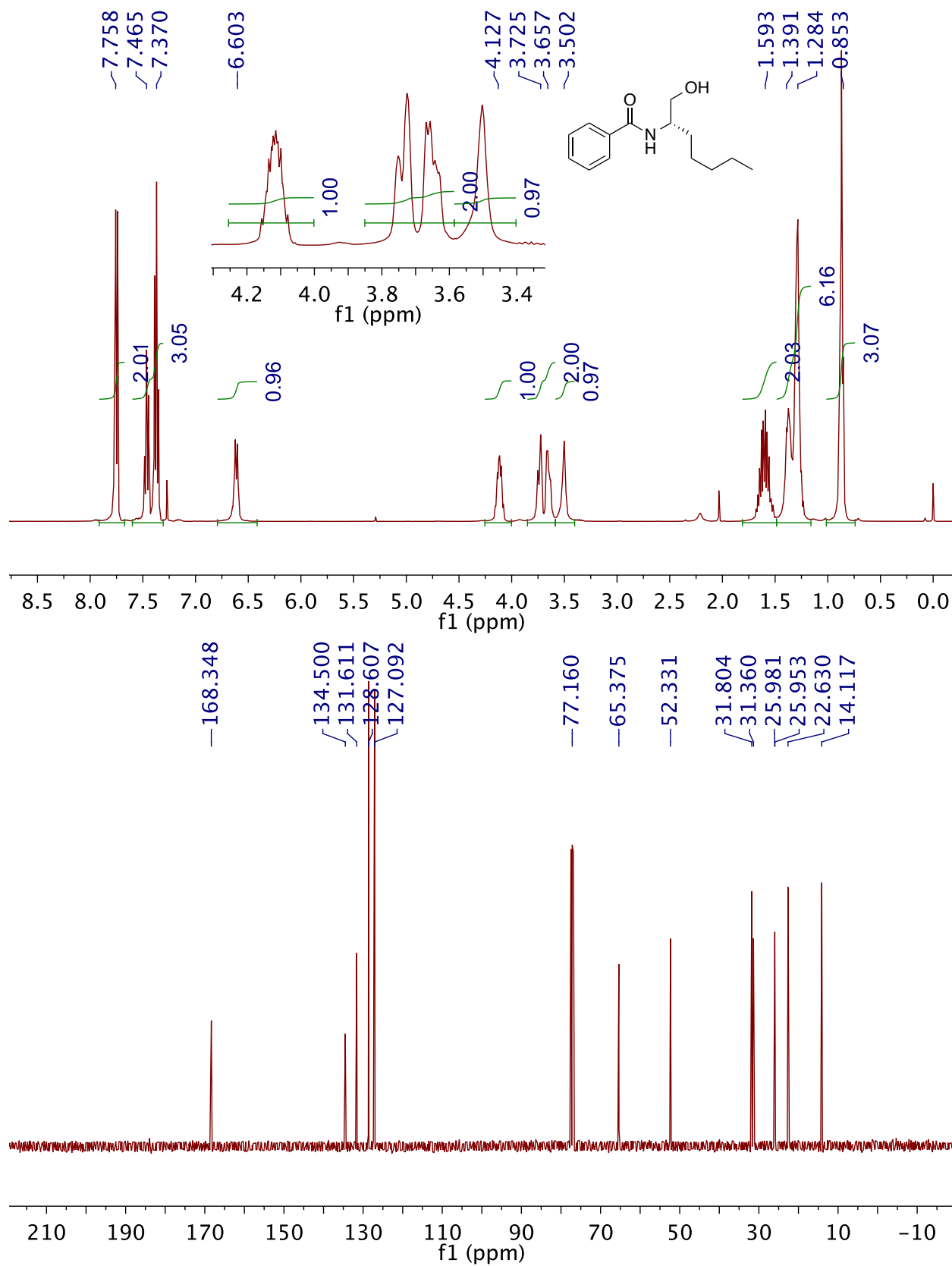


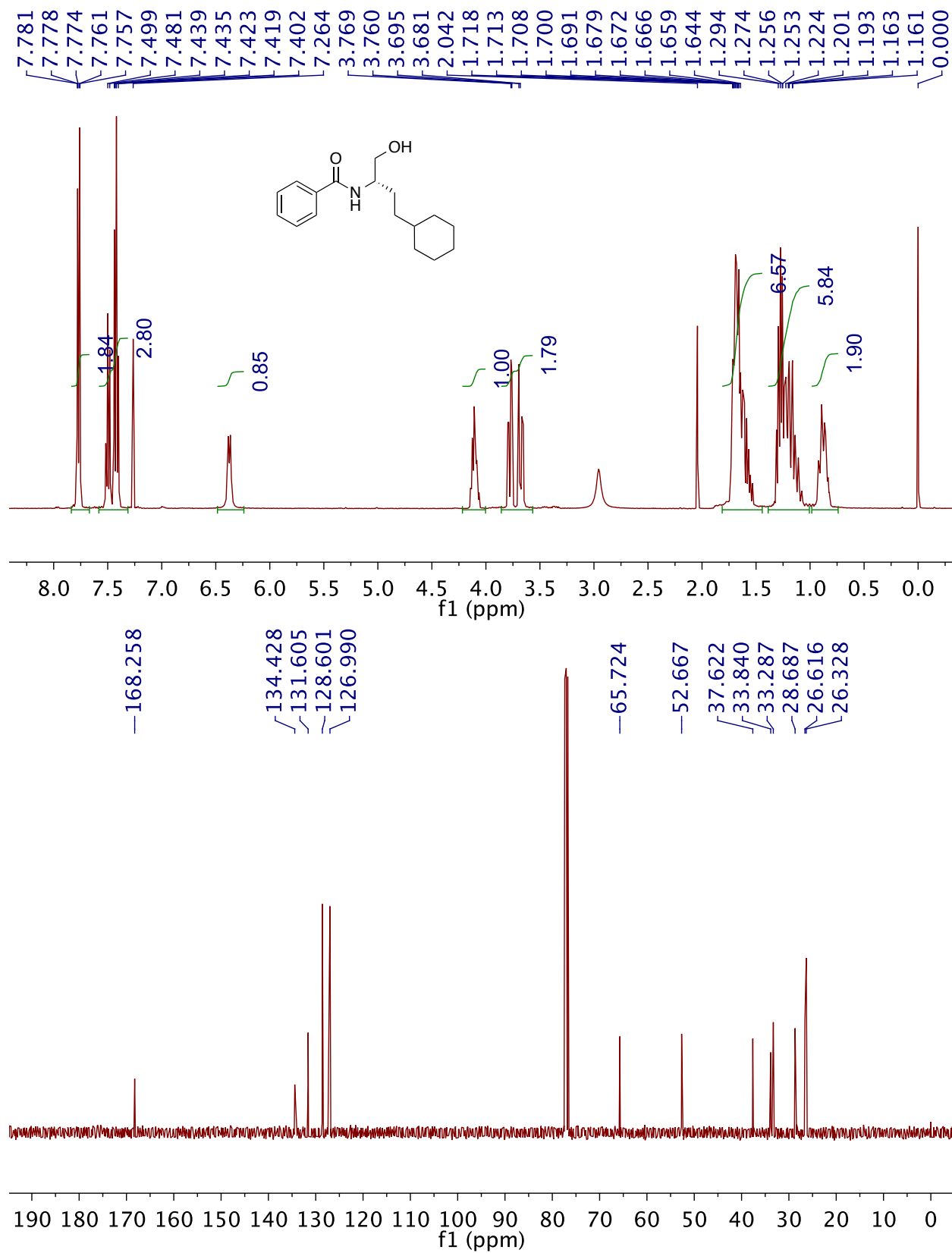


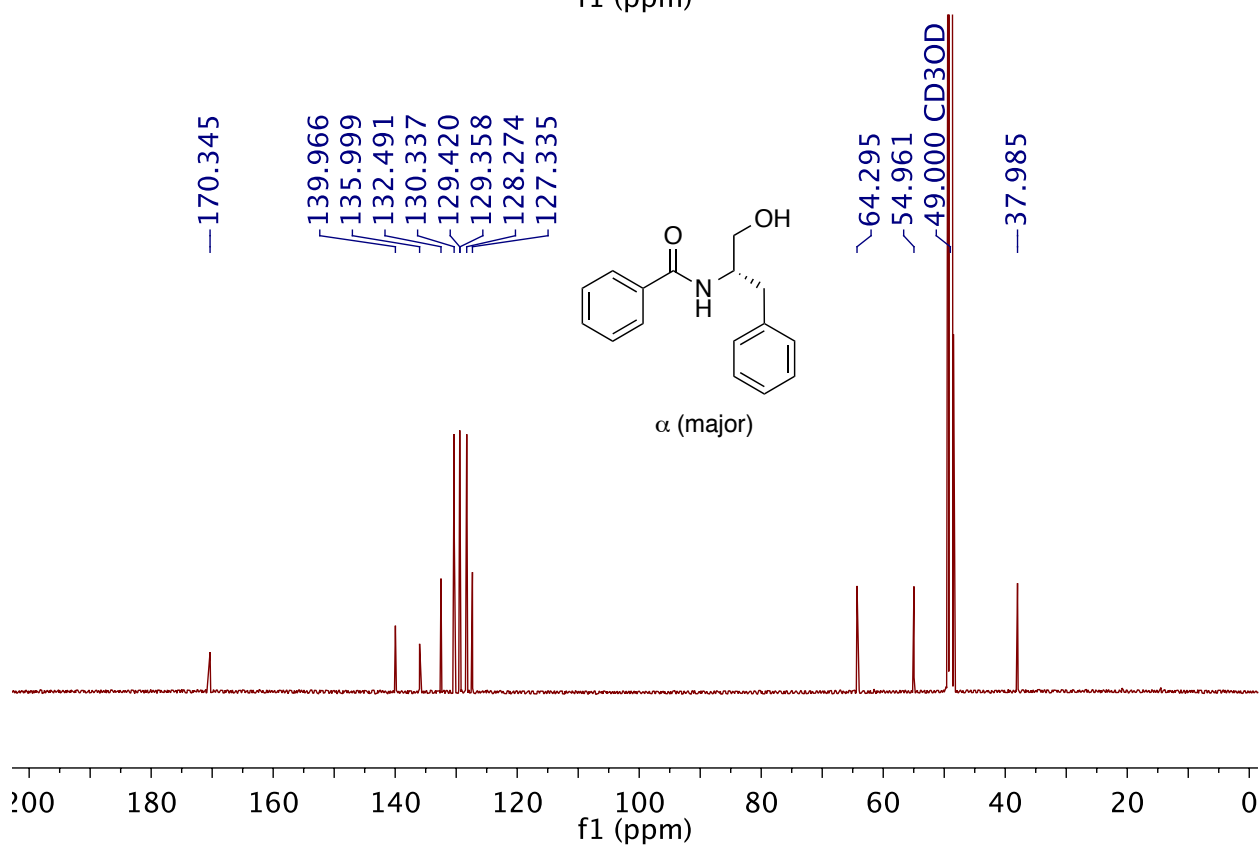
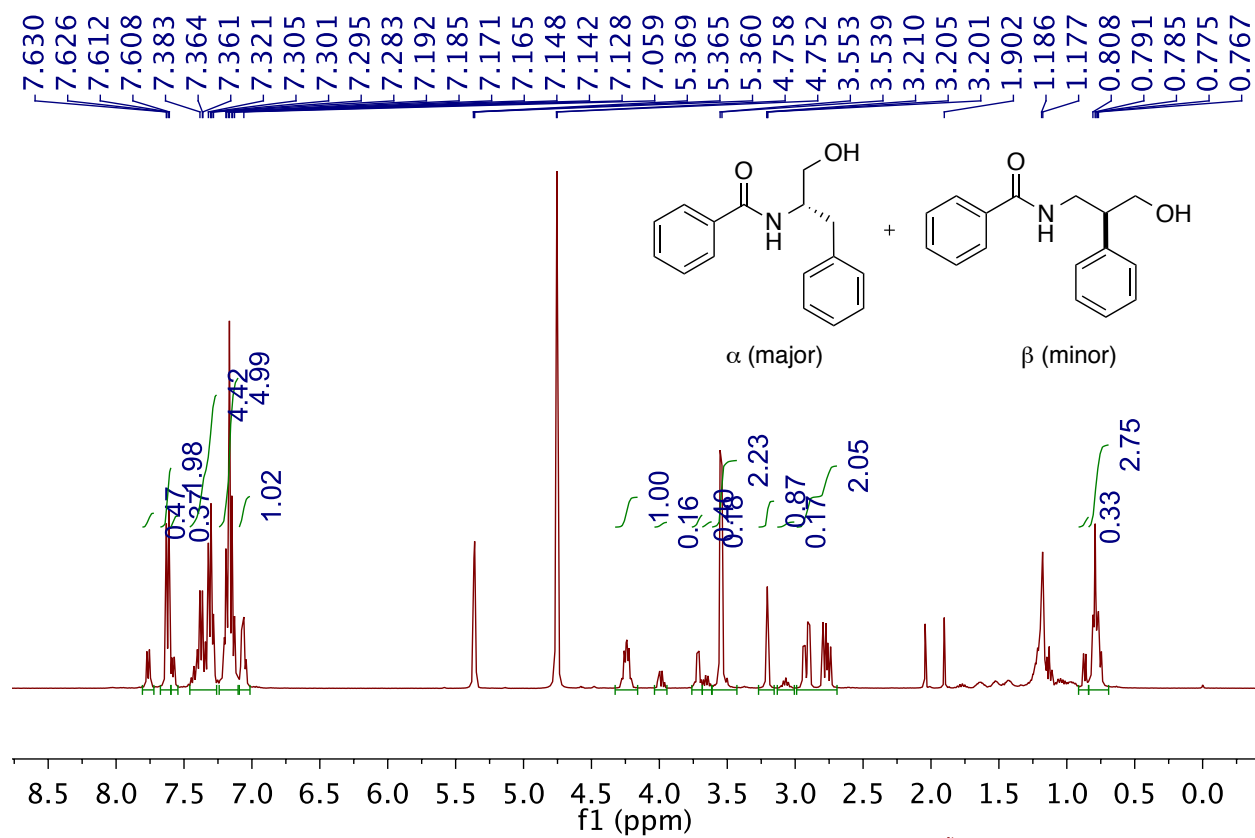


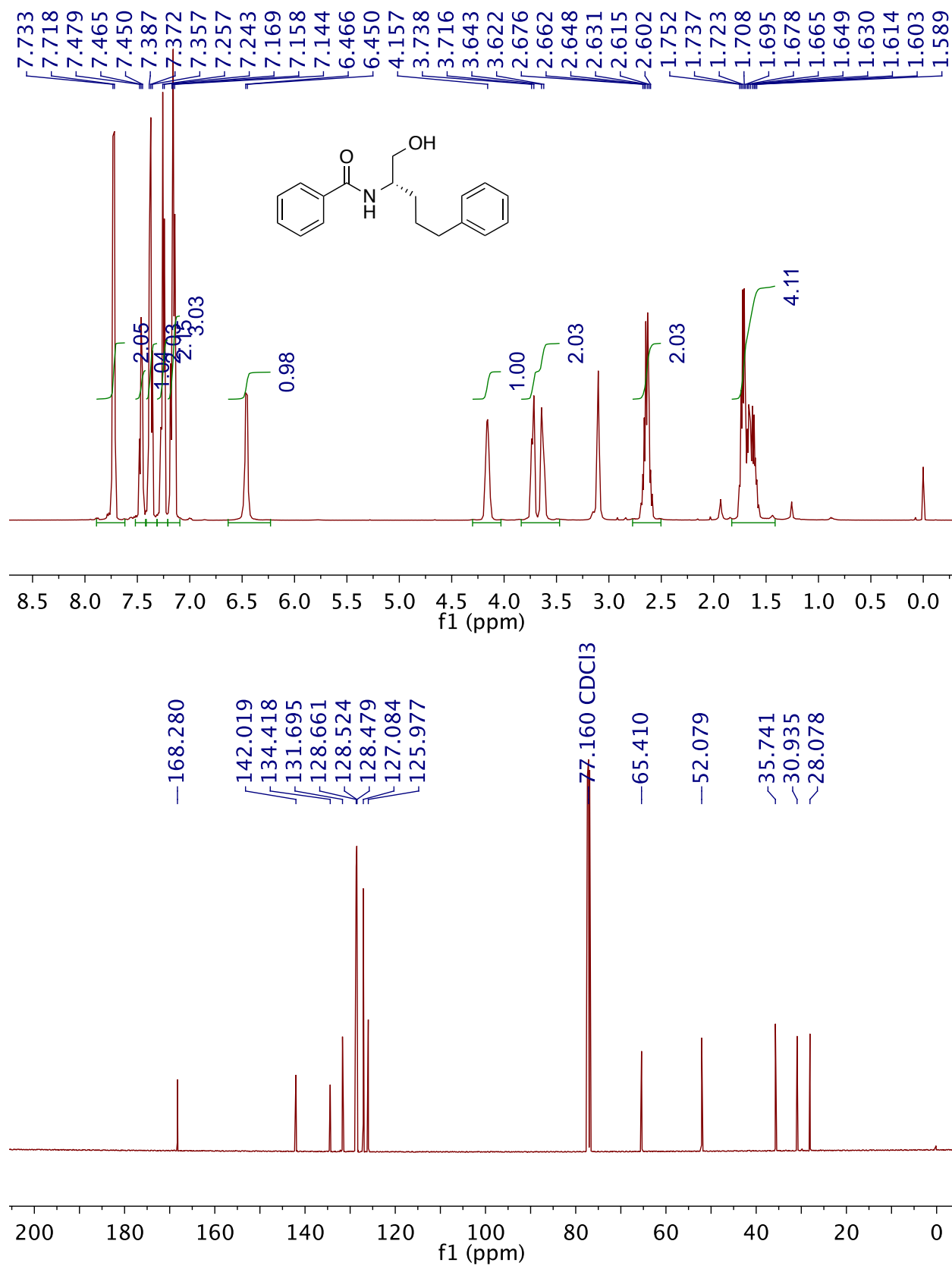


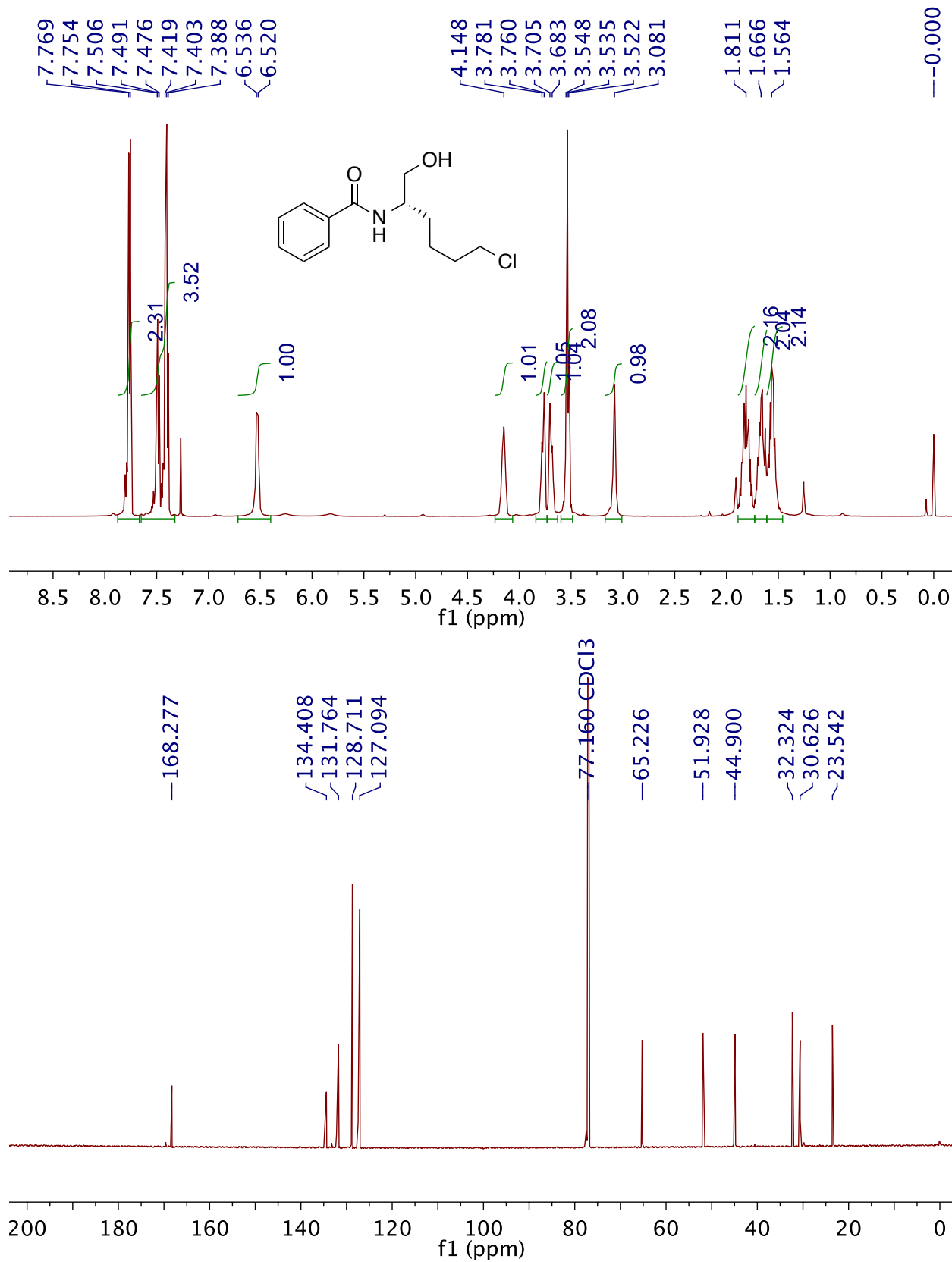


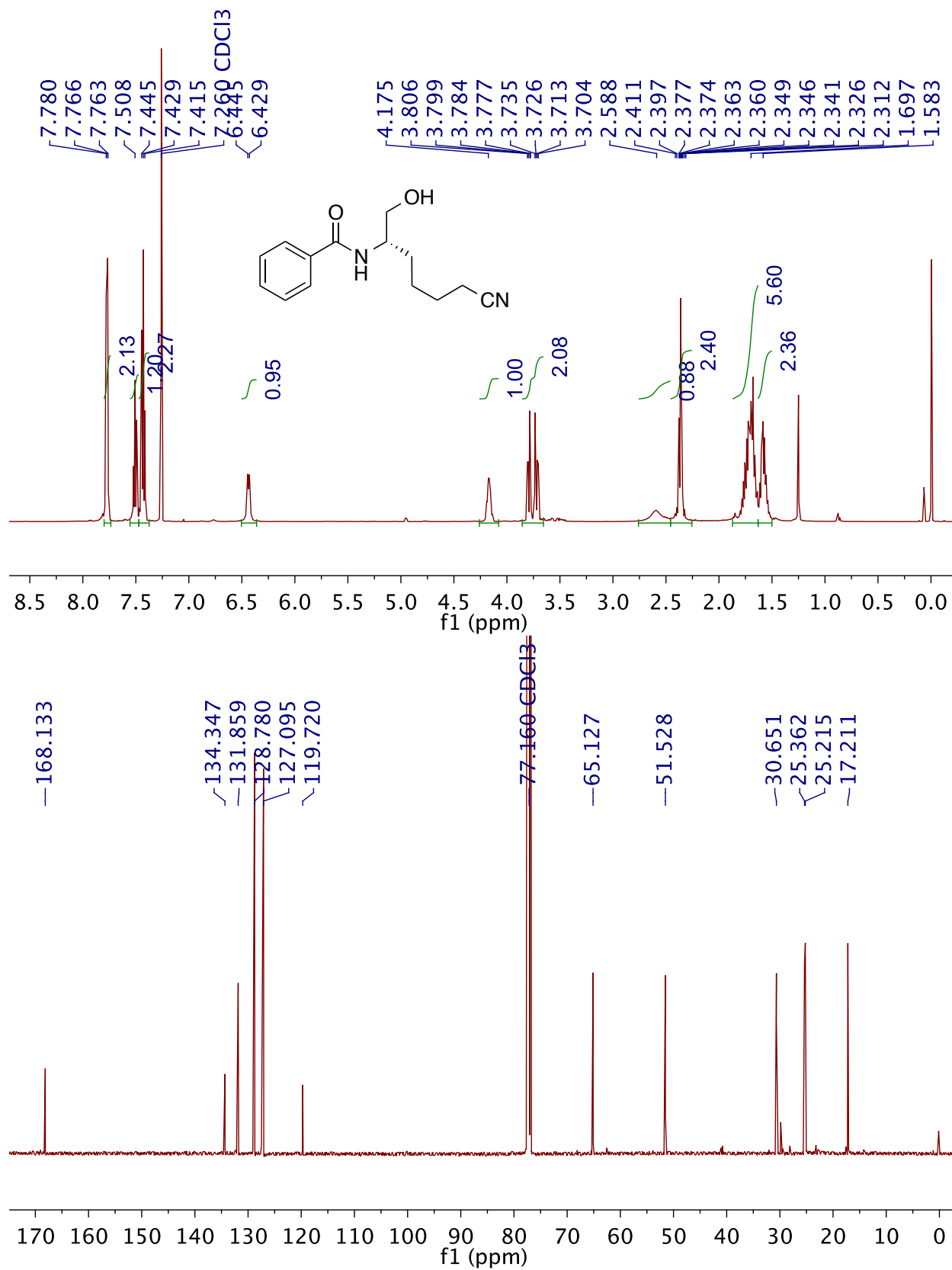


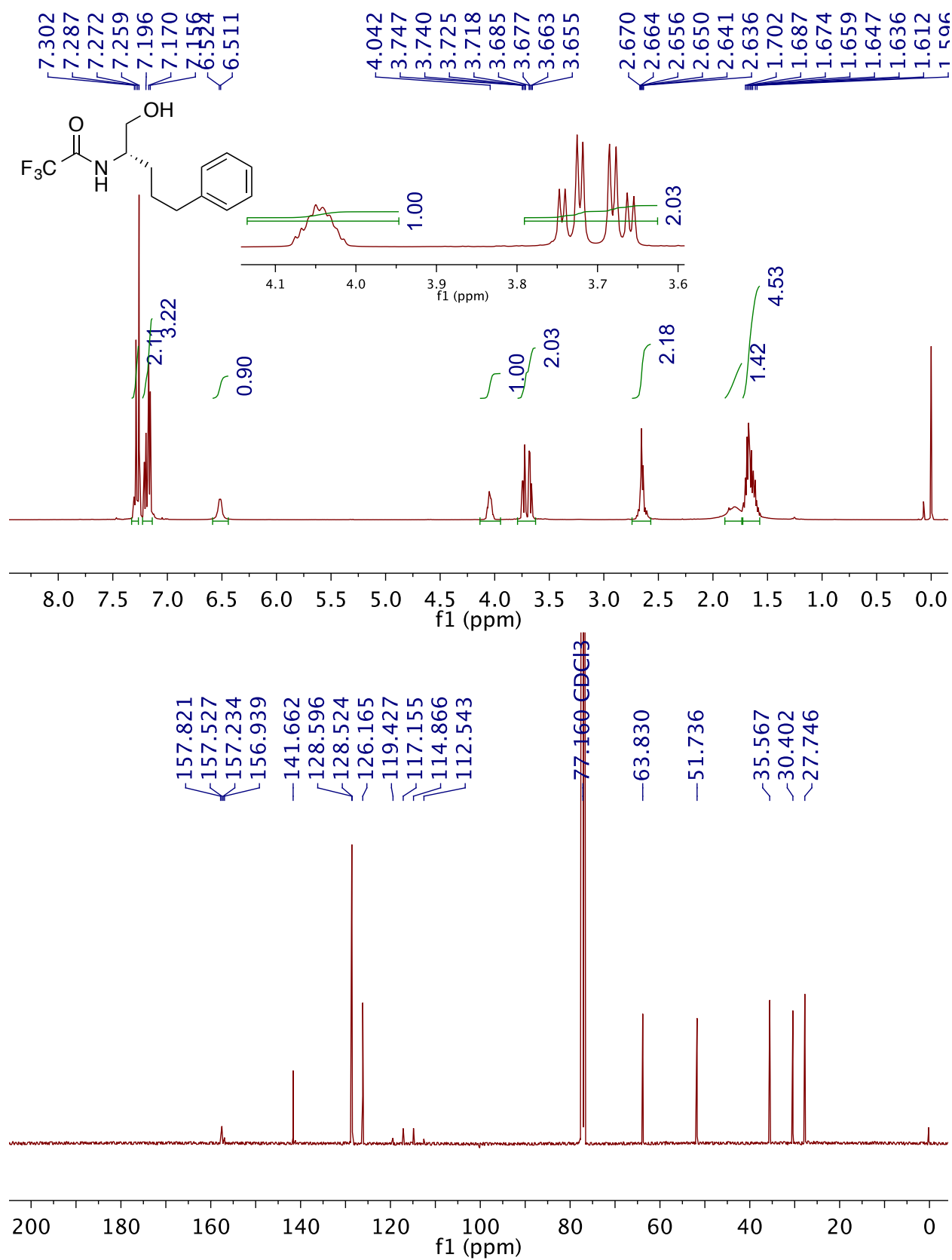


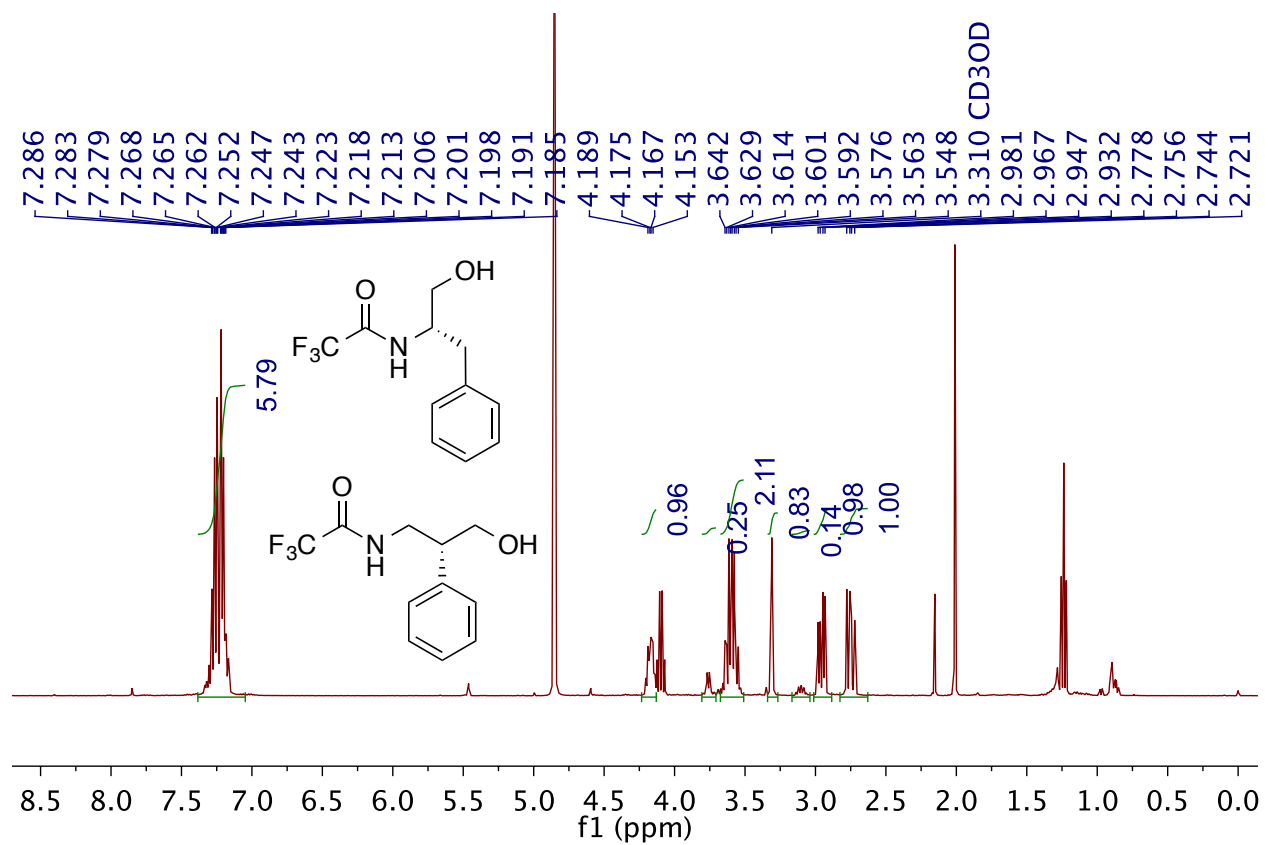


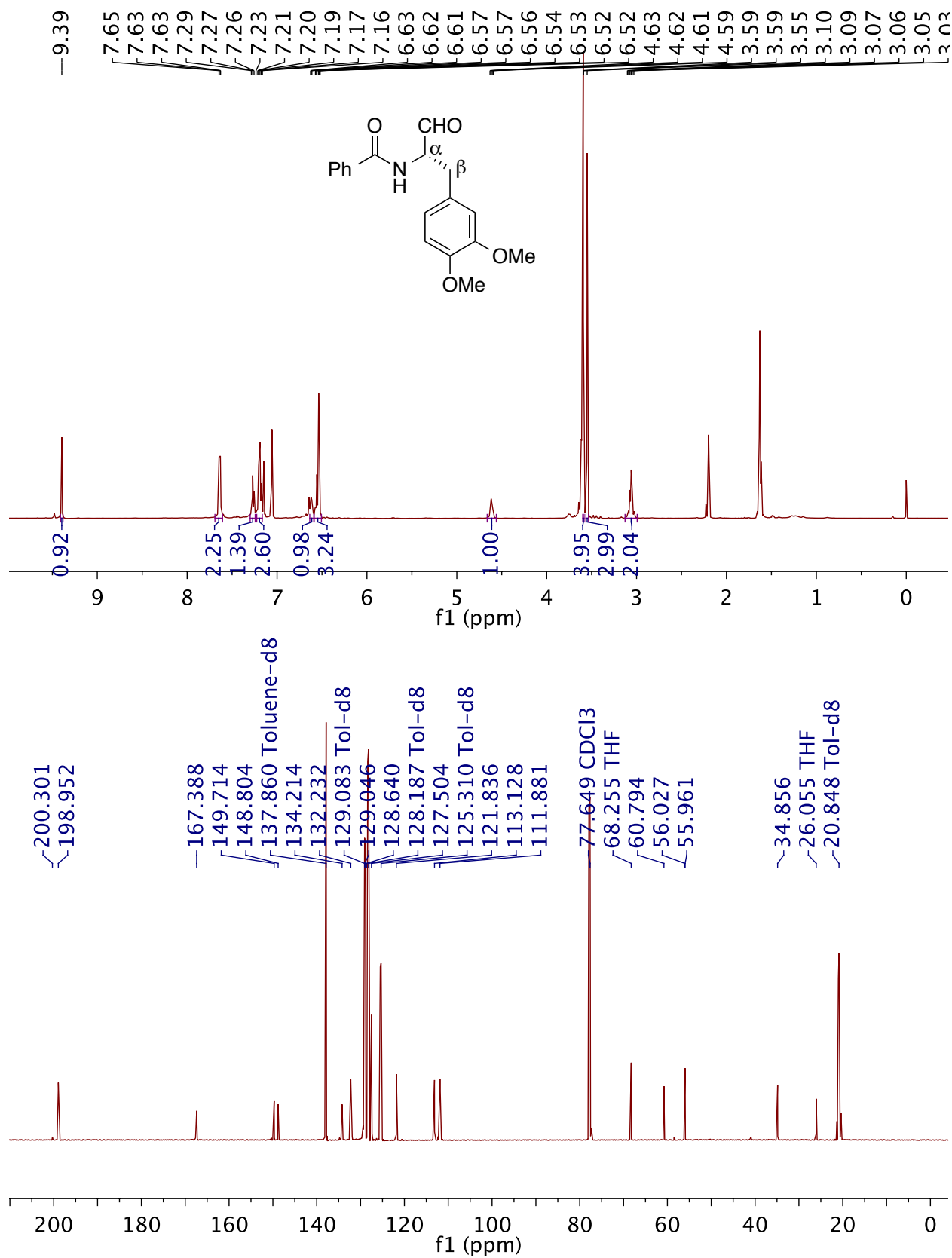




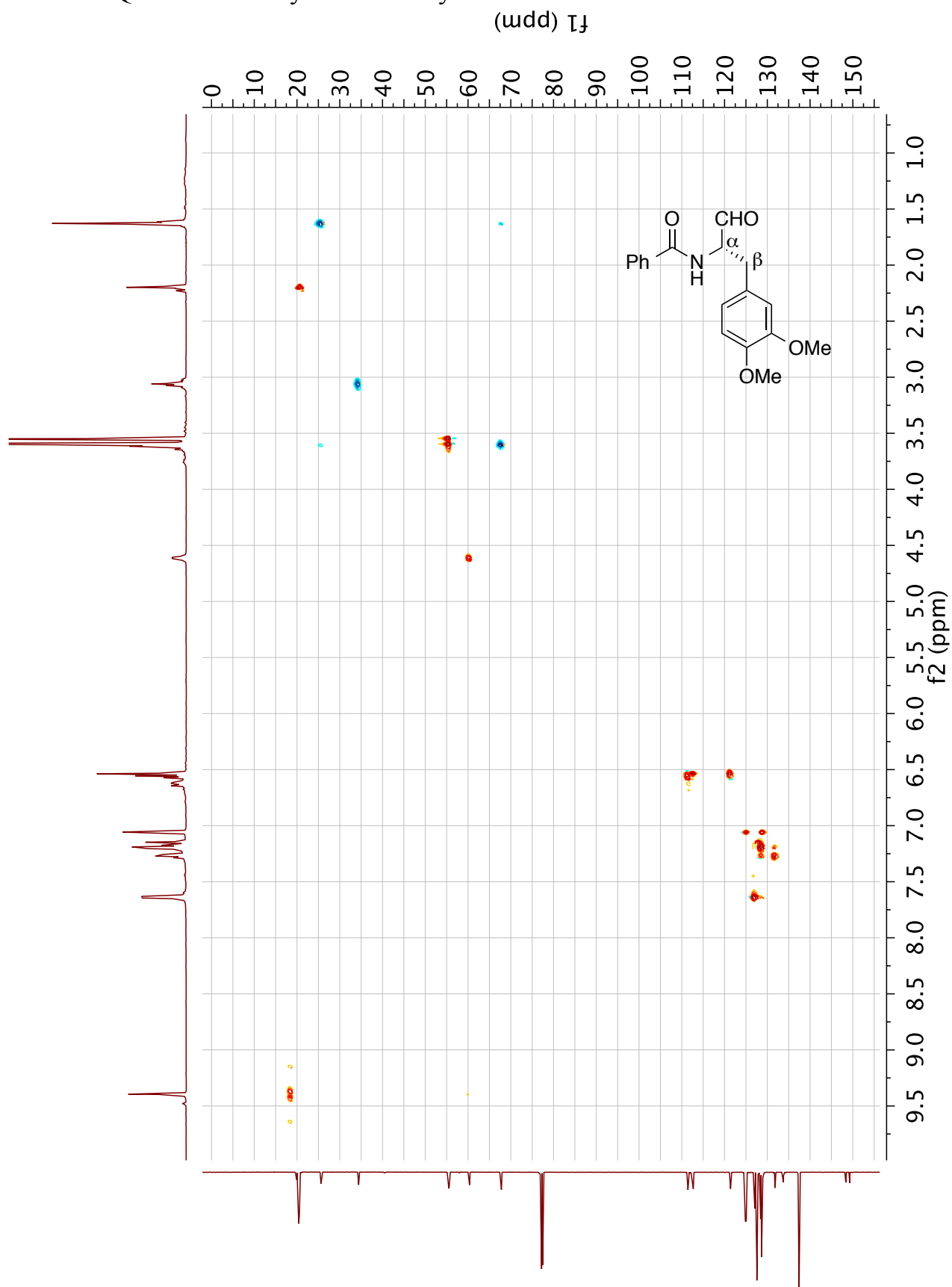


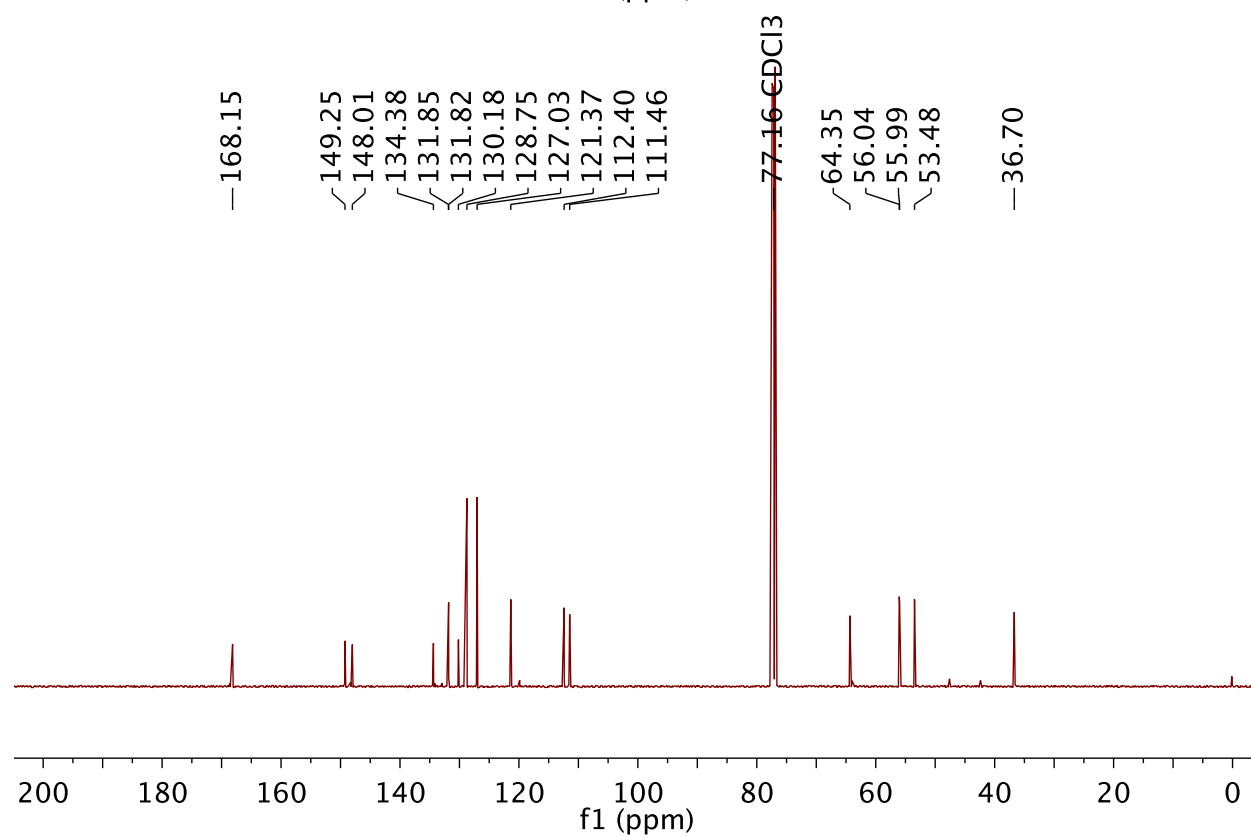
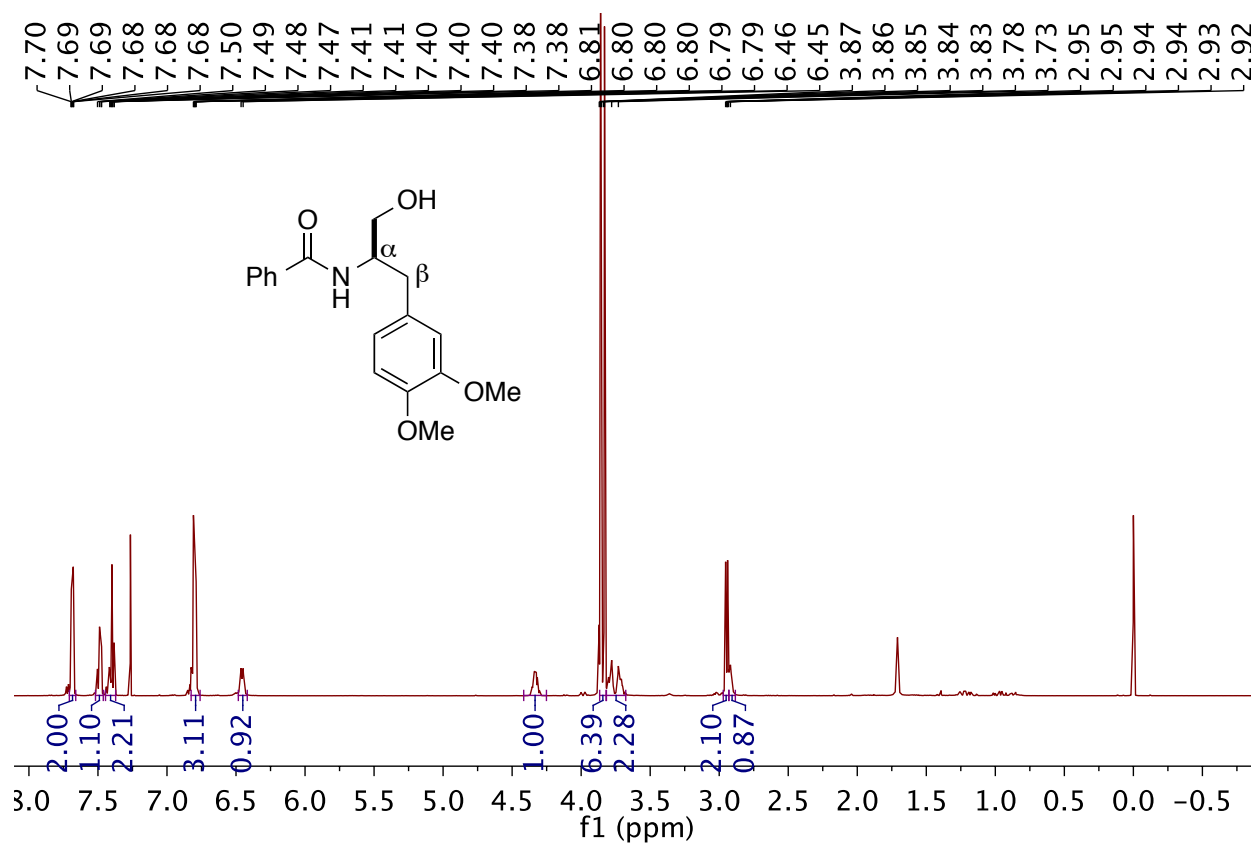




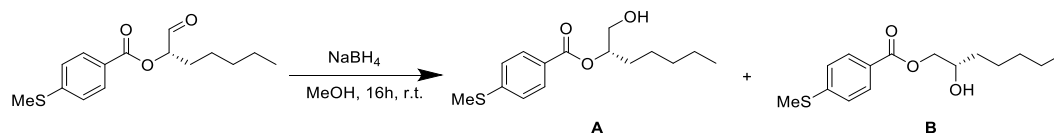


HSQC of the aldehyde to identify isomers



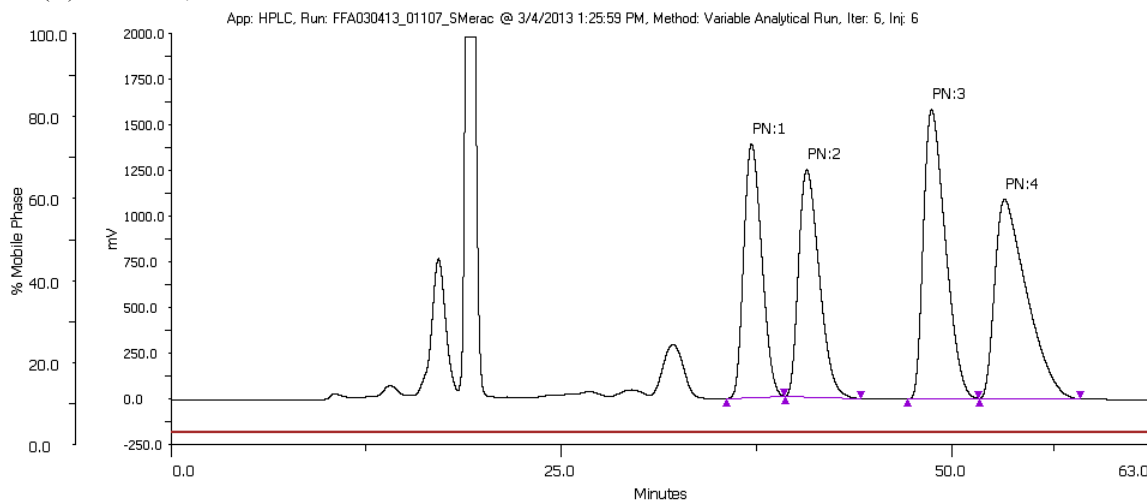


VII. HPLC and SFC traces

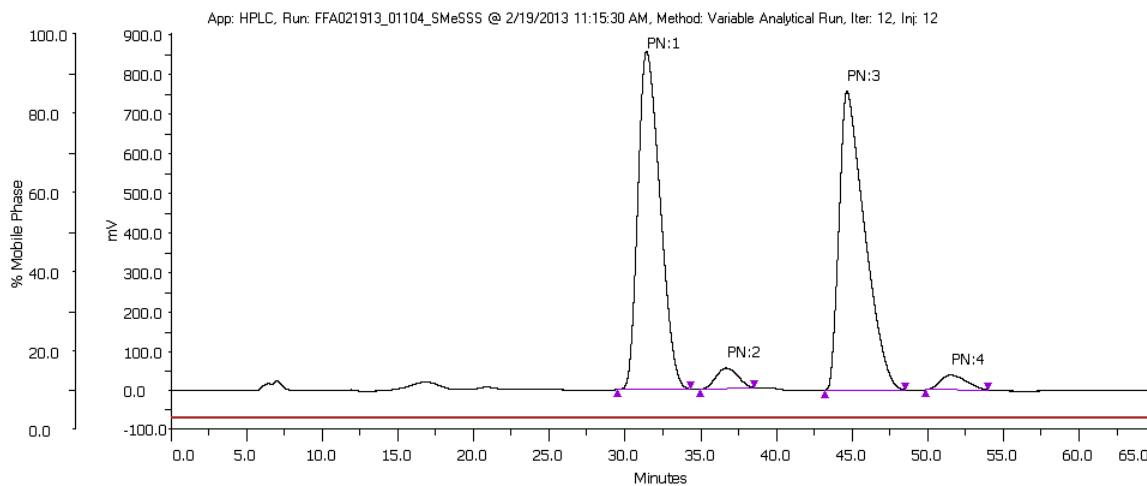


Resolution by HPLC:

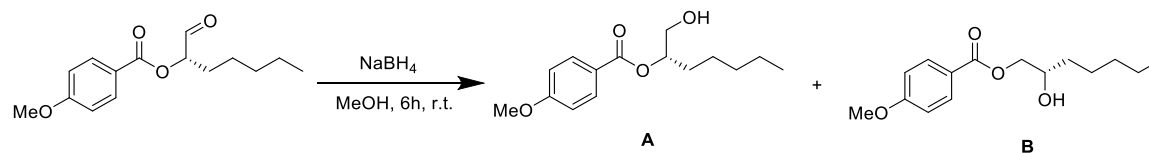
Racemic run: CHIRALPAK 1A (AD-H), 3% iPrOH/hexanes, 0.9 ml/min, 220 nm, t_R (**A**): 37.2 min, 40.8 min, t_R (**B**): 48.8 min, 53.4 min



Chiral run: CHIRALPAK 1A (AD-H), 3% iPrOH/hexanes, 0.9 ml/min, 220 nm, t_R (**A**): 31.5 min, 36.7 min, t_R (**B**): 44.7 min, 51.6 min, 90% ee

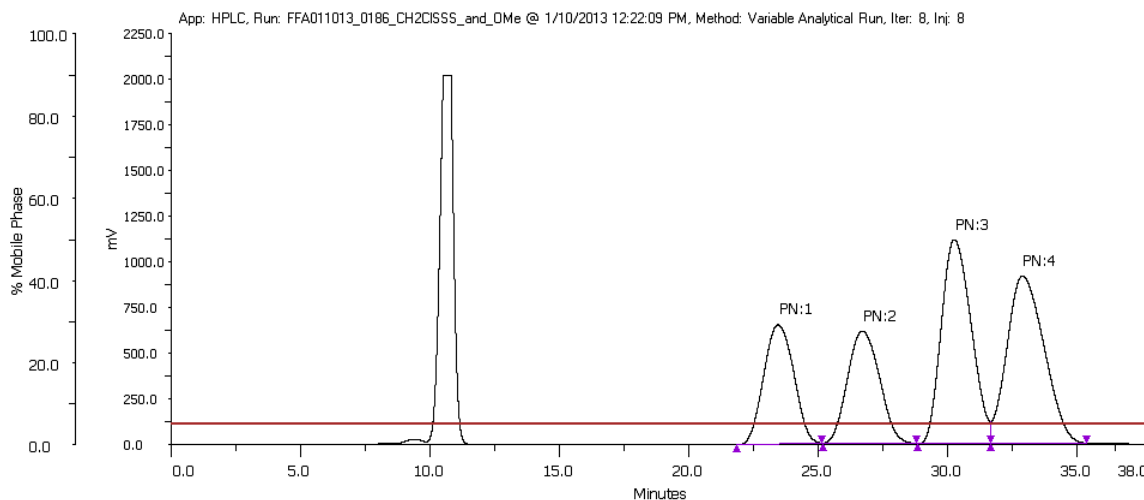


Peak Number (PN)	isomer	t_R (min)	Area (uVmin x100)	% Area
1	A	31.5	144958230.8322	46.905
2	A	36.7	8599526.6365	2.783
3	B	44.7	148067052.4987	47.911
4	B	51.6	7419669.9993	2.401

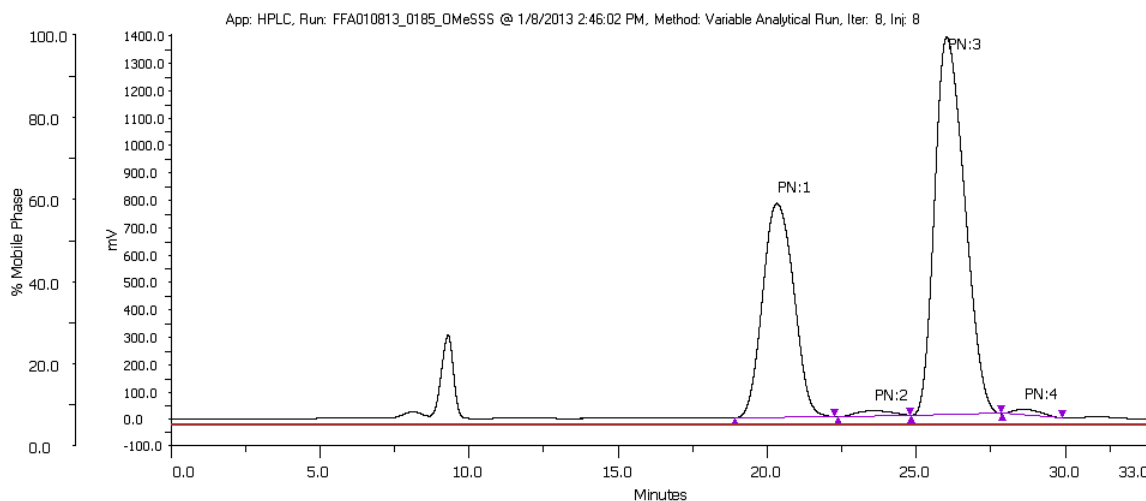


Resolution by HPLC:

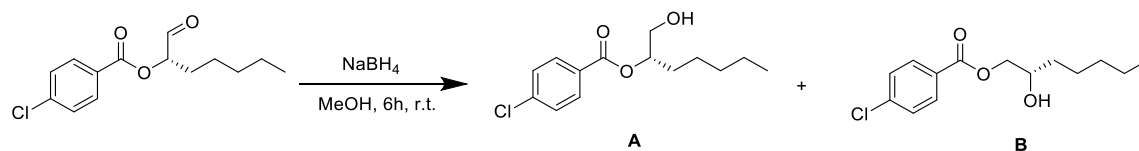
Racemic run: CHIRALPAK 1A (AD-H), 5% iPrOH/hexanes, 0.7 ml/min, 254 nm, t_R (**A**): 23.5 min, 26.8 min, t_R (**B**): 30.3 min, 33.0 min



Chiral run: CHIRALPAK 1A (AD-H), 5% iPrOH/hexanes, 0.8 ml/min, 254 nm, t_R (**A**): 20.3 min, 23.6 min, t_R (**B**): 26.0 min, 28.7 min, 96% ee

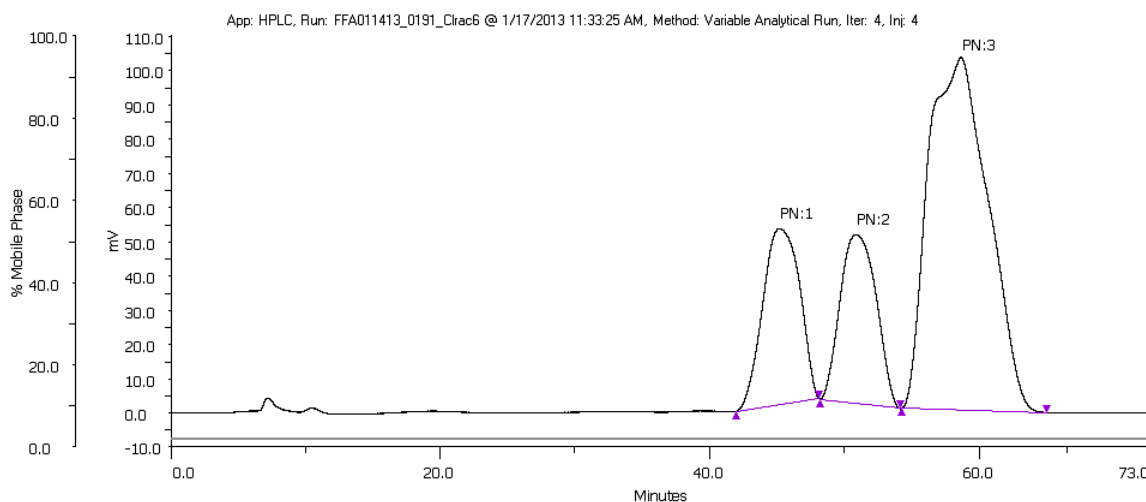


Peak Number (PN)	isomer	t_R (min)	Area (uVmin x100)	% Area
1	A	20.3	94911962.1362	36.417
2	A	23.6	2720385.831	1.044
3	B	26.1	160681660.8333	61.653
4	B	28.7	2308812.7922	0.886

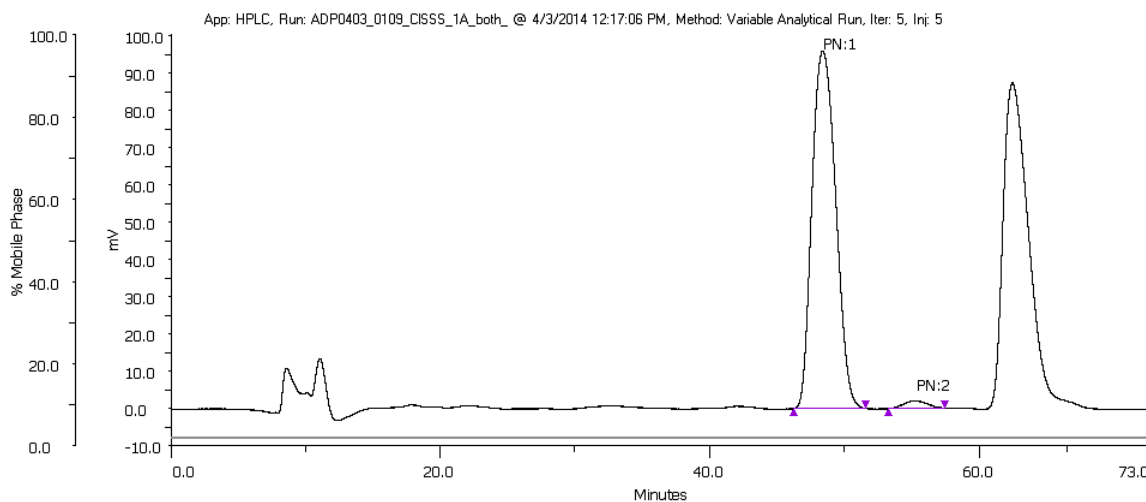


Resolution by HPLC:

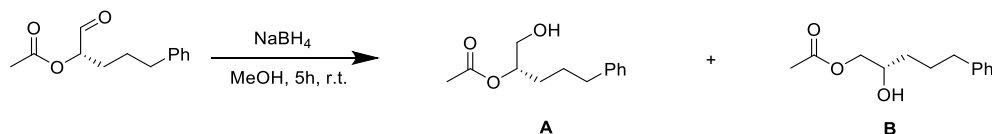
Racemic run: CHIRALPAK 1A (AD-H), 2% iPrOH/hexanes, 0.6 ml/min, 254 nm, t_R (A): 45.1 min, 51.0 min, t_R (B, unresolved): 58.7 min



Chiral run: CHIRALPAK 1A (AD-H), 2% iPrOH/hexanes, 0.6 ml/min, 254 nm, t_R (A): 48.4 min, 55.3 min, 96% ee

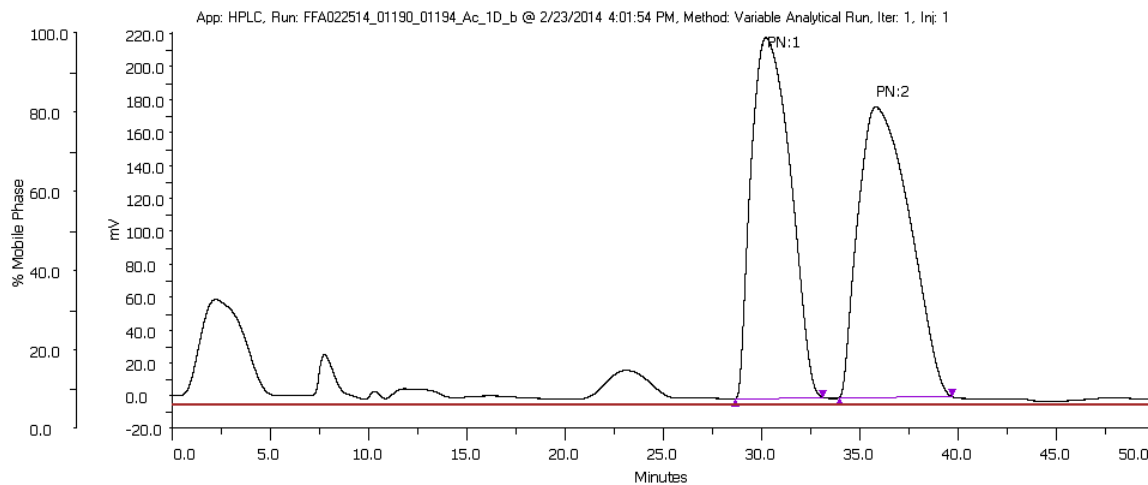


Peak Number (PN)	isomer	t_R (min)	Area (uVmin x100)	% Area
1	A	48.4	19554047.9174	98.008
2	A	55.3	397457.6244	1.992

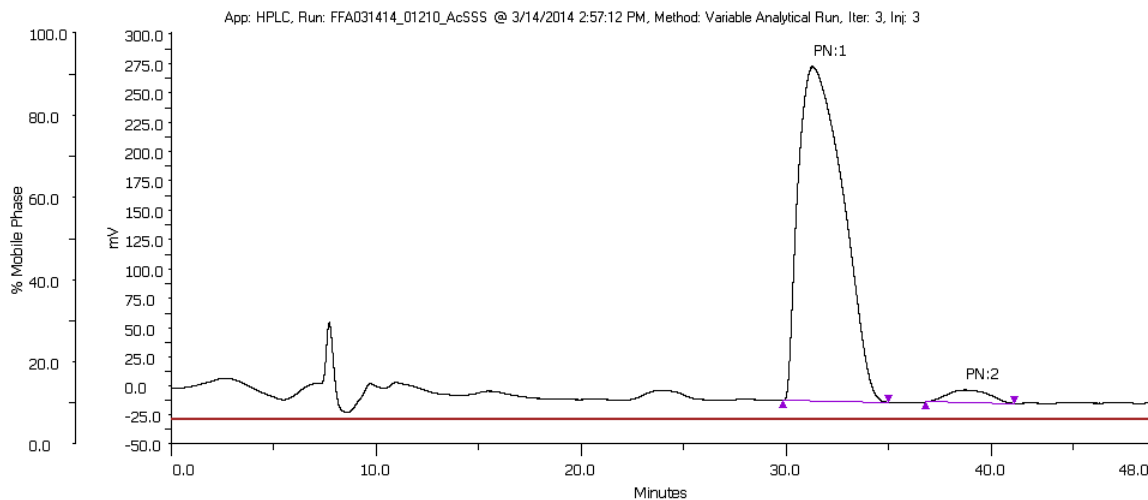


Resolution by HPLC:

Racemic run: CHIRALPAK 1D, 6% iPrOH/hexanes, 0.6 ml/min, 220 nm, t_R (**B**): 30.3 min, 35.9 min

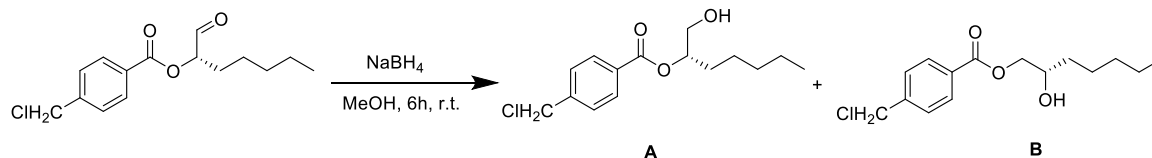


Chiral run: CHIRALPAK 1D, 6% iPrOH/hexanes/0.1% TFA, 0.6 ml/min, 220 nm, t_R (**B**): 31.3min, 88.8 min, 93%ee



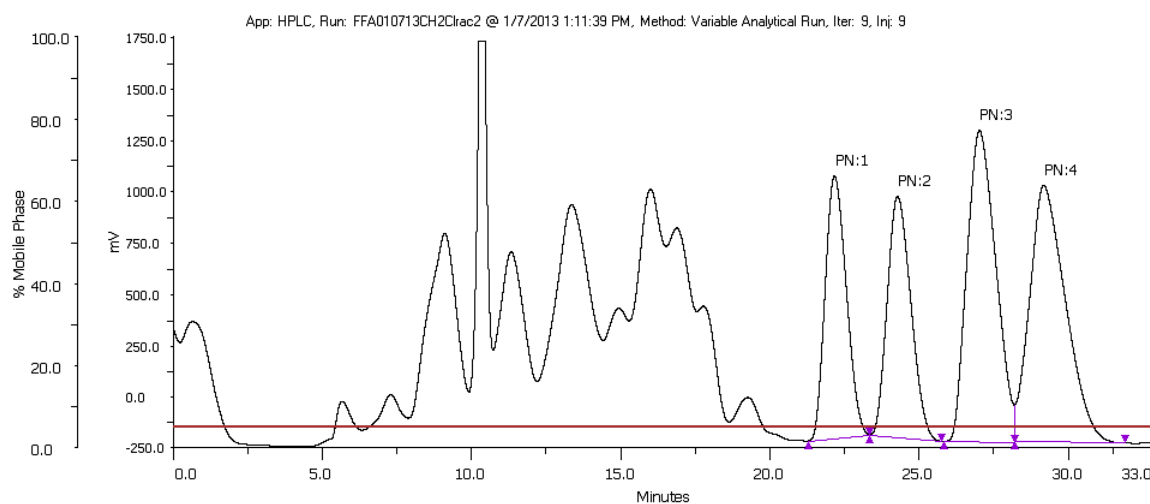
Enantioenriched run shows no **A** isomer because sample was purified before HPLC and only **B** isomer was collected.

Peak Number (PN)	isomer	t_R (min)	Area (uVmin x100)	% Area
1	B	31.3	71835284.9266	96.533
2	B	38.8	2579833.1423	3.467

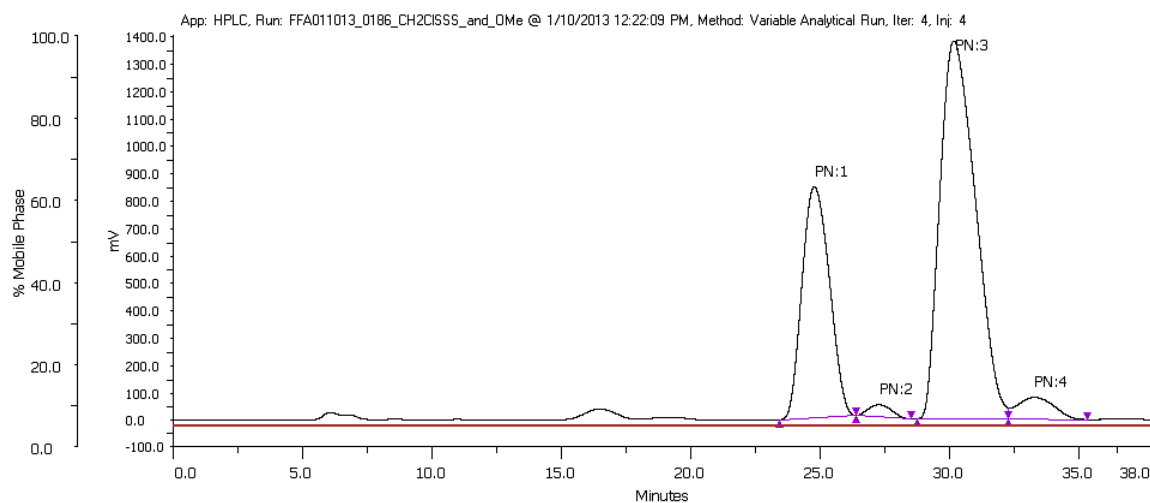


Resolution by HPLC:

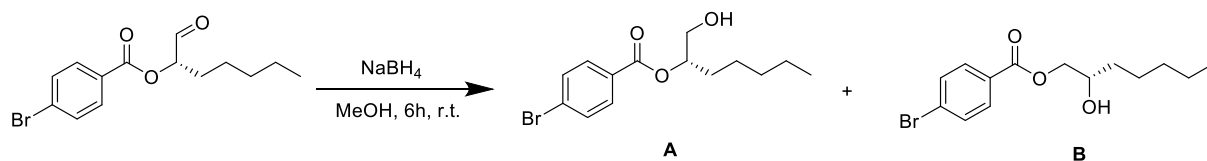
Racemic run: CHIRALPAK 1A (AD-H), 5% iPrOH/hexanes, 0.7 ml/min, 254 nm, t_R (**A**): 23.5 min, 26.8 min, t_R (**B**): 30.3 min, 33.0 min



Chiral run: CHIRALPAK 1A (AD-H), 5% iPrOH/hexanes, 0.8 ml/min, 254 nm, t_R (**A**): 20.3 min, 23.6 min, t_R (**B**): 26.0 min, 28.7 min, 92% ee

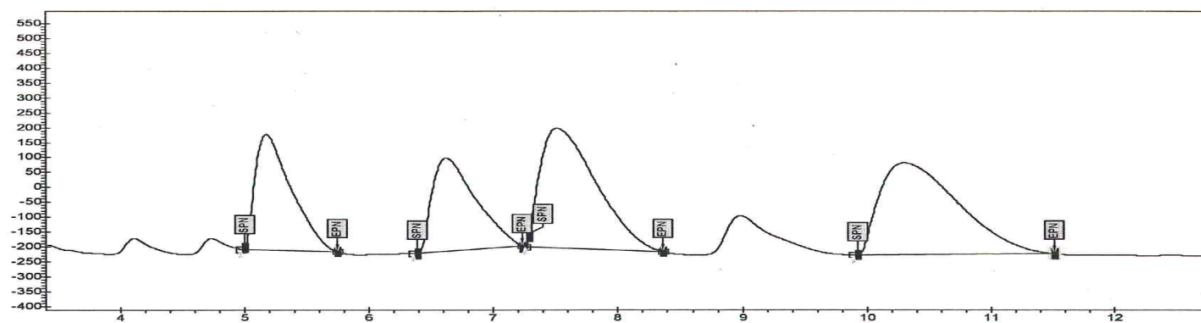


Peak Number (PN)	isomer	t_R (min)	Area (uVmin x100)	% Area
1	A	24.8	103527229.1501	30.298
2	A	27.3	4598088.8746	1.346

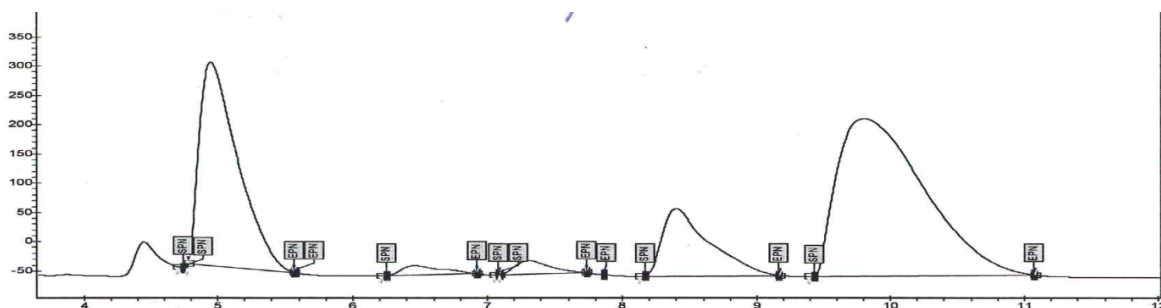


Resolution by SFC:

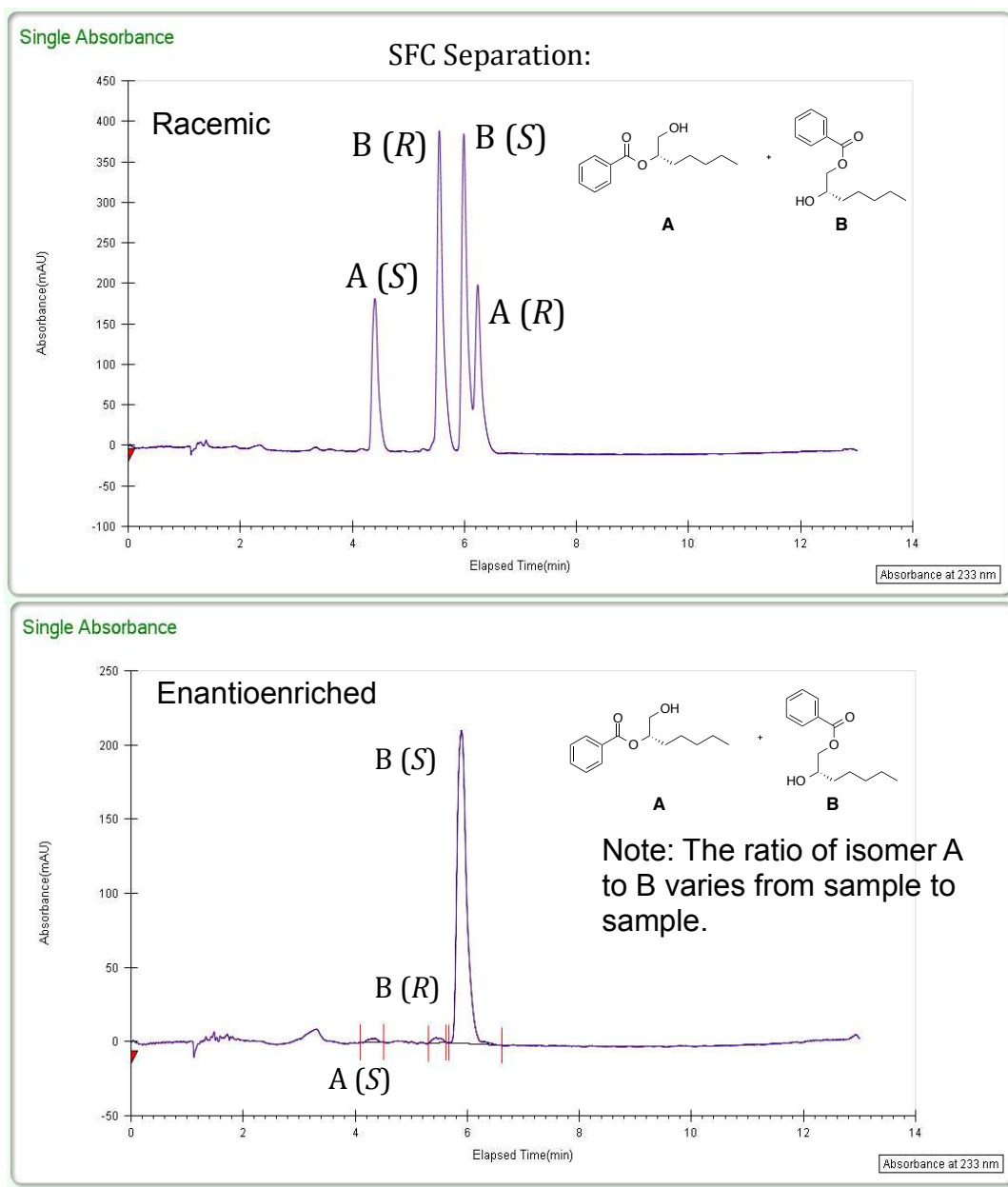
Racemic run: OJ-H, 4% modifier, 4 ml/min, methanol, 50°C, t_R (**A**): 5.2 min, 6.6 min, t_R (**B**): 7.5 min, 10.3 min



Chiral run: OJ-H, 4% modifier, 4 ml/min, methanol, 50°C, t_R (**A**): 5.0 min, 6.5 min, t_R (**B**): 7.3 min, 9.8 min, 92% ee



t_R (min)	isomer	Area (uVmin)	% Area
5.0	A	115.7	23.651
6.5	A	5.6	1.143
7.3	B	6.9	1.414
9.81	B	203.1	41.535



General Info

Log Author

Log Date 11/30/2013 5:46:05 PM
 Report By current_User
 Report Date 12/12/2013
 Method Name Gradient_5_50_3flow.met

Notes

Injection Info

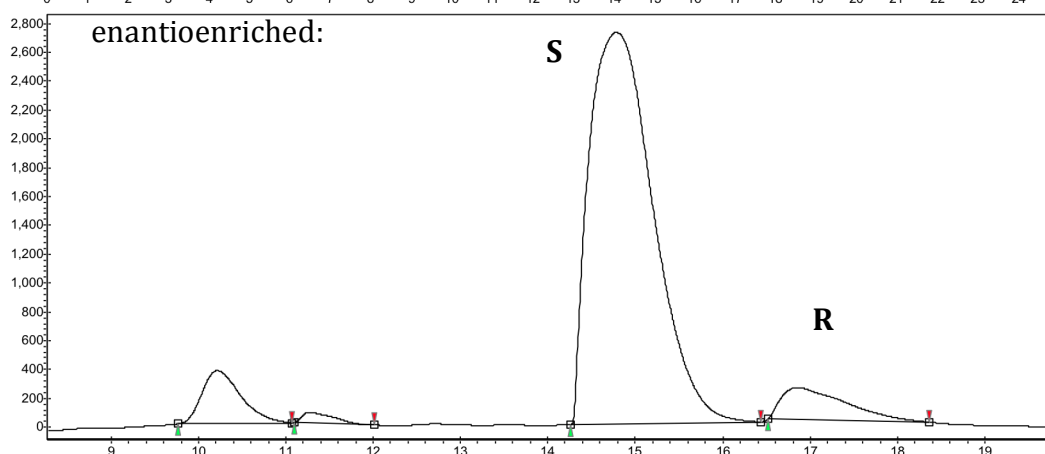
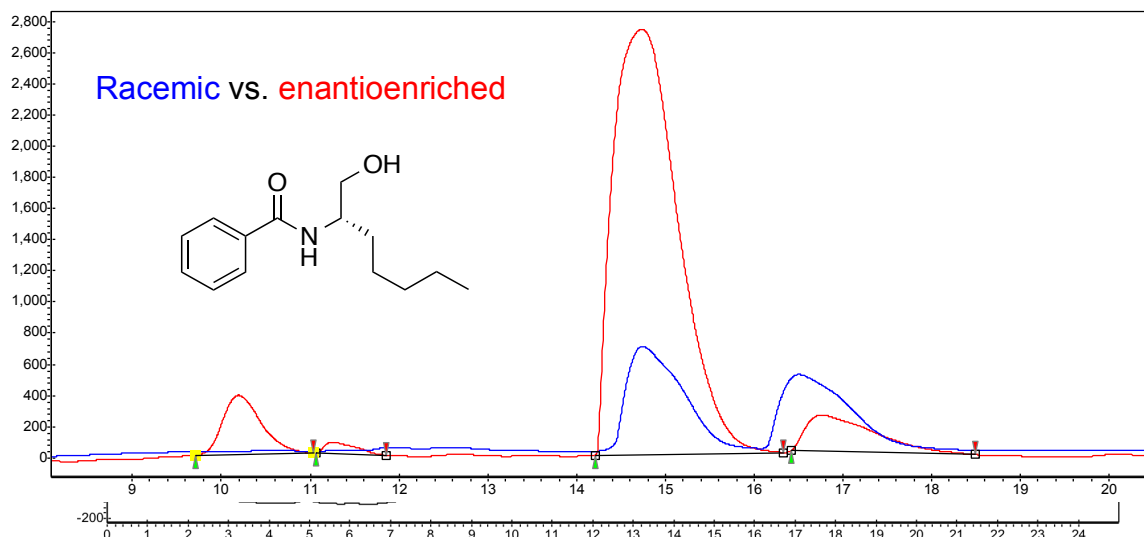
Inj Vol 10
 Solvent MeOH
 Column AD-H
 Sample MLA2276r
 Well location P1: 1E

Temp 35
 Flow 3
 % Modifier 5
 Pressure 100

Peak Info

Peak No	% Area	Area	RT (min)	Height (mV)	K'
1	1.0416	26.525	4.36	2.3412	0.0041
2	1.6264	41.4194	5.45	3.5302	0.0051
3	97.332	2478.6963	5.9	210.691	0.0055
Total:	100	2546.6407			

SFC separation:



#	Name	Start [Min]	Time [Min]	End [Min]	RT Offset [Min]	Quantity [% Area]	Height [μV]	Area [μV.Min]	Area [%]
1	UNKNOWN	9.77	10.21	11.07	0.00	6.89	366.1	187.5	6.886
4	UNKNOWN	11.10	11.28	12.01	0.00	1.12	74.4	30.6	1.122
2	UNKNOWN	14.26	14.78	16.44	0.00	84.94	2714.9	2313.1	84.937
3	UNKNOWN	16.52	16.86	18.36	0.00	7.05	224.6	192.1	7.055

Total 100.00 3380.0 2723.3 100.000
 MLA2085r_22 10/12/12 method MLAgredientC3_2to8mod_2flow_50C.METH

Column: 3 (OJ-H)

Temp: 50C

Pressure: 150 bar

Flow: 2mL/min

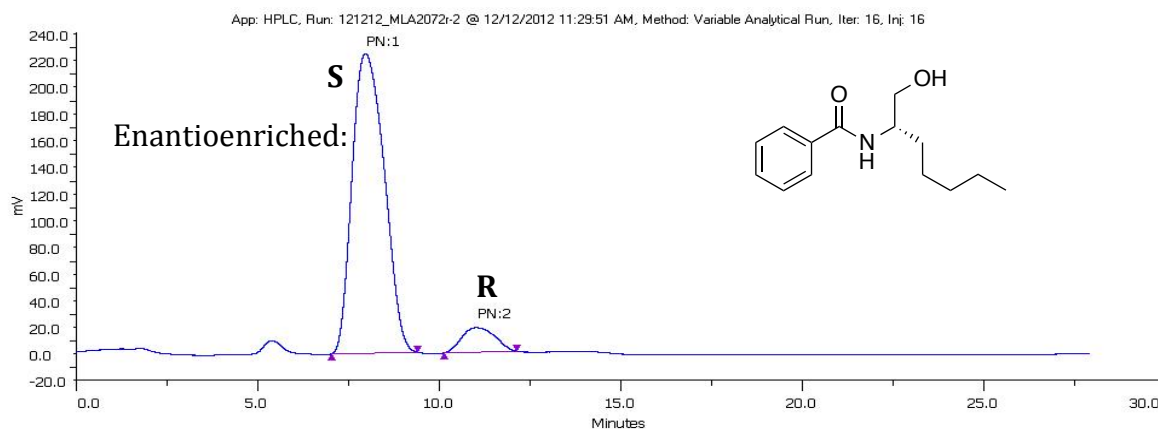
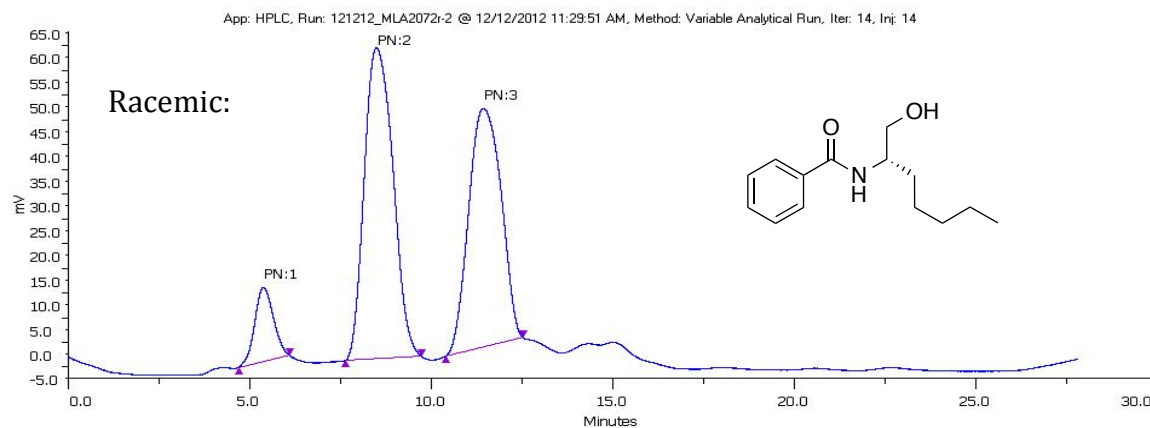
210 nm Detection

MeOH modifier in CO2

Modifier Program:

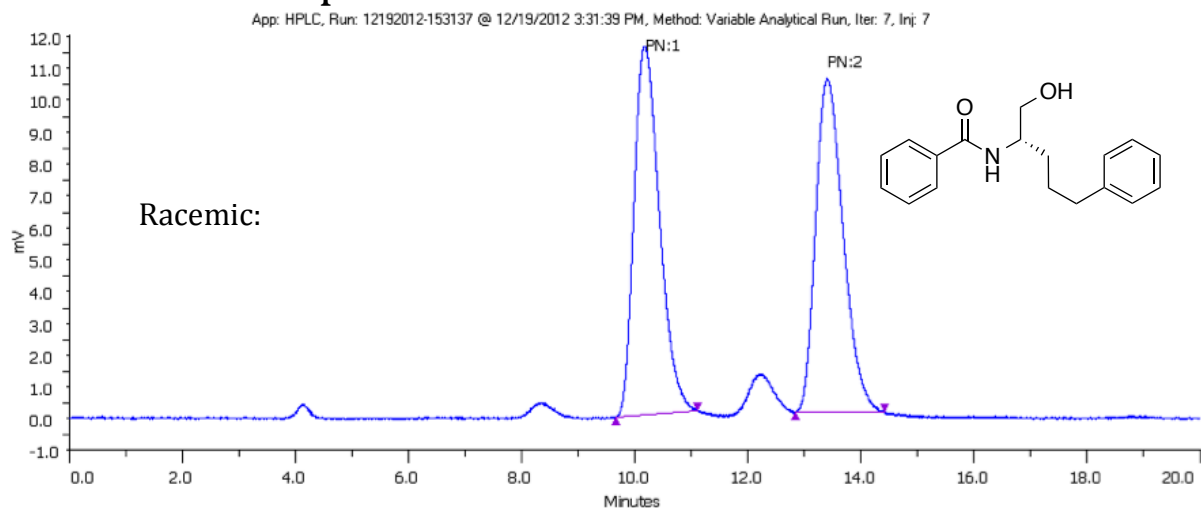
Rate	final	hold (min)
0	2	1
1	8	20
1	8	EOR

HPLC separation:

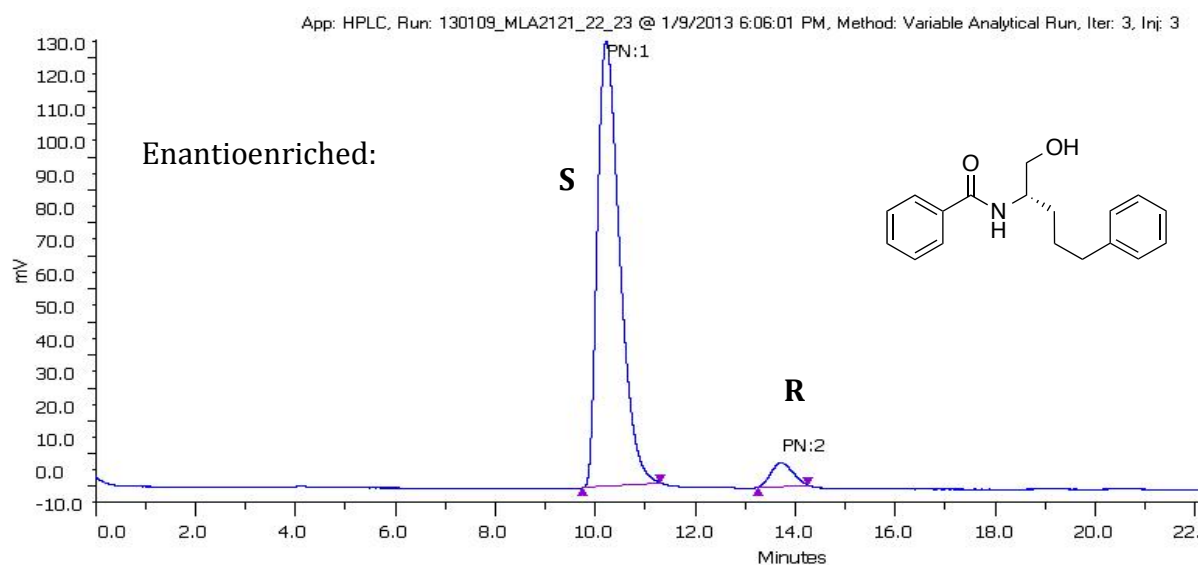


Peak Name	Retention Time (min)	Area (uVmin x100)	Area %
1	7.98	23098779.1658	92.214
2	11.026	1950412.4969	7.786

HPLC separation:

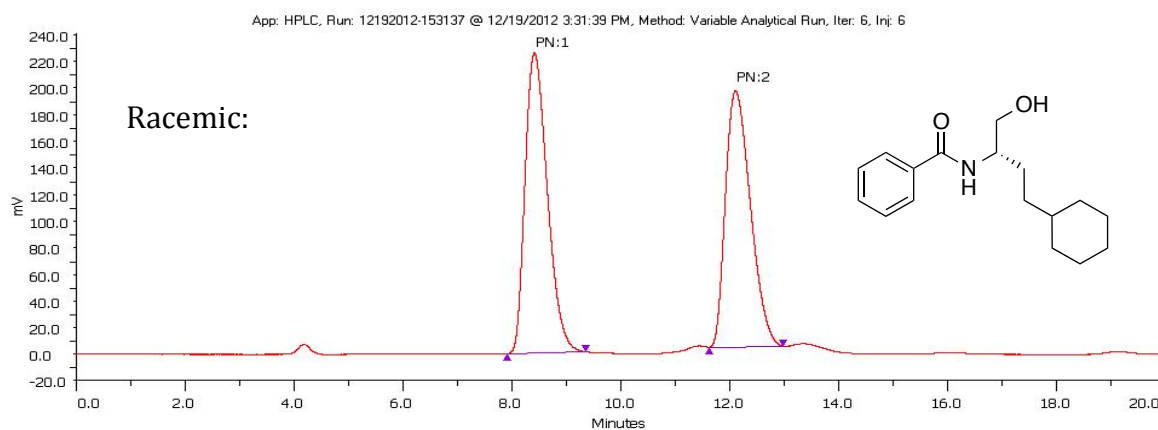


*Note that scales are different on the enantioenriched vs racemic traces.

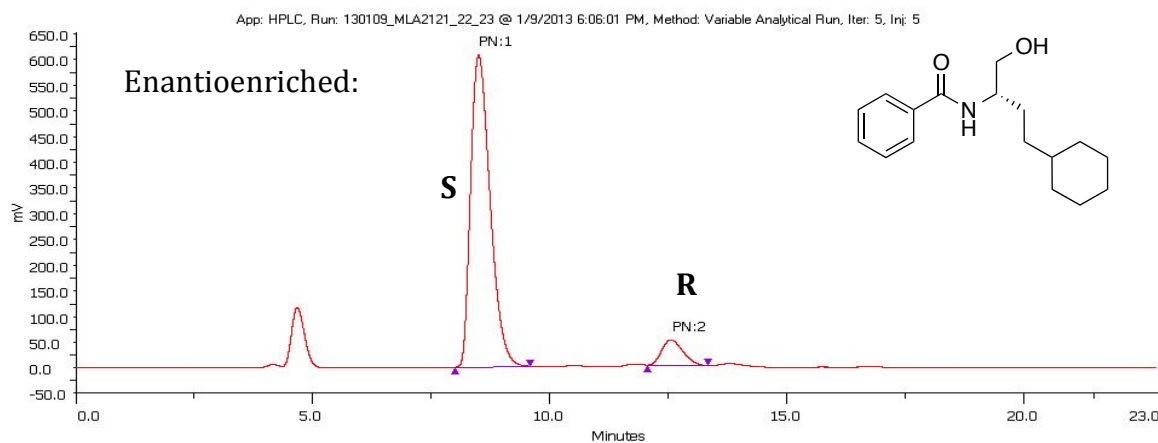


Peak Name	Retention Time (min)	Area (uVmin x100)	Area %
1	10.229	6971986.2537	95.077
2	13.728	361028.7597	4.923

HPLC separation:

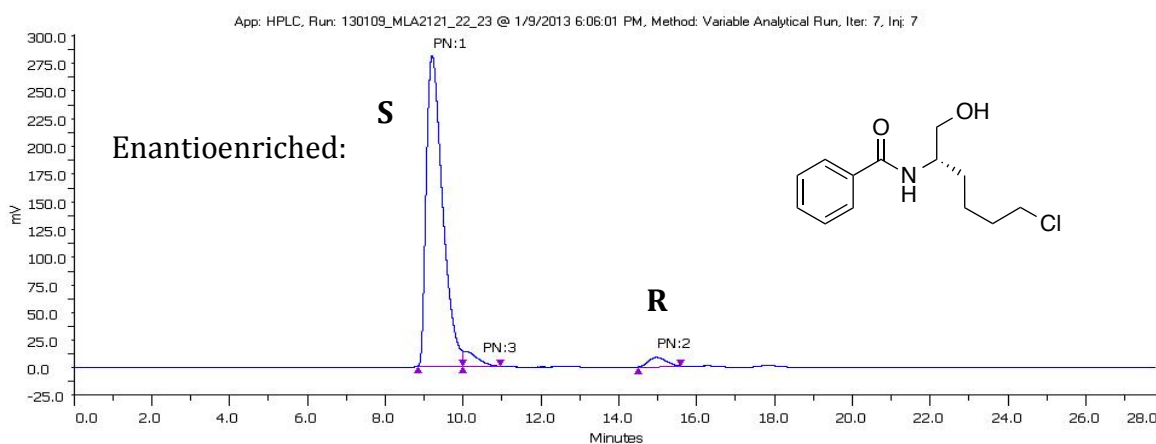
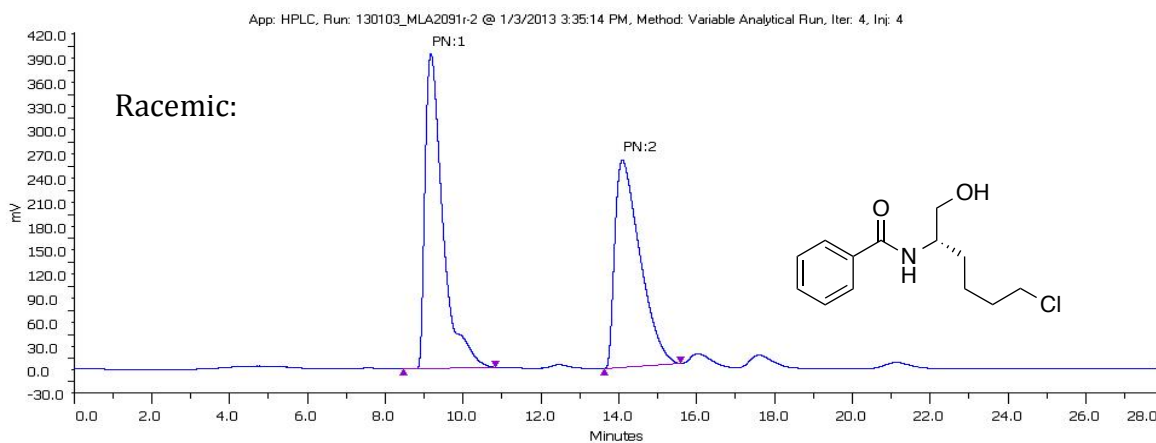


*Note that scales are different on the enantioenriched vs racemic traces.



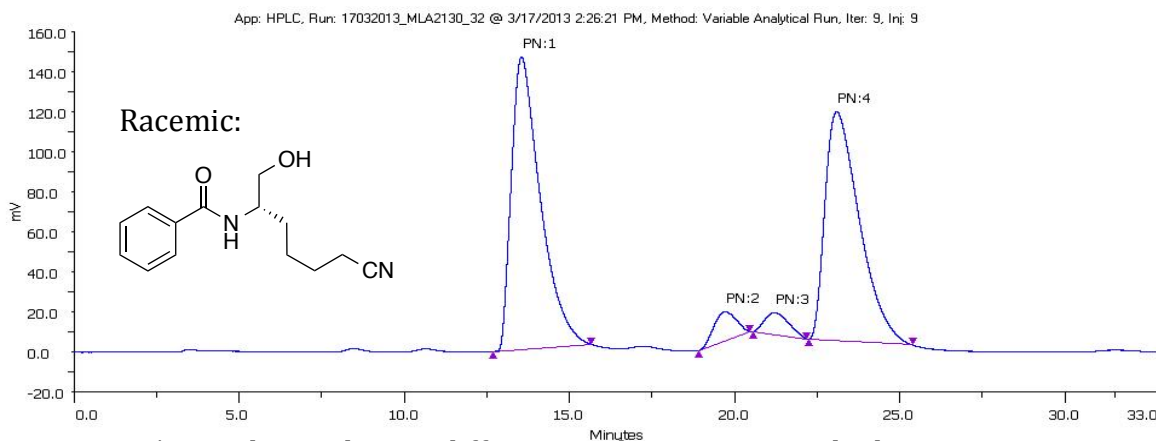
Peak Name	Retention Time (min)	Area (uVmin x100)	Area %
1	8.509	28931946.6674	91.896
2	12.571	2551569.1691	8.104

HPLC separation:

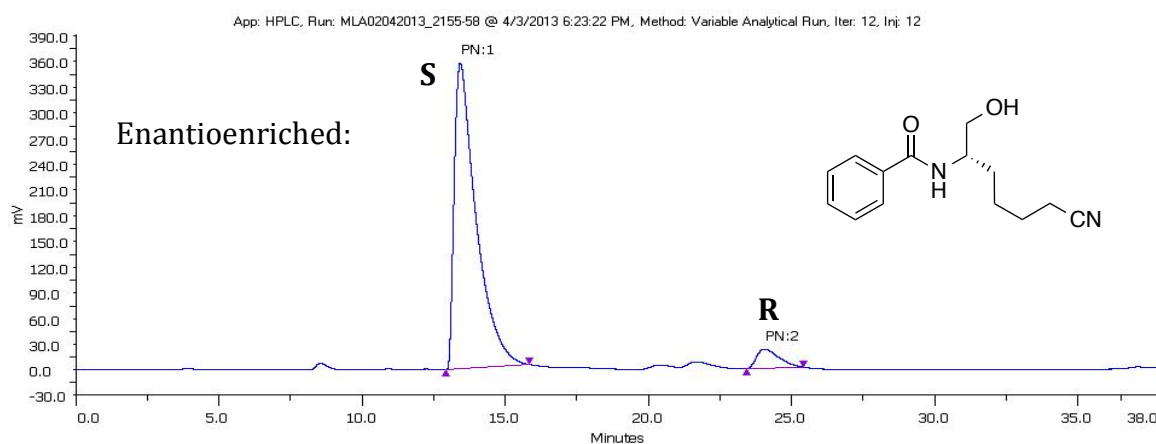


Peak Name	Retention Time (min)	Area (uVmin x100)	Area %
1	9.216	13707290.7953	93.202
2	14.983	441835.835	3.004
3 (impurity)	10.014	557908.081	3.793

HPLC separation:

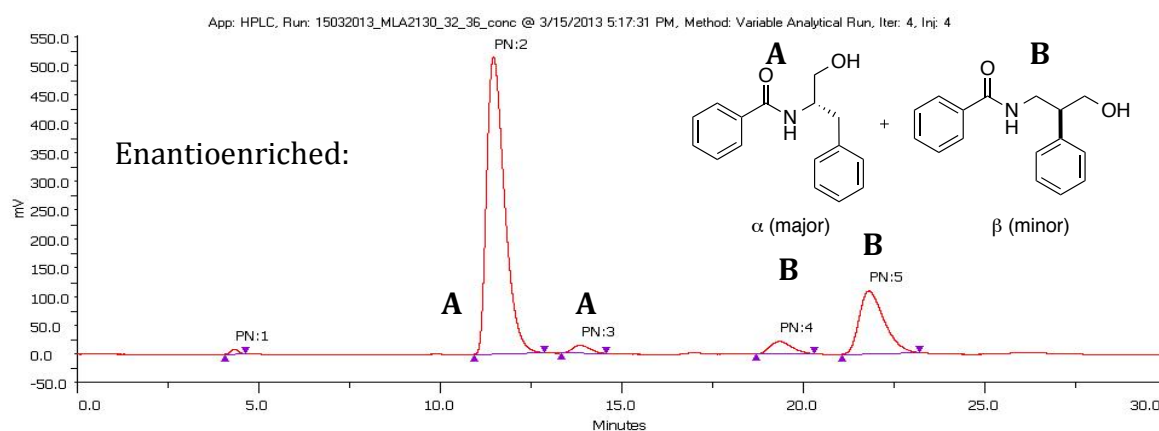
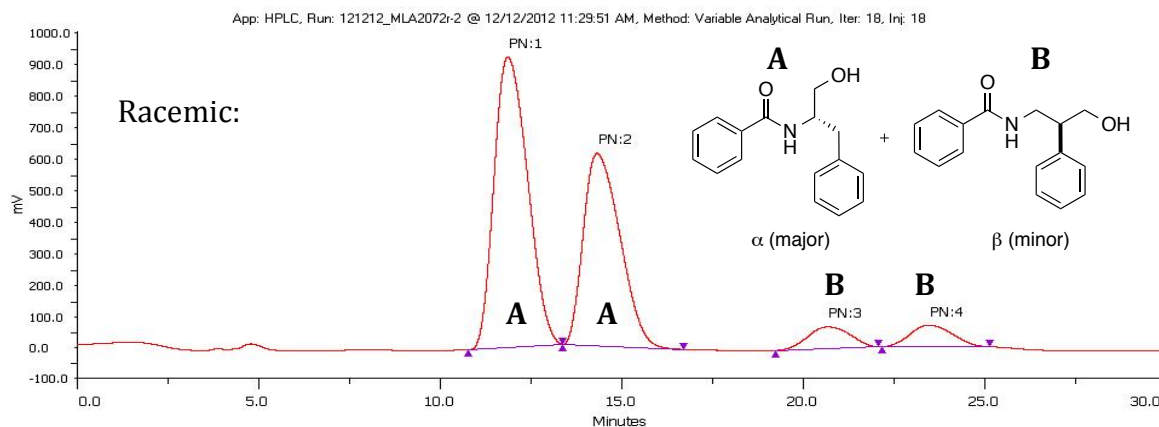


*Note that scales are different on the enantioenriched vs racemic traces.



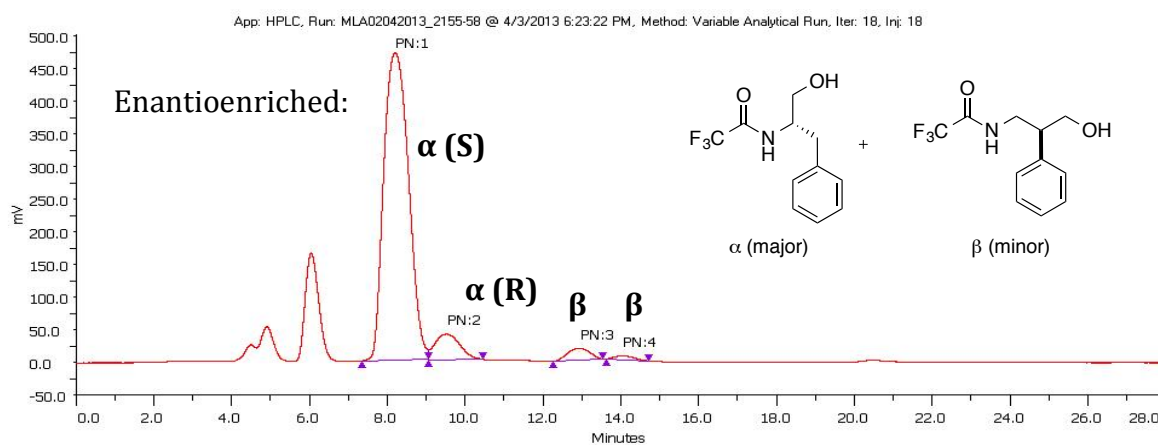
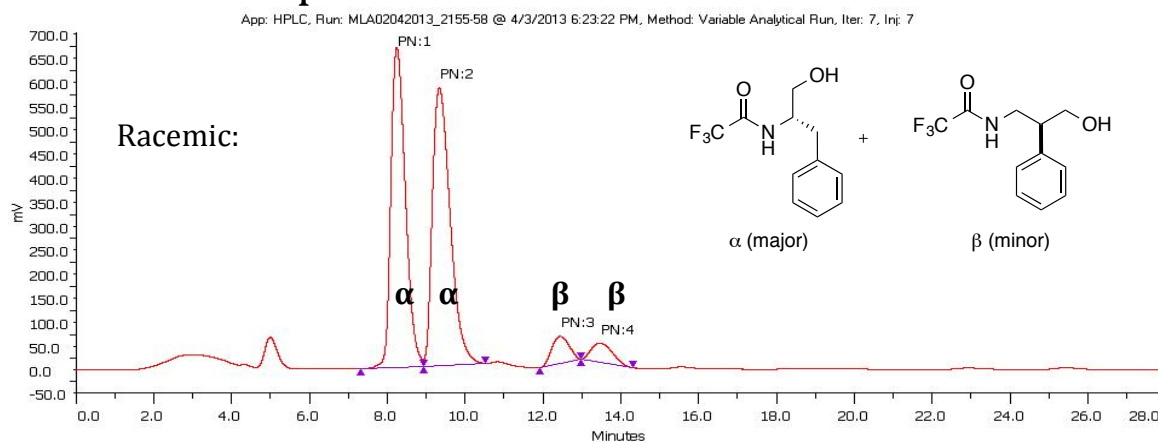
Peak Name	Retention Time (min)	Area (uVmin x100)	Area %
1	13.446	31690445.414	93.997
2	24.071	2024017.91	6.003

HPLC separation:



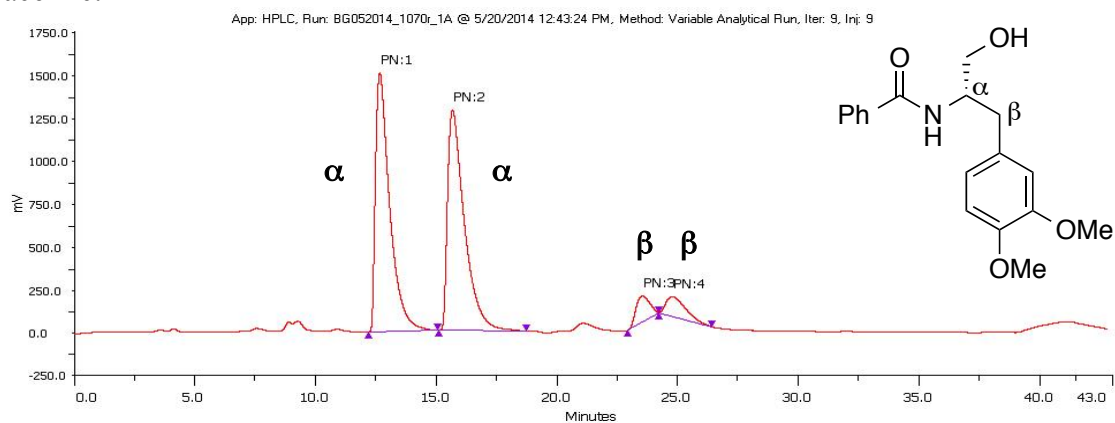
Peak Name	Retention Time (min)	Area (uVmin x100)	Area %
2	11.483	29252597.4926	72.508
3	13.885	768988.3313	1.906
4	19.352	1472231.6663	3.649
5	21.825	8638956.6561	21.413

HPLC separation:

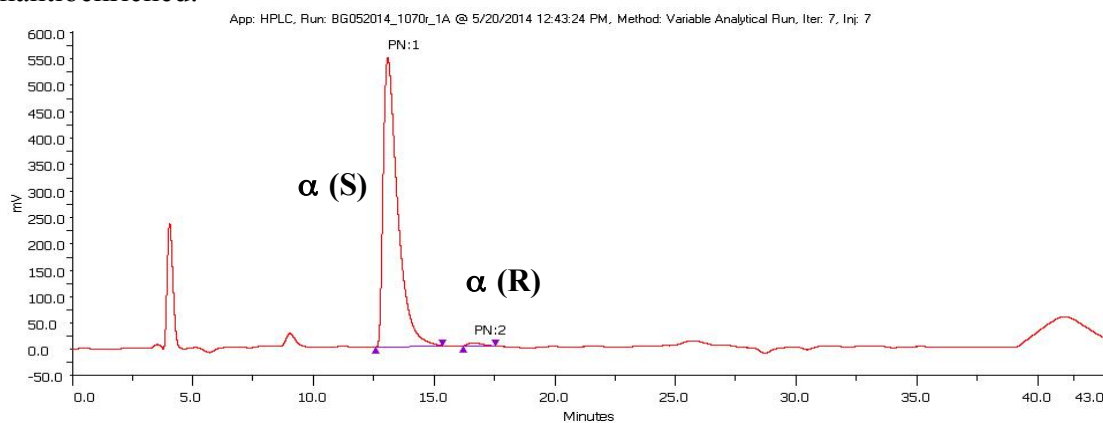


Peak Name	Retention Time (min)	Area (uVmin x100)	Area %
1	8.211	34620060.4828	88.619
2	9.528	2875018.0774	7.359
3	12.898	1206989.9988	3.09
4	14.11	364094.1667	0.932

Racemic:



Enantioenriched:



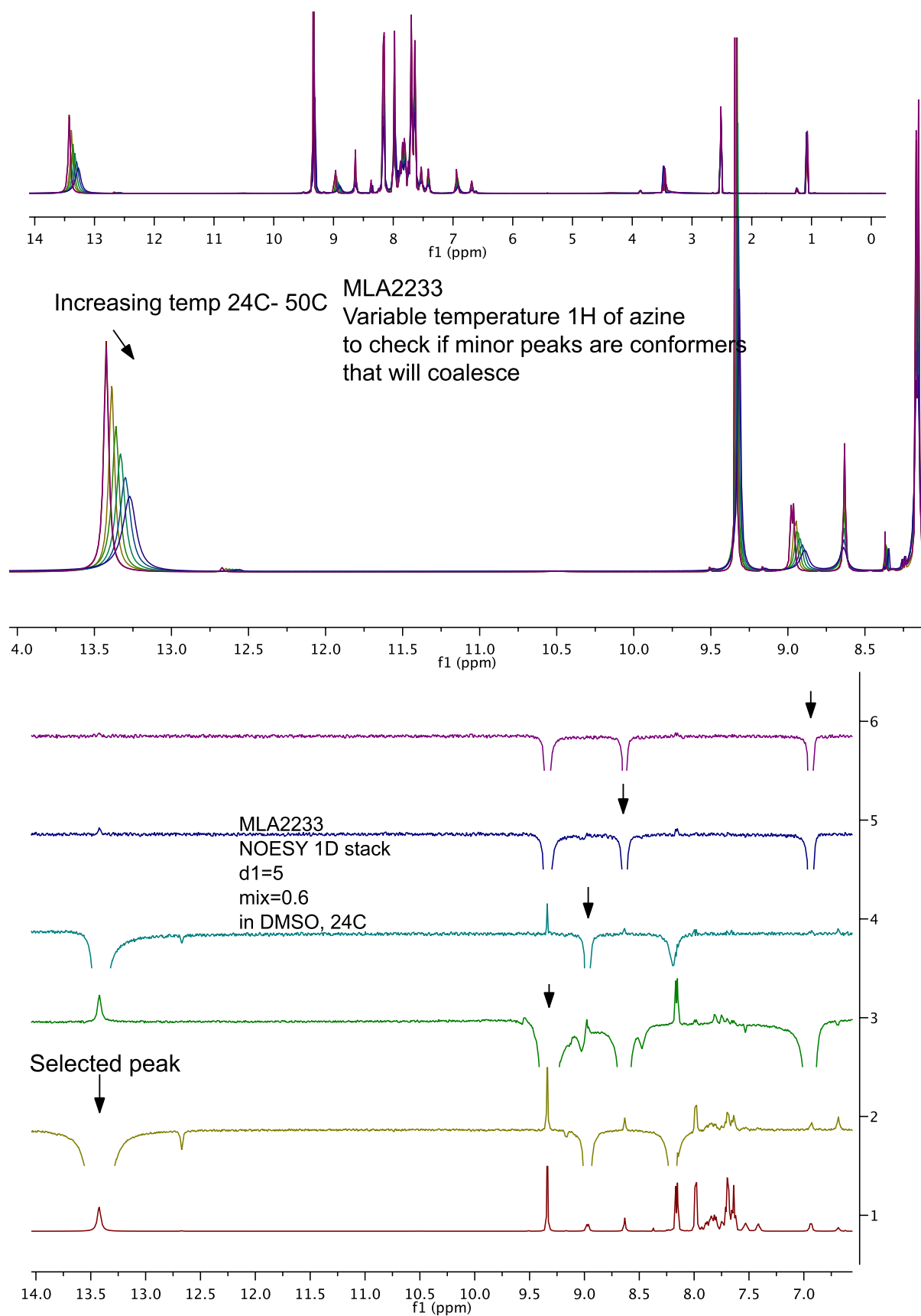
Enantioenriched run shows no β isomer because sample was purified before HPLC and only α isomer was collected.

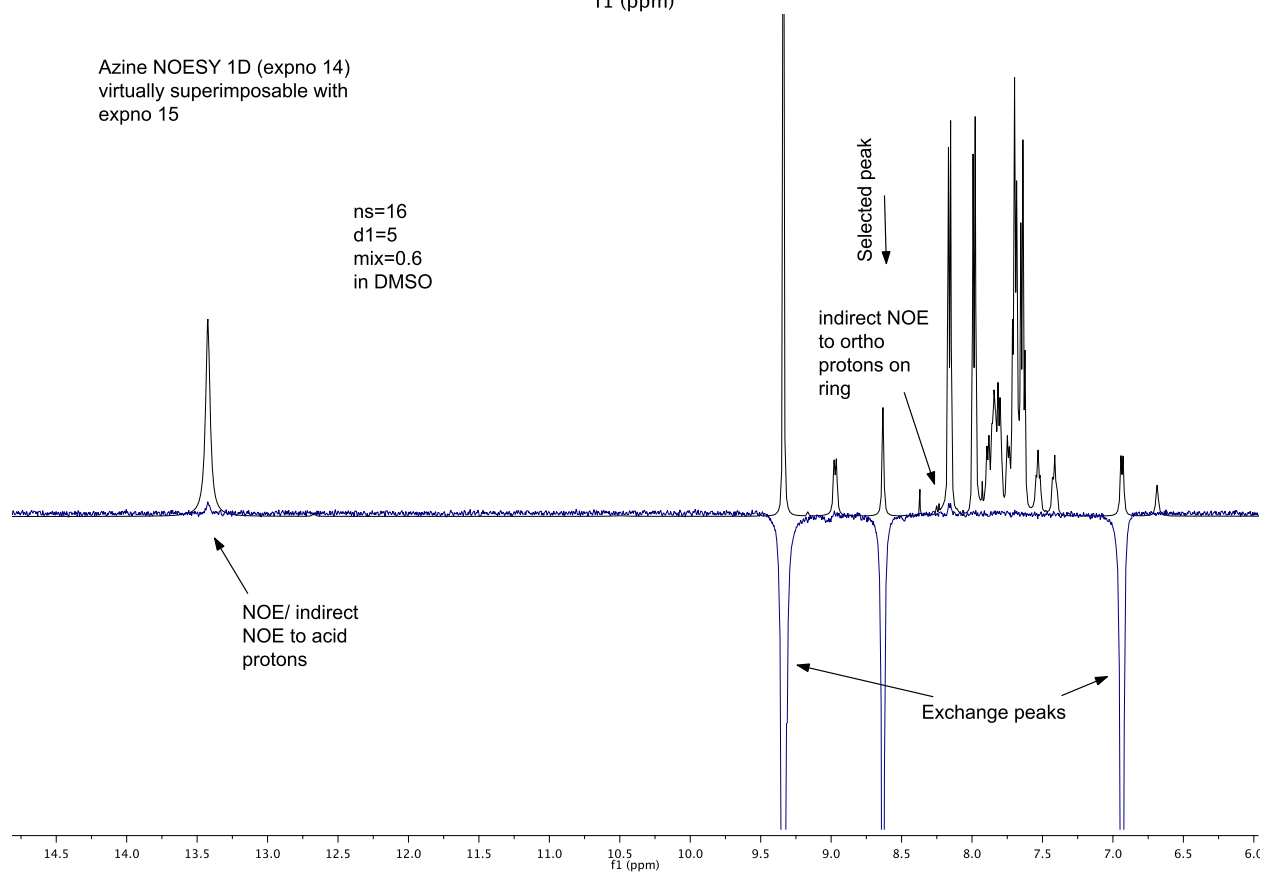
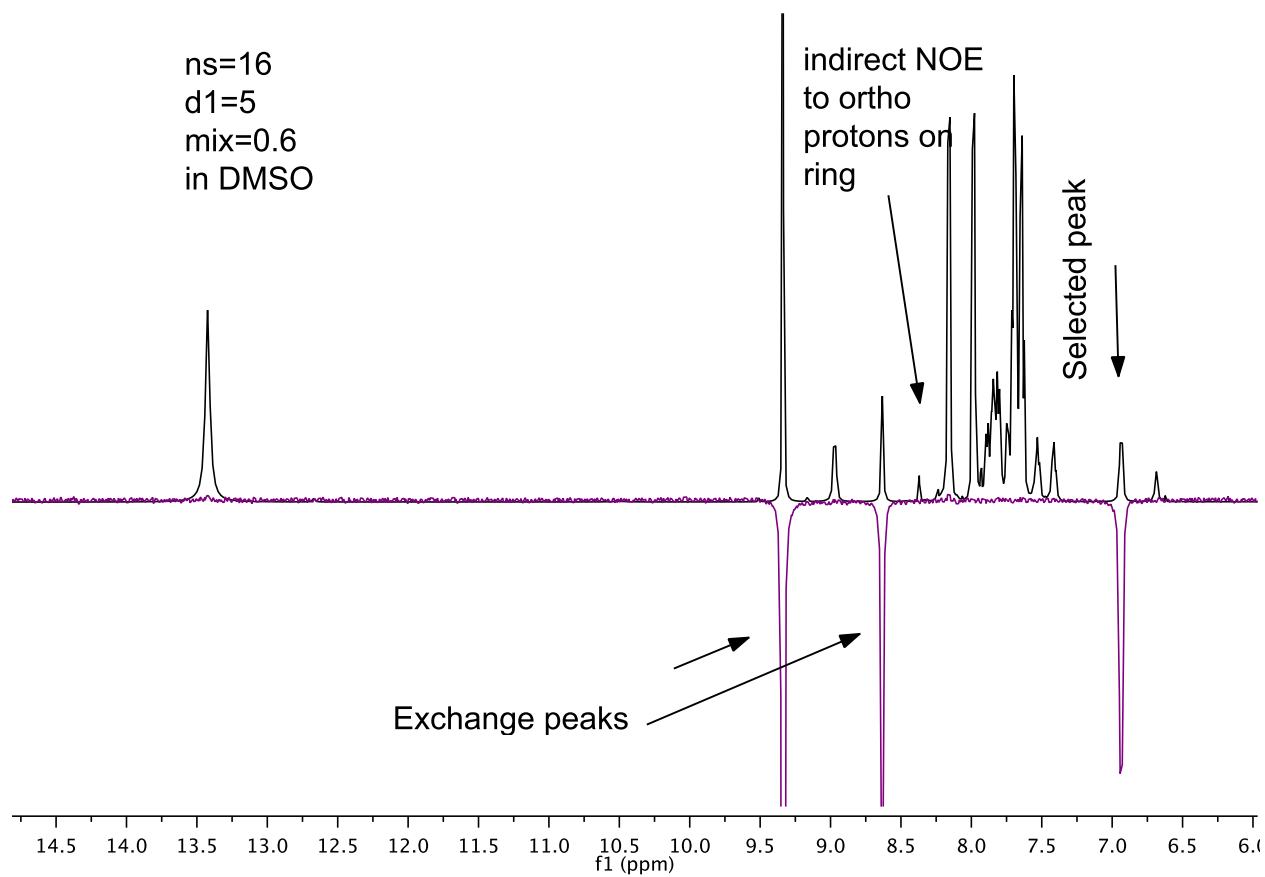
Retention Time (min)	Area (uVmin x100)	Area %
13.092	37901592.4973	98.899
16.678	422008.3301	1.101

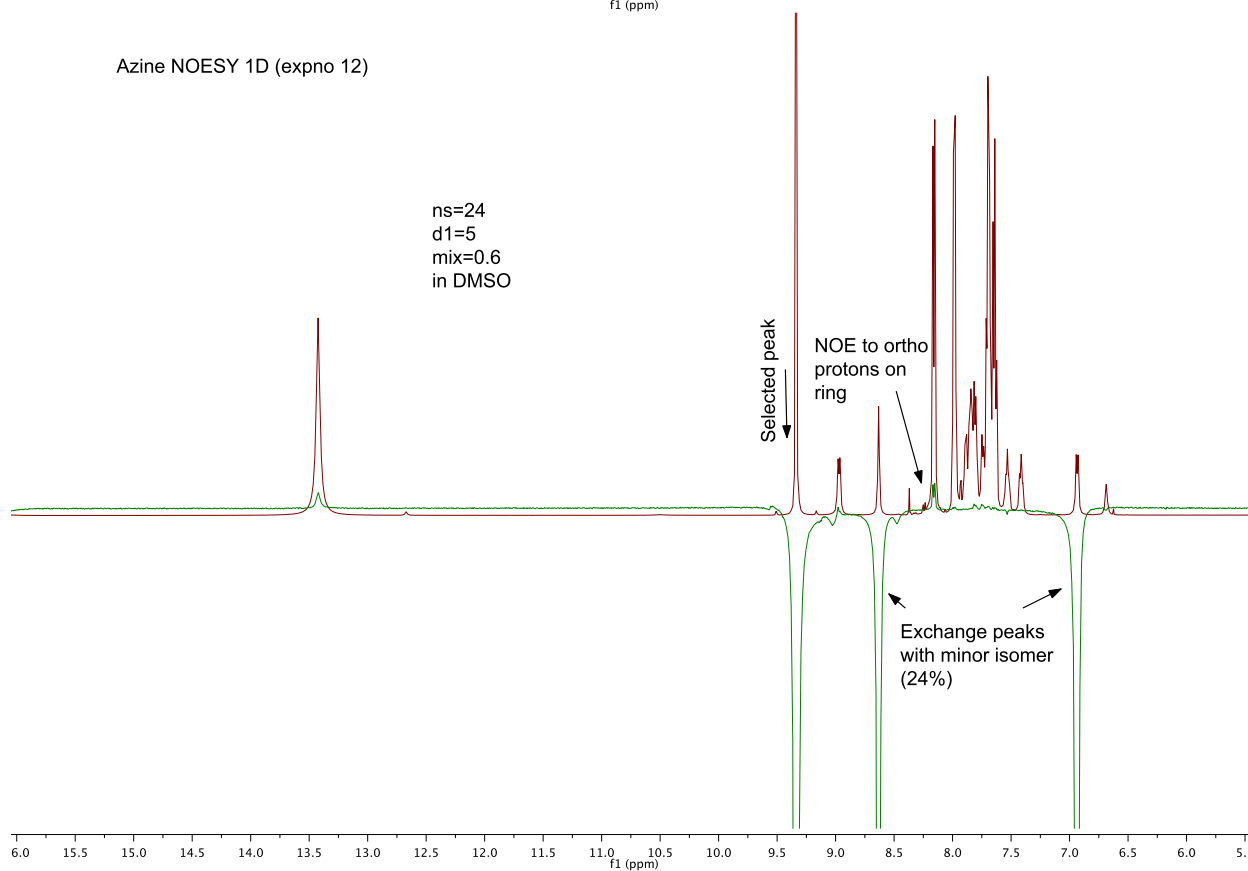
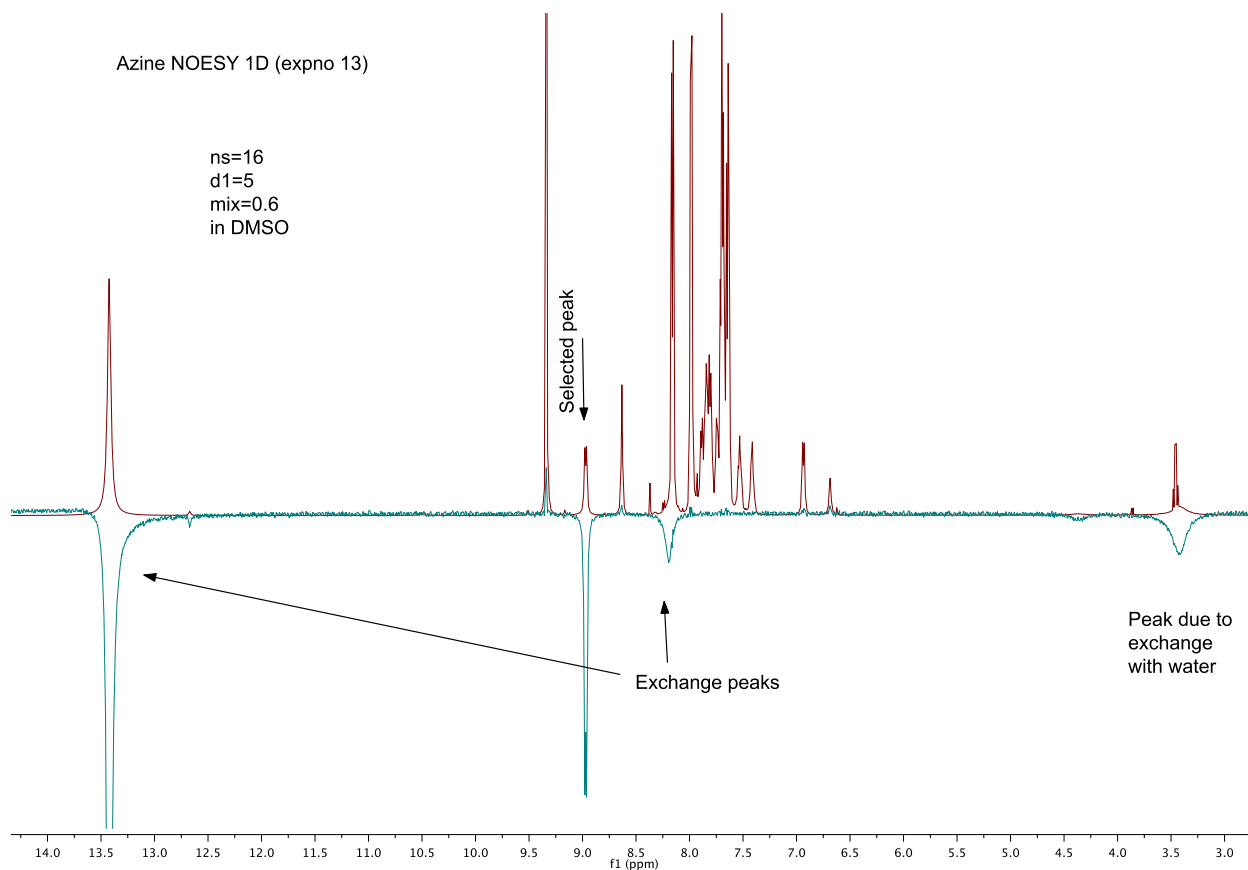
Chapter 3 Supporting data and spectra.

Data used for Table 3.1.

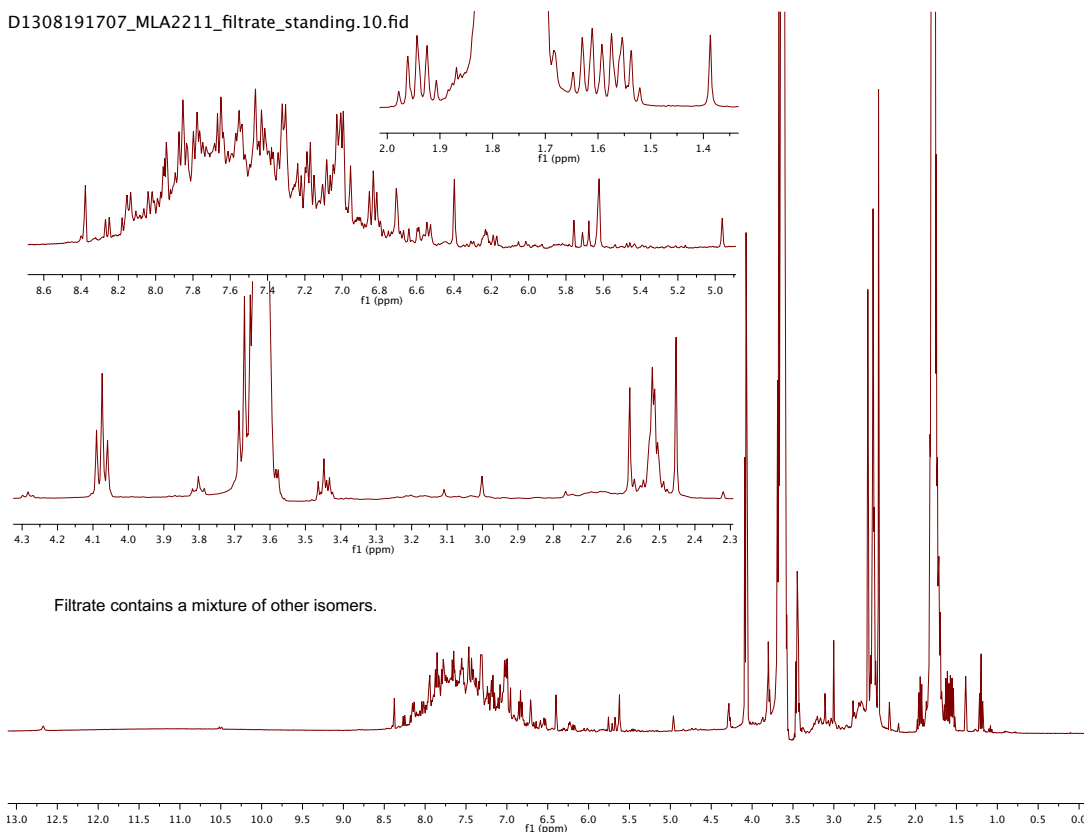
Entry	Scale	Yield (%) ^a	mL THF/ g phosphine
GW1123	1.3 g	31.8	154
GW1121	1.3 g	27.1	154
TTA1026	0.5 g	11.3	200
TTA1032	0.5 g	15.2	--
TTA1036	1.3 g	19.0	115
TTA1042	1.1 g	29	--
TTA1087	1.43 g	14.4	70
EW1008	0.95 g	29.3	79
EW1051	2.3 g	20 ^b	43
EW1083	2.3 g	18 ^b	17
ERN2184	4.4 g	30.5 ^b	45
MLA1147	1.9 g	13	26
MLA1022	0.86	18.7	41
MLA1096	2.25 g	12.6	44
MLA1143	1.7 g	23.9	30
MLA2063	2.5 g (17.5 mmol)	36.7	30
MLA2191	2.5 g (17.5 mmol)	17.7	60



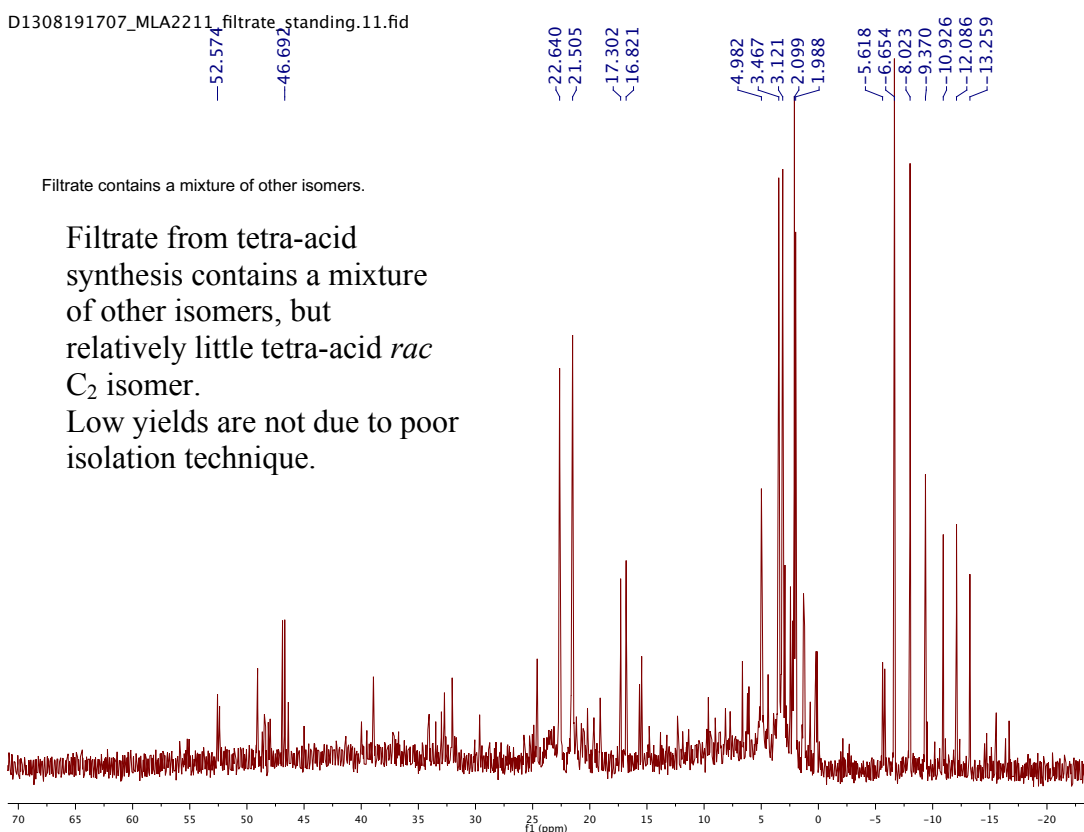




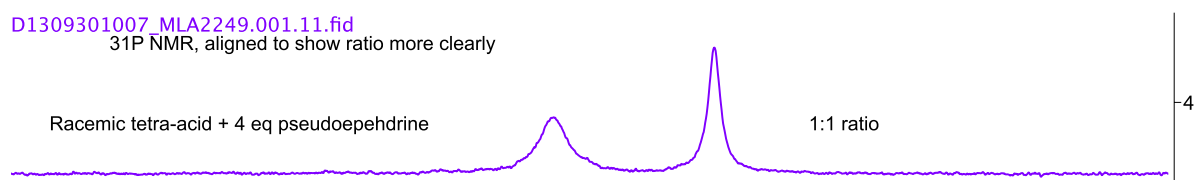
D1308191707_MLA2211_filtrate_standing.10.fid



D1308191707_MLA2211_filtrate_standing.11.fid



D1309301007_MLA2249.001.11.fid

³¹P NMR, aligned to show ratio more clearly

D1309301007_MLA2244-4.001.11.fid

Racemic tetra-acid + 4 eq pseudoephedrine,
mother liquor from first separation

4.3:1 ratio

Solids from various crops showing
separation of diastereomers
(Crystallization solvent was
unoptimized, 9:1 2-propanol:water)

D1309251118_MLA2244-1.001.11.fid

Racemic tetra-acid + 4 eq pseudoephedrine,
Solids from first separation

1:10.7 ratio

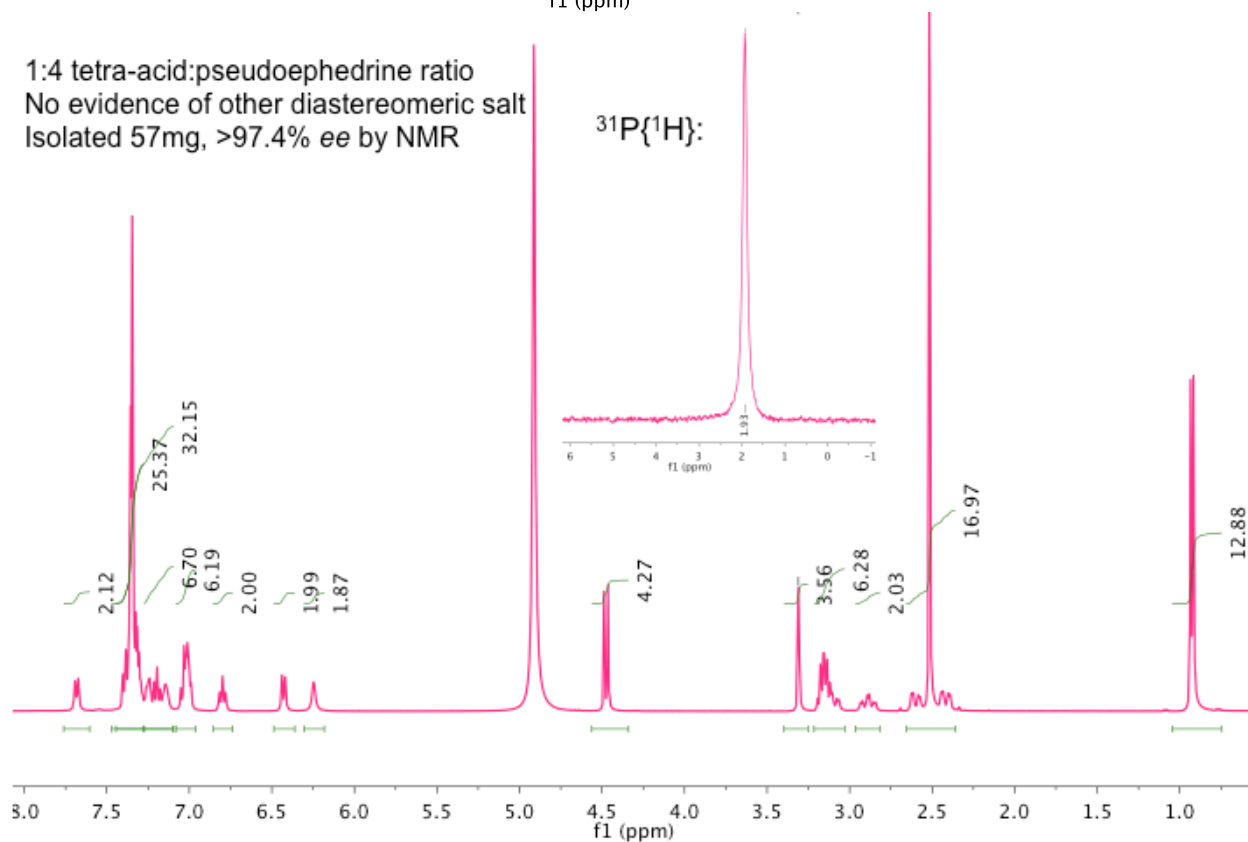
D1309251118_MLA2244-6.005.11.fid

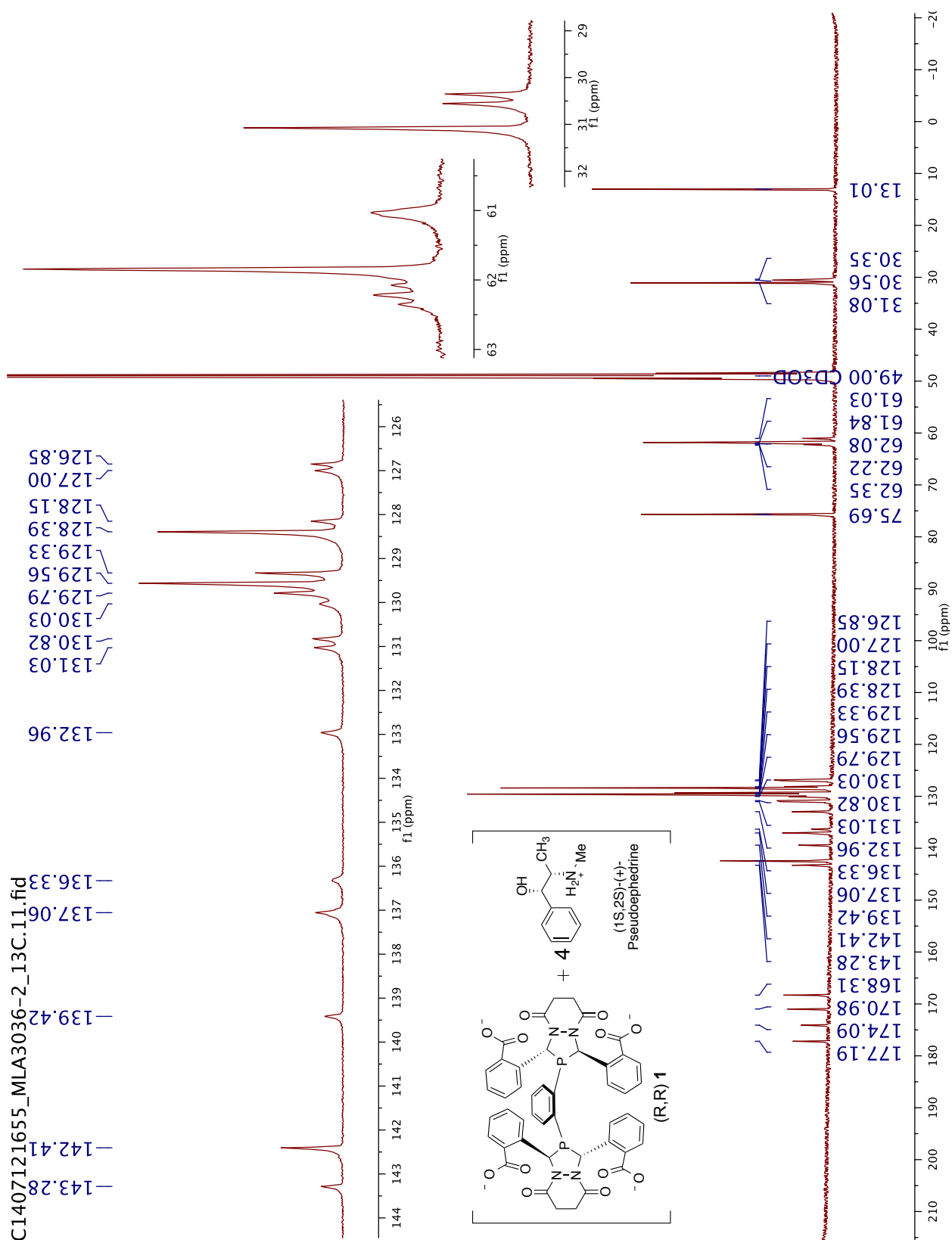
Racemic tetra-acid + 4 eq pseudoephedrine,
mother liquor from recrystallization of crude solids

1:6.0 ratio

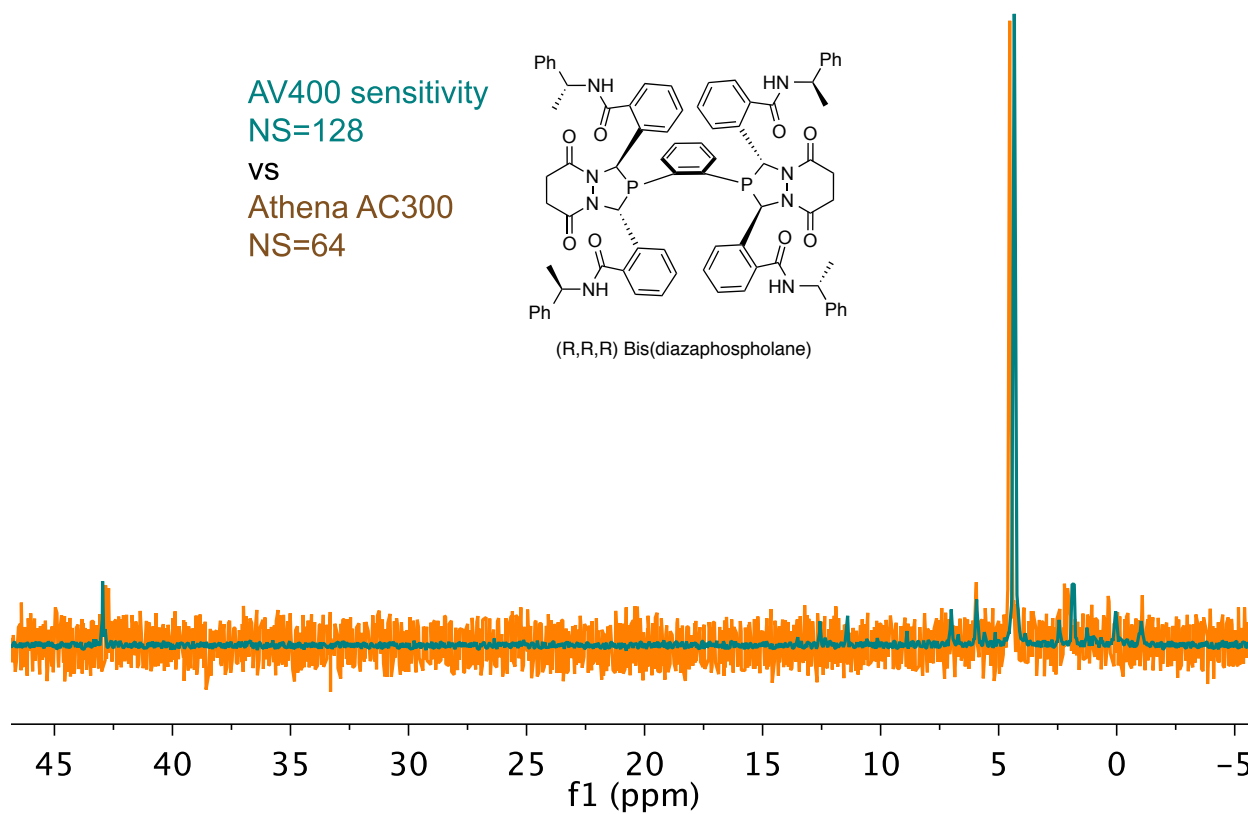
f1 (ppm)

1:4 tetra-acid:pseudoephedrine ratio
No evidence of other diastereomeric salt
Isolated 57mg, >97.4% ee by NMR

³¹P{¹H}:¹H NMR of (R,R) tetra-acid (S,S) pseudoephedrine salt

$^{13}\text{C}\{^1\text{H}\}$ NMR of (R,R) tetra-acid (S,S)pseudoephedrine salt

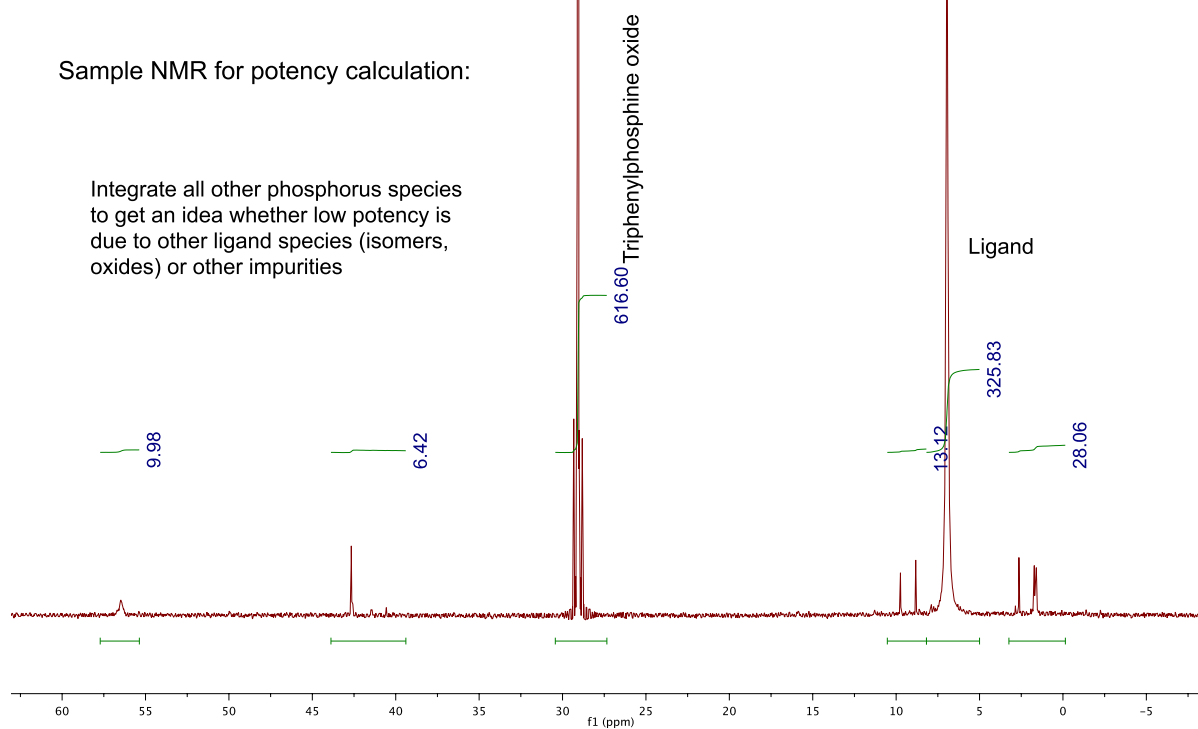
Spectra on older, less sensitive NMR instrument made it difficult to see ligand impurities.



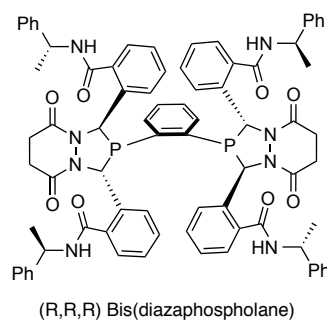
MLA3083_col_F3.1-9.3.2.fid

Sample NMR for potency calculation:

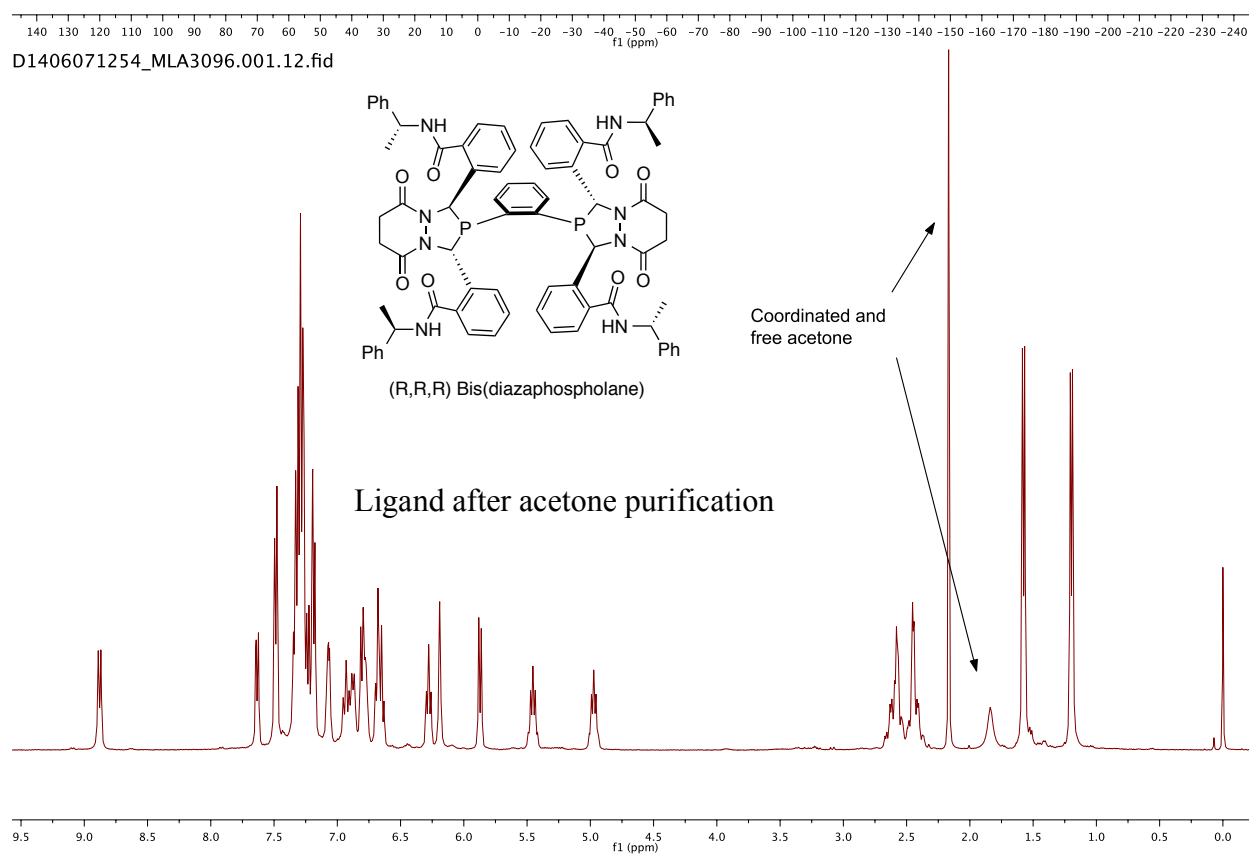
Integrate all other phosphorus species to get an idea whether low potency is due to other ligand species (isomers, oxides) or other impurities



Parameter	Value
D1406071254_MLA3096.001.11.fid	
Title	D1406071254_MLA3096.001.11.fid
Comment	Group Landis P31CPD CDCl ₃ / home/ mabrams/ av400 mabrams [2 At - 201]
Origin	Bruker BioSpin GmbH
Solvent	CDCl ₃
Temperature	297.3
Pulse Sequence	zgpg30
Experiment	1D
Number of Scans	512
Receiver Gain	193
Relaxation Delay	2.0000
Pulse Width	15.0000
Acquisition Time	0.5112
Acquisition Date	2014-06-07T13:08:00
Modification Date	2014-06-07T13:30:22
expno	
Spectrometer Frequency	161.99
Spectral Width	64102.6
Lowest Frequency	-40151.1
Nucleus	31P
Acquired Size	32768
Spectral Size	65536

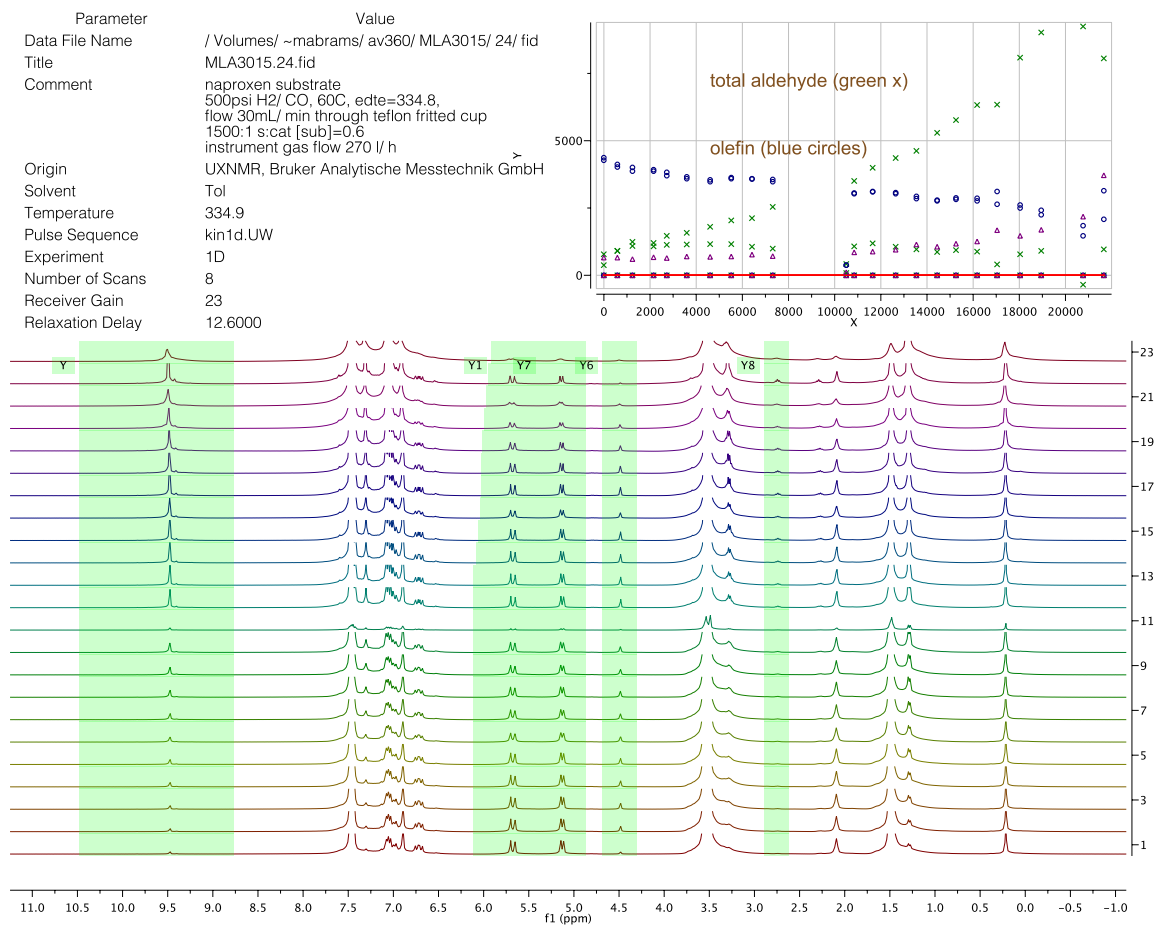


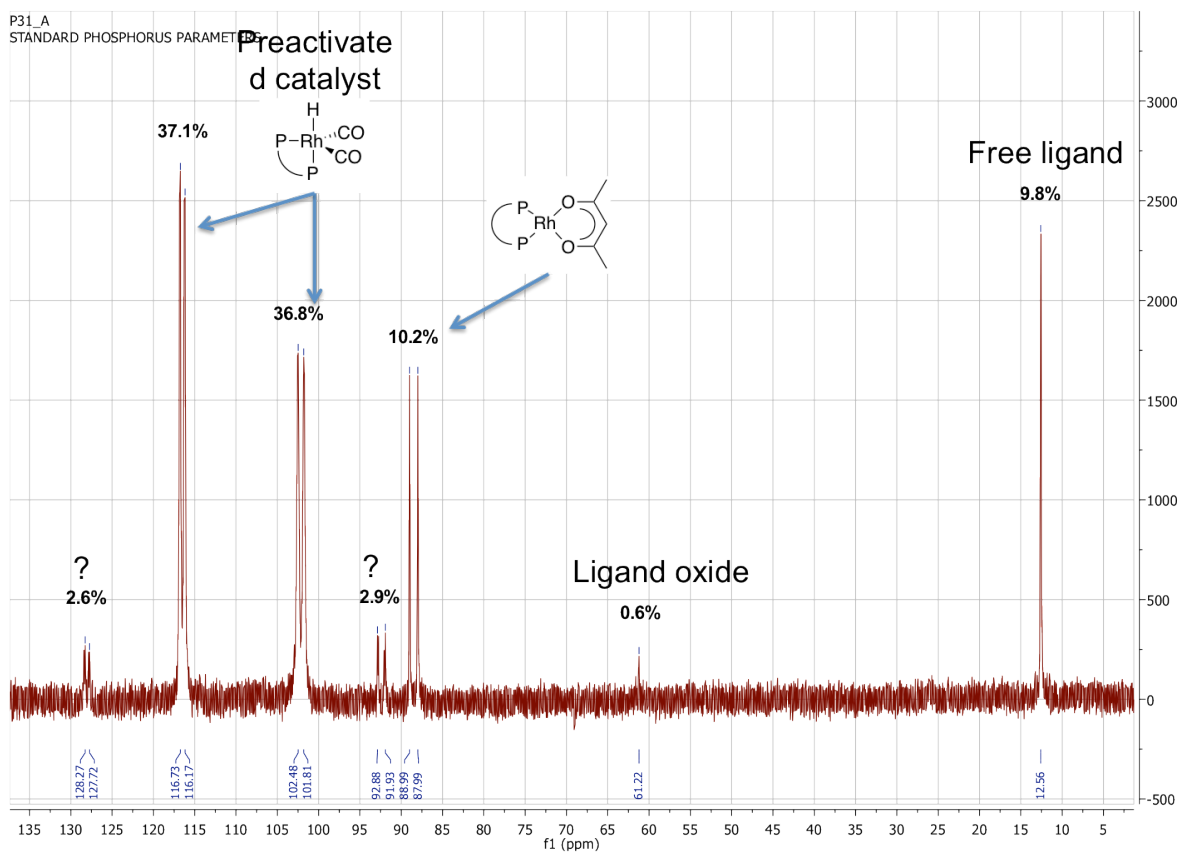
Ligand after acetone purification
NS=512



Chapter 5: Spectra and supporting data.

Timecourse with integrals graph for starved HP-NMR run (naproxen)



^{31}P NMR of pre-activated catalyst

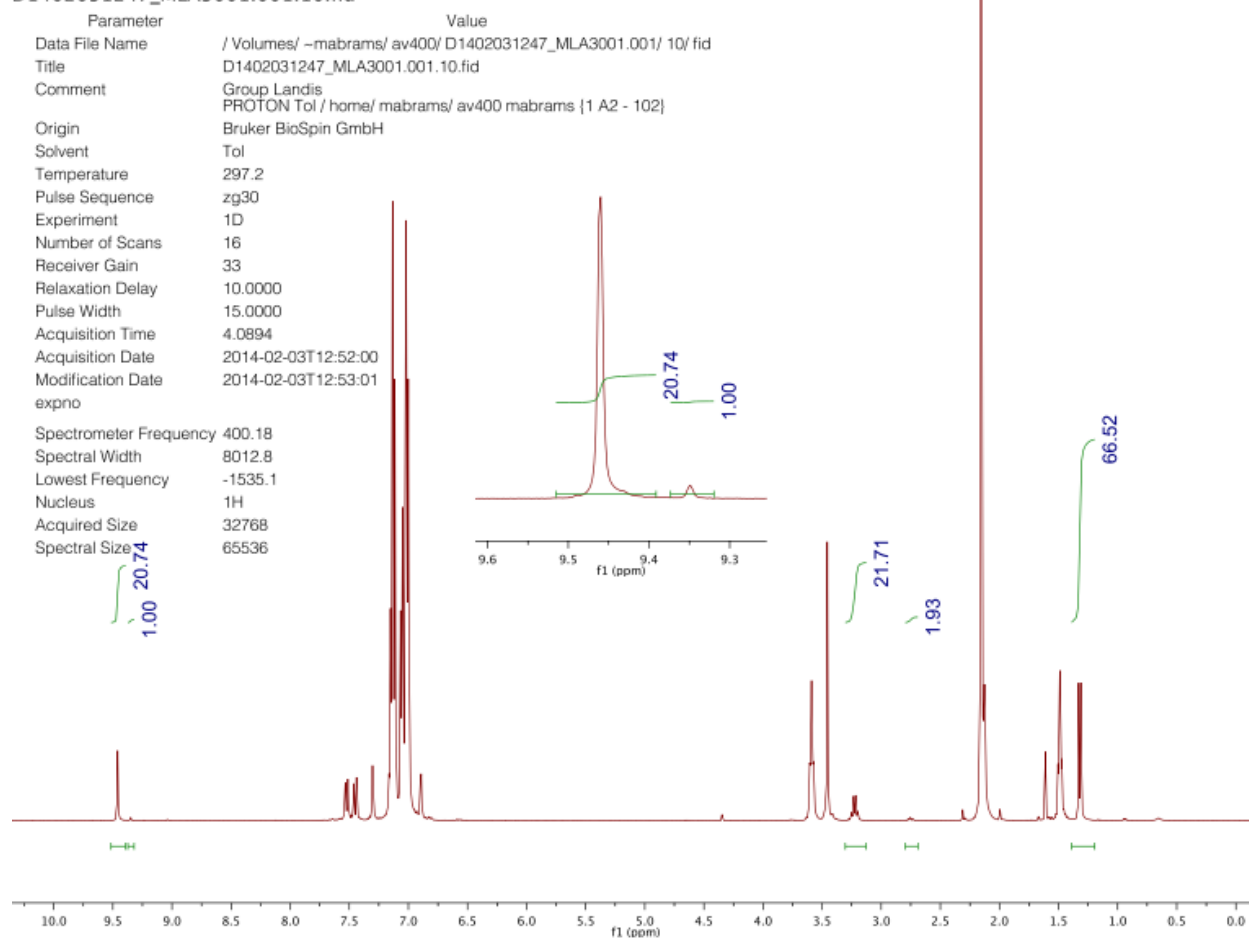
Endeavor runs during July 2014 Eli Lilly visit

<u>Run</u>	<u>Sampl</u> <u>e</u>	<u>SM</u>	<u>BP1</u>	<u>BP2</u>	<u>LP</u>	<u>ee</u>	<u>B/L</u>	<u>Conditions</u>
Day 1 Batch Runs	-032- B1	3.6	86.2	4.6	5.6	89.9	16.2	preact/new cat, new ole, 60C, 400#
	-032- B2	3.3	84.1	6.2	6.4	86.3	14.1	new cat, new ole, 60C, 400#
	-032- B3	8.5	82.6	3.9	5	91.0	17.3	new cat, old ole, 60C, 400#
	-032- B4	5.3	85.1	4	5.6	91.0	15.9	old cat, new ole, 60C, 400#
	-032- B5	5.8	82.3	3.8	8	91.2	10.8	new cat, new ole, 60C, 150#
	-032- B6	48.8	46	2.5	2.7	89.7	18.0	new cat, new ole, 42C, 300#
	-032- B7	55.2	38.9	3.2	2.7	84.8	15.6	new cat, new ole, 40C, 400#
	-032- B8	57.8	38.3	1.7	2.2	91.5	18.2	new cat, new ole, 40C, 150#
	All runs at S/C=1343 for 6h							
Day 2 Batch Runs	-032- B21	58.4	35.2	3.5	2.8	81.9	13.8	39C, 400#, S/C=1343
	-032- B22	51.3	40.9	4.6	3.2	79.8	14.2	41C, 400#, S/C=1343
	-032- B23	100	ND	ND	ND	ND	ND	Endeavor failure
	-032- B24	6.8	79.7	6.3	7.2	85.3	11.9	60C, 400#, S/C=1343
	-032- B25	47.1	42.3	4.8	5.8	79.6	8.1	60C, 400#, S/C=5983
	-032- B26	0.8	86.1	5	8.1	89.0	11.2	70C, 400#, S/C=1343
	-032- B27	0.8	77.5	12.1	9.6	73.0	9.3	80C, 400#, S/C=1343
	-032- B28	0.8	53.7	29.8	15.7	28.6	5.3	100C, 400#, S/C=1343
	All runs for 6h.							
Thurs. AM Runs	-032- B31	64.9	31.99	1.47	1.64	91.2	20.4	pre-act cat, 40C, 400#, S/C=1343
	-032- B32	49.44	46.26	1.65	2.64	93.1	18.1	pre-act cat, 40C, 150#, S/C=1343
	-032- B33	10.38	78.07	3.71	7.85	90.9	10.4	pre-act cat, 60C, 150#, S/C=1343
	-032- B34	27.34	65.44	2.8	4.42	91.8	15.4	pre-act cat, 60C, 400#, S/C=1343
	-032- B35	21.04	71.89	2.88	4.19	92.3	17.8	not pre-act cat from Wed, 60C, 400#, S/C=1343
	-032- B36	22.91	70.02	2.87	4.2	92.1	17.4	not pre-act cat from Mon., 60C, 400#, S/C=1343
	-032- B37	1.65	79.94	5.83	12.59	86.4	6.8	pre-act cat, 70C, 150#, S/C=1343
	-032-	2.41	85.23	4.3	8.07	90.4	11.1	pre-act cat, 70C, 400#, S/C=1343

B38		All runs for 3h.						
Thurs. PM Runs	-032-B41	64.12	31.59	1.37	2.92	91.7	11.3	pre-act cat, 40C, 400#, S/C=1343
	-032-B42	48.8	45.84	2.02	3.34	91.6	14.3	pre-act cat, 40C, 150#, S/C=1343
	-032-B43	27.34	63.59	3.02	6.05	90.9	11.0	pre-act cat, 60C, 150#, S/C=1343
	-032-B44	14.07	75.35	3.85	6.74	90.3	11.8	pre-act cat, 60C, 400#, S/C=1343
	-032-B45	23.49	68.76	3.03	4.71	91.6	15.2	not pre-act cat from Wed, 60C, 400#, S/C=1343
	-032-B46	22.87	69.26	3.03	4.84	91.6	14.9	not pre-act cat from Mon., 60C, 400#, S/C=1343
	-032-B47	1.76	80	5.95	12.3	86.2	7.0	pre-act cat, 70C, 150#, S/C=1343
	-032-B48	3.75	83.92	4.73	7.6	89.3	11.7	pre-act cat, 70C, 400#, S/C=1343
	All runs for 3h.							
Fri. AM Runs	-032-B51	66.36	30.83	1.58	1.23	90.2	26.3	pre-act cat, 40C, 400#, S/C=1343
	-032-B52	53.64	42.87	1.47	2.02	93.4	22.0	pre-act cat, 40C, 150#, S/C=1343
	-032-B53	10.99	77.47	3.74	7.8	90.8	10.4	pre-act cat, 60C, 150#, S/C=1343
	-032-B54	15.48	75.38	3.52	5.63	91.1	14.0	pre-act cat, 60C, 400#, S/C=1343
	-032-B55	20.7	71.05	3.57	4.68	90.4	15.9	not pre-act cat from Wed, 60C, 400#, S/C=1343
	-032-B56	21.94	70.45	3.24	4.38	91.2	16.8	not pre-act cat from Mon., 60C, 400#, S/C=1343
	-032-B57	1.82	79.53	5.64	13.01	86.8	6.5	pre-act cat, 70C, 150#, S/C=1343
	-032-B58	6.94	81.22	4.28	7.56	90.0	11.3	pre-act cat, 70C, 400#, S/C=1343
	All runs for 3h.							

Representative naproxen aldehyde **3** ^1H NMR (crude, Tol- d_8)

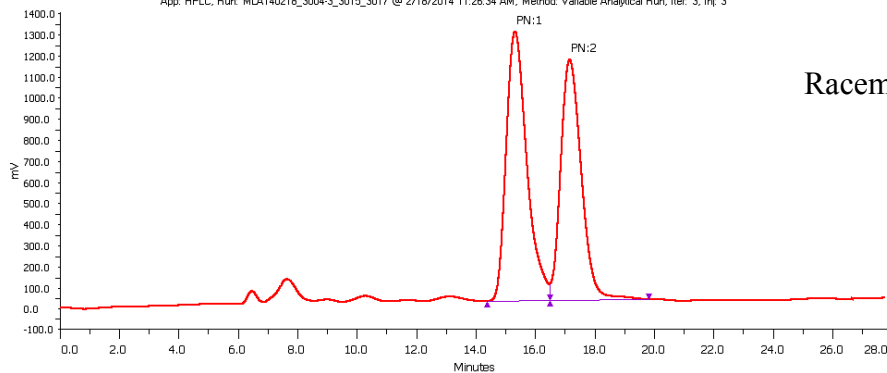
D1402031247_MLA3001.001.10.fid



HPLC traces of naproxen aldehyde **3****Graph**

Sample Name MLA3001_rac_1D_0.7_ft_4
Application Name HPLC (Administrator)
Method Name Variable Analytical Run
Configuration Name Configuration 1
Version 12
Data Instrument Name Detector
Data Channel Name WL 2
Notes
Injection Number 3

App: HPLC, Run: MLA140218_3004-3_3015_3017 @ 2/18/2014 11:26:34 AM, Method: Variable Analytical Run, Iter: 3, Inj: 3



Racemic run

Sample Table

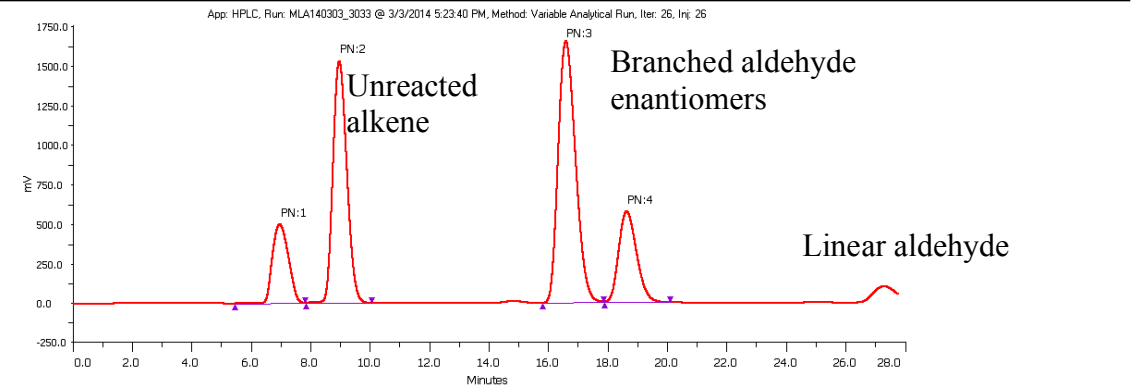
Sample Name	Peak Name	Retention Time (min)	Area (uVmin x100)	Area %	Height (mV)	Notes	Plate Number	Peak Width 10% (min)	
MLA3001_rac_1D_0.7_ft_4	1	15.337	103248481.0724	52.878	1275.245		2415.627	1.497	
MLA3001_rac_1D_0.7_ft_4	2	17.178	92008518.6025	47.122	1138.154		2948.772	1.364	

Run Variables

Name	Type	Value
#Sample Well	Well	6
#Column	VALVEMATE POSITION	1

Graph	
Sample Name	MLA3033-B_2
Application Name	HPLC (Administrator)
Method Name	Variable Analytical Run
Configuration Name	Configuration 1
Version	12
Data Instrument Name	Detector
Data Channel Name	WL 2
Notes	
Injection Number	26

Enantioenriched run

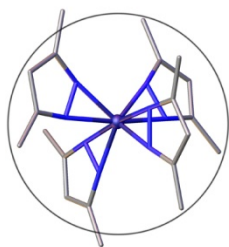


Sample Table									
Sample Name	Peak Name	Retention Time (min)	Area (uVmin x100)	Area %	Height (mV)	Notes	Plate Number	Peak Width 10% (min)	
MLA3033-B_2	1	6.975	30842755.8249	11.622	498.447		713.872	0.977	
MLA3033-B_2	2	8.982	82927054.1651	31.249	1528.916		1703.996	0.915	
MLA3033-B_2	3	16.611	111834285.0118	42.142	1651.061		3706.358	1.145	
MLA3033-B_2	4	18.66	39772300.4251	14.987	572.785		4521.651	1.183	

Run Variables		
Name	Type	Value

Appendix C

Crystal structure of tetra-acid/pseudoephedrine salt



MOLECULAR STRUCTURE LABORATORY

DR. MATT BENNING (BRUKER), PROF. KATRINA FOREST, DR. ILIA
A. GUZEI, DR. KEN SATYSHUR (UW-MADISON)

University of Wisconsin-Madison
2124 Chemistry Department
1101 University Ave
Madison, WI 53706

☎ 608-263-4694
Fax 608-262-0381

E-mail: iguzei@chem.wisc.edu

Low quality structure – connectivity and absolute configuration only

Structural report on Landis48

JUNE 11, 2014

Crystallographic Experimental Section

Data Collection

A colorless crystal with approximate dimensions $0.40 \times 0.30 \times 0.20 \text{ mm}^3$ was selected under oil under ambient conditions and attached to the tip of a MiTeGen MicroMount©. The crystal was mounted in a stream of cold nitrogen at 100(1) K and centered in the X-ray beam by using a video camera.

The crystal evaluation and data collection were performed on a Bruker Venture diffractometer with Cu K_α ($\lambda = 1.54178 \text{ \AA}$) radiation.

The initial cell constants were obtained from three series of ω scans at different starting angles. The reflections were successfully indexed by an automated indexing routine built in the APEXII program. The final cell constants were calculated from a set of 9813 strong reflections from the actual data collection.

The data were collected by using the full sphere data collection routine to survey the reciprocal space to the extent of a full sphere to a resolution of 0.82 \AA . A total of 127871 data were harvested by collecting 10 sets of frames with 0.5° scans in ω and ϕ with an exposure time 60 sec per frame. These highly redundant datasets were corrected for Lorentz and polarization effects. The absorption correction was based on fitting a function to the empirical transmission surface as sampled by multiple equivalent measurements. [1]

Structure Solution and Refinement

The systematic absences in the diffraction data were uniquely consistent for the space group $P2_12_12_1$ that yielded chemically reasonable and computationally stable results of refinement [2-4].

A successful solution by the direct methods provided most non-hydrogen atoms from the E -map. The remaining non-hydrogen atoms were located in an alternating series of least-squares cycles and difference Fourier maps. All non-hydrogen atoms were refined with anisotropic displacement coefficients unless otherwise specified. All hydrogen atoms were included in the

structure factor calculation at idealized positions and were allowed to ride on the neighboring atoms with relative isotropic displacement coefficients.

The atomic connectivity, absolute structure, and absolute configuration were unequivocally established by this X-ray single-crystal study. All chiral centers in the two diphosphine anions are R whereas the chiral carbons in the eight protonated pseudoephedrine cations are S, (Fig 1,2). The two anions have very similar geometries and so do the eight cations (Fig. 3,4). Despite numerous recrystallizations and multiple data collections on several crystals at different temperatures the data and refinement quality is substandard. Whereas the connectivity and composition of the main molecules have been reliably established, they were refined with restraints and constraints, and it was not possible to identify and properly refine solvent molecules occupying lattice voids.

There are two quadruply deprotonated diphosphine anions and eight singly protonated pseudoephedrine cations in the asymmetric unit. Additionally there are unidentified solvent molecules in the lattice – all positions of atoms in these solvent molecules were modelled as oxygen atoms (most of them with partial occupancy, and all of them with identical isotropic displacement coefficients).

All phenyl groups were refined with an idealized geometry.

There are disordered fragments in the structure, in all cases the disorder is over two positions in a 1:1 ratio.

In molecule P1 the benzoate at C27 is disordered over two positions. The disordered atoms were refined isotropically. Atoms O5 and O6 are also disordered due to rotation of the carboxylate and were refined isotropically.

Similarly, in molecule P2 the benzoate at C27 and atoms O5a and O6a are disordered and were refined isotropically. The carboxylate groups involving atoms O5, O6, O5a, O6a were refined with restraints.

Only protonated pseudoephedrine cations N5, N5b, and N5e were refined anisotropically, the rest – isotropically. Atom C54a is almost sp²-hybridized and attempt to impose a tetrahedral geometry on it were unfruitful. Within four groups of atoms C47A - C52A, C47B - C52B, C47D - C52D, C47F - C52F all atoms were constrained to have the same anisotropic displacement parameters.

The final least-squares refinement of 1550 parameters against 35688 data resulted in residuals R (based on F^2 for $I \geq 2\sigma$) and wR (based on F^2 for all data) of 0.1501 and 0.4728, respectively. The final difference Fourier map contained several peaks (smaller than ca. ~ 1.2 e/Å³) that were considered either noise or minor positions of disordered solvent molecules.

Summary

Crystal Data for C₈₆H₉₆N₈O_{24.21}P₂ ($M=1690.99$ g/mol): orthorhombic, space group P2₁2₁2₁ (no. 19), $a = 19.2424(6)$ Å, $b = 19.6060(7)$ Å, $c = 50.4378(16)$ Å, $V = 19028.5(11)$ Å³, $Z = 8$, $T = 100$ K, $\mu(\text{CuK}\alpha) = 1.022$ mm⁻¹, $D_{\text{calc}} = 1.181$ g/cm³, 127871 reflections measured ($4.836^\circ \leq 2\theta \leq 145.31^\circ$), 35688 unique ($R_{\text{int}} = 0.0382$, $R_{\text{sigma}} = 0.0325$) which were used in all calculations. The final R_1 was 0.1501 ($I > 2\sigma(I)$) and wR_2 was 0.4728 (all data).

References

- [1] Bruker-AXS. (2007-2014) APEX2 (Ver. 2014.1-1), SADABS (2012-1), and SAINT+ (Ver. 8.32A) Software Reference Manuals. Bruker-AXS, Madison, Wisconsin, USA.
- [2] Sheldrick, G. M. (2008) SHELXL. *Acta Cryst.* **A64**, 112-122.
- [3] Dolomanov, O.V.; Bourhis, L.J.; Gildea, R.J.; Howard, J.A.K.; Puschmann, H. "OLEX2: a complete structure solution, refinement and analysis program". *J. Appl. Cryst.* (2009) **42**, 339-341.
- [4] Guzei, I.A. (2013). Internal laboratory computer programs Gn.

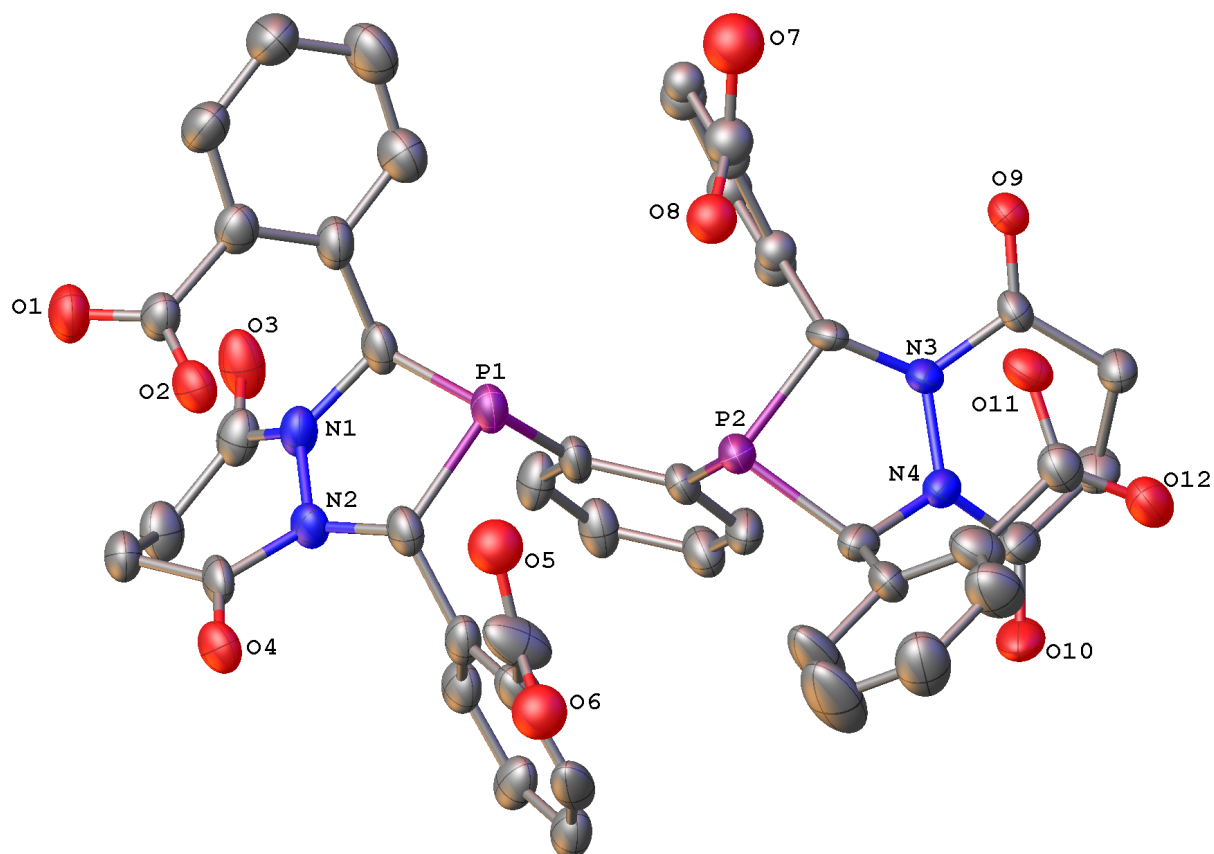


Figure 1. A molecular drawing of one symmetry-independent diphosphine anion shown with 30% probability ellipsoids. One part of the disorder and H atoms are omitted for clarity.

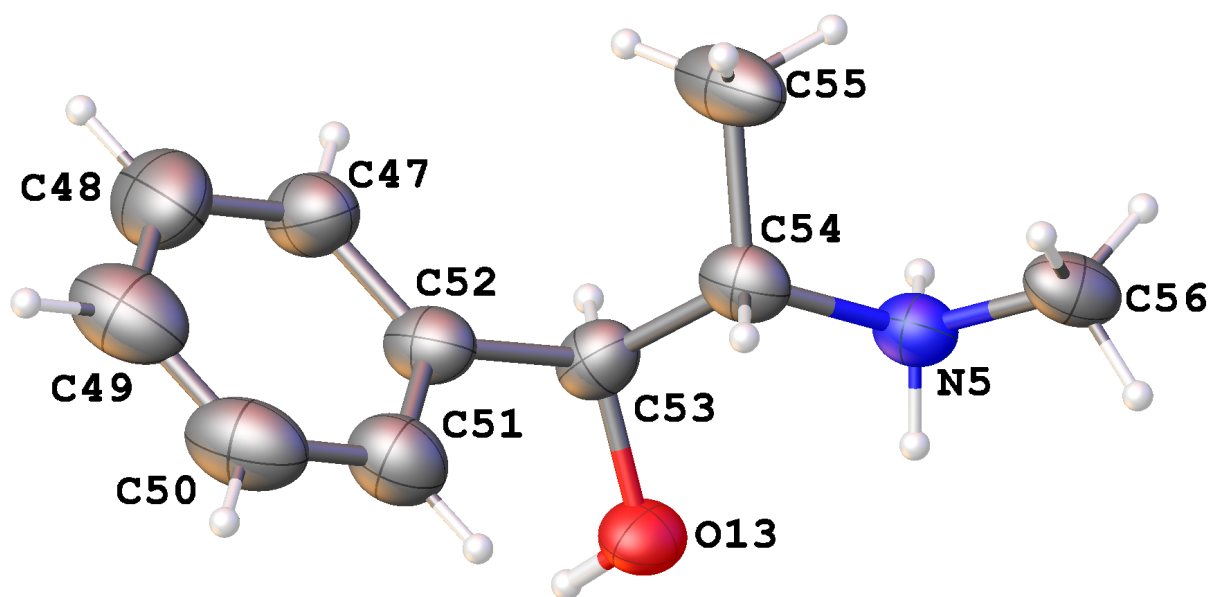


Figure 2. A molecular drawing of one symmetry-independent protonated pseudoephedrine cation shown with 30% probability ellipsoids.

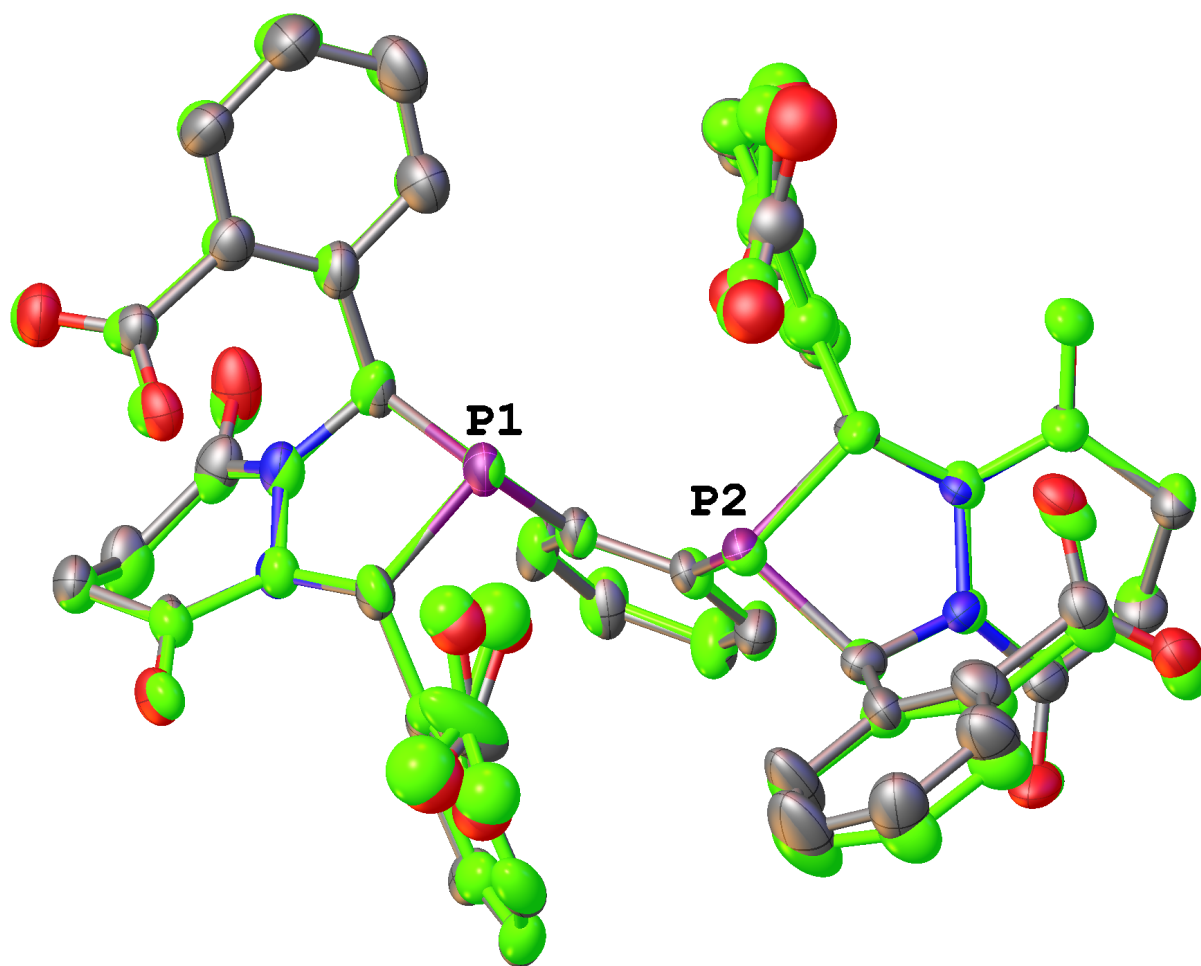


Figure 3. A superposition of the diphosphine anions. All disorder component are included but the H atoms are omitted.

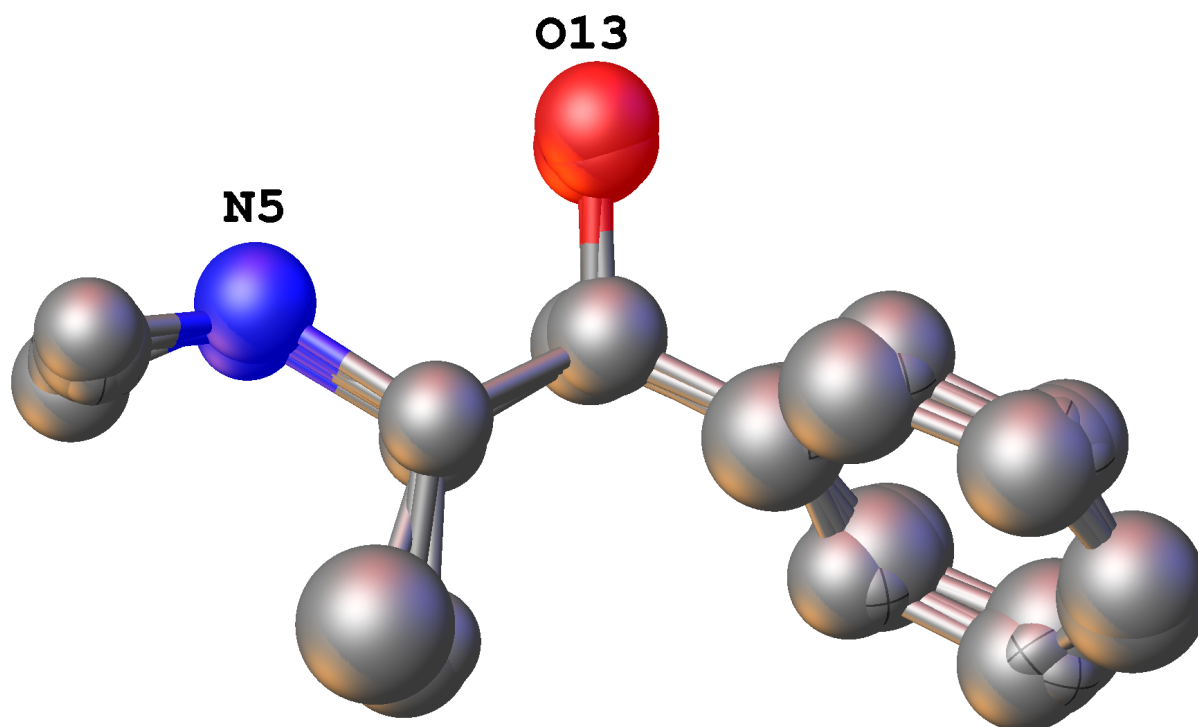


Figure 4. A superposition of the eight protonated pseudoephedrine cations. All H atoms are omitted.

Table 1 Crystal data and structure refinement for Landis48.

Identification code	Landis48
Empirical formula	C ₄₆ H ₃₂ N ₄ O ₁₂ P ₂ x 4 C ₁₀ H ₁₆ NO x solvent (8.21 O)
Formula weight	1690.99
Temperature/K	100
Crystal system	orthorhombic
Space group	P2 ₁ 2 ₁ 2 ₁
a/Å	19.2424(6)
b/Å	19.6060(7)
c/Å	50.4378(16)
α/°	90
β/°	90
γ/°	90
Volume/Å ³	19028.5(11)
Z	8
ρ _{calc} /cm ³	1.181
μ/mm ⁻¹	1.022
F(000)	7133.0
Crystal size/mm ³	0.4 × 0.3 × 0.2
Radiation	CuKα (λ = 1.54178)
2θ range for data collection/°	4.836 to 145.31
Index ranges	-23 ≤ h ≤ 23, -18 ≤ k ≤ 24, -61 ≤ l ≤ 61
Reflections collected	127871
Independent reflections	35688 [R _{int} = 0.0382, R _{sigma} = 0.0325]
Data/restraints/parameters	35688/85/1550
Goodness-of-fit on F ²	1.010
Final R indexes [I ≥ 2σ (I)]	R ₁ = 0.1501, wR ₂ = 0.4166
Final R indexes [all data]	R ₁ = 0.1688, wR ₂ = 0.4728
Largest diff. peak/hole / e Å ⁻³	1.20/-0.85
Flack parameter	0.03(5)

Table 2 Fractional Atomic Coordinates (×10⁴) and Equivalent Isotropic Displacement Parameters (Å²×10³) for Landis48. U_{eq} is defined as 1/3 of the trace of the orthogonalised U_{ij} tensor.

Atom	x	y	z	U(eq)
P1	1580.3 (12)	7998.4 (14)	3224.7 (5)	59.4 (5)
P2	3166.0 (11)	7979.8 (13)	3039.5 (4)	54.4 (5)
N3	3843 (4)	7587 (4)	2597.8 (13)	51.3 (15)

C27	3285(5)	8041(5)	2669.5(14)	55(2)
O7	2204(15)	9578(14)	2285(4)	104(7)
O8	2617(10)	9310(9)	2684(3)	69(4)
C28	2620(4)	7849(6)	2512(2)	47(4)
C29	2448(5)	7170(5)	2466(2)	49(3)
C30	1852(6)	7007(6)	2324(2)	57(4)
C31	1428(5)	7524(7)	2227(2)	60(4)
C32	1600(5)	8203(6)	2272(2)	46(3)
C33	2195(5)	8365(5)	2414(2)	44(3)
C34	2372(13)	9112(14)	2462(4)	66(5)
O7C	2430(20)	9814(15)	2321(6)	133(10)
O8C	2831(14)	9495(12)	2714(4)	95(6)
C28C	2625(5)	8037(7)	2521(3)	59(5)
C29C	2381(7)	7387(7)	2461(3)	81(7)
C30C	1772(8)	7310(8)	2315(3)	76(6)
C31C	1407(6)	7881(10)	2230(3)	81(6)
C32C	1651(6)	8530(8)	2290(3)	69(5)
C33C	2260(6)	8608(7)	2435(3)	59(4)
C34C	2526(16)	9328(14)	2500(5)	85(8)
O1	-989(4)	8602(6)	3563.9(17)	82(2)
O2	103(4)	8927(4)	3624.2(14)	67.4(17)
O3	-405(5)	6798(5)	3267.9(19)	89(3)
O4	876(4)	7997(4)	4086.7(13)	65.1(16)
O5	2453(9)	9040(9)	3658(4)	83(5)
O6	3241(10)	8867(9)	3968(3)	84(5)
O5C	2622(8)	8837(8)	3580(2)	64(3)
O6C	2934(16)	9057(10)	3993(3)	107(7)
O9	3874(3)	7971(4)	2171.9(11)	57.0(14)
O10	5036(5)	6660(5)	2983.8(18)	85(3)
O11	4803(4)	8752(4)	2601.1(13)	64.9(16)
O12	5788(5)	8174(6)	2696.5(15)	81(2)
N1	396(4)	7500(5)	3439.8(16)	61.1(18)
N2	845(4)	7645(5)	3661.3(14)	56.8(17)
N4	4288(4)	7414(4)	2816.1(14)	54.0(16)
C1	647(5)	7749(6)	3183.5(18)	62(2)
C2	197(4)	8306(4)	3058.4(13)	66(2)
C3	291(5)	8368(5)	2786.3(13)	88(4)
C4	-100(5)	8837(6)	2643.2(10)	99(4)
C5	-585(5)	9244(5)	2772.2(14)	102(5)
C6	-680(4)	9181(5)	3044.3(14)	89(4)
C7	-289(4)	8712(4)	3187.4(10)	66(2)
C8	-403(5)	8747(6)	3481.9(18)	61(2)

C9	-95(5)	7015(6)	3467(2)	70(3)
C10	-258(6)	6830(7)	3749(3)	77(3)
C11	-184(5)	7460(7)	3926(2)	69(3)
C12	539(5)	7734(5)	3902.2(18)	58(2)
C13	1519(5)	7956(5)	3599.1(17)	59(2)
C14	2111(3)	7557(3)	3736.6(12)	61(2)
C15	2039(3)	6855(3)	3763.5(13)	67(2)
C16	2569(4)	6473(3)	3877.3(14)	75(3)
C17	3172(3)	6793(4)	3964.0(13)	73(3)
C18	3245(3)	7495(4)	3937.1(13)	84(4)
C19	2714(3)	7877(3)	3823.3(13)	76(3)
C20	2795(8)	8662(7)	3808(2)	100(5)
C21	1989(5)	7180(6)	3146.8(17)	61(2)
C22	1635(5)	6563(6)	3169(2)	70(3)
C23	1957(6)	5926(7)	3129(2)	72(3)
C24	2647(6)	5920(7)	3061(2)	72(3)
C25	3012(5)	6542(7)	3041(2)	70(3)
C26	2693(4)	7165(6)	3076.4(16)	56(2)
C35	4152(4)	7641(5)	2349.0(16)	51.6(18)
C36	4828(5)	7246(5)	2321.7(18)	58(2)
C37	4859(6)	6645(5)	2504(2)	69(3)
C38	4757(5)	6883(6)	2790(2)	62(2)
C39	4091(4)	7684(5)	3068.4(18)	58(2)
C40	4576(4)	8215(4)	3186.7(12)	66(2)
C41	4468(5)	8342(7)	3454.6(12)	116(7)
C42	4874(7)	8823(8)	3585.7(13)	148(11)
C43	5387(6)	9176(7)	3448.7(18)	106(5)
C44	5495(5)	9049(6)	3180.7(16)	99(4)
C45	5089(5)	8569(5)	3049.7(11)	80(3)
C46	5250(6)	8476(6)	2756(2)	66(2)
P1A	5391.8(15)	4125.0(13)	4279.8(4)	61.1(6)
P2A	5354.0(13)	5693.3(12)	4470.0(4)	58.4(5)
N3A	4946(4)	6319(4)	4925.3(15)	53.9(16)
C27A	5440(6)	5794(4)	4842.1(17)	58(2)
O7A	7205(11)	4748(11)	5167(4)	85(5)
O8A	6882(9)	5301(10)	4794(4)	72(5)
C28A	5434(7)	5125(5)	4983(3)	64(6)
C29A	4776(7)	4872(8)	5040(4)	83(7)
C30A	4704(8)	4264(8)	5179(4)	86(7)
C31A	5290(10)	3910(6)	5262(3)	66(5)
C32A	5949(8)	4163(6)	5206(3)	67(5)
C33A	6021(7)	4771(6)	5067(3)	56(4)

C34A	6729(12)	4970(12)	5007(5)	65(6)
O7B	6985(12)	4645(12)	5243(4)	91(6)
O8B	6769(9)	5184(10)	4863(4)	69(5)
C28B	5286(6)	5127(4)	4997(2)	48(4)
C29B	4595(6)	4961(6)	5044(3)	61(4)
C30B	4432(6)	4373(6)	5185(3)	62(4)
C31B	4959(8)	3952(5)	5278(2)	60(4)
C32B	5650(7)	4119(5)	5231(2)	47(3)
C33B	5814(6)	4706(5)	5090(2)	49(4)
C34B	6545(13)	4855(13)	5067(5)	69(6)
O1A	5975(6)	1592(4)	3918.3(16)	81(2)
O2A	6339(4)	2669(4)	3866.0(15)	71.7(18)
O3A	4123(6)	2200(4)	4190.3(19)	87(3)
O4A	5461(4)	3513(4)	3413.3(11)	60.1(15)
O5A	6522(9)	4949(8)	3858(4)	76(4)
O6A	6390(11)	5803(10)	3578(4)	101(6)
O5B	6356(12)	5128(15)	3932(3)	105(7)
O6B	6560(11)	5458(17)	3521(4)	119(8)
O9A	5349(4)	6329(3)	5341.2(12)	61.5(15)
O10A	3934(4)	7482(4)	4546.1(16)	71.9(19)
O11A	6066(4)	7349(4)	4911.4(13)	64.5(16)
O12A	5440(5)	8290(4)	4829.7(16)	81(2)
N1A	4897(5)	2997(5)	4047.2(17)	67(2)
N2A	5078(5)	3443(4)	3835.5(15)	58.8(17)
N4A	4749(4)	6761(4)	4707.6(14)	53.6(16)
C1A	5142(8)	3186(5)	4305(2)	74(3)
C2A	5698(4)	2751(4)	4429.1(12)	71(3)
C3A	5729(5)	2820(4)	4703.2(12)	85(4)
C4A	6183(6)	2418(5)	4849.7(10)	101(5)
C5A	6607(5)	1947(5)	4722.1(14)	97(4)
C6A	6576(5)	1878(4)	4448.1(15)	80(3)
C7A	6122(5)	2280(4)	4301.6(10)	70(2)
C8A	6144(7)	2169(6)	4004(2)	70(3)
C9A	4387(7)	2500(5)	4005(3)	76(3)
C10A	4202(8)	2381(7)	3718(3)	85(3)
C11A	4877(6)	2464(5)	3555(2)	65(2)
C12A	5181(5)	3166(5)	3586.2(17)	55.2(19)
C13A	5385(6)	4091(5)	3902.5(16)	58(2)
C14A	5017(3)	4693(3)	3768.9(11)	57(2)
C15A	4300(3)	4654(3)	3738.3(12)	64(2)
C16A	3940(3)	5191(4)	3622.2(13)	70(3)
C17A	4296(5)	5767(3)	3536.6(13)	80(4)

C18A	5013(5)	5806(3)	3567.2(13)	88(4)
C19A	5374(3)	5269(4)	3683.3(13)	73(3)
C20A	6165(9)	5311(8)	3707(2)	138(10)
C21A	4556(6)	4524(5)	4349.3(17)	60(2)
C22A	3936(8)	4165(6)	4327(2)	75(3)
C23A	3295(7)	4460(6)	4369(3)	77(3)
C24A	3284(7)	5147(7)	4438(3)	85(3)
C25A	3885(6)	5520(5)	4466(2)	67(2)
C26A	4527(5)	5223(5)	4433.6(17)	58(2)
C35A	5010(5)	6606(5)	5163.1(19)	59(2)
C36A	4570(6)	7256(5)	5209(2)	65(2)
C37A	3975(5)	7269(5)	5021(2)	61(2)
C38A	4191(5)	7186(5)	4741(2)	61(2)
C39A	5039(6)	6580(5)	4450.5(18)	60(2)
C40A	5551(4)	7086(3)	4332.9(12)	63(2)
C41A	5697(6)	6987(4)	4065.7(12)	92(4)
C42A	6135(7)	7435(5)	3933.3(11)	117(7)
C43A	6428(6)	7983(5)	4068.0(15)	94(4)
C44A	6283(5)	8082(4)	4335.2(15)	85(3)
C45A	5844(4)	7633(4)	4467.6(10)	71(3)
C46A	5767(6)	7772(6)	4761(2)	69(3)
O13G	-3065(9)	6835(9)	2500(3)	132(4)
N5G	-3216(11)	7456(11)	2977(4)	126(5)
C47G	-1177(8)	6834(8)	2546(3)	130(7)
C48G	-603(6)	6952(11)	2385(4)	153(9)
C49G	-675(8)	7327(12)	2153(4)	198(15)
C50G	-1322(10)	7584(10)	2082(3)	133(7)
C51G	-1896(7)	7466(8)	2243(3)	140(7)
C52G	-1824(6)	7091(7)	2475(3)	97(4)
C53G	-2398(13)	6969(14)	2637(5)	128(6)
C54G	-2550(11)	7627(11)	2826(4)	112(5)
C55G	-1897(18)	7730(19)	3031(6)	159(10)
C56G	-3357(12)	7814(13)	3218(4)	121(6)
O13E	-1106(5)	8575(5)	4356(2)	85(2)
N5E	-52(5)	9239(5)	4152.5(16)	66(2)
C47E	-2490(5)	9685(5)	4133.4(13)	87(3)
C48E	-3075(4)	10008(6)	4235.7(19)	109(5)
C49E	-3147(5)	10091(6)	4508(2)	95(4)
C50E	-2633(6)	9851(6)	4678.1(14)	108(5)
C51E	-2049(5)	9528(6)	4575.8(14)	89(4)
C52E	-1977(4)	9445(5)	4303.5(14)	80(3)
C53E	-1324(6)	9123(6)	4199(2)	70(3)

C54E	-710(7)	9629(6)	4210(2)	73(3)
C55E	-787(11)	10224(8)	4014(4)	114(6)
C56E	593(7)	9630(7)	4187(2)	76(3)
O13D	3538(8)	10103(9)	4825(3)	123(4)
N5D	4359(6)	9762(6)	4419(2)	85(3)
C47D	3974(13)	11831(14)	4874(4)	183(5)
C48D	4154(15)	12306(11)	5066(5)	183(5)
C49D	4518(15)	12101(13)	5291(4)	183(5)
C50D	4701(13)	11420(14)	5322(4)	183(5)
C51D	4522(15)	10945(11)	5130(5)	183(5)
C52D	4158(15)	11151(13)	4905(5)	183(5)
C53D	3910(13)	10627(13)	4710(5)	123(6)
C54D	4541(9)	10356(9)	4580(3)	96(4)
C55D	4992(10)	10895(10)	4454(4)	102(4)
C56D	4935(10)	9261(10)	4321(4)	102(4)
O13	3989(4)	6574(5)	1888.6(17)	74.1(19)
N5	3299(4)	7600(5)	1660.8(17)	64.8(19)
C47	2888(6)	5204(5)	1646.4(13)	92(4)
C48	2561(6)	4625(5)	1745(2)	117(6)
C49	2460(6)	4551(5)	2016(2)	116(6)
C50	2687(6)	5055(6)	2189.1(15)	116(6)
C51	3014(6)	5634(5)	2090.9(14)	93(4)
C52	3115(5)	5709(4)	1819.6(15)	75(3)
C53	3437(6)	6356(6)	1718(2)	67(2)
C54	2913(5)	6933(7)	1718(2)	70(3)
C55	2321(8)	6828(11)	1516(3)	107(6)
C56	2896(6)	8223(8)	1692(2)	75(3)
O13F	1244(5)	9587(5)	3474.9(18)	83(2)
N5F	2422(6)	9756(6)	3189(2)	81(2)
C47F	96(8)	10639(8)	3108(2)	123(2)
C48F	-404(7)	11137(8)	3154(3)	123(2)
C49F	-370(7)	11536(7)	3382(3)	123(2)
C50F	164(8)	11437(8)	3563(2)	123(2)
C51F	664(7)	10939(8)	3517(3)	123(2)
C52F	630(7)	10540(7)	3290(3)	123(2)
C53F	1172(7)	9986(7)	3244(3)	81(3)
C54F	1887(7)	10317(7)	3196(3)	79(3)
C55F	1923(9)	10726(9)	2950(3)	96(4)
C56F	3162(9)	9999(9)	3222(3)	92(4)
O13A	2994(7)	8741(7)	963(2)	108(3)
N5A	2791(7)	9913(7)	659(3)	93(3)
C47A	1915(11)	7626(12)	599(3)	156(4)

C48A	1404(12)	7143(10)	651(4)	156(4)
C49A	1018(10)	7182(10)	883(4)	156(4)
C50A	1143(11)	7704(11)	1063(3)	156(4)
C51A	1654(11)	8187(10)	1011(4)	156(4)
C52A	2040(10)	8148(10)	779(4)	156(4)
C53A	2568(10)	8676(10)	741(4)	105(5)
C54A	2286(9)	9330(10)	647(4)	99(4)
C55A	1640(20)	9640(30)	528(9)	216(17)
C56A	2589(12)	10613(12)	693(4)	120(6)
O13B	4071(5)	3208(4)	3123.9(19)	80(2)
N5B	5013(5)	4054(4)	2921.4(16)	61.8(18)
C47B	2630(6)	3950(8)	2775(2)	115(2)
C48B	1936(5)	4111(8)	2820(2)	115(2)
C49B	1695(4)	4194(8)	3078(3)	115(2)
C50B	2147(6)	4115(8)	3291(2)	115(2)
C51B	2841(5)	3954(8)	3246(2)	115(2)
C52B	3082(4)	3871(8)	2988(3)	115(2)
C53B	3820(6)	3701(6)	2935(2)	67(2)
C54B	4302(7)	4306(5)	2964(2)	69(3)
C55B	4141(8)	4870(8)	2760(3)	93(4)
C56B	5614(8)	4554(6)	2975(2)	77(3)
O13C	575(5)	6546(5)	4330.3(17)	80(2)
N5C	1398(4)	7481(4)	4566.0(17)	59.2(17)
C47C	1135(7)	5117(6)	4722.8(17)	107(5)
C48C	1291(10)	4431(6)	4687(3)	150(9)
C49C	1460(10)	4189(5)	4436(3)	154(9)
C50C	1475(9)	4632(7)	4221(2)	141(8)
C51C	1319(7)	5318(6)	4257.2(17)	99(4)
C52C	1150(6)	5561(5)	4507.9(19)	80(3)
C53C	996(5)	6303(5)	4538(2)	61(2)
C54C	1650(6)	6754(6)	4540(2)	67(2)
C55C	2165(8)	6575(8)	4753(3)	83(3)
C56C	1941(7)	7997(7)	4535(3)	77(3)
O14	5320(20)	4760(20)	2207(7)	90.7(9)
O15	5592(6)	5105(6)	2271(2)	90.7(9)
O16	7396(13)	6884(18)	4731(5)	90.7(9)
O17	7412(9)	7217(13)	4709(3)	90.7(9)
O18	2338(19)	2244(19)	3568(7)	90.7(9)
O19	2580(13)	3200(13)	3916(5)	90.7(9)
O20	-3281(10)	5550(10)	2589(4)	90.7(9)
O21	7885(8)	6072(8)	4990(3)	90.7(9)
O22	2093(15)	10014(15)	3890(5)	90.7(9)

O23	554(19)	5234(19)	3544(7)	90.7(9)
O24	8360(20)	6090(20)	3190(7)	90.7(9)
O25	7553(14)	6502(14)	3579(5)	90.7(9)
O26	3410(6)	8739(6)	4496(2)	90.7(9)
O27	7610(15)	4703(15)	3632(5)	90.7(9)
O28	-801(6)	6244(6)	4383(2)	90.7(9)
O30	3822(8)	10108(8)	3923(3)	90.7(9)
O31	2240(20)	10040(20)	1797(7)	90.7(9)
O32	4422(7)	9111(7)	5099(2)	90.7(9)
O33	3614(7)	1906(7)	3056(2)	90.7(9)
O34	-1769(6)	7358(6)	4300(2)	90.7(9)
O35	5012(8)	5722(8)	1334(3)	90.7(9)
O36	7900(20)	4390(20)	3899(8)	90.7(9)
O37	-2015(10)	7741(10)	3780(3)	90.7(9)
O38	5291(6)	5961(6)	1858(2)	90.7(9)
O39	6307(6)	6108(6)	3058(2)	90.7(9)
O40	1974(13)	895(13)	4297(5)	90.7(9)
O41	3128(11)	1266(11)	3997(4)	90.7(9)
O42	2580(20)	1680(20)	3518(9)	90.7(9)

Table 3 Anisotropic Displacement Parameters ($\text{\AA}^2 \times 10^3$) for Landis48. The Anisotropic displacement factor exponent takes the form: $-2\pi^2[h^2a^{*2}U_{11}+2hka^*b^*U_{12}+\dots]$.

Atom	U_{11}	U_{22}	U_{33}	U_{23}	U_{13}	U_{12}
P1	50.3(10)	74.7(14)	53.2(11)	-6.6(10)	12.9(9)	3.3(10)
P2	46.5(10)	71.3(13)	45.3(10)	10.9(9)	7.6(8)	8.2(9)
N3	47(3)	65(4)	41(3)	19(3)	5(3)	10(3)
C27	62(4)	71(5)	33(3)	13(3)	0(3)	20(4)
O1	63(4)	107(6)	76(4)	-11(4)	18(4)	7(4)
O2	73(4)	73(4)	56(3)	-11(3)	13(3)	1(3)
O3	81(5)	101(6)	87(5)	-36(5)	25(4)	-23(5)
O4	72(4)	70(4)	53(3)	-11(3)	15(3)	1(3)
O9	55(3)	69(4)	47(3)	12(3)	8(2)	1(3)
O10	74(4)	96(6)	85(5)	47(5)	12(4)	29(4)
O11	75(4)	69(4)	50(3)	13(3)	2(3)	-6(3)
O12	73(5)	111(7)	60(4)	8(4)	8(3)	-4(5)
N1	44(3)	83(5)	56(4)	-13(4)	8(3)	0(4)
N2	51(4)	79(5)	41(3)	-12(3)	5(3)	5(3)
N4	42(3)	68(4)	52(4)	16(3)	4(3)	8(3)
C1	55(4)	83(6)	49(4)	-16(4)	17(4)	-1(4)
C2	54(5)	82(6)	62(5)	-9(5)	16(4)	5(4)

C3	88(8)	109(10)	66(6)	-4(6)	11(6)	9(7)
C4	107(10)	127(12)	63(6)	-21(7)	13(7)	-3(9)
C5	81(8)	139(14)	86(8)	14(9)	3(7)	30(9)
C6	65(6)	129(12)	72(6)	-9(7)	-6(5)	25(7)
C7	53(5)	82(6)	62(5)	-12(5)	0(4)	0(4)
C8	50(4)	79(6)	55(4)	-12(4)	5(4)	8(4)
C9	57(5)	75(6)	79(6)	-22(5)	8(4)	4(5)
C10	63(5)	81(7)	85(7)	-7(6)	17(5)	-14(5)
C11	53(5)	91(7)	63(5)	-1(5)	16(4)	11(5)
C12	54(4)	66(5)	55(5)	-2(4)	25(4)	15(4)
C13	58(4)	70(5)	49(4)	-8(4)	17(4)	3(4)
C14	46(4)	86(6)	52(4)	-15(4)	10(3)	3(4)
C15	61(5)	84(7)	58(5)	-17(4)	13(4)	11(5)
C16	61(5)	101(8)	64(5)	-29(5)	0(4)	19(6)
C17	54(5)	105(9)	61(5)	-17(5)	5(4)	9(5)
C18	50(5)	160(14)	43(4)	-7(6)	-4(4)	-12(7)
C19	72(6)	109(9)	48(4)	-2(5)	6(4)	-17(6)
C20	116(11)	109(10)	74(7)	24(7)	-11(7)	-62(9)
C21	44(4)	95(7)	44(4)	-4(4)	14(3)	2(4)
C22	50(4)	79(6)	82(6)	-22(5)	14(4)	4(4)
C23	63(5)	86(7)	68(6)	-20(5)	20(5)	-11(5)
C24	74(6)	78(6)	63(5)	8(5)	23(5)	9(5)
C25	57(5)	86(7)	66(5)	18(5)	19(4)	23(5)
C26	47(4)	81(6)	41(4)	11(4)	12(3)	3(4)
C35	51(4)	62(4)	42(4)	8(3)	14(3)	1(4)
C36	55(4)	64(5)	55(4)	9(4)	11(4)	11(4)
C37	75(6)	57(5)	76(6)	20(4)	9(5)	11(4)
C38	49(4)	73(6)	63(5)	24(4)	7(4)	3(4)
C39	47(4)	76(6)	53(4)	21(4)	1(3)	3(4)
C40	58(4)	97(7)	41(4)	14(4)	11(4)	11(5)
C41	101(10)	200(20)	44(5)	-5(8)	6(6)	-50(12)
C42	139(16)	250(30)	58(7)	-34(11)	5(9)	-53(19)
C43	86(8)	146(15)	87(8)	-21(9)	2(7)	-17(10)
C44	91(9)	135(13)	70(7)	-1(8)	-9(6)	-23(9)
C45	91(8)	86(7)	62(6)	17(5)	0(5)	-10(6)
C46	64(5)	76(6)	60(5)	1(4)	7(4)	-7(5)
P1A	74.9(14)	60.4(12)	47.8(10)	-11.5(9)	-0.2(10)	14.4(11)
P2A	64.7(12)	60.8(12)	49.7(10)	-8.5(9)	-10.5(9)	12.9(10)
N3A	55(4)	56(4)	51(3)	-11(3)	-10(3)	3(3)
C27A	73(5)	48(4)	53(4)	-8(3)	-17(4)	20(4)
O1A	109(6)	63(4)	71(4)	-7(3)	9(4)	11(4)
O2A	77(4)	76(4)	62(4)	-5(3)	7(3)	9(4)

O3A	107(6)	59(4)	94(5)	-8(4)	36(5)	-11(4)
O4A	67(4)	72(4)	41(3)	-10(3)	2(3)	8(3)
O9A	73(4)	61(3)	51(3)	-5(3)	-14(3)	-2(3)
O10A	75(4)	66(4)	75(4)	-1(3)	-28(4)	18(3)
O11A	53(3)	91(5)	50(3)	-2(3)	-9(3)	-12(3)
O12A	97(6)	75(5)	69(4)	-16(4)	-1(4)	1(4)
N1A	82(5)	60(4)	60(4)	-12(3)	13(4)	6(4)
N2A	74(5)	53(4)	49(4)	-10(3)	4(3)	5(3)
N4A	57(4)	50(3)	54(4)	-9(3)	-11(3)	14(3)
C1A	114(9)	46(4)	62(5)	-1(4)	18(6)	14(5)
C2A	98(8)	58(5)	55(5)	-7(4)	5(5)	3(5)
C3A	129(11)	72(6)	54(5)	1(5)	7(6)	14(7)
C4A	140(14)	97(10)	66(7)	4(6)	3(8)	13(10)
C5A	116(11)	89(9)	87(8)	23(7)	0(8)	13(8)
C6A	96(8)	75(6)	67(6)	2(5)	8(6)	16(6)
C7A	85(7)	59(5)	66(5)	5(4)	11(5)	3(5)
C8A	80(6)	66(6)	66(5)	8(5)	0(5)	14(5)
C9A	84(7)	52(5)	91(7)	-8(5)	23(6)	6(5)
C10A	96(8)	68(6)	90(8)	-10(6)	6(7)	1(6)
C11A	82(6)	53(5)	61(5)	-10(4)	-5(5)	7(4)
C12A	60(4)	60(5)	46(4)	-9(3)	-3(3)	3(4)
C13A	73(5)	60(4)	41(4)	-18(3)	1(4)	5(4)
C14A	83(6)	48(4)	39(3)	-5(3)	-3(4)	4(4)
C15A	79(6)	65(5)	47(4)	-4(4)	7(4)	10(5)
C16A	89(7)	65(5)	56(5)	-5(4)	9(5)	17(5)
C17A	129(11)	58(5)	54(5)	1(4)	18(6)	20(6)
C18A	146(13)	71(7)	48(5)	1(4)	-3(6)	-19(8)
C19A	95(7)	77(6)	47(4)	-11(4)	5(5)	-24(6)
C20A	190(20)	157(17)	63(7)	31(9)	-31(10)	-97(17)
C21A	80(6)	59(5)	42(4)	-7(3)	6(4)	19(4)
C22A	100(8)	60(5)	65(5)	-20(4)	11(5)	6(5)
C23A	72(6)	65(6)	95(8)	-22(5)	11(6)	-11(5)
C24A	78(7)	80(7)	98(8)	-33(7)	4(6)	6(6)
C25A	68(6)	57(5)	76(6)	-28(4)	-10(5)	8(4)
C26A	62(5)	63(5)	50(4)	-17(4)	-5(4)	9(4)
C35A	63(5)	58(5)	55(4)	-6(4)	-15(4)	8(4)
C36A	67(5)	58(5)	69(5)	-16(4)	0(5)	13(4)
C37A	55(4)	59(5)	68(5)	-13(4)	-7(4)	7(4)
C38A	57(4)	60(5)	64(5)	-13(4)	-16(4)	8(4)
C39A	82(6)	50(4)	48(4)	-7(3)	-15(4)	2(4)
C40A	75(6)	60(5)	54(4)	4(4)	-6(4)	12(4)
C41A	143(13)	82(7)	52(5)	-2(5)	0(7)	-13(8)

C42A	178(19)	125(13)	48(6)	14(7)	12(8)	-36(13)
C43A	106(10)	112(11)	65(6)	4(7)	14(6)	-4(9)
C44A	83(7)	94(8)	78(7)	10(6)	-3(6)	-1(7)
C45A	75(6)	77(6)	61(5)	10(5)	-9(5)	7(5)
C46A	67(5)	75(6)	65(5)	-5(5)	-5(5)	-24(5)
O13E	73(5)	80(5)	101(6)	19(4)	11(4)	18(4)
N5E	80(5)	65(4)	53(4)	5(3)	13(4)	8(4)
C47E	81(7)	98(9)	81(7)	13(7)	5(6)	19(7)
C48E	86(9)	103(11)	138(14)	29(10)	3(9)	18(8)
C49E	90(8)	78(7)	118(11)	0(7)	36(8)	18(7)
C50E	123(13)	113(12)	88(9)	8(8)	33(9)	10(10)
C51E	99(9)	100(9)	68(6)	-1(6)	21(6)	1(8)
C52E	94(8)	71(6)	76(6)	3(5)	22(6)	19(6)
C53E	70(6)	78(6)	62(5)	-1(5)	8(5)	17(5)
C54E	92(7)	65(5)	63(5)	-11(4)	18(5)	13(5)
C55E	135(13)	83(8)	125(11)	43(8)	61(11)	47(9)
C56E	79(7)	78(6)	70(6)	9(5)	4(5)	-11(5)
O13	52(3)	83(5)	87(5)	-4(4)	-9(3)	7(3)
N5	55(4)	80(5)	59(4)	8(4)	0(3)	-4(4)
C47	96(9)	100(9)	79(7)	17(7)	-10(7)	-24(8)
C48	98(11)	114(13)	140(15)	21(11)	-12(10)	-35(10)
C49	74(8)	160(18)	113(12)	45(12)	8(8)	1(10)
C50	89(9)	169(19)	90(9)	39(11)	2(8)	-15(11)
C51	86(8)	112(10)	81(8)	18(7)	6(6)	0(8)
C52	62(5)	95(8)	69(6)	16(6)	0(5)	-17(5)
C53	68(5)	76(6)	58(5)	0(4)	9(4)	-17(5)
C54	59(5)	93(7)	58(5)	15(5)	9(4)	-7(5)
C55	75(7)	142(14)	103(9)	60(10)	-22(7)	-38(9)
C56	57(5)	104(8)	63(5)	2(5)	-2(4)	21(5)
O13B	84(5)	59(4)	97(5)	7(4)	-16(4)	-10(4)
N5B	77(5)	57(4)	52(4)	-6(3)	5(4)	-3(4)
C47B	88(4)	116(5)	141(6)	25(5)	8(4)	8(4)
C48B	88(4)	116(5)	141(6)	25(5)	8(4)	8(4)
C49B	88(4)	116(5)	141(6)	25(5)	8(4)	8(4)
C50B	88(4)	116(5)	141(6)	25(5)	8(4)	8(4)
C51B	88(4)	116(5)	141(6)	25(5)	8(4)	8(4)
C52B	88(4)	116(5)	141(6)	25(5)	8(4)	8(4)
C53B	75(6)	63(5)	63(5)	1(4)	-5(5)	18(5)
C54B	100(8)	49(4)	57(5)	1(4)	19(5)	10(5)
C55B	95(9)	101(9)	84(7)	26(7)	39(7)	40(8)
C56B	107(9)	65(6)	57(5)	-11(4)	8(5)	-30(6)

Table 4 Bond Lengths for Landis48.

Atom	Atom	Length/Å	Atom	Atom	Length/Å
P1	C1	1.873(10)	C1A	C2A	1.505(14)
P1	C13	1.894(9)	C2A	C3A	1.3900
P1	C21	1.831(11)	C2A	C7A	1.3900
P2	C27	1.884(8)	C3A	C4A	1.3900
P2	C26	1.849(11)	C4A	C5A	1.3900
P2	C39	1.877(9)	C5A	C6A	1.3900
N3	C27	1.440(11)	C6A	C7A	1.3900
N3	N4	1.435(10)	C7A	C8A	1.517(12)
N3	C35	1.393(10)	C9A	C10A	1.50(2)
C27	C28	1.554(11)	C10A	C11A	1.547(19)
C27	C28C	1.475(11)	C11A	C12A	1.505(14)
O7	C34	1.32(2)	C13A	C14A	1.532(11)
O8	C34	1.27(3)	C14A	C15A	1.3900
C28	C29	1.3900	C14A	C19A	1.3900
C28	C33	1.3900	C15A	C16A	1.3900
C29	C30	1.3900	C16A	C17A	1.3900
C30	C31	1.3900	C17A	C18A	1.3900
C31	C32	1.3900	C18A	C19A	1.3900
C32	C33	1.3900	C19A	C20A	1.530(17)
C33	C34	1.52(3)	C21A	C22A	1.389(18)
O7C	C34C	1.33(3)	C21A	C26A	1.436(13)
O8C	C34C	1.27(3)	C22A	C23A	1.378(19)
C28C	C29C	1.3900	C23A	C24A	1.393(17)
C28C	C33C	1.3900	C24A	C25A	1.376(18)
C29C	C30C	1.3900	C25A	C26A	1.375(15)
C30C	C31C	1.3900	C35A	C36A	1.546(13)
C31C	C32C	1.3900	C36A	C37A	1.487(15)
C32C	C33C	1.3900	C37A	C38A	1.479(15)
C33C	C34C	1.54(3)	C39A	C40A	1.518(12)
O1	C8	1.233(14)	C40A	C41A	1.3900
O2	C8	1.260(13)	C40A	C45A	1.3900
O3	C9	1.244(15)	C41A	C42A	1.3900
O4	C12	1.246(13)	C42A	C43A	1.3900
O5	C20	1.246(9)	C43A	C44A	1.3900
O6	C20	1.245(9)	C44A	C45A	1.3900
O5C	C20	1.243(9)	C45A	C46A	1.514(12)
O6C	C20	1.244(9)	O13G	C53G	1.48(3)
O9	C35	1.226(11)	N5G	C54G	1.53(3)

O10	C38	1.196(12)	N5G C56G	1.43(3)
O11	C46	1.282(14)	C47G C48G	1.3900
O12	C46	1.231(15)	C47G C52G	1.3900
N1	N2	1.441(11)	C48G C49G	1.3900
N1	C1	1.464(13)	C49G C50G	1.3900
N1	C9	1.348(15)	C50G C51G	1.3900
N2	C12	1.362(11)	C51G C52G	1.3900
N2	C13	1.466(12)	C52G C53G	1.40(3)
N4	C38	1.385(13)	C53G C54G	1.63(3)
N4	C39	1.429(13)	C54G C55G	1.64(4)
C1	C2	1.530(13)	O13E C53E	1.403(15)
C2	C3	1.3900	N5E C54E	1.508(15)
C2	C7	1.3900	N5E C56E	1.469(16)
C3	C4	1.3900	C47E C48E	1.3900
C4	C5	1.3900	C47E C52E	1.3900
C5	C6	1.3900	C48E C49E	1.3900
C6	C7	1.3900	C49E C50E	1.3900
C7	C8	1.503(10)	C50E C51E	1.3900
C9	C10	1.502(18)	C51E C52E	1.3900
C10	C11	1.530(18)	C52E C53E	1.503(12)
C11	C12	1.497(15)	C53E C54E	1.543(19)
C13	C14	1.546(11)	C54E C55E	1.536(18)
C14	C15	1.3900	O13D C53D	1.38(3)
C14	C19	1.3900	N5D C54D	1.46(2)
C15	C16	1.3900	N5D C56D	1.56(2)
C16	C17	1.3900	C47D C48D	1.3900
C17	C18	1.3900	C47D C52D	1.3900
C18	C19	1.3900	C48D C49D	1.3900
C19	C20	1.547(15)	C49D C50D	1.3900
C21	C22	1.392(17)	C50D C51D	1.3900
C21	C26	1.399(12)	C51D C52D	1.3900
C22	C23	1.407(18)	C52D C53D	1.50(3)
C23	C24	1.371(16)	C53D C54D	1.48(3)
C24	C25	1.411(19)	C54D C55D	1.51(3)
C25	C26	1.379(15)	O13 C53	1.431(14)
C35	C36	1.519(12)	N5 C54	1.531(15)
C36	C37	1.496(13)	N5 C56	1.456(16)
C37	C38	1.529(17)	C47 C48	1.3900
C39	C40	1.522(12)	C47 C52	1.3900
C40	C41	1.3900	C48 C49	1.3900
C40	C45	1.3900	C49 C50	1.3900
C41	C42	1.3900	C50 C51	1.3900

C42	C43	1.3900	C51	C52	1.3900
C43	C44	1.3900	C52	C53	1.501(12)
C44	C45	1.3900	C53	C54	1.514(18)
C45	C46	1.523(11)	C54	C55	1.542(18)
P1A	C1A	1.906(11)	O13F	C53F	1.411(17)
P1A	C13A	1.904(8)	N5F	C54F	1.507(18)
P1A	C21A	1.822(10)	N5F	C56F	1.51(2)
P2A	C27A	1.894(9)	C47F	C48F	1.3900
P2A	C26A	1.848(11)	C47F	C52F	1.3900
P2A	C39A	1.844(10)	C48F	C49F	1.3900
N3A	C27A	1.463(11)	C49F	C50F	1.3900
N3A	N4A	1.449(11)	C50F	C51F	1.3900
N3A	C35A	1.331(12)	C51F	C52F	1.3900
C27A	C28A	1.493(12)	C52F	C53F	1.524(18)
C27A	C28B	1.550(11)	C53F	C54F	1.54(2)
O7A	C34A	1.30(2)	C54F	C55F	1.48(2)
O8A	C34A	1.29(3)	O13A	C53A	1.39(2)
C28A	C29A	1.3900	N5A	C54A	1.50(2)
C28A	C33A	1.3900	N5A	C56A	1.44(3)
C29A	C30A	1.3900	C47A	C48A	1.3900
C30A	C31A	1.3900	C47A	C52A	1.3900
C31A	C32A	1.3900	C48A	C49A	1.3900
C32A	C33A	1.3900	C49A	C50A	1.3900
C33A	C34A	1.45(3)	C50A	C51A	1.3900
O7B	C34B	1.29(2)	C51A	C52A	1.3900
O8B	C34B	1.29(3)	C52A	C53A	1.46(2)
C28B	C29B	1.3900	C53A	C54A	1.47(3)
C28B	C33B	1.3900	C54A	C55A	1.50(2)
C29B	C30B	1.3900	O13B	C53B	1.442(13)
C30B	C31B	1.3900	N5B	C54B	1.471(16)
C31B	C32B	1.3900	N5B	C56B	1.539(14)
C32B	C33B	1.3900	C47B	C48B	1.3900
C33B	C34B	1.44(3)	C47B	C52B	1.3900
O1A	C8A	1.255(16)	C48B	C49B	1.3900
O2A	C8A	1.260(15)	C49B	C50B	1.3900
O3A	C9A	1.218(15)	C50B	C51B	1.3900
O4A	C12A	1.231(12)	C51B	C52B	1.3900
O5A	C20A	1.245(9)	C52B	C53B	1.484(14)
O6A	C20A	1.244(9)	C53B	C54B	1.512(17)
O5B	C20A	1.244(9)	C54B	C55B	1.542(16)
O6B	C20A	1.244(9)	O13C	C53C	1.407(14)
O9A	C35A	1.236(11)	N5C	C54C	1.511(14)

O10A	C38A	1.244(12)	N5C	C56C	1.463(16)
O11A	C46A	1.261(15)	C47C	C48C	1.3900
O12A	C46A	1.244(16)	C47C	C52C	1.3900
N1A	N2A	1.424(13)	C48C	C49C	1.3900
N1A	C1A	1.430(15)	C49C	C50C	1.3900
N1A	C9A	1.399(16)	C50C	C51C	1.3900
N2A	C12A	1.384(11)	C51C	C52C	1.3900
N2A	C13A	1.440(12)	C52C	C53C	1.493(13)
N4A	C38A	1.369(12)	C53C	C54C	1.537(15)
N4A	C39A	1.456(12)	C54C	C55C	1.501(18)

Table 5 Bond Angles for Landis48.

Atom	Atom	Atom	Angle/°	Atom	Atom	Atom	Angle/°
C1	P1	C13	92.3(4)	C6A	C7A	C2A	120.0
C21	P1	C1	99.2(5)	C6A	C7A	C8A	115.2(6)
C21	P1	C13	101.7(4)	O1A	C8A	O2A	126.0(11)
C26	P2	C27	102.4(4)	O1A	C8A	C7A	117.6(10)
C26	P2	C39	101.1(4)	O2A	C8A	C7A	116.4(10)
C39	P2	C27	88.9(4)	O3A	C9A	N1A	120.8(12)
N4	N3	C27	113.5(7)	O3A	C9A	C10A	124.3(12)
C35	N3	C27	119.9(6)	N1A	C9A	C10A	115.0(11)
C35	N3	N4	117.0(7)	C9A	C10A	C11A	107.3(11)
N3	C27	P2	107.5(5)	C12A	C11A	C10A	111.5(8)
N3	C27	C28	109.7(8)	O4A	C12A	N2A	119.3(9)
N3	C27	C28C	120.7(9)	O4A	C12A	C11A	126.9(8)
C28	C27	P2	113.1(7)	N2A	C12A	C11A	113.6(8)
C28C	C27	P2	113.6(8)	N2A	C13A	P1A	105.6(6)
C29	C28	C27	120.8(7)	N2A	C13A	C14A	112.8(7)
C29	C28	C33	120.0	C14A	C13A	P1A	114.6(5)
C33	C28	C27	119.2(7)	C15A	C14A	C13A	117.7(6)
C30	C29	C28	120.0	C15A	C14A	C19A	120.0
C29	C30	C31	120.0	C19A	C14A	C13A	122.3(6)
C32	C31	C30	120.0	C16A	C15A	C14A	120.0
C31	C32	C33	120.0	C15A	C16A	C17A	120.0
C28	C33	C34	120.9(9)	C16A	C17A	C18A	120.0
C32	C33	C28	120.0	C19A	C18A	C17A	120.0
C32	C33	C34	119.1(9)	C14A	C19A	C20A	120.6(7)
O7	C34	C33	120(2)	C18A	C19A	C14A	120.0
O8	C34	O7	118(3)	C18A	C19A	C20A	119.3(7)
O8	C34	C33	120.9(15)	O5A	C20A	C19A	124.5(11)

C29C C28C C27	114.0(9)	O6A C20A O5A	124.8(13)
C29C C28C C33C	120.0	O6A C20A C19A	110.2(13)
C33C C28C C27	126.0(9)	O5B C20A O6B	125.2(13)
C28C C29C C30C	120.0	O5B C20A C19A	110.5(14)
C31C C30C C29C	120.0	O6B C20A C19A	124.1(13)
C32C C31C C30C	120.0	C22A C21A P1A	121.7(7)
C31C C32C C33C	120.0	C22A C21A C26A	118.3(9)
C28C C33C C34C	120.5(10)	C26A C21A P1A	120.0(9)
C32C C33C C28C	120.0	C23A C22A C21A	123.0(10)
C32C C33C C34C	119.5(10)	C22A C23A C24A	117.2(12)
O7C C34C C33C	118(2)	C25A C24A C23A	121.8(12)
O8C C34C O7C	117(3)	C24A C25A C26A	121.2(10)
O8C C34C C33C	124.9(18)	C21A C26A P2A	118.2(8)
N2 N1 C1	114.9(7)	C25A C26A P2A	123.4(7)
C9 N1 N2	118.7(9)	C25A C26A C21A	118.3(10)
C9 N1 C1	123.8(9)	N3A C35A C36A	115.6(8)
N1 N2 C13	116.5(7)	O9A C35A N3A	121.2(9)
C12 N2 N1	117.2(7)	O9A C35A C36A	122.9(8)
C12 N2 C13	121.4(8)	C37A C36A C35A	109.9(8)
C38 N4 N3	119.6(8)	C38A C37A C36A	113.0(9)
C38 N4 C39	122.3(7)	O10A C38A N4A	120.0(9)
C39 N4 N3	116.0(7)	O10A C38A C37A	126.2(9)
N1 C1 P1	107.8(7)	N4A C38A C37A	113.8(8)
N1 C1 C2	114.6(7)	N4A C39A P2A	107.9(6)
C2 C1 P1	113.7(7)	N4A C39A C40A	116.0(7)
C3 C2 C1	113.3(5)	C40A C39A P2A	115.1(7)
C3 C2 C7	120.0	C41A C40A C39A	114.8(5)
C7 C2 C1	126.7(5)	C41A C40A C45A	120.0
C2 C3 C4	120.0	C45A C40A C39A	125.2(5)
C5 C4 C3	120.0	C42A C41A C40A	120.0
C4 C5 C6	120.0	C43A C42A C41A	120.0
C7 C6 C5	120.0	C42A C43A C44A	120.0
C2 C7 C8	125.9(6)	C43A C44A C45A	120.0
C6 C7 C2	120.0	C40A C45A C46A	125.3(6)
C6 C7 C8	113.9(6)	C44A C45A C40A	120.0
O1 C8 O2	125.4(9)	C44A C45A C46A	114.6(6)
O1 C8 C7	117.0(9)	O11A C46A C45A	115.1(10)
O2 C8 C7	117.5(8)	O12A C46A O11A	127.0(10)
O3 C9 N1	119.7(11)	O12A C46A C45A	117.9(10)
O3 C9 C10	125.7(11)	C56G N5G C54G	118.5(19)
N1 C9 C10	114.4(9)	C48G C47G C52G	120.0
C9 C10 C11	109.8(10)	C47G C48G C49G	120.0

C12	C11	C10	109.2(8)	C50G C49G C48G	120.0
O4	C12	N2	119.6(8)	C51G C50G C49G	120.0
O4	C12	C11	124.9(8)	C50G C51G C52G	120.0
N2	C12	C11	115.4(9)	C47G C52G C53G	119.6(14)
N2	C13	P1	106.6(6)	C51G C52G C47G	120.0
N2	C13	C14	110.2(8)	C51G C52G C53G	120.4(14)
C14	C13	P1	115.1(5)	O13G C53G C54G	104.9(18)
C15	C14	C13	118.1(6)	C52G C53G O13G	116.2(18)
C15	C14	C19	120.0	C52G C53G C54G	110.5(19)
C19	C14	C13	121.9(6)	N5G C54G C53G	105.7(17)
C14	C15	C16	120.0	N5G C54G C55G	110.6(18)
C17	C16	C15	120.0	C53G C54G C55G	109(2)
C16	C17	C18	120.0	C56E N5E C54E	114.9(9)
C19	C18	C17	120.0	C48E C47E C52E	120.0
C14	C19	C20	121.1(6)	C49E C48E C47E	120.0
C18	C19	C14	120.0	C48E C49E C50E	120.0
C18	C19	C20	118.9(6)	C49E C50E C51E	120.0
O5	C20	C19	124.7(10)	C52E C51E C50E	120.0
O6	C20	O5	124.3(13)	C47E C52E C53E	121.3(7)
O6	C20	C19	110.9(12)	C51E C52E C47E	120.0
O5C	C20	O6C	125.4(13)	C51E C52E C53E	118.7(7)
O5C	C20	C19	107.2(10)	O13E C53E C52E	111.9(9)
O6C	C20	C19	127.0(11)	O13E C53E C54E	104.0(10)
C22	C21	P1	122.3(6)	C52E C53E C54E	111.0(10)
C22	C21	C26	118.4(10)	N5E C54E C53E	108.1(9)
C26	C21	P1	119.2(9)	N5E C54E C55E	110.0(10)
C21	C22	C23	123.0(9)	C55E C54E C53E	113.0(14)
C24	C23	C22	117.9(11)	C54D N5D C56D	120.3(13)
C23	C24	C25	119.6(11)	C48D C47D C52D	120.0
C26	C25	C24	122.2(9)	C49D C48D C47D	120.0
C21	C26	P2	119.0(8)	C48D C49D C50D	120.0
C25	C26	P2	122.2(7)	C49D C50D C51D	120.0
C25	C26	C21	118.9(10)	C52D C51D C50D	120.0
N3	C35	C36	114.1(7)	C47D C52D C53D	120(2)
O9	C35	N3	120.6(7)	C51D C52D C47D	120.0
O9	C35	C36	125.2(7)	C51D C52D C53D	120(2)
C37	C36	C35	112.3(8)	O13D C53D C52D	113(2)
C36	C37	C38	109.6(9)	O13D C53D C54D	110.2(19)
O10	C38	N4	119.4(10)	C54D C53D C52D	106(2)
O10	C38	C37	126.9(10)	N5D C54D C53D	109.5(16)
N4	C38	C37	113.7(8)	N5D C54D C55D	117.6(14)
N4	C39	P2	107.3(6)	C53D C54D C55D	114.0(17)

N4	C39	C40	116.1(7)	C56	N5	C54	116.0(9)
C40	C39	P2	113.6(7)	C48	C47	C52	120.0
C41	C40	C39	114.4(5)	C47	C48	C49	120.0
C41	C40	C45	120.0	C50	C49	C48	120.0
C45	C40	C39	125.6(5)	C49	C50	C51	120.0
C42	C41	C40	120.0	C50	C51	C52	120.0
C41	C42	C43	120.0	C47	C52	C53	121.2(7)
C44	C43	C42	120.0	C51	C52	C47	120.0
C45	C44	C43	120.0	C51	C52	C53	118.7(7)
C40	C45	C46	124.6(6)	O13	C53	C52	110.7(9)
C44	C45	C40	120.0	O13	C53	C54	105.8(9)
C44	C45	C46	115.4(6)	C52	C53	C54	110.9(9)
O11	C46	C45	114.1(9)	N5	C54	C55	110.3(9)
O12	C46	O11	128.2(10)	C53	C54	N5	108.4(8)
O12	C46	C45	117.8(10)	C53	C54	C55	113.1(13)
C13AP1A	C1A		91.7(4)	C54F	N5F	C56F	114.2(11)
C21AP1A	C1A		100.3(6)	C48F	C47F	C52F	120.0
C21AP1A	C13A		101.6(4)	C49F	C48F	C47F	120.0
C26AP2A	C27A		103.1(5)	C48F	C49F	C50F	120.0
C39AP2A	C27A		89.0(4)	C51F	C50F	C49F	120.0
C39AP2A	C26A		100.5(5)	C50F	C51F	C52F	120.0
N4A	N3A	C27A	111.9(7)	C47F	C52F	C53F	120.3(10)
C35AN3A	C27A		119.8(7)	C51F	C52F	C47F	120.0
C35AN3A	N4A		117.0(7)	C51F	C52F	C53F	119.7(10)
N3A	C27AP2A		107.5(5)	O13F	C53F	C52F	109.7(11)
N3A	C27AC28A		118.4(10)	O13F	C53F	C54F	105.9(11)
N3A	C27AC28B		109.0(9)	C52F	C53F	C54F	109.6(12)
C28AC27AP2A			112.4(8)	N5F	C54F	C53F	107.9(11)
C28B	C27AP2A		113.2(7)	C55F	C54F	N5F	110.1(12)
C29AC28AC27A			114.7(9)	C55F	C54F	C53F	113.6(12)
C29AC28AC33A			120.0	C56A	N5A	C54A	123.8(16)
C33AC28AC27A			125.2(9)	C48A	C47AC52A		120.0
C30AC29AC28A			120.0	C47A	C48AC49A		120.0
C29AC30AC31A			120.0	C48A	C49AC50A		120.0
C30AC31AC32A			120.0	C51A	C50AC49A		120.0
C31AC32AC33A			120.0	C52A	C51AC50A		120.0
C28AC33AC34A			124.5(11)	C47A	C52AC53A		123.6(16)
C32AC33AC28A			120.0	C51A	C52AC47A		120.0
C32AC33AC34A			115.4(11)	C51A	C52AC53A		116.4(16)
O7A	C34AC33A		116(2)	O13A	C53AC52A		111.6(17)
O8A	C34AO7A		122(2)	O13A	C53AC54A		113.2(16)
O8A	C34AC33A		121.5(14)	C52A	C53AC54A		113.7(17)

C29B C28B C27A	117.9(7)	C53A C54A N5A	114.4(15)
C29B C28B C33B	120.0	C53A C54A C55A	142(3)
C33B C28B C27A	122.1(7)	C55A C54A N5A	104(2)
C30B C29B C28B	120.0	C54B N5B C56B	117.3(9)
C31B C30B C29B	120.0	C48B C47B C52B	120.0
C32B C31B C30B	120.0	C49B C48B C47B	120.0
C33B C32B C31B	120.0	C48B C49B C50B	120.0
C28B C33B C34B	124.5(11)	C51B C50B C49B	120.0
C32B C33B C28B	120.0	C52B C51B C50B	120.0
C32B C33B C34B	115.4(11)	C47B C52B C53B	118.9(9)
O7B C34B O8B	119(2)	C51B C52B C47B	120.0
O7B C34B C33B	121(2)	C51B C52B C53B	121.1(9)
O8B C34B C33B	119.4(14)	O13B C53B C52B	110.5(10)
N2A N1A C1A	116.1(9)	O13B C53B C54B	104.8(9)
C9A N1A N2A	119.0(9)	C52B C53B C54B	113.1(10)
C9A N1A C1A	123.5(10)	N5B C54B C53B	107.1(8)
N1A N2A C13A	117.8(7)	N5B C54B C55B	109.3(9)
C12AN2A N1A	118.3(8)	C53B C54B C55B	112.0(12)
C12AN2A C13A	120.1(8)	C56C N5C C54C	114.6(9)
N3A N4A C39A	115.4(6)	C48C C47C C52C	120.0
C38AN4A N3A	118.5(8)	C47C C48C C49C	120.0
C38AN4A C39A	123.9(8)	C50C C49C C48C	120.0
N1A C1A P1A	105.9(7)	C49C C50C C51C	120.0
N1A C1A C2A	117.8(8)	C50C C51C C52C	120.0
C2A C1A P1A	113.3(9)	C47C C52C C53C	121.8(8)
C3A C2A C1A	113.0(6)	C51C C52C C47C	120.0
C3A C2A C7A	120.0	C51C C52C C53C	118.2(8)
C7A C2A C1A	126.9(6)	O13C C53C C52C	111.6(9)
C4A C3A C2A	120.0	O13C C53C C54C	106.4(8)
C3A C4A C5A	120.0	C52C C53C C54C	113.5(9)
C4A C5A C6A	120.0	N5C C54C C53C	106.3(8)
C7A C6A C5A	120.0	C55C C54C N5C	111.8(10)
C2A C7A C8A	124.8(6)	C55C C54C C53C	114.3(10)

Table 6 Torsion Angles for Landis48.

A	B	C	D	Angle/°	A	B	C	D	Angle/°
C35	N3	C27	C28C_b	62.4(13)	N1A	N2A	C13A	P1A	-2.8(10)
P1	C1	C2	C3	76.4(7)	N1A	N2A	C13A	C14A	-128.7(8)
P1	C1	C2	C7	-106.0(7)	N1A	C1A	C2A	C3A	-158.9(9)
P1	C13	C14	C15	-86.3(7)	N1A	C1A	C2A	C7A	16.4(15)

P1	C13	C14	C19	91.4(7)	N1A	C9A	C10A	C11A	35.5(13)
P1	C21	C22	C23	-174.9(9)	N2A	N1A	C1A	P1A	17.2(11)
P1	C21	C26	P2	-4.7(10)	N2A	N1A	C1A	C2A	-110.8(11)
P1	C21	C26	C25	174.3(7)	N2A	N1A	C9A	O3A	-165.8(10)
P2	C27	C28	C29	-80.7(9)	N2A	N1A	C9A	C10A	14.0(14)
P2	C27	C28	C33	99.6(8)	N2A	C13A	C14A	C15A	36.0(8)
P2	C27	C28C	C29C	-86.8(9)	N2A	C13A	C14A	C19A	-145.0(6)
P2	C27	C28C	C33C	94.7(12)	N4A	N3A	C27A	P2A	-21.4(9)
P2	C39	C40	C41	69.9(8)	N4A	N3A	C27A	C28A	-150.0(9)
P2	C39	C40	C45	-109.4(8)	N4A	N3A	C27A	C28B	-144.4(8)
N3	C27	C28	C29	39.2(10)	N4A	N3A	C35A	O9A	-160.0(9)
N3	C27	C28	C33	-140.5(7)	N4A	N3A	C35A	C36A	26.4(13)
N3	C27	C28C	C29C	42.9(12)	N4A	C39A	C40A	C41A	-165.8(7)
N3	C27	C28C	C33C	-135.5(11)	N4A	C39A	C40A	C45A	11.3(12)
N3	N4	C38	O10	-166.6(9)	C1A	P1A	C21A	C22A	-18.4(9)
N3	N4	C38	C37	13.4(12)	C1A	P1A	C21A	C26A	160.5(8)
N3	N4	C39	P2	15.4(9)	C1A	N1A	N2A	C12A	148.0(9)
N3	N4	C39	C40	-112.8(8)	C1A	N1A	N2A	C13A	-10.1(13)
N3	C35	C36	C37	27.1(13)	C1A	N1A	C9A	O3A	0.0(17)
C27	P2	C26	C21	-108.0(7)	C1A	N1A	C9A	C10A	179.8(11)
C27	P2	C26	C25	73.1(9)	C1A	C2A	C3A	C4A	175.6(9)
C27	P2	C39	N4	-22.0(7)	C1A	C2A	C7A	C6A	-175.0(10)
C27	P2	C39	C40	107.7(6)	C1A	C2A	C7A	C8A	6.2(13)
C27	N3	N4	C38	167.1(8)	C2A	C3A	C4A	C5A	0.0
C27	N3	N4	C39	3.2(11)	C2A	C7A	C8A	O1A	-118.0(10)
C27	N3	C35	O9	-14.5(14)	C2A	C7A	C8A	O2A	62.5(13)
C27	N3	C35	C36	167.2(9)	C3A	C2A	C7A	C6A	0.0
C27	C28	C29	C30	-179.7(10)	C3A	C2A	C7A	C8A	-178.8(10)
C27	C28	C33	C32	179.7(10)	C3A	C4A	C5A	C6A	0.0
C27	C28	C33	C34	-0.5(13)	C4A	C5A	C6A	C7A	0.0
C27	C28C	C29C	C30C	-178.5(12)	C5A	C6A	C7A	C2A	0.0
C27	C28C	C33C	C32C	178.3(14)	C5A	C6A	C7A	C8A	178.9(9)
C27	C28C	C33C	C34C	-1.6(19)	C6A	C7A	C8A	O1A	63.1(13)
C28	C27	C28C	C29C	4(3)	C6A	C7A	C8A	O2A	-116.3(9)
C28	C27	C28C	C33C	-174(4)	C7A	C2A	C3A	C4A	0.0
C28	C29	C30	C31	0.0	C9A	N1A	N2A	C12A	-45.1(13)
C28	C33	C34	O7	148.1(19)	C9A	N1A	N2A	C13A	156.7(9)
C28	C33	C34	O8	-39(2)	C9A	N1A	C1A	P1A	-149.0(9)
C29	C28	C33	C32	0.0	C9A	N1A	C1A	C2A	83.1(14)
C29	C28	C33	C34	179.8(13)	C9A	C10A	C11A	C12A	-59.9(12)
C29	C30	C31	C32	0.0	C10A	C11A	C12A	O4A	-141.7(11)
C30	C31	C32	C33	0.0	C10A	C11A	C12A	N2A	33.6(13)

C31	C32	C33	C28	0.0	C12A N2A	C13A P1A	-160.6(7)
C31	C32	C33	C34	-179.8(13)	C12A N2A	C13A C14A	73.6(11)
C32	C33	C34	O7	-32(3)	C13A P1A	C21A C22A	75.5(9)
C32	C33	C34	O8	140.4(17)	C13A P1A	C21A C26A	-105.6(8)
C33	C28	C29	C30	0.0	C13A N2A	C12A O4A	-8.9(14)
C28C	C27	C28	C29	-176(4)	C13A N2A	C12A C11A	175.3(9)
C28C	C27	C28	C33	5(3)	C13A C14A	C15A C16A	179.0(6)
C28C	C29C	C30C	C31C	0.0	C13A C14A	C19A C18A	-178.9(6)
C28C	C33C	C34C	O7C	144(3)	C13A C14A	C19A C20A	3.0(10)
C28C	C33C	C34C	O8C	-35(3)	C14A C15A	C16A C17A	0.0
C29C	C28C	C33C	C32C	0.0	C14A C19A	C20A O5A	-19(2)
C29C	C28C	C33C	C34C	-179.9(17)	C14A C19A	C20A O6A	167.9(15)
C29C	C30C	C31C	C32C	0.0	C14A C19A	C20A O5B	-47(2)
C30C	C31C	C32C	C33C	0.0	C14A C19A	C20A O6B	128(2)
C31C	C32C	C33C	C28C	0.0	C15A C14A	C19A C18A	0.0
C31C	C32C	C33C	C34C	179.9(16)	C15A C14A	C19A C20A	-178.0(9)
C32C	C33C	C34C	O7C	-36(3)	C15A C16A	C17A C18A	0.0
C32C	C33C	C34C	O8C	145(2)	C16A C17A	C18A C19A	0.0
C33C	C28C	C29C	C30C	0.0	C17A C18A	C19A C14A	0.0
O3	C9	C10	C11	-140.9(12)	C17A C18A	C19A C20A	178.1(9)
O9	C35	C36	C37	-151.2(10)	C18A C19A	C20A O5A	162.7(16)
N1	N2	C12	O4	-165.0(9)	C18A C19A	C20A O6A	-10.2(19)
N1	N2	C12	C11	18.4(13)	C18A C19A	C20A O5B	135.0(17)
N1	N2	C13	P1	-4.1(10)	C18A C19A	C20A O6B	-50(3)
N1	N2	C13	C14	-129.6(8)	C19A C14A	C15A C16A	0.0
N1	C1	C2	C3	-159.1(7)	C21A C22A	C23A C24A	-1(2)
N1	C1	C2	C7	18.5(12)	C22A C21A	C26A P2A	178.6(8)
N1	C9	C10	C11	33.4(14)	C22A C21A	C26A C25A	-5.5(14)
N2	N1	C1	P1	13.1(10)	C22A C23A	C24A C25A	-1(2)
N2	N1	C1	C2	-114.6(9)	C23A C24A	C25A C26A	-2(2)
N2	N1	C9	O3	-167.6(10)	C24A C25A	C26A P2A	-179.7(11)
N2	N1	C9	C10	17.8(13)	C24A C25A	C26A C21A	4.6(17)
N2	C13	C14	C15	34.3(8)	C26A P2A	C27A N3A	-74.5(7)
N2	C13	C14	C19	-148.0(6)	C26A P2A	C27A C28A	57.5(9)
N4	N3	C27	P2	-20.1(9)	C26A P2A	C27A C28B	45.8(8)
N4	N3	C27	C28	-143.3(7)	C26A P2A	C39A N4A	79.1(7)
N4	N3	C27	C28C	-152.4(9)	C26A P2A	C39A C40A	-149.6(6)
N4	N3	C35	O9	-158.4(9)	C26A C21A	C22A C23A	3.5(17)
N4	N3	C35	C36	23.3(12)	C35A N3A	C27A P2A	-164.0(8)
N4	C39	C40	C41	-165.0(8)	C35A N3A	C27A C28A	67.3(13)
N4	C39	C40	C45	15.7(12)	C35A N3A	C27A C28B	73.0(11)
C1	P1	C13	N2	9.6(7)	C35A N3A	N4A C38A	-49.1(12)

C1	P1	C13	C14	132.2(7)	C35A N3A N4A C39A	147.1(9)
C1	P1	C21	C22	-22.3(10)	C35A C36A C37A C38A	-53.2(12)
C1	P1	C21	C26	161.3(7)	C36A C37A C38A O10A	-142.3(11)
C1	N1	N2	C12	149.6(9)	C36A C37A C38A N4A	34.6(12)
C1	N1	N2	C13	-6.0(12)	C38A N4A C39A P2A	-145.8(8)
C1	N1	C9	O3	-6.6(16)	C38A N4A C39A C40A	83.4(12)
C1	N1	C9	C10	178.8(10)	C39A P2A C27A N3A	26.0(7)
C1	C2	C3	C4	177.8(8)	C39A P2A C27A C28A	158.1(9)
C1	C2	C7	C6	-177.5(9)	C39A P2A C27A C28B	146.4(8)
C1	C2	C7	C8	8.4(12)	C39A P2A C26A C21A	159.3(7)
C2	C3	C4	C5	0.0	C39A P2A C26A C25A	-16.4(10)
C2	C7	C8	O1	-121.1(10)	C39A N4A C38A O10A	-5.3(15)
C2	C7	C8	O2	59.5(13)	C39A N4A C38A C37A	177.7(9)
C3	C2	C7	C6	0.0	C39A C40A C41A C42A	177.3(8)
C3	C2	C7	C8	-174.2(9)	C39A C40A C45A C44A	-177.0(9)
C3	C4	C5	C6	0.0	C39A C40A C45A C46A	7.3(12)
C4	C5	C6	C7	0.0	C40A C41A C42A C43A	0.0
C5	C6	C7	C2	0.0	C40A C45A C46A O11A	68.1(11)
C5	C6	C7	C8	174.8(8)	C40A C45A C46A O12A	-113.8(10)
C6	C7	C8	O1	64.4(12)	C41A C40A C45A C44A	0.0
C6	C7	C8	O2	-114.9(9)	C41A C40A C45A C46A	-175.7(10)
C7	C2	C3	C4	0.0	C41A C42A C43A C44A	0.0
C9	N1	N2	C12	-47.7(13)	C42A C43A C44A C45A	0.0
C9	N1	N2	C13	156.6(9)	C43A C44A C45A C40A	0.0
C9	N1	C1	P1	-148.6(9)	C43A C44A C45A C46A	176.1(9)
C9	N1	C1	C2	83.8(12)	C44A C45A C46A O11A	-107.8(8)
C9	C10	C11	C12	-58.2(13)	C44A C45A C46A O12A	70.3(11)
C10	C11	C12	O4	-144.5(10)	C45A C40A C41A C42A	0.0
C10	C11	C12	N2	32.0(13)	O13G C53G C54G N5G	50(2)
C12	N2	C13	P1	-158.7(8)	O13G C53G C54G C55G	169(2)
C12	N2	C13	C14	75.8(11)	C47G C48G C49G C50G	0.0
C13	P1	C1	N1	-12.8(8)	C47G C52G C53G O13G	-142.0(17)
C13	P1	C1	C2	115.3(6)	C47G C52G C53G C54G	99(2)
C13	P1	C21	C22	72.0(9)	C48G C47G C52G C51G	0.0
C13	P1	C21	C26	-104.5(8)	C48G C47G C52G C53G	180.0(18)
C13	N2	C12	O4	-10.6(14)	C48G C49G C50G C51G	0.0
C13	N2	C12	C11	172.8(9)	C49G C50G C51G C52G	0.0
C13	C14	C15	C16	177.7(6)	C50G C51G C52G C47G	0.0
C13	C14	C19	C18	-177.6(6)	C50G C51G C52G C53G	-180.0(18)
C13	C14	C19	C20	5.3(8)	C51G C52G C53G O13G	38(3)
C14	C15	C16	C17	0.0	C51G C52G C53G C54G	-81(2)
C14	C19	C20	O5	-21(2)	C52G C47G C48G C49G	0.0

C14	C19	C20	O6	157.9(13)	C52G C53G C54G N5G	175.8(17)
C14	C19	C20	O5C	-48.6(15)	C52G C53G C54G C55G	-65(2)
C14	C19	C20	O6C	124(2)	C56G N5G C54G C53G	159(2)
C15	C14	C19	C18	0.0	C56G N5G C54G C55G	41(3)
C15	C14	C19	C20	-177.1(8)	O13E C53E C54E N5E	48.9(11)
C15	C16	C17	C18	0.0	O13E C53E C54E C55E	170.9(10)
C16	C17	C18	C19	0.0	C47E C48E C49E C50E	0.0
C17	C18	C19	C14	0.0	C47E C52E C53E O13E	-142.5(9)
C17	C18	C19	C20	177.2(8)	C47E C52E C53E C54E	101.9(10)
C18	C19	C20	O5	161.6(16)	C48E C47E C52E C51E	0.0
C18	C19	C20	O6	-19.2(17)	C48E C47E C52E C53E	-177.1(11)
C18	C19	C20	O5C	134.2(11)	C48E C49E C50E C51E	0.0
C18	C19	C20	O6C	-53(2)	C49E C50E C51E C52E	0.0
C19	C14	C15	C16	0.0	C50E C51E C52E C47E	0.0
C21	P1	C1	N1	89.4(7)	C50E C51E C52E C53E	177.2(10)
C21	P1	C1	C2	-142.5(6)	C51E C52E C53E O13E	40.4(13)
C21	P1	C13	N2	-90.2(7)	C51E C52E C53E C54E	-75.3(11)
C21	P1	C13	C14	32.3(8)	C52E C47E C48E C49E	0.0
C21	C22	C23	C24	-1.3(18)	C52E C53E C54E N5E	169.4(8)
C22	C21	C26	P2	178.7(8)	C52E C53E C54E C55E	-68.7(12)
C22	C21	C26	C25	-2.3(14)	C56E N5E C54E C53E	-173.1(9)
C22	C23	C24	C25	1.8(18)	C56E N5E C54E C55E	63.2(15)
C23	C24	C25	C26	-2.7(17)	O13D C53D C54D N5D	47(2)
C24	C25	C26	P2	-178.1(9)	O13D C53D C54D C55D	-178.4(17)
C24	C25	C26	C21	2.9(15)	C47D C48D C49D C50D	0.0
C26	P2	C27	N3	-77.3(7)	C47D C52D C53D O13D	-123(2)
C26	P2	C27	C28	43.9(8)	C47D C52D C53D C54D	116(2)
C26	P2	C27	C28C	58.8(9)	C48D C47D C52D C51D	0.0
C26	P2	C39	N4	80.4(7)	C48D C47D C52D C53D	175(3)
C26	P2	C39	C40	-149.9(6)	C48D C49D C50D C51D	0.0
C26	C21	C22	C23	1.6(16)	C49D C50D C51D C52D	0.0
C35	N3	C27	P2	-165.2(7)	C50D C51D C52D C47D	0.0
C35	N3	C27	C28	71.5(11)	C50D C51D C52D C53D	-175(3)
C35	N3	N4	C38	-46.7(11)	C51D C52D C53D O13D	52(3)
C35	N3	N4	C39	149.3(8)	C51D C52D C53D C54D	-69(2)
C35	C36	C37	C38	-56.7(12)	C52D C47D C48D C49D	0.0
C36	C37	C38	O10	-143.6(11)	C52D C53D C54D N5D	170.4(17)
C36	C37	C38	N4	36.3(12)	C52D C53D C54D C55D	-55(2)
C38	N4	C39	P2	-148.1(7)	C56D N5D C54D C53D	-163.8(16)
C38	N4	C39	C40	83.7(11)	C56D N5D C54D C55D	64(2)
C39	P2	C27	N3	23.8(7)	O13 C53 C54 N5	50.0(10)
C39	P2	C27	C28	144.9(7)	O13 C53 C54 C55	172.7(9)

C39	P2	C27	C28C	159.9(9)	C47	C48	C49	C50	0.0
C39	P2	C26	C21	160.7(7)	C47	C52	C53	O13	-143.0(8)
C39	P2	C26	C25	-18.3(9)	C47	C52	C53	C54	99.9(10)
C39	N4	C38	O10	-3.7(15)	C48	C47	C52	C51	0.0
C39	N4	C38	C37	176.4(9)	C48	C47	C52	C53	-176.8(10)
C39	C40	C41	C42	-179.4(8)	C48	C49	C50	C51	0.0
C39	C40	C45	C44	179.3(9)	C49	C50	C51	C52	0.0
C39	C40	C45	C46	-0.2(13)	C50	C51	C52	C47	0.0
C40	C41	C42	C43	0.0	C50	C51	C52	C53	176.8(10)
C40	C45	C46	O11	75.1(13)	C51	C52	C53	O13	40.2(12)
C40	C45	C46	O12	-107.2(12)	C51	C52	C53	C54	-76.9(10)
C41	C40	C45	C44	0.0	C52	C47	C48	C49	0.0
C41	C40	C45	C46	-179.5(12)	C52	C53	C54	N5	170.2(8)
C41	C42	C43	C44	0.0	C52	C53	C54	C55	-67.2(11)
C42	C43	C44	C45	0.0	C56	N5	C54	C53	-171.1(9)
C43	C44	C45	C40	0.0	C56	N5	C54	C55	64.6(14)
C43	C44	C45	C46	179.5(11)	O13F	C53F	C54F	N5F	54.2(13)
C44	C45	C46	O11	-104.4(9)	O13F	C53F	C54F	C55F	176.5(12)
C44	C45	C46	O12	73.4(12)	C47F	C48F	C49F	C50F	0.0
C45	C40	C41	C42	0.0	C47F	C52F	C53F	O13F	-130.2(11)
P1A	C1A	C2A	C3A	76.8(8)	C47F	C52F	C53F	C54F	114.0(12)
P1A	C1A	C2A	C7A	-108.0(8)	C48F	C47F	C52F	C51F	0.0
P1A	C13A	C14A	C15A	-84.8(7)	C48F	C47F	C52F	C53F	178.7(15)
P1A	C13A	C14A	C19A	94.2(7)	C48F	C49F	C50F	C51F	0.0
P1A	C21A	C22A	C23A	-177.5(10)	C49F	C50F	C51F	C52F	0.0
P1A	C21A	C26A	P2A	-0.3(10)	C50F	C51F	C52F	C47F	0.0
P1A	C21A	C26A	C25A	175.6(8)	C50F	C51F	C52F	C53F	-178.7(15)
P2A	C27A	C28A	C29A	-84.9(10)	C51F	C52F	C53F	O13F	48.5(15)
P2A	C27A	C28A	C33A	97.5(12)	C51F	C52F	C53F	C54F	-67.3(14)
P2A	C27A	C28B	C29B	-81.4(9)	C52F	C47F	C48F	C49F	0.0
P2A	C27A	C28B	C33B	99.5(9)	C52F	C53F	C54F	N5F	172.3(11)
P2A	C39A	C40A	C41A	66.8(7)	C52F	C53F	C54F	C55F	-65.3(16)
P2A	C39A	C40A	C45A	-116.0(7)	C56F	N5F	C54F	C53F	-163.5(11)
N3A	C27A	C28A	C29A	41.5(12)	C56F	N5F	C54F	C55F	72.0(16)
N3A	C27A	C28A	C33A	-136.1(11)	O13A	C53A	C54A	N5A	40(2)
N3A	C27A	C28B	C29B	38.1(10)	O13A	C53A	C54A	C55A	-144(4)
N3A	C27A	C28B	C33B	-141.0(8)	C47A	C48A	C49A	C50A	0.0
N3A	N4A	C38A	O10A	-167.6(9)	C47A	C52A	C53A	O13A	-129.4(16)
N3A	N4A	C38A	C37A	15.4(12)	C47A	C52A	C53A	C54A	101.1(19)
N3A	N4A	C39A	P2A	17.0(9)	C48A	C47A	C52A	C51A	0.0
N3A	N4A	C39A	C40A	-113.8(8)	C48A	C47A	C52A	C53A	180(2)
N3A	C35A	C36A	C37A	22.1(14)	C48A	C49A	C50A	C51A	0.0

C27AP2A C26AC21A	-109.2(7)	C49A C50A C51A C52A	0.0
C27AP2A C26AC25A	75.1(10)	C50A C51A C52A C47A	0.0
C27AP2A C39AN4A	-24.0(7)	C50A C51A C52A C53A	-180(2)
C27AP2A C39AC40A	107.3(7)	C51A C52A C53A O13A	50(2)
C27AN3A N4A C38A	167.1(8)	C51A C52A C53A C54A	-79(2)
C27AN3A N4A C39A	3.3(11)	C52A C47A C48A C49A	0.0
C27AN3A C35AO9A	-19.2(15)	C52A C53A C54A N5A	168.5(16)
C27AN3A C35AC36A	167.2(9)	C52A C53A C54A C55A	-15(5)
C27AC28AC29AC30A	-177.7(12)	C56A N5A C54A C53A	-151.3(17)
C27AC28AC33AC32A	177.5(14)	C56A N5A C54A C55A	31(3)
C27AC28AC33AC34A	-6(2)	O13B C53B C54B N5B	56.1(10)
C27AC28B C29B C30B	-179.1(10)	O13B C53B C54B C55B	175.9(9)
C27AC28B C33B C32B	179.1(11)	C47B C48B C49B C50B	0.0
C27AC28B C33B C34B	3.5(16)	C47B C52B C53B O13B	-139.7(9)
C28AC27AC28B C29B	-169(5)	C47B C52B C53B C54B	103.1(11)
C28AC27AC28B C33B	11(5)	C48B C47B C52B C51B	0.0
C28AC29AC30AC31A	0.0	C48B C47B C52B C53B	-179.8(13)
C28AC33AC34AO7A	156.7(17)	C48B C49B C50B C51B	0.0
C28AC33AC34AO8A	-29(3)	C49B C50B C51B C52B	0.0
C29AC28AC33AC32A	0.0	C50B C51B C52B C47B	0.0
C29AC28AC33AC34A	176.7(18)	C50B C51B C52B C53B	179.8(14)
C29AC30AC31AC32A	0.0	C51B C52B C53B O13B	40.4(14)
C30AC31AC32AC33A	0.0	C51B C52B C53B C54B	-76.7(12)
C31AC32AC33AC28A	0.0	C52B C47B C48B C49B	0.0
C31AC32AC33AC34A	-177.0(16)	C52B C53B C54B N5B	176.6(9)
C32AC33AC34AO7A	-26(2)	C52B C53B C54B C55B	-63.6(12)
C32AC33AC34AO8A	147.7(17)	C56B N5B C54B C53B	-172.6(8)
C33AC28AC29AC30A	0.0	C56B N5B C54B C55B	65.9(13)
C28B C27AC28AC29A	12(5)	O13C C53C C54C N5C	55.8(10)
C28B C27AC28AC33A	-166(6)	O13C C53C C54C C55C	179.5(10)
C28B C29B C30B C31B	0.0	C47C C48C C49C C50C	0.0
C28B C33B C34B O7B	149.1(18)	C47C C52C C53C O13C	-138.0(9)
C28B C33B C34B O8B	-33(3)	C47C C52C C53C C54C	101.9(11)
C29B C28B C33B C32B	0.0	C48C C47C C52C C51C	0.0
C29B C28B C33B C34B	-175.6(16)	C48C C47C C52C C53C	-179.1(12)
C29B C30B C31B C32B	0.0	C48C C49C C50C C51C	0.0
C30B C31B C32B C33B	0.0	C49C C50C C51C C52C	0.0
C31B C32B C33B C28B	0.0	C50C C51C C52C C47C	0.0
C31B C32B C33B C34B	176.0(14)	C50C C51C C52C C53C	179.2(11)
C32B C33B C34B O7B	-27(3)	C51C C52C C53C O13C	42.9(12)
C32B C33B C34B O8B	150.9(17)	C51C C52C C53C C54C	-77.3(11)
C33B C28B C29B C30B	0.0	C52C C47C C48C C49C	0.0

O3A	C9A	C10A	C11A	-144.7(12)	C52C	C53C	C54C	N5C	178.8(8)
O9A	C35A	C36A	C37A	-151.3(11)	C52C	C53C	C54C	C55C	-57.4(13)
N1A	N2A	C12A	O4A	-166.5(9)	C56C	N5C	C54C	C53C	-171.9(9)
N1A	N2A	C12A	C11A	17.7(13)	C56C	N5C	C54C	C55C	62.8(12)

Table 7 Hydrogen Atom Coordinates ($\text{\AA} \times 10^4$) and Isotropic Displacement Parameters ($\text{\AA}^2 \times 10^3$) for Landis48.

Atom	<i>x</i>	<i>y</i>	<i>z</i>	U(eq)
H27	3421	8518	2623	66
H27A	3479	8508	2640	66
H29	2738	6817	2533	59
H30	1735	6544	2293	68
H31	1021	7413	2129	72
H32	1310	8556	2205	55
H29C	2630	6997	2519	97
H30C	1605	6866	2274	91
H31C	991	7828	2131	97
H32C	1402	8921	2232	83
H1	638	7352	3059	75
H3	623	8091	2698	105
H4	-35	8880	2457	119
H5	-853	9564	2674	122
H6	-1012	9459	3132	106
H10A	64	6469	3811	92
H10B	-738	6652	3761	92
H11A	-523	7813	3871	83
H11B	-281	7337	4113	83
H13	1520	8433	3669	71
H15	1627	6637	3704	81
H16	2520	5994	3896	90
H17	3535	6532	4042	88
H18	3657	7714	3996	101
H22	1155	6572	3212	84
H23	1704	5514	3149	87
H24	2877	5500	3028	86
H25	3495	6531	3001	84
H36A	4877	7086	2136	70
H36B	5223	7554	2360	70
H37A	5315	6416	2487	83
H37B	4491	6314	2457	83

H39	4088	7290	3194	70
H41	4118	8101	3548	139
H42	4800	8910	3769	178
H43	5664	9504	3538	127
H44	5845	9290	3087	118
H27B	5913	5992	4873	69
H27C	5923	5950	4885	69
H29A	4375	5114	4983	100
H30A	4254	4091	5217	103
H31A	5241	3495	5358	80
H32A	6349	3921	5263	81
H29B	4235	5249	4980	73
H30B	3959	4259	5217	74
H31B	4847	3550	5375	72
H32B	6010	3831	5295	57
H1A	4732	3164	4426	88
H3A	5439	3142	4790	102
H4A	6204	2465	5037	122
H5A	6917	1672	4822	117
H6A	6866	1556	4361	95
H10C	3849	2716	3660	102
H10D	4010	1916	3695	102
H11C	5221	2120	3613	78
H11D	4774	2381	3365	78
H13A	5878	4086	3840	69
H15A	4057	4260	3797	77
H16A	3450	5164	3601	84
H17A	4050	6134	3457	96
H18A	5257	6200	3509	106
H22A	3955	3695	4282	90
H23A	2878	4204	4351	92
H24A	2849	5365	4467	102
H25A	3856	5991	4509	81
H36C	4395	7262	5393	78
H36D	4863	7665	5182	78
H37C	3648	6898	5067	73
H37D	3726	7708	5040	73
H39A	4636	6570	4325	72
H41A	5496	6613	3974	111
H42A	6235	7368	3751	140
H43A	6728	8289	3977	113
H44A	6483	8456	4427	102

H13G	-3111	7110	2373	197
H5GA	-3581	7527	2866	152
H5GB	-3207	7003	3016	152
H47G	-1127	6578	2705	156
H48G	-161	6777	2434	184
H49G	-283	7408	2043	238
H50G	-1371	7841	1923	160
H51G	-2338	7642	2194	168
H53G	-2290	6570	2754	153
H54G	-2618	8045	2715	135
H55A	-2058	7662	3213	238
H55B	-1710	8192	3012	238
H55C	-1533	7396	2990	238
H56A	-2981	8139	3253	181
H56B	-3389	7488	3365	181
H56C	-3798	8061	3201	181
H13E	-743	8405	4292	127
H5EA	-36	8868	4261	79
H5EB	-71	9084	3983	79
H47E	-2442	9629	3947	104
H48E	-3426	10173	4119	131
H49E	-3546	10312	4578	114
H50E	-2682	9907	4864	130
H51E	-1698	9364	4692	106
H53E	-1398	8967	4012	84
H54E	-680	9818	4394	88
H55D	-391	10227	3892	171
H55E	-800	10655	4112	171
H55F	-1219	10170	3913	171
H56D	480	10095	4243	113
H56E	845	9646	4018	113
H56F	883	9410	4321	113
H13D	3810	9848	4910	185
H5DA	4131	9918	4273	102
H5DB	4047	9512	4514	102
H47D	3726	11972	4720	219
H48D	4029	12772	5045	219
H49D	4641	12425	5422	219
H50D	4950	11279	5476	219
H51D	4647	10479	5151	219
H53D	3613	10855	4573	148
H54D	4829	10168	4728	116

H55G	5104	10761	4272	153
H55H	5422	10943	4556	153
H55I	4742	11331	4453	153
H56G	5390	9418	4384	153
H56H	4936	9248	4127	153
H56I	4843	8803	4390	153
H13B	4302	6276	1891	111
H5B	3674	7624	1770	78
H5C	3461	7584	1491	78
H47	2957	5255	1461	110
H48	2406	4280	1626	141
H49	2236	4155	2083	139
H50	2618	5004	2375	139
H51	3169	5979	2209	112
H53	3618	6284	1535	81
H54	2704	6965	1899	84
H55J	2391	6397	1422	160
H55K	2320	7205	1389	160
H55L	1874	6816	1610	160
H56J	2422	8108	1747	112
H56K	2881	8469	1523	112
H56L	3113	8512	1827	112
H13F	854	9431	3519	124
H5FA	2385	9532	3032	97
H5FB	2325	9452	3320	97
H47F	73	10367	2953	147
H48F	-769	11205	3030	147
H49F	-712	11876	3413	147
H50F	187	11709	3719	147
H51F	1029	10871	3641	147
H53F	1038	9694	3090	97
H54F	1994	10622	3350	94
H55M	2288	10544	2835	144
H55N	2029	11202	2994	144
H55O	1475	10704	2858	144
H56M	3166	10496	3243	138
H56N	3433	9873	3065	138
H56O	3367	9786	3379	138
H13C	3281	8419	966	162
H5AA	3093	9816	792	112
H5AB	3041	9896	505	112
H47A	2179	7600	440	187

H48A	1319	6786	527	187
H49A	669	6852	919	187
H50A	879	7731	1222	187
H51A	1739	8544	1135	187
H53A	2876	8506	595	126
H54A	2115	9439	830	119
H55P	1292	9285	503	324
H55Q	1761	9843	356	324
H55R	1463	9994	646	324
H56P	2082	10642	708	180
H56Q	2745	10881	541	180
H56R	2802	10793	855	180
H13H	3890	2827	3093	119
H5BA	5047	3911	2750	74
H5BB	5077	3682	3027	74
H47B	2795	3893	2599	138
H48B	1627	4165	2675	138
H49B	1221	4304	3109	138
H50B	1982	4172	3467	138
H51B	3150	3901	3391	138
H53B	3864	3510	2752	81
H54B	4261	4495	3147	82
H55S	4547	4941	2646	140
H55T	4032	5295	2854	140
H55U	3743	4734	2652	140
H56S	5425	4994	3033	115
H56T	5884	4619	2812	115
H56U	5916	4369	3114	115
H13I	291	6832	4390	121
H5CA	1064	7556	4442	71
H5CB	1199	7533	4728	71
H47C	1019	5283	4894	129
H48C	1281	4128	4834	180
H49C	1567	3720	4412	185
H50C	1591	4466	4050	169
H51C	1329	5622	4110	118
H53C	742	6372	4709	73
H54C	1886	6706	4365	81
H55V	2238	6970	4868	125
H55W	2607	6444	4671	125
H55X	1986	6193	4858	125
H56V	2387	7773	4502	116

H56W	1973	8270	4697	116
H56X	1826	8295	4385	116

Table 8 Atomic Occupancy for Landis48.

Atom	<i>Occupancy</i>	Atom	<i>Occupancy</i>	Atom	<i>Occupancy</i>
H27	0.5	H27A	0.5	O7	0.5
O8	0.5	C28	0.5	C29	0.5
H29	0.5	C30	0.5	H30	0.5
C31	0.5	H31	0.5	C32	0.5
H32	0.5	C33	0.5	C34	0.5
O7C	0.5	O8C	0.5	C28C	0.5
C29C	0.5	H29C	0.5	C30C	0.5
H30C	0.5	C31C	0.5	H31C	0.5
C32C	0.5	H32C	0.5	C33C	0.5
C34C	0.5	O5	0.5	O6	0.5
O5C	0.5	O6C	0.5	H27B	0.5
H27C	0.5	O7A	0.5	O8A	0.5
C28A	0.5	C29A	0.5	H29A	0.5
C30A	0.5	H30A	0.5	C31A	0.5
H31A	0.5	C32A	0.5	H32A	0.5
C33A	0.5	C34A	0.5	O7B	0.5
O8B	0.5	C28B	0.5	C29B	0.5
H29B	0.5	C30B	0.5	H30B	0.5
C31B	0.5	H31B	0.5	C32B	0.5
H32B	0.5	C33B	0.5	C34B	0.5
O5A	0.5	O6A	0.5	O5B	0.5
O6B	0.5	O14	0.30(3)	O16	0.47(4)
O17	0.65(4)	O18	0.29(3)	O19	0.42(3)
O20	0.55(3)	O21	0.67(3)	O22	0.37(3)
O23	0.30(3)	O24	0.27(3)	O25	0.40(3)
O27	0.37(3)	O30	0.74(3)	O31	0.28(3)
O32	0.79(3)	O33	0.85(3)	O35	0.68(3)
O36	0.26(3)	O37	0.58(3)	O40	0.42(3)
O41	0.52(3)	O42	0.23(3)		